

MEIOTIC AND MITOTIC FUNCTIONS OF MAMMALIAN  
RAD18 IN DNA DOUBLE-STRAND BREAK REPAIR

Akiko Inagaki

---

ISBN: 978-94-90371-41-8

Layout & printing: Off Page, Amsterdam

Cover images: Lake Wakatipu in Queenstown, New Zealand (Front); Traffic sign in Wellington, New Zealand (Back)

The work described in this thesis was performed at the Department of Reproduction and Development at the Erasmus MC in Rotterdam, The Netherlands.

Printing of this thesis was financially supported by Erasmus University Rotterdam, Department of Reproduction and Development, Erasmus MC, Stichting tot Bevordering van de Electronenmicroscopie in Nederland (SEN), Greiner Bio-One B.V., Carl Zeiss B.V., and Millipore B.V.



Copyright © 2010 by A. Inagaki. All rights reserved.  
No part of this book may be reproduced, stored in a retrieval system or transmitted in any form or by any means, without prior permission of the author.

---

Meiotic and mitotic functions of mammalian RAD18  
in DNA double-strand break repair

Thesis

to obtain the degree of Doctor from the Erasmus University Rotterdam  
by command of the rector magnificus

Prof.dr. H.G. Schmidt

and in accordance with the decision of the Doctorate Board

The public defence shall be held on  
Friday 22 October 2010 at 13.30 o'clock

by

**Akiko Inagaki**  
born in Osaka, Japan



## DOCTORAL COMMITTEE

**Promotors:** Prof.dr. J.A. Grootegoed  
Prof.dr. J.H.J. Hoeijmakers

**Copromotor:** Dr. W.M. Baarends

**Other members:** Prof.dr. T.K. Sixma  
Dr. H. Jacobs  
Dr. D.C. van Gent

## TABLE OF CONTENTS

<b>Outline of this thesis</b>		7
<b>Chapter 1</b>	DNA repair in mitotic and meiotic cells	
	<i>I. DNA repair in mitotic cells</i>	11
	<i>II. DNA repair in meiotic cells</i>	33
<b>Chapter 2</b>	Dynamic localization of human RAD18 during the cell cycle and a functional connection with DNA double-strand break repair	69
<b>Chapter 3</b>	Human RAD18 interacts with ubiquitylated chromatin components and facilitates RAD9 recruitment to DNA double strand breaks	99
<b>Chapter 4</b>	Meiotic functions of RAD18	133
<b>Chapter 5</b>	Meiotic recombination is controlled by PCNA K164 modification	163
<b>Chapter 6</b>	Relation between radiation-induced DNA double-strand breaks, synapsis and the MSUC response in spermatocytes and oocytes of Spo11 mutant mice	181
<b>Chapter 7</b>	General discussion	199
<b>Addendum</b>	Summary	212
	Samenvatting	214
	List of Abbreviations	216
	Curriculum vitae	218
	PhD portfolio	219
	List of publications	221
	Acknowledgements	222



## OUTLINE OF THIS THESIS

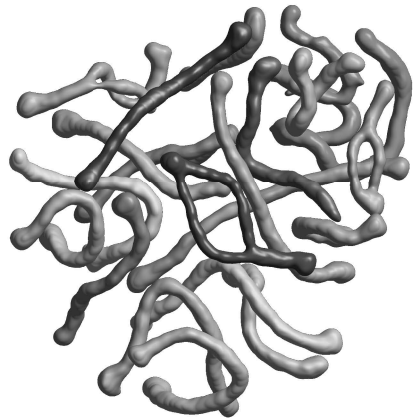
This thesis focuses on the role of RAD18 in DNA double-strand break (DSB) repair. Much is known about the role of RAD18, and its critical substrate PCNA in replication damage bypass (RDB) repair. However, the roles of RAD18 in DSB repair are still elusive, although several interaction partners of RAD18 have been identified, and the radiation-sensitivity of *Rad18* knockout cells has shown that this E3 ligase is active in DSB repair.

First, a general introduction on the possible involvement of RAD18 in DSB repair mechanisms and RDB that operate in mitotic and meiotic cells is presented in **Chapter 1**. In **Chapter 2**, we examined the dynamic localization of human RAD18 during the cell cycle and after DNA damage in living cells. The DNA damage response functions of RAD18 after different types of damages (UV and IR) were analyzed. In order to distinguish DSB repair functions of RAD18 from functions in the RDB pathway, the dynamics of the known substrate of RAD18 in RDB, PCNA, was also examined in living cells. Subsequently, we performed a structure-function analysis of RAD18 and examined the requirements for RAD18 localization to DSBs in mitotic cells. We also show that RAD18 facilitates recruitment of the checkpoint protein RAD9 to DSB repair sites (**Chapter 3**). Next, we examined the role of mouse RAD18 in meiotic DSB repair by analysing the testicular phenotype of *Rad18* knockdown mice (**Chapter 4**). Also, the function of PCNA modification in meiosis was examined in **Chapter 5**. We propose a possible role of SUMOylated PCNA in meiotic crossover control. Based upon our observations on RAD18 localization to DSBs in meiosis, we have performed a detailed analysis of the accumulation of DSB-repair proteins in the presence and absence of meiotic (SPO11-induced) DSBs in spermatocytes, in relation to chromosome pairing (**Chapter 6**). Finally, we present a general discussion of the results described in Chapter 2 - 6 and present a model of RAD18 functions in DSB repair (**Chapter 7**).

1

# DNA REPAIR IN MITOTIC AND MEIOTIC CELLS

Akiko Inagaki



Department of Reproduction and Development, Erasmus MC – University  
Medical Center, PO BOX 2040, 3000 CA, Rotterdam, the Netherlands

## **DNA REPAIR IN MITOTIC AND MEIOTIC CELLS**

In somatic cells, DNA damage may arise due to exogenous and endogenous sources. Correct repair of DNA lesions is essential for the maintenance of genome integrity. In meiotic cells, formation and repair of meiosis-specific DNA double-strand breaks (DSB) is required for homologous chromosome pairing. In this chapter, we describe DSB repair mechanisms that operate in mitotic and meiotic cells.

## I. DNA REPAIR IN MITOTIC CELLS

- Types of damage and repair mechanisms, Double strand break repair pathways, DNA damage tolerance, DNA damage response, and cell cycle checkpoint activation

**Akiko Inagaki**

Department of Reproduction and Development, Erasmus MC – University Medical Center, Rotterdam, the Netherlands

**Key words:** DNA double-strand break repair, homologous recombination, non-homologous DNA end-joining, cell cycle checkpoint, replication damage bypass, DNA damage response

### 1. TYPES OF DAMAGE AND REPAIR MECHANISMS

Cells are constantly exposed to internal and external factors that may cause DNA damage. To maintain genomic integrity, cells have developed elaborate DNA repair systems and various cell cycle checkpoints that ensure the repair of DNA lesions before cell cycle progression resumes. Depending on the type of DNA damage, different DNA repair mechanisms may be activated. For example, base excision repair is used to repair oxidized, alkylated or some types of mismatched bases, whereas nucleotide excision repair is used for bulky helix-distorting DNA lesions. Interstrand cross-link repair and DNA double-strand break repair are two other major repair pathways. In contrast, there is a special pathway called replication damage bypass (RDB) that allows progression of DNA replication in the presence of unrepaired DNA lesions in the template. Checkpoint signaling is activated in response to various situations that threaten genome integrity such as incomplete DNA replication, repair at stalled replication forks, and damaged DNA induced by both internal and external sources such as UV light, ionizing radiation, reactive oxygen species or DNA-damaging agents. Active checkpoints prevent further progression of the cell cycle. If DNA repair mechanisms fail in repair DNA lesions, additional signaling pathways are activated, which lead to cell death via apoptosis. In this chapter, the mechanisms of double-strand break repair and replication damage bypass, as well as DNA damage response pathways and checkpoint signaling will be described in the mammalian system as well as in yeast (Table 1).

### 2. DOUBLE-STRAND BREAK REPAIR PATHWAYS

One of the most genotoxic lesions is a DNA double-strand break (DSB). During S phase, DSBs can arise when the replication fork collapses. In addition, DSBs may arise from exogenous factors such as ionizing radiation. Two distinct repair pathways have been identified in mammalian cells; non-homologous end-joining (NHEJ) (Figure 1), and homologous recombination (HR) (Figure 2-6). NHEJ is an error-prone form of

**Table 1.** Proteins involved in DSB repair, Checkpoint, and RDB pathways

	mammals	<i>S. pombe</i>	<i>S. cerevisiae</i>
NHEJ	KU70	Pku70	Hdf1
	KU80	Pku80	Hdf2
	DNA-PKs	-	-
	ARTEMIS	-	-
	POL $\mu$	Pol4	Pol4
	POL $\lambda$	Pol4	Pol4
	DNAIigase4	Lig4	Dnl4
	XRCC4	-	Lif1
	XLJ	Xlf1	Nej1
HR	MRE11	Rad32	Mre11
	RAD50	Rad50	Rad50
	NBS1	Nbs1	Xrs2
	CTIP	Ctp1	Sae2
	EXO1	Exo1	Exo1
	DNA2	Dna2	Dna2
	BLM	Rqh1	Sgs1
	RTEL1	Srs2	Srs2
	FBH1	Fbh1	-
	RAD51	Rhp51	Rad51
	RAD51D	Rdl1	-
	RPA	Ssb/Rad11	Rfa
	RAD52	Rad22 Rti1/Rad22B	Rad52
	RAD54	Rhp54	Rad54
	-	Rph55	Rad55
	XRCC2	Rlp1	-
	XRCC3	Rhp57	Rad57
	GEN1	-	Yen1
	TOPIII $\alpha$	Top3	Top3
	RMI1	Rmi1	Rmi1
	MUS81	Mus81	Mus81
	EME1	Eme1	Mms4

Table 1. Continuation

	mammals	<i>S. pombe</i>	<i>S. cerevisiae</i>
Checkpoint	ATR	Rad3	Mec1
	ATM	Tel1	Tel1
	ATRIP	Rad26	Ldc1/Ddc2
	CHK1	Chk1	Chk1
	CHK2	Cds1	Rad53
	RAD9	Rad9	Ddc1
	RAD1	Rad1	Rad17
	HUS1	Hus1	Mec3
	RAD17	Rad17	Rad24
	53BP1	Crb2/Rhp9	Rad9
	TOPBP1	Cut5	Dpb11
RDB	PCNA	Pcn1	Pol30
	RAD18	Rhp18	Rad18
	HR6A	Rhp6	Rad6
	HR6B	Rhp6	Rad6
	HLTF	Rad8	Rad5
	SHPRH	Rad8	Rad5
	POL $\eta$	Eso1	Rad30
	POL $\iota$	-	-
	POL $\kappa$	-	-
	REV3(POL $\zeta$ )	Rev3	Rev3
	REV7(POL $\zeta$ )	Rev7	Rev7
	REV1	Rev1	Rev1
	Ubiquitin	Ubi4	Ubi4
	SUMO1	Pmt3	Smt3
	SUMO2	-	-
	SUMO3	-	-
	UBC13	Ubc13	Ubc13
	MMS2	mms2	Mms2
	SAE1	Rad31	Aos1
	SAE2	Fub2	Uba2
UBC9	Hus5	Ubc9	

DSB repair, in which the two ends of the broken DNA are processed for direct ligation. This mechanism is thought to be operative mainly during the G1 phase but may also function in S and G2 phases. In contrast, HR is an error-free mechanism, in which a homologous sequence of the sister chromatid is used as a template to process repair in the S and G2 phases.

## 2.1 Non-homologous DNA end-joining

In non-dividing haploid organisms or in diploid organisms that are not in S phase, a homologous template of sister chromatid is not available, and of homologous chromosome is not situated nearby. Therefore, DSBs can be repaired only by NHEJ. NHEJ involves several separate steps (Figure 1), 1) DNA-end cleavage, 2) DNA synthesis, and 3) ligation to restore integrity to the DNA strands. While HR appears to be the predominant mechanism of DSB repair in yeast, NHEJ is thought to be the main DSB-repair pathway in mammals, especially during G1 phase.

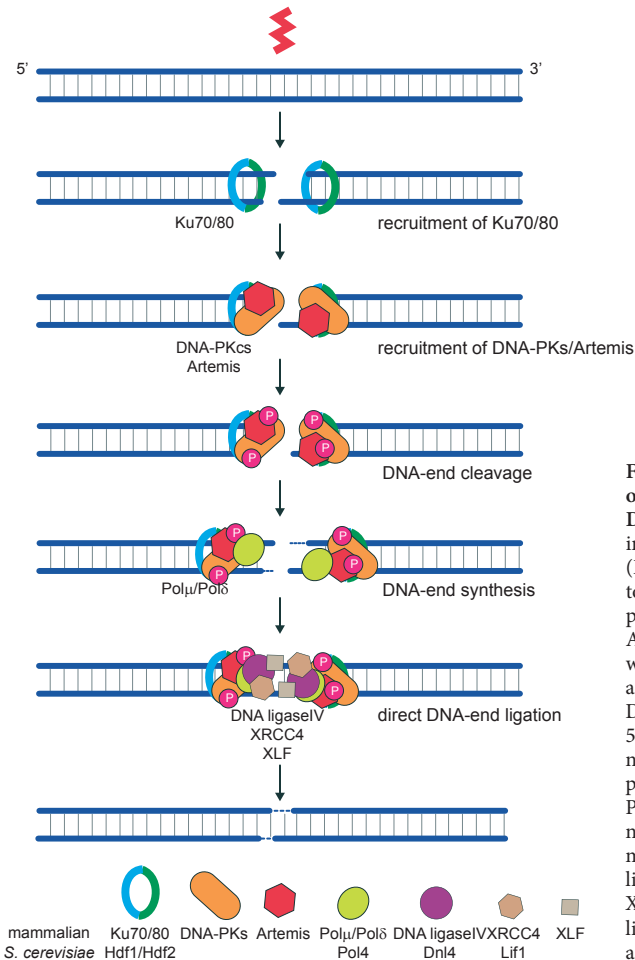


**Figure 1. Schematic representation of the mammalian nonhomologous DNA end-joining pathway.** With induction of a double-strand break (DSB), a Ku70/80 heterodimer binds to the DNA ends. Subsequently, DNA protein kinase (DNA-PKcs) and Artemis are recruited, and interact with Ku70/80. Both DNA-PKcs and Artemis are phosphorylated by DNA-PKcs. Non-complementary 5' nucleotides are processed by the nuclease activity of Artemis. DNA polymerases of the PolX family, Polμ or Polλ, synthesize several nucleotides to generate terminal microhomology, if necessary. DNA ligase IV and its associated factors XRCC4 and XLF are recruited and ligate incompatible DNA ends. Polμ and Polλ fill the DNA gaps.

### 2.1.1 DNA-end cleavage

When a DSB arises, Ku is the first protein that binds to the two broken DNA ends [1-5]. Ku is a ring-like heterodimer composed of Ku70 and Ku80, which displays high affinity to DNA ends and serves as a platform for the core components of NHEJ (reviewed in [6]). Once Ku binds to DNA ends, it recruits Artemis and the DNA-dependent protein kinase catalytic subunit (DNA-PKcs) [7]. When DNA-PKcs binds to DSB ends, the serine/threonine kinase activity of DNA-PKcs becomes active [8-11]. Upon activation, both DNA-PKcs itself as well as Artemis are phosphorylated [12,13]. This phosphorylation of Artemis activates its 5'- and 3'- endonuclease activity at overhangs, hairpins, gaps, flaps, and various loop conformations [12,14]. Artemis appears to be involved in processing various damaged DNA ends to remove nucleotides that cannot be directly ligated [12,15,16]. In addition, the DNA-bound DNA-PKcs molecules bridge and connect the two DNA ends [17-19].

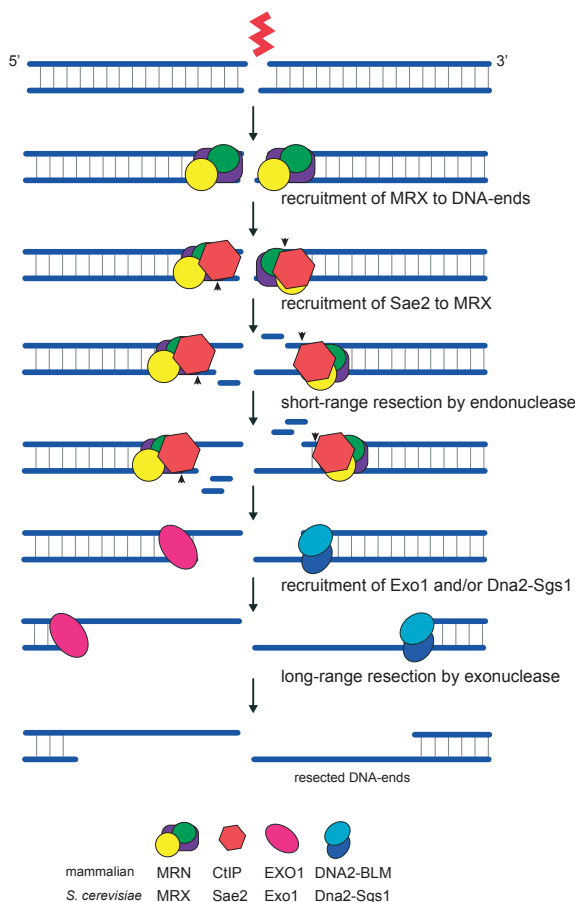


**Figure 2. Schematic mechanism of yeast DNA-end resection in the homologous recombination pathway.** Mammalian orthologs are also shown in the figure. DSBs are detected by the Mre11-Rad50-Xrs2 complex (MRX), followed by Sae2. Endonuclease activity of Mre11 and Sae2 initiates DNA-end resection. The DNA-end resection is further processed by either the 5'-3'exonuclease Exo1, or the helicase Sgs1 / 5'flap endonuclease Dna2 complex for long-range resection.

### 2.1.2 DNA synthesis

Three DNA polymerases of the PolX family are involved in mammalian NHEJ; Pol $\mu$ , Pol $\lambda$ , and terminal deoxynucleotidyl transferase (TdT) [20-25]. These three DNA polymerases all contain BRCT domains, and bind to the Ku-DNA complexes [21]. TdT functions only during V(D)J recombination, since it is expressed only in pre-B and pre-T cells [26]. Pol $\lambda$  displays template-dependent DNA synthesis, while Pol $\mu$  shows both template-dependent and -independent DNA synthesis [20,27-29]. The template-independent polymerase activities are crucial to join two incompatible DNA ends (reviewed in [6]). Random addition of nucleotides by Pol $\mu$  possibly generates the terminal microhomology, which allows efficient annealing of the DNA ends (reviewed in [30]).

### 2.1.3 DNA-end ligation

A complex of three proteins, named DNA ligase IV, XRCC4, and XLF, mediates the final step of NHEJ. The DNA ligase IV/XRCC4/XLF is a very flexible ligase, with the capability to ligate one strand independent of the other strand [21], across gaps of several nucleotides [27], and incompatible DNA ends [27,31,32]. Each broken DNA-end associates with Ku during the three enzymatic steps of NHEJ, and Ku functions as a central platform that interacts with the Artemis/DNA-PKcs complex, the DNA polymerases, and the DNA ligase IV/XRCC4/XLF complex [6,12,17,30,33,34].

## 2.2 Homologous recombination

During homologous recombination (HR) genetic information is exchanged between two homologous sequences. When DSBs are induced by endogenous or exogenous factors, a template DNA sequence is used to repair the breaks, and this template is usually provided by the sister chromatid in mitotic cells. However, when the template sequence that is used is not the sister chromatid but another homologous region, the HR process can result in loss of heterozygosity or gross chromosomal rearrangements such as translocations, deletions or inversions (reviewed in [35]). HR proceeds in several distinguishable steps; 1) resection of double-stranded DNA (dsDNA) to generate single-stranded DNA (ssDNA) tails (Figure 2), 2) formation of a recombinase filament on the ssDNA ends (Figure 3), 3) strand invasion into a homologous sequence

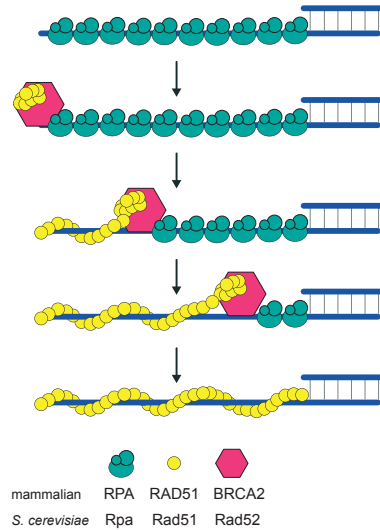


**Figure 3. RAD51 filament formation in the HR pathway.** The resected ssDNA is initially bound by the ssDNA-binding protein RPA (replication protein A), which has higher affinity and specificity for ssDNA than RAD51. BRCA2 in mammals (Rad52 in yeast) interacts with both RAD51 and RPA, and accelerates displacement of RPA from ssDNA by RAD51, thereby allowing efficient RAD51-mediated recombination involving RPA-coated ssDNA.

to form a D-loop intermediate (Figure 4), 4) DNA synthesis (Figure 4), capture of the second DSB end, and formation of a cruciform intermediate, called Holliday junction (HJ) (Figure 5), and 5) resolution of the HJs to give either crossover or non-crossover products (Figure 6). Instead of capturing the second DSB end at step 4, the invaded strand may also be displaced and anneal with the second resected DSB end. This specific subpathway generates only non-crossover products, and has been called synthesis-dependent strand annealing (SDSA) (Figure 7). A second subpathway is called break-induced replication (BIR), and during this process the invading strand at step 4 is postulated to establish a replication fork to copy the entire distal arm of the template chromosome, resulting in loss of heterozygosity (Figure 8) [36,37].

### 2.2.1 DNA-end resection of dsDNA to ssDNA

All HR pathways are initiated by 5'-3' degradation of one strand at both sides of the break; the so-called DNA-end resection, generating stretches of ssDNA, that are subsequently

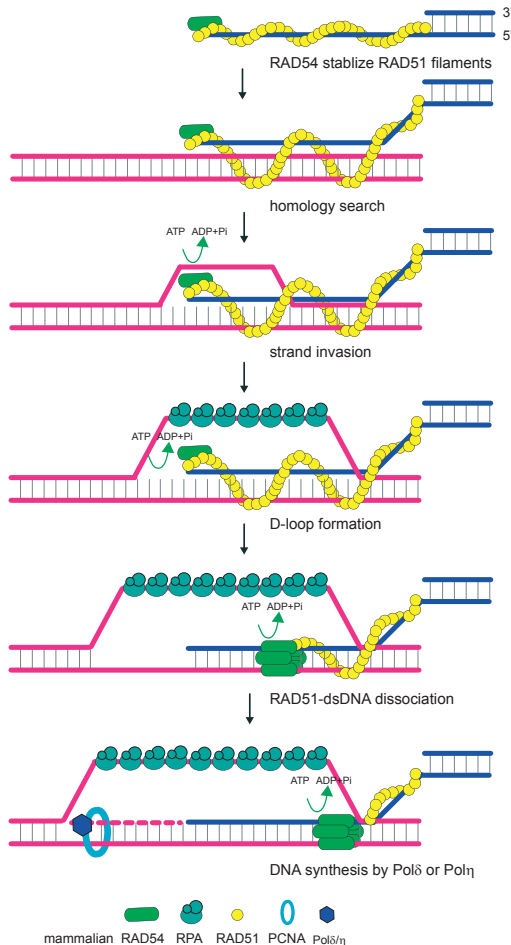


**Figure 4. Homology search, strand invasion, and DNA synthesis in the HR pathway.** RAD54 binds to the RAD51-ssDNA filaments to stabilize the RAD51 filament. The RAD51 filament binds duplex DNA and searches for DNA homology in the duplex DNA molecules. Subsequently, RAD54 stimulates RAD51-mediated joint molecule (D-loop) formation (figures are adapted from Sung, 2006 [326]). The D-loops are stabilized by RPA binding to the displaced strand. After DNA strand exchange, RAD54 forms a hexameric complex, and dissociates RAD51-dsDNA filaments by translocating on the DNA. DNA synthesis from the invading 3' ssDNA tail of the broken chromosome is performed by DNA polymerase  $\delta$  or  $\eta$ . PCNA functions as a sliding clamp.

coated by the ssDNA binding protein complex RPA (reviewed in [38]). DNA resection is a highly complex and regulated process. A crucial protein complex involved in the DNA resection process is the MRN complex (MRX in *Saccharomyces cerevisiae*), composed of MRE11, RAD50, and a third protein known as NBS1 in most eukaryotes and as Xrs2 in *S. cerevisiae* [39-44]. In addition to acting as a nuclease during resection, the RAD50 and MRE11 components of the MRN complex form an oligomeric complex on linear DNA to tether broken DNA ends, and keep them in close proximity before repair [45-47].

Loss of any of the three components of the MRN complex leads to hypersensitivity to DNA-damaging agents [48-50], defects in HR [51,52] and embryonic lethality [48,50,53], suggesting that the MRN complex operates as a single functional unit. MRE11 shows both endonuclease and exonuclease activity *in vitro* although its exonuclease activity operates in the 3'-5' direction, opposite to the direction for the DNA resection *in vivo* [42,54]. In *S. cerevisiae*, an endonuclease, Sae2, cooperates with Mre11 and together they initiate DNA resection [55]. Further processing occurs by either the 5'-3' exonuclease Exo1, or the helicase Sgs1-5' flap endonuclease Dna2 complex for long-range resection [54,56-59]. It seems that the Sgs1-Dna2 complex functions in a parallel pathway to Exo1 [59] (Figure 2). DNA resection is barely affected upon single deletion of *sae2*, *exo1*, or *sgs1*, or in *mre11* nuclease-defective mutants, suggesting that their functions

can be bypassed, although triple deletion of *sae2*, *exo1* and *sgs1* blocks DNA resection [55-61]. In addition, overexpression of Exo1 partially suppresses the phenotype of *mre11* mutants [57,59,62]. In mammalian cells, a functional ortholog of yeast Sae2, CtIP, has been identified [42,63,64]. Human CtIP physically interacts with MRE11 [42,63,64], and CtIP together with MRE11 show increased nuclease activity compared to MRE11 alone [63]. In addition, downregulation of CtIP or expression of a MRE11 nuclease-defective mutant completely abolishes ssDNA formation, as measured by the lack of

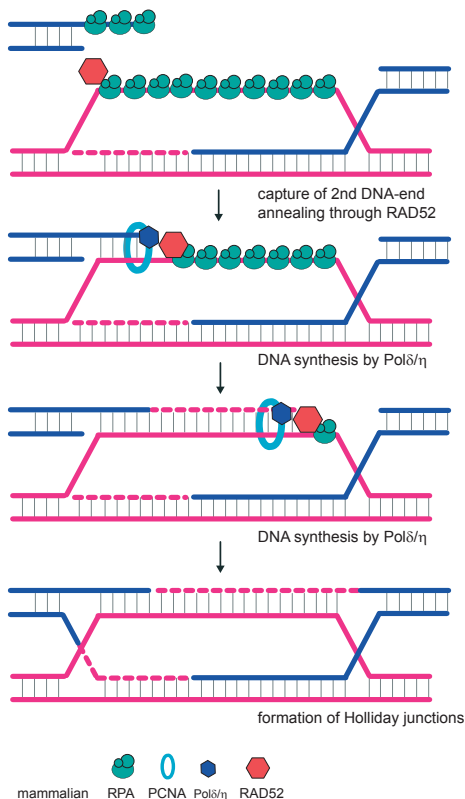


**Figure 5.** Second DNA capture and DNA synthesis in the HR pathway. At the D-loop, RPA binds to the displaced strand. Mammalian RAD52 protein binds RPA, forms a stable complex with RPA-ssDNA, and is capable of annealing complementary DNA strands bound by RPA. DNA synthesis from the 3' terminus of the captured second end can be performed by Pol $\eta$ .

RPA foci formation [56,63-65]. BLM (mutated in Bloom syndrome) is considered to be the Sgs1 ortholog in mammals, based on protein-protein interactions and mutant phenotypes; mutation of *Blm* causes genome instability and cancer development in mice and humans [66-68]. Recently, the human ortholog of Dna2 was characterized [69,70]. Biochemical analysis revealed that, similar to its yeast counterpart, the human DNA2 (hDNA2) protein possesses nuclease and limited helicase activities [69,70], suggesting analogous functions of Dna2 and hDNA2 in yeast and human cells, respectively. Depletion of hDNA2 leads to the appearance of aneuploid cells and the formation of intranuclear chromatin bridges, indicating that hDNA2, like its yeast counterpart, is essential for DNA stability [71]. Another crucial factor, the tumor suppressor protein BRCA1, has been identified in mammalian cells; this protein is absent from the yeast genome. Interaction of CtIP and BRCA1 is essential for CtIP recruitment to sites of DNA damage [72] and proper DNA resection [64,73].

### 2.2.2 RAD51 filament formation

The enzymes that mediate the pairing and shuffling of DNA sequences during HR are called recombinases. Two recombinases, Rad51 and Dmc1, are present in eukaryotes.

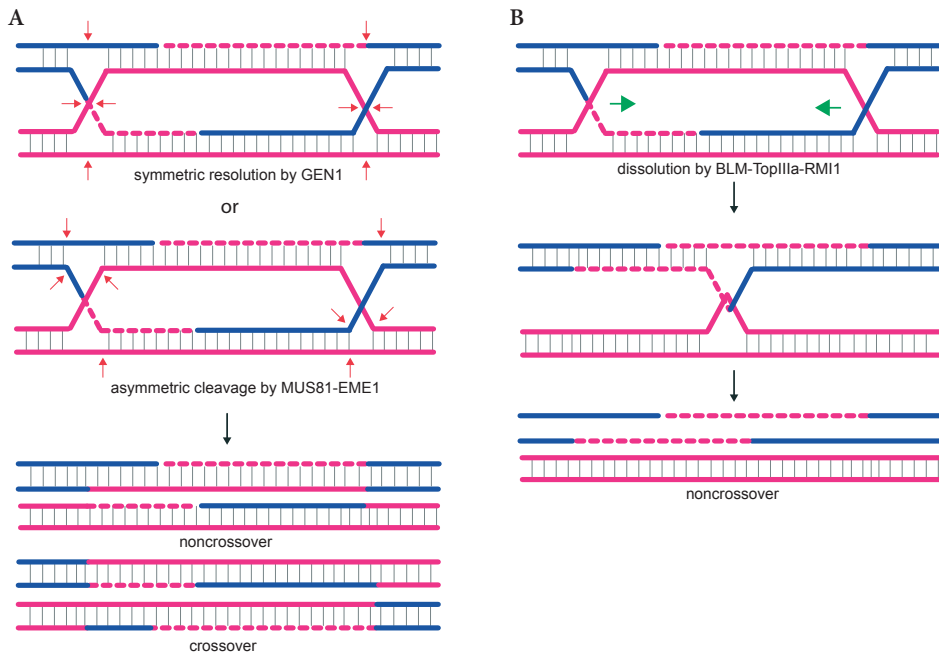


**Figure 6. Resolution of Holliday junctions in the HR pathway.** Three available pathways to resolve double Holliday junctions resulted from strand exchanges between sister chromatids (blue and red). (A) GEN1/Yen1 promotes Holliday junction resolution by a symmetrical cleavage mechanism, and the MUS81-EME1 heterodimer (Mus81-Mms4 in yeast) cleaves asymmetrically. Both symmetrical and asymmetrical cleavages produce either crossover or non-crossover recombinants. (B) Dissolution of Holliday junctions catalyzed by BLM-TopIIIa-RMI1 (Sgs1-Top3-Rmi1 in yeast). Two HJ structures are pushed toward each other by DNA helicase, and dissolved by topoisomerase to generate non-crossover recombinants. Figures are adapted from West, 2009 [327].

Rad51 is required for mitotic and meiotic HR, whereas Dmc1 functions only in meiotic HR (Chapter 1, part II). *S. cerevisiae* Rad51 assembles onto ssDNA or dsDNA to form a right-handed helical polymer that can span thousands of bases or base pairs [74,75]. Mammalian RAD51 also forms helical filaments on both ssDNA and dsDNA, similar to *S. cerevisiae* Rad51 [76]. Both in yeast and mammalian HR, RAD51-coated single-stranded DNA can invade duplex DNA and pair with homologous nucleotides to initiate the strand exchange reactions that result in genetic recombination. In the nucleus, ssDNA is initially bound by the ssDNA-binding protein RPA (replication protein A), which displays higher affinity and specificity for ssDNA than RAD51 [38]. RPA is a heterotrimeric ssDNA-binding protein involved in all DNA metabolic processes involving ssDNA [38]. *In vitro*, RPA inhibits nucleation of the RAD51 filament on ssDNA, but stimulates recombination by eliminating secondary structure in ssDNA and by binding to the displaced strand of the D-loop [77,78]. The inhibitory

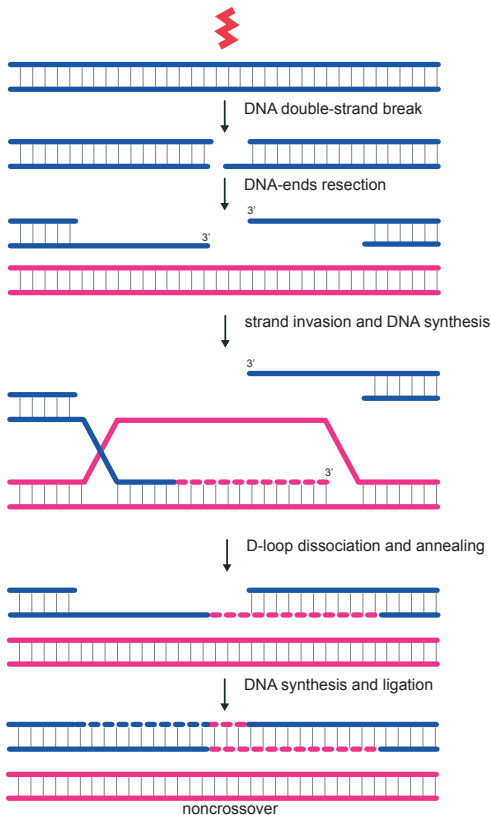


**Figure 7. Synthesis-dependent strand annealing in the HR pathway.** If the second DNA end does not capture the displaced D-loop, the invaded strand may be displaced and anneal with the second resected DSB end. This pathway generates only non-crossover products.

effect of RPA on RAD51 filament formation is overcome by RAD51 mediator proteins [79]. In *S. cerevisiae*, the Rad55-Rad57 complex and Rad52 have been identified as the key mediators of Rad51 filament formation [80,81]. Rad55 and Rad57 are two paralogs of Rad51 and form a heterodimer with mediator activity, as they enable Rad51-mediated *in vitro* recombination in the presence of RPA-coated ssDNA [80]. There are five mammalian RAD51 paralogs (RAD51B, RAD51C, RAD51D, XRCC2, and XRCC3) [82-84]. All RAD51 paralogs are required *in vivo* for RAD51 filament formation. They function in the assembly and/or maintenance of the RAD51 presynaptic filament [85,86]. A complex of RAD51B and RAD51C enhances the homologous DNA pairing activity of RAD51 [87], which could derive from the ability of RAD51C to promote the melting of duplex DNA [88].

*S. cerevisiae* Rad52 forms a multimeric ring structure that binds preferentially to ssDNA [89,90]. Yeast Rad52 interacts

with both Rad51 and RPA [91,92], accelerates displacement of RPA from ssDNA by Rad51 [93], and allows efficient Rad51-mediated recombination involving RPA-coated ssDNA [81,94,95]. Rad52 is also involved in the annealing of homologous ssDNA coated by RPA [96]. This activity is thought to be critical in second-end capture [97,98], synthesis-dependent strand annealing (SDSA), and single-strand annealing (SSA). In contrast to the severe HR-defective phenotype of the yeast Rad52 mutant, mouse *Rad52* mutants display a very mild recombination defect and no IR sensitivity [99], suggesting redundancy in function of RAD52 with other mediator proteins in mammalian cells. The tumour suppressor BRCA2 is an intriguing protein among the mediator proteins. Cells deficient in BRCA2 are sensitive to DNA-damaging agents and impaired for HR [100,101]. BRCA2 is also required for IR-induced RAD51 foci formation [102,103]. BRCA2 functions via two mechanisms to favour RAD51 filament formation; nucleation and filament stabilization. Human BRCA2 interacts with RAD51 protein through a motif called the BRC repeat [100,104,105], and also via a structurally distinct motif located at its extreme carboxyl terminus [106,107]. In addition to an interaction with RAD51, BRCA2 has also been found to associate with RPA [108]. These properties make this protein an excellent candidate for performing functions that are redundant with RAD52 (Figure 3).

### 2.2.3 Homology search and strand invasion into a homologous sequence

During pre-synapsis, mediator proteins function in the replacement of RPA with RAD51 on the single-stranded tails of the processed DSB. During synapsis, the RAD51 filament

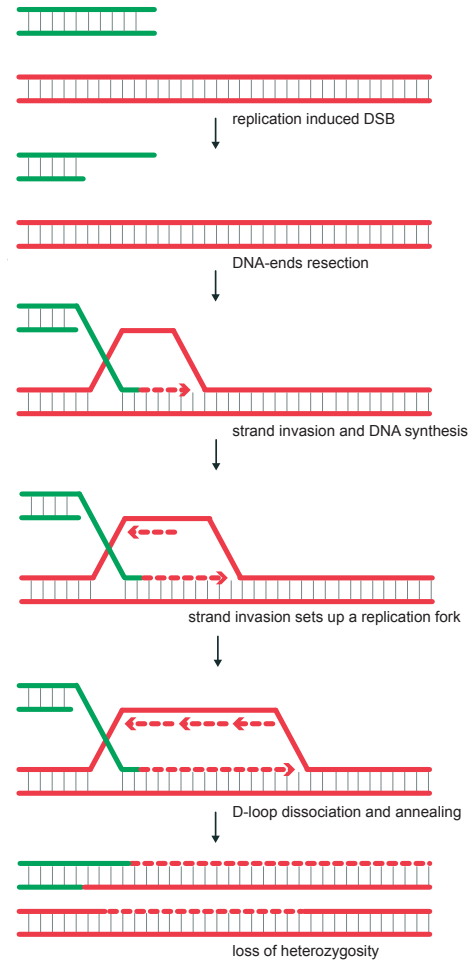


**Figure 8. Break-induced replication in the HR pathway.** When only one DSB end shares homology to a template elsewhere in the genome, a less-efficient HR mechanism, break-induced replication (BIR), can be used to repair the break. In BIR, recombination is used to establish a uni-directional replication fork that can copy the template DNA to the end of the chromosome. BIR will result in loss of the distal part of the broken chromosome, hence loss of heterozygosity.

performs the homology search and DNA strand invasion. During these enzymatic steps, RAD54, a member of the Swi2/Snf2-like family of dsDNA-dependent ATPases, is required at multiple stages in yeast and mammalian cells. In the early stages, RAD54 stimulates for the DNA homology search and joint molecule formation (reviewed in [109]). RAD54 stabilizes the RAD51 filament by forming a complex with the RAD51-ssDNA filaments independent of its ATPase activity [87,110-113]. Subsequently, RAD54 stimulates RAD51-mediated joint molecule (D-loop) formation in an ATPase-dependent manner [87,111,113-117]. The D-loops are stabilized by RPA binding to the displaced strand [77]. The mammalian paralogue of RAD54, RAD54B, also has a dsDNA-dependent ATPase activity, interacts with RAD51, and can translocate on duplex DNA to result in topological changes in the DNA and the transient opening of the DNA strands (Figure 4). Similar to RAD54, RAD54B enhances the activity of RAD51, which promotes D-loop formation [118-120].

#### 2.2.4 DNA synthesis, capture of the second DSB end and formation of a Holliday junction

After DNA strand exchange, RAD54, which may act as hexameric complex, progressively dissociates RAD51-dsDNA filaments by translocating on the DNA towards a terminus of the filament in yeast and mammalian cells [112,121,122]. Intriguingly, *rad54* shows a synthetic lethal interaction with *srs2* in *S. cerevisiae* [123]. Srs2 is a 3'-5' helicase that strips Rad51 from ssDNA [124,125]. Notably, only *rad54* mutant cells are synthetically lethal in combination with *srs2*, but *rad51*, *rad52*, *rad55* or *rad57* mutants are not [123]. It might be crucial to keep Rad51 away from sites where recombination is not needed, and this may be achieved through actions of Srs2 and/or Rad54 (reviewed in [109]). The dissociation of Rad51 from the heteroduplex DNA by the Rad54 motor allows the transition from strand invasion and homologous pairing to DNA synthesis. Once the joint molecule has been formed, the invading 3' ssDNA tail of the broken chromosome, which can subsequently serve as a primer, is extended by DNA polymerase, restoring the information that was lost at the site of the break (Figure 4). The translesion polymerase Pol $\eta$  participates in this DNA synthesis reaction by preferentially binding and extending DNA synthesis from D-loop recombination intermediates *in vitro* [126]. The DNA replication polymerase  $\delta$  can also be loaded to DNA through the actions of replication factor C (RFC) and the DNA clamp homotrimeric PCNA ring (see also 3. Replication bypass, below), then it binds to the D-loop and performs efficient DNA synthesis from the invading 3' end [127]. The *in vitro* system identified a preference of Pol  $\delta$  over Pol  $\eta$  in D-loop extension both in yeast and mammalian cells [127,128]. At the displaced strand of the D-loop, RAD52 and RPA collaborate to promote D-loop extension, annealing to the second end of a DSB, and DNA synthesis from the 3' terminus of the captured second DSB by Pol $\eta$  (Figure 5) [97]. This cross-stranded structure formed through invasion of the ends of a broken DNA molecule into homologous duplex DNA has been named Holliday junction (HJ) [129,130]. A HJ is able to undergo branch migration along DNA to generate increasing or decreasing length of heteroduplex DNA, and Rad54 promotes the bidirectional DNA branch-migration [131].

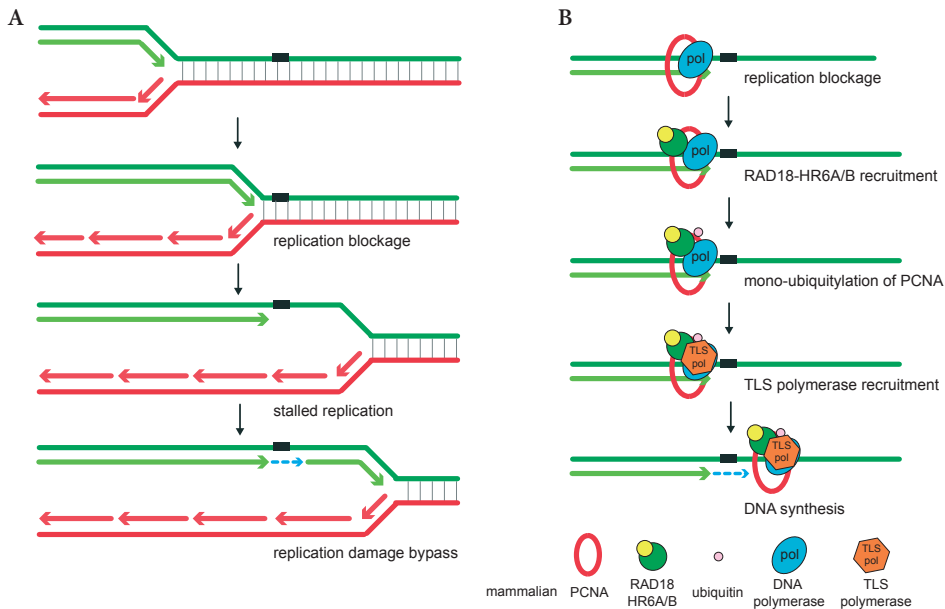


**Figure 9. Replication damage bypass; error-prone pathway.** (A) When the replication machinery encounters damage, the DNA replication polymerase cannot incorporate nucleotides opposite sites of the damage. Subsequently, a translesion synthesis (TLS) polymerase which has a lower fidelity than the replication polymerase is recruited and bypasses the replication without repairing the damage. (B) Recruitment of translesion polymerases to a stalled replication site. Proliferation cell nuclear antigen (PCNA) is a sliding clamp, which functions as a platform for the replication machinery. When the replication machinery is stalled, the RAD18-HR6A/B complex is recruited and mono-ubiquitylates PCNA, which recruits a TLS polymerase to the replication machinery. Subsequently, the TLS polymerase bypasses the damage to allow restart of the replication.

### 2.2.5 Resolution of HJs

Holliday junctions can be dissolved in several different ways. The Holliday junction resolvase GEN1 (Yen1 in *S. cerevisiae*) cuts junctions symmetrically to give rise to nicked duplex products, and produces either crossover or non-crossover products [132]. Holliday junctions also can be dissociated by the Bloom's syndrome complex (BLM helicase-topoisomerase III $\alpha$  - RMI1) (Sgs1-Top3-Rmi1 complex in *S. cerevisiae* and *S. pombe*), which gives rise to non-crossover products only [133,134], or they can be cleaved asymmetrically by MUS81-EME1, a heterodimeric 5'- flap endonuclease, (Mus81-Mms4 in *S. cerevisiae*, and Mus81-Eme1 in *S. pombe*), which produces either crossover or non-crossovers (Figure 6) [135-138].

When the migrating D-loop does not capture the second DSB end, SDSA may occur and the invading strand is displaced and anneals with the second resected DSB end (Figure 7) (reviewed in [139]). Dissociation of the D-loop is promoted by the branch-migration activity of Rad54 [131,140]. Some DSBs that arise at telomeres or at broken replication forks are single-ended, and these are repaired through the single-ended invasion process called break-induced replication (BIR) to copy the entire information

from the donor chromosome by DNA synthesis, skipping the involvement of the second end of the DSB (Figure 8) [36,37,141-145].

### 2.3 Choice of DSB repair pathway

How do cells determine either NHEJ or HR will be used to repair DSBs? HR is operative only in the S/G2 phases of the cell cycle when a sister chromatid is available. NHEJ can function in all phases of the cell cycle and is the predominant repair pathway in somatic mammalian cells (reviewed in [30]). The choice between different DSBs repair pathways is tightly regulated, and DNA-end resection represents a primary regulatory step towards HR. The resection machinery is a downstream substrate of the checkpoint kinase, ATM. A component of the MRN complex, NBS1, is required for the recruitment [146] and activation [147] of ATM. Subsequently, ATM phosphorylates CtIP in response to DNA damage, and these phosphorylations are essential for the resection activity [63]. In *S. cerevisiae*, the ATM ortholog Tel1 phosphorylates Sae2 [148]. Resection is needed for all HR pathways, and resected DNA decreases NHEJ efficiency, as a result of poor binding of the NHEJ factor Ku to ssDNA [149]. In the absence of Ku, DNA-end resection processes faster, and overexpression of Ku reduces the DNA-end resection [150,151]. DNA resection takes place only when cyclin-dependent kinases (CDKs) are active (thus in S/G2 phases) [152-155]. *S. cerevisiae* Rad9 (note that this protein is not the ortholog of *S. pombe* or mammalian Rad9, which is a component of the 9-1-1 complex; see below) and Sae2 have been implicated in the CDK-dependent regulation of DNA resection in *S. cerevisiae* [156]. Rad9 is a large chromatin-binding protein, and could pose as a physical obstacle for processive DNA resection [156]. Sae2 is directly phosphorylated by CDK, and impairment of this phosphorylation leads to a reduction in DNA-end resection, a delay of HR, and an increase in NHEJ [153]. The putative mammalian ortholog of *S. cerevisiae* Rad9, 53BP1, also undergoes multiple CDK-dependent phosphorylations [157,158]. Phosphorylation of the mammalian Sae2 ortholog, CtIP, controls DNA-end resection in a manner similar to its yeast ortholog, indicating that this mechanism may be conserved [63-65,73,153]. CDK-dependent phosphorylation of CtIP promotes its interaction with BRCA1 in S/G2 [159], which is essential for CtIP recruitment to DSB sites and CtIP-mediated DNA-end resection [64,73,159]. In addition, CtIP protein levels are minimal in G1 and increase in S/G2 phases [73]. *Brca1* deficiency prevents normal HR, leading to aberrant chromatid fusions mediated by NHEJ [160], while deletion of *53BP1* rescues Rad51-dependent HR to WT levels in *Brca1*-deficient cells, indicating that 53BP1 interferes with HR by blocking the broken DNA-ends resection [160]. In cells lacking both BRCA1 and 53BP1, genomic stability is rescued because the HR pathway is largely restored [160]. In contrast, BRCA1-deficient repair is not restored by deletion of a NHEJ factor, DNA ligase 4. Mechanistically, 53BP1 could block DNA-end resection either directly by binding to di-methylation of histone H4 at lysine residue 9 (H4K9me2) in the vicinity of the DSB or by acting as an adaptor that mediates the recruitment of additional factors, which in turn would prevent nuclease access (reviewed in [161]). BRCA1 might play a role in the removal of 53BP1 from replication-associated breaks

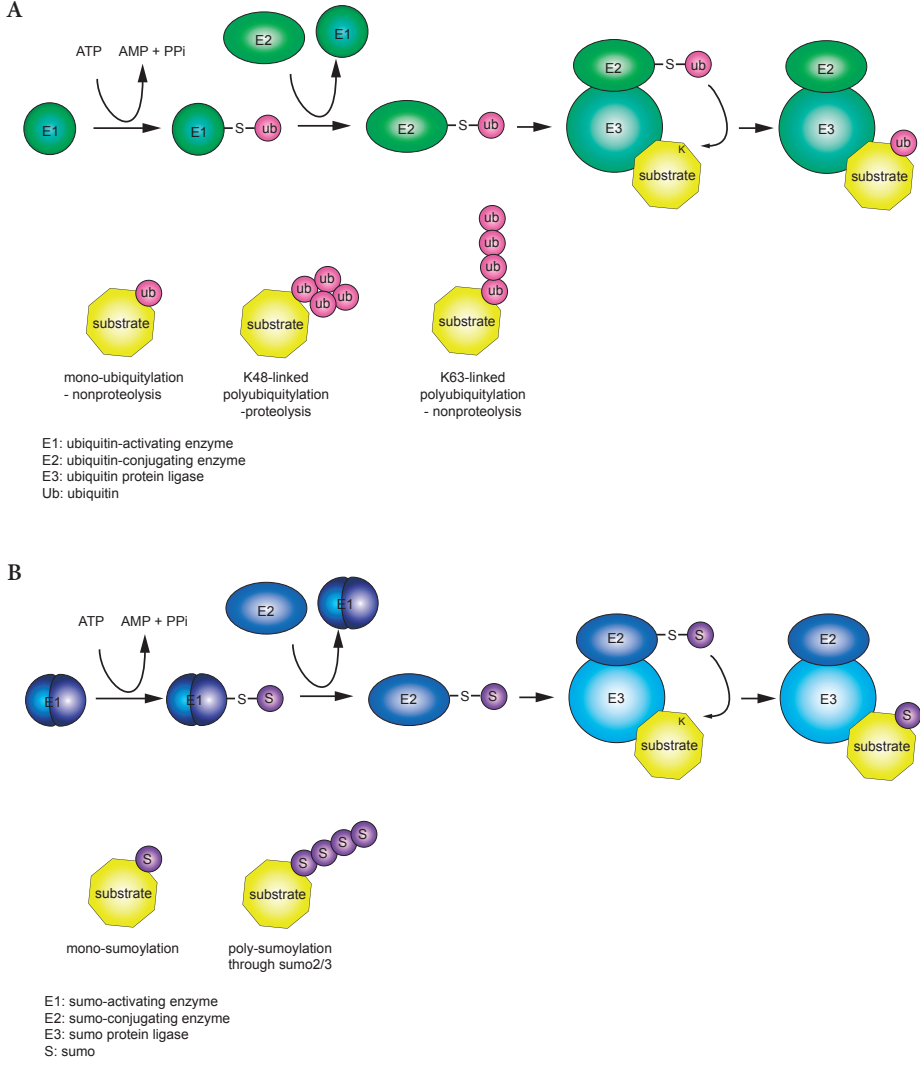


**Figure 10. Ubiquitylation and SUMOylation.** (A) Ubiquitylation pathway. E1 activates ubiquitin through ATP, and forms a thioester linkage with the C-terminal of ubiquitin at glycine 76 (G76). Subsequently, the E1 is replaced by an E2 and generates thioester bonds with ubiquitin at G76. This E2-S-ubiquitin complex binds to an E3-substrate complex, and the activated ubiquitin is transferred from E2 to a lysine residue of a target substrate. The transferred ubiquitin attaches on a substrate through an isopeptide linkage. E3s modify protein substrates by either monoubiquitylation or sequential attachment of ubiquitin molecules to form polyubiquitin chains. All seven lysine residues of ubiquitin (Lys6, Lys11, Lys27, Lys29, Lys33, Lys48, Lys63) can form chain linkages *in vivo*. Lys48- and Lys63-linked chains are the best characterized and are probably the most common. The Lys63-linked chains function in signaling, and Lys48-linked chains target substrates to the proteasome for degradation [328]. (B) SUMOylation pathway. Similar to ubiquitylation pathway, SUMOylation occurs in an ATP-dependent manner and involves SUMO-activating enzyme (E1), SUMO-conjugating enzyme (E2) and SUMO ligase (E3). SUMO interacts with substrates through the C-terminal glycine of SUMO. SUMO-activating enzyme is a heterodimer. In contrast to the ubiquitylation pathway, the SUMOylation pathway also involves an E1 (heterodimer), a single E2 (UBC9), and several E3 ligases (approximately 10 E3 ligases). In yeast, only one SUMO is present, while mammalian cells contain three SUMO isoforms (SUMO1, SUMO2, and SUMO3). Only SUMO2 and 3 are able to form SUMO chains.

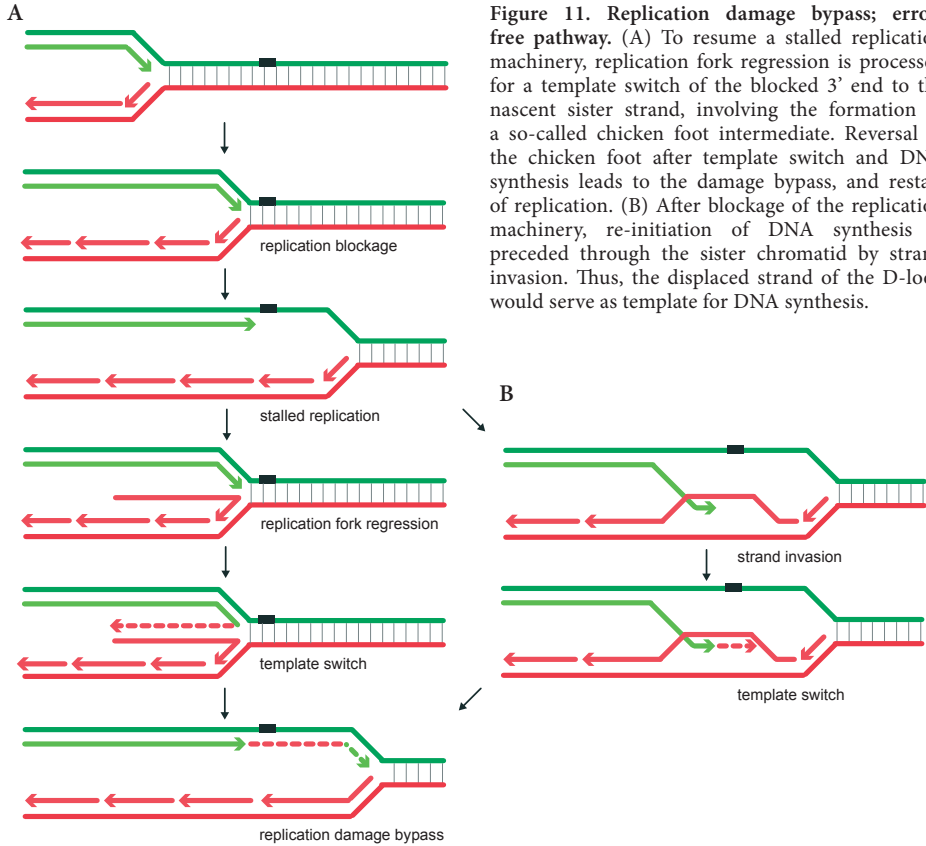


**Figure 11. Replication damage bypass; error-free pathway.** (A) To resume a stalled replication machinery, replication fork regression is processed for a template switch of the blocked 3' end to the nascent sister strand, involving the formation of a so-called chicken foot intermediate. Reversal of the chicken foot after template switch and DNA synthesis leads to the damage bypass, and restart of replication. (B) After blockage of the replication machinery, re-initiation of DNA synthesis is preceded through the sister chromatid by strand invasion. Thus, the displaced strand of the D-loop would serve as template for DNA synthesis.

to facilitate HR, suggesting that the balance between BRCA1 and 53BP1 activities regulates the choice between HR and NHEJ, probably via stimulation and inhibition of DNA-end resection, respectively.

### 3. DNA DAMAGE TOLERANCE

#### 3.1 PCNA ubiquitylation - replication damage bypass

During DNA replication, the presence of unrepaired DNA lesions may block progression of the replication machinery, which might result in DNA double-strand breaks and gross chromosomal rearrangements, or even to a permanent cell-cycle arrest and cell death. Replication damage bypass (RDB) is a special pathway that allows progression of DNA replication without actually removing the lesion (Figure 9A) (reviewed in [162]). Proliferating cell nuclear antigen (PCNA) plays a crucial role in the RDB pathway (Figure 9B). PCNA is a processive clamp for the replicative DNA polymerases and an essential binding platform for numerous proteins involved in DNA replication, repair, and cell cycle regulation. PCNA forms a homo-trimer that encircles

double-stranded DNA, and operates as a sliding clamp to keep the DNA polymerase machinery firmly on the DNA during DNA replication (reviewed in [163]).

The genes controlling RDB in *S. cerevisiae* are known as the Rad6 epistasis group. It has been shown that the RDB pathway is conserved from yeast to mammals (reviewed in [164]). Rad6 is an E2 ubiquitin-conjugating enzyme that is essential for this pathway [165]. Ubiquitin is a small protein that consists of 76 amino acids (approximately 7 kDa), and is highly conserved from yeast to human. The glycine residue of ubiquitin attaches covalently to lysine residues on a substrate protein. This process is called 'ubiquitylation'. Ubiquitylation is an essential cellular process operated by a multienzyme cascade of an ubiquitin-activating enzyme (E1), an ubiquitin-conjugating enzyme (E2), and an ubiquitin ligase (E3). Structurally distinct forms of ubiquitylated substrates, mono-, poly-, or multi-ubiquitylation, transmit various intracellular signals (reviewed in [166]). Poly-ubiquitylation through the lysine 48 residue (K48) of ubiquitin marks proteins for degradation by the 26S proteasome [167]. In contrast, mono-ubiquitylation, or poly-ubiquitylation chains through other lysines including K63 of ubiquitin, generate nonproteolytic signals, such as in endocytosis [168], in ribosome biogenesis [169], in DNA damage tolerance [170], and the DNA damage response pathway (Figure 10A, [171-173], reviewed in [162,166,174]).

In the RDB pathway, ubiquitylation of PCNA plays an important role, and several E2 and E3 enzymes are essential. Depending on the interactions with downstream components, error-free or error-prone sub-pathways can be activated. The first step in both pathways involves mono-ubiquitylation of PCNA at the conserved lysine residue 164 (K164) by the Rad6-Rad18 complex in yeast, in which Rad18 acts as an ubiquitin E3 ligase [175]. In mammalian cells, RAD18 complexes with the mammalian orthologs of yeast Rad6, HR6A (UBE2A) and HR6B (UBE2B) [176], and similar to the mechanism in yeast, the HR6A/B/RAD18 complex also regulates site-specific PCNA mono-ubiquitylation at K164 when the replication machinery is stalled by UV-induced DNA damage [177,178]. Mono-ubiquitylation of PCNA by the yeast Rad6-Rad18 complex recruits specific translesion synthesis (TLS) polymerases that can incorporate nucleotides in the strand opposite the site of the DNA lesions, and this process may usually be error-prone (Figure 9B, reviewed in [179,180]). In mammals, DNA polymerases which belong to the Y family (Pol $\eta$ , Pol $\iota$ , Pol $\kappa$ , and Rev1), and DNA polymerase  $\zeta$ , which is a member of the B family, promote replication through DNA lesions [181-189]. Yeast also has several Y family polymerases, although Pol $\iota$  and Pol $\kappa$  orthologs are missing (Reviewed in [164]).

The Y-family polymerases differ from replicative polymerases by their low fidelity, which is due to the lack of 3'-5' proofreading exonuclease activity [190,191], and by their ability to replicate through DNA lesions (reviewed in [192]). Pol $\zeta$  is strikingly different from other TLS polymerases since it functions as the proficient extender of primer termini opposite from DNA lesions [185]. Thus, replication through many DNA lesions requires the action of two different polymerases, one that carries out the nucleotide insertion reaction opposite the lesion site, and the other for the subsequent extension reaction (reviewed in [164]). All these Y-family polymerases have ubiquitin binding motifs, either as a so-called UBZ domain (Pol $\eta$  and Pol $\kappa$ ) or a UBM domain

(Polt and Rev1), and these appear to be required to bind to the mono-ubiquitylated form of PCNA [193].

Mono-ubiquitylation by the Rad6-Rad18 complex may be followed by Rad5-Mms2-Ubc13-mediated poly-ubiquitylation [175], and this activates an error-free sub-pathway of RDB. The E3 ubiquitin ligase Rad5 interacts with both the Rad6-Rad18 and the Mms2-Ubc13 complexes, to stimulate K63-linked poly-ubiquitylation of PCNA. Subsequently, polyubiquitylated PCNA enables template switching to the intact sister chromatid, and as a consequence, error-free damage bypass replication may occur (Figure 11) [194]. Two mammalian orthologs of yeast Rad5, named HLTf and SHPRH, mediate PCNA polyubiquitylation together with the mammalian MMS2-UBC13 complex in this conserved error-free pathway of RDB [195-198], although polyubiquitylated PCNA is barely detectable in mammalian cells [199].

### 3.2 PCNA SUMOylation

In *S. cerevisiae*, K164 of PCNA is known to be modified not only by ubiquitin but also by the small ubiquitin like modifier (SUMO) [175]. SUMO is evolutionary related to ubiquitin, but this modification does not target proteins for degradation. In contrast to yeast, which has only one SUMO, mammals have three SUMO variants. SUMOylation also occurs via a three-step enzymatic cascade, mechanistically similar to ubiquitylation, through a SUMO-activating enzyme (E1), a SUMO-conjugating enzyme (E2) and a SUMO ligase (E3) (Figure 10B). Both ubiquitin and SUMO can target lysine residues on a substrate (reviewed in [162,200]).

PCNA sumoylation is mediated by the SUMO ligase Siz1 and causes recruitment of the helicase Srs2 to replication forks during S phase. Srs2 then prevents unscheduled crossover events through its ability to disrupt Rad51 nucleoprotein filaments in *S. cerevisiae* [124,125,201-203]. Since HR at stalled replication forks can lead to genomic rearrangements, SUMOylation of PCNA may be used to keep this mechanism under tight control. Srs2 was originally identified as a suppressor of *rad6* and *rad18* mutants, and has been proposed to be a regulator of the Rad6-dependent pathways [165]. Branzei et al. recently reported that SUMOylation of PCNA by Siz1 regulates the Rad18-Rad5 mediated error-free pathway (Figure 11) [204]. They show that when PCNA SUMOylation is functional, error-free RDB can occur through formation of a sister chromatid junction (SCJ) at damaged replication forks, and this pathway then requires Rad18-Rad5-Mms2-Ubc13-mediated PCNA polyubiquitylation, and Rad51. Rad18 and Rad51 work together to promote replication bypass of the lesion by using the information of the newly synthesized chromatid. In this pathway, PCNA SUMOylation suppresses the formation of SCJs by homologous recombination alone, independent of Rad18. This may be mediated by the filament-disruptive activity of Srs2, and indicates that homologous recombination may be toxic in the absence of a functional Rad18 pathway [204]. This finding provides mechanistic details, which may help to explain how *Rad18* knockout leads to increased mitotic recombination and sister chromatid exchanges in mouse embryonic stem cells [205].

Sequence homologs of *SRS2* are not apparent in the genomes of higher eukaryotes. Therefore, it has been proposed that other helicases act in combination to substitute

for Srs2 in order to negatively regulate HR and ensure genome stability. The function of the Srs2-related DNA helicase FBH1 overlaps with Srs2 in its capability to displace RAD51 filaments to suppress HR in human cells [206,207], although this enzyme is not conserved in budding yeast, *C. elegans*, or *Drosophila*. FBH1 orthologs are found in mouse, chicken, and fission yeast [208,209]. In addition, the RecQ family helicases BLM and RECQL5 are able to disrupt RAD51 filaments *in vitro* and inhibit the initiation of HR [210-216]. Recently, another functional ortholog of Srs2, RTEL1 has been found in human and *C. elegans*, and it functions as an antagonist of HR by disrupting D-loop recombination intermediates [217]. Taken together, there appear to be several candidate proteins that could inhibit HR during S phase in mammalian cells in a manner analogous to Srs2 in yeast. However, it is not at all certain that this mechanism is completely conserved, since SUMOylated forms of PCNA have not yet been detected in mammalian cells.

#### 4. DNA DAMAGE RESPONSE AND CELL CYCLE CHECKPOINT ACTIVATION

Various cell cycle checkpoints ensure that repair of DNA lesions is completed before cell cycle progression resumes. Checkpoint signaling is activated in response to incomplete DNA replication due to stalled replication forks, and by damaged DNA induced by both internal and external sources such as UV light, ionizing radiation, reactive oxygen species, or other DNA-damaging agents. If repair mechanisms fail in repair the genotoxic damage, additional signaling pathways are activated, which leads to cell death via apoptosis [218-220]. The DNA damage response is a signal transduction pathway that coordinates cell cycle transitions, DNA replication, DNA repair and apoptosis. Two related protein kinases, ATM (serine/threonine protein kinase ataxia telangiectasia mutated) and ATR (ataxia-telangiectasia and Rad3-related), are the critical upstream kinases that control the DNA damage-induced cell cycle checkpoint machinery [218,221]. Both ATM and ATR are members of the phosphatidylinositol 3-kinase-like kinase (PIKK) family. The DNA damage response pathway consists of three major groups of proteins that act together to translate the signal of damaged DNA into cell cycle arrest and DNA repair. These groups comprise a) sensor proteins that recognize damaged DNA directly or indirectly, b) transducer proteins that relay and amplify the damage signal, and c) effector proteins that control cell cycle progression, chromatin restructuring and DNA repair [221-224].

Sensor proteins are required to recognize DNA damage. In this paragraph, activation of the DNA damage response and cell cycle checkpoints in response to DSBs and lesions caused by replication stress will be discussed. The MRN complex is known to be a damage sensor for DSBs [146,147,225-227], and it recruits and activates the transducer kinase ATM [146]. The 9-1-1 complex, a PCNA-like, ring-shaped heterotrimer [228], and ATRIP are sensors for lesions caused by replication stress [228-230]. ATRIP is a protein that recruits and activates the transducer kinase ATR [9,231,232]. In general, the checkpoint response to DSBs, initiated by ATM, results in

activation of an effector kinase named CHK2 through phosphorylation at T68, whereas the checkpoint response to stalled replication forks, DNA crosslinks, and UV radiation damage, induced by ATR, activates another effector kinase named CHK1 through phosphorylation at S317 and S345 [218,233,234]. However, the functions of CHK1 and CHK2 in mammalian cells are most likely at least partially overlapping, which will be discussed below.

#### 4.1 IR-induced damage

A conserved region in the C terminus of the NBS1 subunit of the MRN sensor complex recruits activated ATM to sites of DNA damage, thus promoting the phosphorylation of ATM-targets and ensuing events of the DNA damage response [146]. ATM activation involves its autophosphorylation on Ser 1981, and the autophosphorylated ATM forms ionizing-radiation (IR)-induced foci [235-237]. NBS1-ATM interaction is required for the IR-induced intra-S and G2/M checkpoints [146].

Following IR exposure, the surrounding chromatin at DSBs undergoes various modifications. One of the first modifications is phosphorylation of the histone H2A variant H2AX by ATM, generating  $\gamma$ H2AX [238]. MDC1, a mediator protein, is immediately recruited to sites of DSBs, interacts directly with  $\gamma$ H2AX via its BRCT domains, and recruits more ATM to the damaged sites [239-241]. Mediators are substrates and regulators of the transducer and effector kinases, promoting their activation, regulating substrate access, and controlling their associations with damaged DNA. The constitutively phosphorylated N-terminus of MDC1 interacts with the FHA domain (forkhead-associated domain; a phosphopeptide-binding domain) of NBS1, and this interaction is essential for the accumulation and retention of the MRN complex at DSBs [242-246]. MDC1 is also phosphorylated by ATM, and this promotes the subsequent recruitment of an E3 ligase named RNF8 [171-173,247]. RNF8 interacts with  $\gamma$ H2AX through its FHA domain, and this leads to ubiquitylation of H2A (uH2A) and H2AX (uH2AX) at DSBs through its E3-ligase activity together with its E2 partner UBC13 [171-173,241]. RNF8 accumulation promotes the accumulation of multiple DSB-repair-associated proteins, including BRCA1 and 53BP1 [171-173,241,248]. The accumulation of BRCA1 and 53BP1 at damaged sites is also dependent on the E3 ligase RNF168 [248,249]. RNF168 interacts with uH2A and uH2AX in an RNF8-dependent manner, and promotes further histone ubiquitylation on damaged chromosomes [248,250]. Recruitment of BRCA1 to uH2A/uH2AX is dependent on its interaction partner RAP80 [251-253]. RAP80 contains two UIM (ubiquitin interaction motif) domains, and the ubiquitin-binding function of the UIM is critical to mediate BRCA1-RAP80 focus formation at sites of DNA damage [251-254]. 53BP1 can recognize H3K79 methylation and H4K20 methylation [255-258], but the methylation of these histones is not regulated by DNA damage [256,259]. The RCTD motif of 53BP1 at the C-terminus is essential for its recruitment to DNA damage, and it apparently interacts with DNA or some component of chromatin, but not with ubiquitylated H2A nor H2AX [260-263]. In addition to the ubiquitylation cascade which controls recruitment of 53BP1 and BRCA1 to DSBs mediated by RNF8/RNF168, a SUMOylation pathway is also involved in IR-induced DNA damage response pathways [264,265]. E3 SUMOylation enzymes,

PIAS1 and PIAS4, accumulate at sites of DSBs, which are required for the DSB-induced ubiquitylation mediated by RNF8 and RNF168. Moreover, PIAS4 is required to recruit 53BP1 to DSBs, and both PIAS1 and PIAS4 are required for BRCA1 recruitment to sites of DSBs [264].

53BP1 [266-268] and BRCA1 [269-271] are both substrates of ATM, and are crucial in regulation of cell cycle checkpoints and DSB repair. As described above (2.3), 53BP1 and BRCA1 play opposing roles in the regulation of the NHEJ and HR pathways at DSB repair sites. However, 53BP1 is also implicated in activation of the intra-S phase checkpoint [272], and the G2/M phase checkpoint [267,273-275]. Resection of DSBs, stimulated by BRCA1, activates the other checkpoint kinase, ATR [61,63,276], leading to CHK1 phosphorylation in response to IR [155]. Deletion of BRCA1 exon11 (*Brcal<sup>A11/A11</sup>*) causes embryonic lethality [277], but this can be rescued by loss of p53 [277], or deletion of ATM or Chk2 [278]. This indicates a role for BRCA1 in checkpoint activation, separate from its function in DNA repair.

As described above, ATM-mediated CtIP phosphorylation leads to DNA-end resection, which also triggers ATR activation [61,63,276], indicating that both ATM and ATR are required for CHK1 phosphorylation in response to IR [155]. ATR needs to associate with DNA lesions to efficiently phosphorylate its target proteins [221,279,280]. Effective RPA-coated ssDNA formation, ATR recruitment, and CHK1 phosphorylation following IR are restricted to the S/G2 phases [155], most likely because the HR pathway, involving strand resection, is efficiently repressed in G1. In contrast, ATM autophosphorylation and CHK2 phosphorylation in response to DSBs occurs with similar efficiency throughout the cell cycle [155].

#### 4.2 Damage at stalled replication forks

ATR signalling through CHK1 is critical for the regulation of DNA replication. ATR signalling slows DNA replication [281,282], suggesting that it regulates checkpoint activation during recombination at stalled and collapsed replication forks. ATR phosphorylates several proteins that regulate recombination, including BRCA1, WRN, and BLM [283-286]. RPA coats most forms of ssDNA in the cell, including the ssDNA formed during DNA replication and DNA repair [287]. RPA-coated ssDNA is important to localize ATR to sites of DNA repair [280]. ATR recognition of RPA-coated ssDNA depends on ATRIP (ATR-interacting protein) [229,230]. Although RPA-coated ssDNA may be sufficient to localize the ATR-ATRIP complex, it is not sufficient for ATR activation [288-290]. ATR signalling depends on co-localization of the ATR-ATRIP complex with the RAD9-RAD1-HUS1 complex (9-1-1 complex), a PCNA-like ring-shaped heterotrimer [228]. The 9-1-1 complex recognizes a DNA end that is adjacent to a stretch of RPA-coated ssDNA. Subsequently, the 9-1-1 complex brings an activator, TOPBP1 (topoisomerase II $\beta$  binding protein 1), to ATR [291-294]. At DSB repair sites, ATR activation also depends on TOPBP1. In this context, TOPBP1 is phosphorylated by ATM, and this stimulates its capacity to activate ATR [295]. Loss of ATR results in a more severe phenotype than loss of either HUS1 or RAD9 [296-299], suggesting that the 9-1-1 complex is not responsible for all functions of ATR, while we cannot exclude their functional redundancy between the complex. Recruitment of the 9-1-1-TOPBP1

and ATR-ATRIP complexes to sites of DNA damage at stalled replication forks occurs as two largely independent events [223,279,300-302]. This independent recruitment might be important to prevent inappropriate checkpoint activation. Claspin, an adaptor or mediator protein that is found at replication forks, also plays an important role in CHK1 activation, since it is crucial to bring ATR and CHK1 together [303,304]. In addition, Claspin binds to phosphorylated RAD17, a clamp loader of the 9-1-1 complex, and this interaction is essential for CHK1 phosphorylation [305].

### 4.3 Checkpoint effector kinases CHK1 and CHK2

Cell cycle arrest is imposed by the activation of two downstream effector kinases, CHK1 and CHK2 (reviewed in [234]). Activation of the effector kinase CHK1 requires its phosphorylation at S317 and S345 by ATR [306-308]. Once CHK1 is phosphorylated, it is released from chromatin to phosphorylate its substrates [309,310]. Key targets of CHK1 to control cell cycle transitions are the CDC25 phosphatases [311]. CDC25 is a positive regulator of cell cycle progression, and removes inhibitory phosphorylations from cyclin-dependent kinases (CDKs) during the normal cell cycle (reviewed in [311,312]). Dephosphorylation activates CDK, allowing the cell cycle to progress (G1/S checkpoint) and enter mitosis (G2/M checkpoint) [313]. Phosphorylation of CDC25 by CHK1 inactivates its phosphatase activity, leading to maintenance of CDK phosphorylation, and cell cycle arrest.

Another effector kinase, CHK2, is activated by ATM through phosphorylations on T68 and other residues in the N-terminal SCD domain, which leads to multimerization of CHK2 [314,315]. CHK2 plays an accessory role, exerting a partial influence on the intra-S and G2/M checkpoints [316], also through negative regulation of the CDC25s via phosphorylation [317-320]. CHK2 is also required for IR-induced apoptosis, and promotes p53-dependent transcriptional responses in many tissues [321,322]. The transcription factor p53 is a direct target of ATM and of the effector kinases in the regulation of apoptosis, but CHK2 and ATM also phosphorylate p53 regulators, leading to increased stability and activity of the p53 transcriptional activator [323-325].

## II. DNA REPAIR IN MEIOTIC CELLS

### DOUBLE STRAND BREAK REPAIR, SYNAPSIS, AND SILENCING IN MEIOSIS

*Epigenetics*, 2010 May 16, volume 5, issue 4, page 255-266

Akiko Inagaki<sup>1</sup>, Sam Schoenmakers<sup>1,2</sup>, and Willy M Baarends<sup>1\*</sup>

<sup>1</sup>Department of Reproduction and Development and <sup>2</sup>Department of Obstetrics and Gynaecology, Erasmus MC – University Medical Center, PO BOX 2040, 3000 CA, Rotterdam, the Netherlands

**Key words:** meiosis, DNA double-strand break repair, chromosome pairing, MSCI, sex chromosomes, MSUC,  $\gamma$ H2AX, histone modification

#### ABSTRACT

Chromosome pairing and synapsis during meiotic prophase requires the formation and repair of DNA double-strand breaks (DSBs) by the topoisomerase-like enzyme SPO11. Chromosomes, or chromosomal regions, that lack a pairing partner, such as the largely heterologous X and Y chromosomes, show delayed meiotic DSB repair and are transcriptionally silenced. Herein, we review meiosis-specific aspects of DSB repair in relation to homology recognition and meiotic silencing of heterologous regions. We propose that persistent meiotic DSBs play a role in inhibiting heterologous synapsis and stimulate meiotic silencing of the X and Y chromosomes.

## INTRODUCTION

Sexual reproduction requires the formation of specialized germ cells by meiosis. Meiosis consists of two rounds of cell division, preceded by a single phase of DNA replication. The first meiotic division (MI) is preceded by a special and prolonged prophase, during which homologous chromosomes align and pair. In many species, including yeast and mammals, homologous chromosome pairing requires formation and repair of meiosis-specific DNA double-strand breaks (DSBs). In somatic cells, DSBs may also arise due to exogenous and endogenous DNA damage. It is evident that correct repair of DSBs is essential for the maintenance of genome integrity. This is important for cells undergoing mitosis, but it is even more important for germ cells, because upon formation of the zygote, the combination of two parental germ cell genomes forms the basis for a new individual. Therefore, it appears counterintuitive for a cell to generate

DSBs on purpose upon entrance into meiosis. In yeast and mouse, the formation and repair of meiotic DSBs, leading to the formation of crossovers (exchange of chromatid arms between homologs) and noncrossovers, is directly required for proper pairing, synapsis and also for the segregation of homologous chromosomes during the first meiotic division. However, in some species, meiotic DSBs are absent in one sex (for example *D. melanogaster* males) or occur after completion of chromosome pairing (for example *C. elegans*). In this “point of view” we evaluate what is currently known about the differences in DSB repair in mammalian mitotic and meiotic cells. We relate this to the ongoing process of homologous chromosome pairing. Next, we discuss how meiotic DSB-repair may be linked to the transcriptional silencing of nonhomologous regions that occurs for example for the largely heterologous X and Y chromosome in the testis.

## HOMOLOGOUS CHROMOSOME PAIRING

Initiation of chromosome pairing occurs during leptotene, progresses during zygotene and is complete in pachytene nuclei. Synapsis is achieved by the formation of the synaptonemal complex (SC) between the chromosomal axes of the paired homologous chromosomes. The SC consists of lateral elements along the chromosomal axes of each homolog, and a central connecting element (Figure 1A). Chromatin loops protrude from the lateral elements. Prior to synapsis, the lateral elements are called axial elements. Formation of the central element is defined as the achievement of synapsis. During diplotene, the SC is gradually disassembled.

## THE ROLE OF THE BOUQUET CONFIGURATION AND MEIOTIC DSB REPAIR

In budding yeast, the designated initiation sites of synapsis appear to colocalize with designated crossover sites [329]. However, in mammals this may not be the case, since cytological observations have indicated that synapsis proceeds from the telomeric ends of the paired homologous chromosomes in humans [330]. Telomeres function during the initial phase of chromosome pairing in both yeast and mammals. During this phase, all telomeres cluster on the nuclear membrane, and the chromosomal arms loop towards the center of the nucleus, forming the transient bouquet stage. The formation of this configuration and the associated chromosomal movements are essential for correct chromosome pairing [331]. However, the formation and repair of meiotic DSBs is also essential to achieve synapsis, as evidenced by the severe chromosome pairing abnormalities that are observed in mice that lack the enzyme (SPO11) that induces the meiotic DSBs, and in mice that carry mutations in (meiotic) DSB-repair genes such as for example *Dmc1* and *Rad51C* (see below) [332-334].

### The role of components of the SC

The repair of meiotic DSBs in yeast, mouse, and man is accompanied by progression of synapsis. Synapsis critically depends on the central element and transverse filaments of

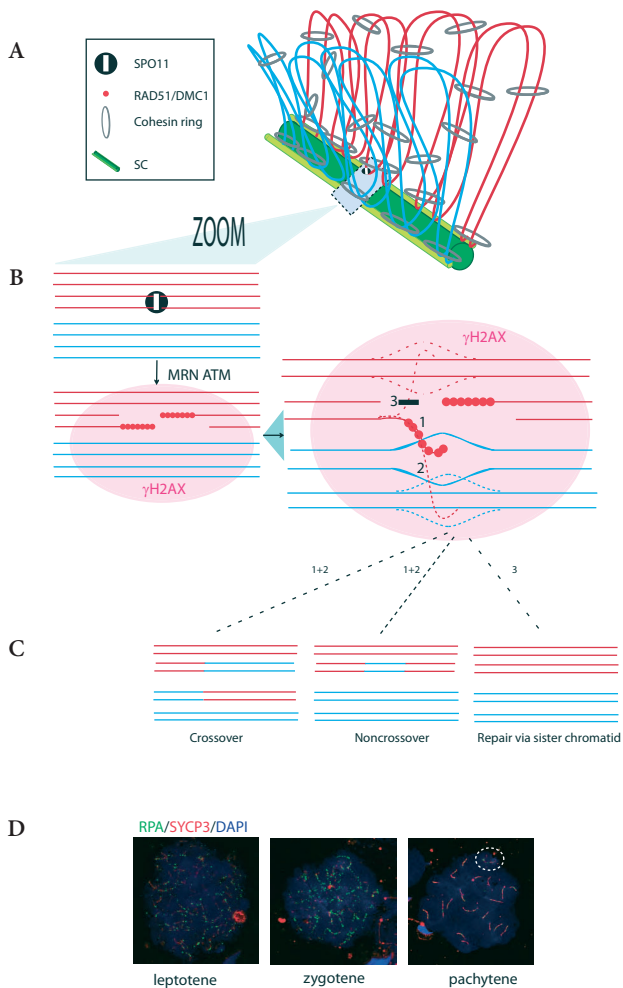


**Figure 1. Homologous chromosome pairing and meiotic DSB repair.** A) Schematic drawing of the synaptonemal complex and associated chromatin in pachytene. The SC consists of lateral elements (light green) that form along the bases of the protruding chromatin loops (red and blue). The homologs are connected via the transversal and central elements of the SC (dark green). Sister chromatids are connected via cohesin rings (grey). Cohesin is enriched at the bases of the chromatin loops. SPO11 and associated proteins mediate the formation of DSBs that are repaired in association with the SC. B) Schematic drawing of the initiation of meiotic DSB repair. Upon formation of a meiotic DSB, the site of the break is recognized by the MRN complex. This complex plays an essential role in the removal of SPO11, resection of the break, and the recruitment of the kinase ATM. This kinase phosphorylates histone H2AX in the chromatin surrounding the DSB. The long ssDNA tails that have been formed during resection are most likely bound by RPA, which is subsequently replaced by RAD51. This protein mediates the homology search. In theory, RAD51 filaments may invade homologous DNA on the sister chromatid, or on one of the two chromatids of the homologous chromosome. In meiosis, interactions with the sister chromatid are somehow repressed, and interaction with one of the chromatids of the homologous chromosome is stimulated. C) Possible outcomes of HR repair of meiotic DSBs. Upon strand invasion, different subpathways of homologous recombination repair using the homologous chromosome as a repair template (1 + 2) (see main text) can lead to the formation of crossovers or noncrossovers (gene conversions). If repair occurs using the sister chromatid as a template (3), the original DNA sequence is restored. D) Localization of RPA (green), SYCP3 (red) and DNA (blue DAPI staining) in spread leptotene, zygotene and pachytene mouse spermatocyte nuclei. Nuclei were spread and immunostained with the indicated antibodies as described in [405]. The anti RPA antibody is described in [366].

the SC. At present, SYCP1, SYCE1, SYCE2 and TEX12 are known components of this structure that connects the two lateral elements that have been formed along the axes of the homologous chromosomes (Figure 1A, reviewed in [335]). Knockout of each of these genes leads to very similar synaptic defects; the chromosomes align but fail to synapse, and meiotic DSB repair is stalled [336-339]. The axial/lateral elements, known to contain SYCP2 and SYCP3 and the meiosis-specific cohesin complex—which keeps the sisters chromatids tied together—are also important for correct homologous chromosome pairing and crossover formation [340-342]. For example, in male *Sycp3* knockout mice, many chromosomes remain asynapsed or show heterologous synapsis, and the spermatocytes become apoptotic around the developmental phase that corresponds to midpachytene in wild type, the stage at which all autosomal chromosomes should have achieved complete synapsis [340]. Many mutants that have pairing and DSB repair abnormalities, show asynapsis at pachytene, resulting in apoptosis around this stage. This is most likely due to the existence of a midpachytene checkpoint linked to the synaptic stage of the chromosomes [343].

In contrast, in *Sycp3*<sup>-/-</sup> females, meiosis is not fully blocked. Many oocytes are lost during the first week of postnatal follicle development, and the ones that survive cause a high frequency of (maternal origin) aneuploidy in embryos following ovulation and fertilization [344]. This sex-difference in severity of the meiotic phenotype of this mutant is illustrative for many genes involved in meiosis [345], and this is thought to be due at least in part to differential regulation of checkpoints [346].

## INDUCTION AND REPAIR OF MEIOTIC DSBs

Meiotic DSBs are induced by the topoisomerase II-like enzyme SPO11. The gene encoding this enzyme is conserved from yeast to worm, flies, and mammals. In yeast and mammals, SPO11 is loaded on the chromatin during the final premeiotic S phase, and disturbance of DNA replication affects meiotic DSB formation in yeast [347]. The DSBs are formed after the final S phase and depend on several accessory factors that may help to localize and activate SPO11 (reviewed in [348]). Meiotic DSBs are not distributed at random in the genome but concentrate in so-called hotspots. Recent evidence indicates that histone modifications such as H3K4 trimethylation are involved in creating the chromatin environment that forms a hotspot [349]. SPO11 functions as a dimer, and one molecule remains covalently attached to each DSB end upon generation of the break (reviewed in [348]). Subsequently, an endonuclease reaction releases a SPO11-coupled oligonucleotide. The MRN complex plays an important role in this reaction. This complex is known to be involved in early steps of DSB repair in somatic cells, and consists of MRE11, RAD50 and a third, less conserved subunit named NBS1 in mammals. MRE11 contains a nuclease domain, but another nuclease that is activated by MRE11, named CtIP, most likely performs the cleavage reaction. End-resection then leads to the formation of long 3' single strand DNA (ssDNA) tails on each end of the break [350-353].

### **Recognition of meiotic DSBs and formation of the RAD51/DMC1 protein filament**

In order for breaks to be repaired, they need to be recognized first. The above mentioned MRN complex is most likely involved in sensing the presence of a DSB, both in mitotic and meiotic cells (reviewed in [58]). When the MRN complex binds a DSB, it immediately recruits a special kinase named ATM, that is essential for activation of DNA repair checkpoints. ATM phosphorylates H2AX at serine 139, forming  $\gamma$ H2AX [354] (Figure 1B). In addition, ATM phosphorylates downstream components of the checkpoint pathway, and the MRN complex itself [355,356]. In mitotic cells, these recognized DSBs may be repaired either through the non-homologous end-joining pathway (NHEJ) or via homologous recombination (HR). In meiotic cells, the inaccurate NHEJ process is repressed [357], leaving HR as the only available pathway for repair. HR may lead to the formation of crossovers, and these are instrumental during the first meiotic metaphase, when sister chromatid cohesion and crossovers keep the homologs attached until loss of sister chromatid cohesion along chromosome arms allows separation of the chromosomes. In mouse and man only a small minority of the DSBs lead to the formation of crossovers, but each chromosome pair has at least one (obligate) crossover. Repair of most meiotic DSBs leads to so-called gene conversions or noncrossovers (Figure 1C).

During HR in mitotic cells, the processed 3' ssDNA ends are first loaded by the ssDNA-binding heterotrimeric protein RPA. RPA is then replaced by RAD51, with the aid of mediators such as RAD52 and the breast cancer related protein 2 (BRCA2) [358]. RAD51 forms a protein filament on the DNA that is required for the homology search. In meiotic cells, RPA foci have been reported to appear as the chromosomes synapse, in zygotene some time after the formation of RAD51 foci in leptotene [359,360]. Also in oocytes, RAD51 foci formation precedes the appearance of visible RPA foci [361]. Thus, RAD51 and RPA seem to accumulate in reversed order on meiotic DSBs, as compared to DSBs in somatic cells. However, it has been suggested that RPA may be present on processed meiotic DSBs before RAD51 accumulates, but only transiently, and therefore not detected by immunocytology [362,363]. In accordance with this suggestion, mouse mutants with impaired loading of RAD51 and its meiosis-specific paralogue DMC1, display RPA foci in high abundance on leptotene and zygotene spermatocytes [332,364,365]. Our own observations, using a RPA antibody that is directed against the two largest subunits of human RPA [366], indicate that RPA foci appear concomitant with RAD51 in mouse spermatocytes (Figure 1D). Partial colocalization of RPA and RAD51/DMC1 on meiotic DSB repair sites during pachytene indicates that RPA may perform an additional function at this later stage. Perhaps RPA and RAD51 filament formation dynamically switches on ssDNA depending on the types of recombination intermediates that are formed. RAD51 and its meiosis-specific paralogue DMC1 appear to colocalize at meiotic DSBs in mouse spermatocytes, and their loading does not require RAD52, but in the absence of BRCA2, the loading of RAD51/DMC1 was severely reduced [364]. BRCA1 performs a similar function in RAD51/DMC1 loading [367], and the RAD51 paralogue RAD51C, and a novel testis-specific protein named TEX15, are also required for this process [332,365,368]. The number of RAD51 foci that can be observed in leptotene nuclei has been used to estimate the number of meiotic DSBs to be around 250-300 [369].

## Interhomolog bias

Upon formation of the RAD51/DMC1 filament, the coated ssDNA will initiate a search for homology. In mitotic cells, the sister chromatid is the preferred template for repair. However, in meiotic cells, repair via the sister chromatid is somehow repressed, and invasion of one of the chromatids of the homologous chromosome is stimulated. A meiosis-specific kinase named Mek1 that localizes to the chromosomal axes in yeast, plays a crucial role in mediating this so-called interhomolog bias [370]. Recent data indicate that Mek1 achieves this function at least in part via phosphorylation of the DNA repair protein Rad54 [371]. This protein interacts with Rad51 and is important for strand invasion and homologous recombination repair in mitotic cells. Phosphorylation of Rad54 by Mek1 inhibits the interaction of Rad54 with Rad51, and this may help to direct repair to the homolog [371]. Another meiosis-specific protein, Hed1, also binds to Rad51 and inhibits its interaction with Rad54 [372]. Activation of the Mek1 kinase requires the function of two components of the axial/lateral elements of the SC; Hop1 and Red1 [370,373]. In budding yeast, a meiosis-specific Rad54 homolog, named Rdh54 acts together with Dmc1 to stimulate the use of the homologous chromosome as a template for repair [374], and this process is aided by the meiosis-specific Hop2/Mnd1 complex [375]. DMC1 and HOP2 homologs have also been identified in mouse [376,377], and both are required for repair of meiotic DSBs and homologous chromosome pairing, indicating that the functions of these proteins may be conserved from yeast to mouse [334,377]. In mouse, two RAD54 homologs have been identified [378], but although these proteins are required for homologous recombination in somatic cells, neither one is required for the formation of crossovers [119,379]. This indicates that DSB repair proceeds normally. Still, in mice deficient for these RAD54 homologs, a few RAD51 foci persist, and RAD51 forms large aggregates in pachytene and diplotene nuclei. This indicates that RAD54 may play a minor role in meiotic recombination in mouse, or perhaps it is only involved in repair of a small subset of the breaks that follow a distinct repair pathway. Taking the yeast data into account, that indicate that repression of RAD54-RAD51 interaction stimulates the interhomolog bias, it is tempting to speculate that RAD54 may function at the minority of sites that still use the sister-chromatid as a template for repair.

## Formation of crossovers and noncrossovers

Upon strand invasion of one of the two sister chromatids of the homologous chromosome, a brief phase of DNA synthesis along the intact template follows. Subsequently, the invaded strand may be released, and re-anneal to the other ssDNA end of the DSB. Repair along this pathway, called synthesis-dependent strand annealing (SDSA), leads to gene conversion events, whereby only a relatively short stretch of DNA (approximately 200 bp-2Kb) is exchanged between homologs [380]. Alternatively, the second end of the DSB may be captured, and a double-holliday junction may be formed. Such a double-holliday junction may be resolved by specific enzymes in two ways, leading to either crossovers or noncrossovers (gene conversions) (reviewed in [381]) (Figure 1B, C). Most meiotic DSBs are thought to be repaired via the SDSA pathway, leaving only a small subset —approximately

5-10% — that will be repaired via the formation double-holliday junctions, and these may mostly generate crossovers.

Many proteins known to be involved in DSB-repair in somatic cells are required for the repair of meiotic DSBs, but the major pathway of crossover formation has a special requirement for proteins involved in DNA mismatch repair. In somatic cells, this pathway removes mismatched nucleotides that may be formed during DNA replication. In meiotic DSB repair, mismatches will occur when the repair template of the homologous chromosome is not identical to the damaged strand of the other chromosome. In *Mlh1* mutants, chromosome pairing occurs normally, indicating that the DSBs that are converted to noncrossovers are normally repaired, but crossovers hardly form, and the spermatocytes undergo apoptosis during metaphase, because all chromosomes are univalent. In mice, a small number of crossovers may be formed by a different pathway that does not require the meiosis-specific mismatch repair proteins [382]. In this pathway, the endonuclease MUS81 cleaves a combination intermediate that is most likely formed just prior to double holliday junction formation, and this cleavage exclusively yields crossovers.

The number and distribution of crossovers is tightly regulated. A special mechanism ensures that each chromosome pair contains at least one crossover, and crossover interference reduces the likelihood of two crossovers occurring in close proximity to each other. The total number of crossovers varies somewhat between different mouse strains and between males and females. Kleckner et al. [383] reported that the number of crossover sites correlates to the length of the SC. This indicates that there is a complex functional interplay between the formation and processing of meiotic DSBs and the structure of the chromosomes. It is not clear what the molecular basis is of crossover interference in mammals. De Boer et al. [384] have shown that two levels of interference exist in mouse spermatocytes. A first level is observed in so-called early recombination foci in late zygotene/early pachytene, most of these will be processed as noncrossovers, and a second level is clear among crossovers marked by MLH1 in mid-to-late pachytene [384]. The crossover pathway that is mediated by MUS81 appears to lack interference [382]. Recently, the ATM kinase that is required for  $\gamma$ H2AX formation upon induction of the meiotic DSBs, was found to play a role in the regulation of crossover numbers and interference [385]. Interestingly, ATM deficiency had both crossover stimulating and inhibiting effects; the formation of the obligate crossover between X and Y was reduced, whereas the total number of MLH1 foci was 13% increased. In addition, crossover interference was mildly affected. These effects were associated with defects in chromosomal axis structure, providing further proof that meiotic recombination and axial chromosome structure are intimately related [385]. ATM activation requires the function of the MRN complex, and hypomorphic mutations in components of this complex also resulted in an increased crossover frequency, although the effect was smaller (8% increase) [386]. These data indicate that ATM may perform multiple functions in meiotic DSB processing, and in propagation of the interference signal. Alternatively, or in addition, a compensating increase in the activity of the related kinase ATR on the ATM null background may regulate types and frequencies of crossover events through phosphorylation of RPA, as has been shown in yeast [387].

The most outspoken change in crossover frequency is observed in mice that are deficient for the ubiquitin conjugating enzyme HR6B [388]. HR6B, and the closely related enzyme HR6A, are involved in mediating post replication repair. This pathway allows replication to proceed in the presence of DNA damage. In addition, HR6B is required for ubiquitylation of H2B [389,390] and most likely ubiquitylates many other substrates. *Hr6b* knockout male mice are infertile, associated with dysregulation of chromatin structure in meiotic and post-meiotic cells [388,391,392]. In late pachytene nuclei of these cells, the SCs are longer, and the number of MLH1 foci is 20% increased in comparison to controls [388], but crossover interference is not affected [393]. It might be suggested that *Hr6b* knockout spermatocytes contain more spontaneous DSB sites that contribute to the increased crossover rates. However, irradiation does not lead to a further increase in the number of MLH1 foci in *Hr6b* knockouts [388], implying that a reduced capacity to repair damage-induced breaks is not involved in mediating the increased crossover frequency. In yeast, mutation of the homolog of HR6B, Rad6, also affects the number of crossover sites, leading to increased as well as decreased frequencies of crossover formation depending on the chromosomal region [394]. This effect is most likely caused by a decrease in the ubiquitylation of H2B, which subsequently leads to a decrease in the level of H3K4 trimethylation, a chromatin mark that has been shown to be associated with hotspot formation [349]. In *Hr6b* knockout spermatocytes, the overall levels of H2B ubiquitylation and H3K4 trimethylation are not changed [392]. However, the regulation of several other histone modifications is disturbed [392], indicating that changes in chromosome structure may be involved in mediating the enhanced recombination frequency in *Hr6b* knockout spermatocytes. Recent data have shown that in, *C. elegans*, a species in which pairing precedes recombination, chromatin condensing complexes regulate meiotic DSB distribution, directly implicating higher order chromosome structure in the regulation of meiotic DSB formation and repair [395].

## DETECTION AND SILENCING OF NONHOMOLOGOUS REGIONS

### Homologous versus heterologous synapsis

In order to ensure that complete genome sets are separated during the metaphase-to-anaphase I transition, pairing between nonhomologous chromosomes needs to be prevented. In the worm *C. elegans*, chromosome movement, and attachment of so-called pairing centers to the nuclear envelope, play important roles in verifying homology before synapsis proceeds [396,397]. In mouse, disruption of telomere attachment during meiotic prophase through targeted disruption of the *Sun1* gene also interferes with chromosome synapsis and meiotic DSB repair, but nonhomologous synapsis is still prevented [331]. In contrast to mammals, worms synapse homologous chromosomes before meiotic recombination is initiated, and therefore basic aspects of homology recognition may differ between worms and mammals [398].

In the absence of meiotic DSBs, in *Spo11* knockout mice, nonhomologous synapsis is observed, in addition to asynapsis [399,400]. Thus, ongoing meiotic DSB repair, or repair-associated signaling, may inhibit nonhomologous synapsis. Still, when

DSB repair is stalled in certain mutant mouse models, nonhomologous synapsis also occurs, indicating that these incompletely repaired DSBs cannot completely prevent heterologous synapsis [334,401-403].

The X and Y chromosome are largely heterologous, and during midpachytene in mouse, synapsis is observed only along the short homologous pseudoautosomal regions, the rest of the chromosomal arms remains unsynapsed. Interestingly, during early pachytene, XY synapsis appears to include nonhomologous regions, since the Y has been observed to synapse with X along almost 90% of its length at this stage [404]. Apparently, this is a transient state, and this observation indicates that progression of synapsis may be dynamic, allowing desynapsis when an unknown control mechanism detects absence of homology. For the XY pair, this mechanism appears to be efficient, since persistent heterologous synapsis between X and Y is not observed. Variable heterologous synapsis is detected when specific translocations cause a pairing problem. For example, in mice carrying two similar but not identical translocations between chromosome 1 and chromosome 13, a heterologous region of approximately 40 Mb is present on both the small 1<sup>13</sup> bivalent and the large 13<sup>1</sup> bivalent. The small translocation bivalent shows complete synapsis in only 40% of the nuclei, whereas the larger bivalent is completely synapsed in more than 95% of the nuclei [405,406]. Such heterologous synapsis is thought to occur via synaptic adjustment, which most likely involves adjustment of chromatin loop length to obtain equalization of chromosomal axes between heterologous regions with a difference in length.

### **Meiotic sex chromosome inactivation**

Already in 1965, Monesi described that the X and Y chromosome show reduced incorporation of tritiated uridine, compared to autosomes in pachytene spermatocytes [407]. This provided the first indications for the meiotic inactivation of the sex chromosomes (MSCI). In addition, it was noted that the X and Y form a more or less separate “body” in the periphery of the nucleus, named sex body or XY body. This transcriptionally silenced chromatin is marked by several histone modifications and associated proteins [392,408-410]. The most well known histone modification that marks the XY body from late zygotene onwards is  $\gamma$ H2AX, the general marker of DSBs [411]. In mice that lack H2AX, the XY body is not formed [412]. Two other modifications that mark the XY body are generally associated with transcriptional silencing but also detected at sites of DSB repair. These are H2AK119 ubiquitylation and sumoylation of chromatin components [413,414]. H2AK119 ubiquitylation is a relatively late (taking approximately 10-20 minutes before maximal levels are achieved) marker of DSB repair in mitotic cells [171,173]. H2A is ubiquitylated by the E3 ligases RNF8 and RNF168 [171,173,250]. RNF8 recruitment depends on MDC1 [171-173], and precedes RNF168 that is recruited by the ubiquitylated H2A generated by RNF8 [250]. SUMOylation of H2A.Z is associated with the presence of persistent DSBs in yeast [415]. Surprisingly, both these modifications do not mark the meiotic DSBs in leptotene and zygotene nuclei.

The chromatin of the XY body is completely reorganized around midpachytene, when all nucleosomes are replaced, as visualized by the complete disappearance of

the replication associated H3.1 variant [410]. Hereafter, during mid-to-late pachytene and diplotene, XY body chromatin accumulates methylated H3K9, which persists and remains present in spermatids [410]. During postmeiotic spermatid development, the X and Y appear to remain globally repressed although a selected set of single- and multi-copy genes is (re) expressed [409,416-418]. Recently, Cocquet et al. [419] showed that the multicopy gene *Sly* is specifically required for the maintenance of postmeiotic X chromosome repression. In addition to SLY, the above-mentioned ubiquitin conjugating enzyme HR6B is also required for the maintenance of meiotic and postmeiotic sex chromosome inactivation [392].

### **Link between asynapsis and persistence of DSB repair proteins**

Chromosomes or chromosomal regions without a pairing partner can only repair their meiotic DSBs (in these regions) through recombination with the sister chromatid or via NHEJ. Since both these pathways appear to be repressed during early meiotic prophase, meiotic DSBs in such regions may remain unrepaired. Indeed, persistent RAD51 foci are observed along the unsynapsed arm of the X chromosome in spermatocytes [369]. Surprisingly, these are only rarely observed along the unsynapsed part of the Y, suggesting that SPO11 generates only a few breaks in this region of the Y. RNA-FISH analyses have provided indications that the Y chromosome is already largely inactive in mouse spermatogonia, and a heterochromatic chromatin structure encompassing most of the Y chromosome may interfere with access of SPO11 to the DNA [418].

The initial formation of RAD51 foci on all chromatin is accompanied by ATM induced phosphorylation of H2AX on surrounding chromatin [420]. However, ATM appears to be gradually replaced by ATR [420]. At DSB sites in somatic cells, ATM recruits ATR to these sites via phosphorylation of the ATR activator TOPBP1 (reviewed in [233]). ATR is partially redundant to ATM in somatic cells, although distinct functions have also been described, for example in activation of the downstream kinases CHK1, and CHK2, respectively (reviewed in [233]). In general, ATM appears to be rapidly recruited to DSB sites, followed by later accumulation of ATR. Conversely, ATR is primarily recruited to stalled replication forks, although ATM may also perform functions at these sites (reviewed in [233]). In meiotic cells, ATR is first observed on a subset of the RAD51 foci in zygotene nuclei [359,421]. Eventually, ATR concentrates along the chromosomal axes of the X and Y chromosome, concomitant with a second wave of  $\gamma$ H2AX formation, selectively on X and Y chromatin, initiating MSC1. This histone modification accumulates on X- and Y-chromosomal chromatin from late zygotene until late diplotene. In addition to RAD51/DMC1, ATR and  $\gamma$ H2AX, several other checkpoint and DSB-related proteins are known to accumulate specifically on the XY body. These include BRCA1, BRCA2, BLM, MDC1, TOPBP1, 53BP1, and RAD1 [422-428]. The above-mentioned post replication repair enzyme HR6B and its E3 ligase partner RAD18 also accumulate on the XY body [429]. All of these proteins, except BLM, 53BP1, and the RAD18/HR6A/B complex, also accumulate on the meiotic DSBs shortly after their formation in leptotene. Apparently, BLM, 53BP1, and the RAD18/HR6A/B are recruited to DSBs in somatic cells, but not to meiotic DSBs in leptotene and zygotene nuclei. Only when these breaks persist until pachytene, like

on the XY body, these proteins are detected. For 53BP1 this apparently differential behaviour towards SPO11 and damage-induced DSBs may simply be due to absence of this protein in leptotene and zygotene spermatocytes; irradiation-induced DSBs in these cells also do not recruit 53BP1 [428]. For RAD18, the situation is different, since this protein does accumulate on irradiation-induced DSBs in leptotene and zygotene nuclei (unpublished). For the BLM helicase, the situation is enigmatic. At DSBs in somatic cells, this protein accumulates within 10 seconds upon formation of the break, independent of ATM and NBS1 [430]. Mutation of the *Blm* gene is embryonic lethal [431], precluding direct analyses of the function of this gene in meiotic recombination. Taking these data together, it appears that the stalled repair of meiotic DSBs on the unsynapsed arms of X (and Y) results in the accumulation of DSB-repair related proteins that do not respond to the meiotic DSBs that are rapidly repaired. This may be either because they are not expressed before these breaks are repaired (53BP1), or because their recruitment to meiotic DSBs is somehow prevented (RAD18, BLM, H2AK119ub1, SUMOylation). This could occur as part of the pathway that prevents recombination with the sister chromatid. Alternatively, or in addition, some of these proteins may accumulate slowly, and reach detectable levels only when repair is stalled, allowing more time to increase the local concentration.

When meiotic DSB-repair is blocked, due to a genetic defect, MSCI usually cannot occur and appears to be inhibited [333,334,336,337,364,365,377,432]. From these observations, it is clear that the DSB-repair pathway and MSCI/MSUC share limiting components. When meiotic DSBs are not formed at all, in the *Spo11* knockout, a so-called pseudo sex body is formed on part of the unsynapsed chromatin in the zygotene-like nuclei [420]. This structure accumulates  $\gamma$ H2AX, and is transcriptionally silenced [433]. These observations show that meiotic DSBs are not absolutely required for the formation of a XY body-like structure during meiotic prophase. However, since the pseudo-XY body forms on only part of the asynapsed chromatin, it also shows that asynapsis by itself is not enough to recruit ATR and trigger  $\gamma$ H2AX formation.

Turner et al. [434] have previously shown that ATR and  $\gamma$ H2AX do not accumulate on XY chromatin in mice that carry a hypomorphic mutation in the *Brca1* gene. In addition, homologous chromosome pairing was severely affected [434]. In a small subfraction of the nuclei in these mutant mice, ATR and  $\gamma$ H2AX did accumulate on X and Y and a normal XY body was formed. From these observations it was concluded that BRCA1 is required for the recruitment of ATR to XY body chromatin. Since BRCA1 is also required for proper repair of meiotic DSBs in mouse, as apparent from the multiple  $\gamma$ H2AX foci that remain in the vast majority of *Brca1* mutant nuclei [434], it might also be suggested that these persistent meiotic DSBs inhibit MSCI, as occurs in many other spermatocytes carrying mutations in the DSB repair pathway. This could explain why  $\gamma$ H2AX is not formed on XY chromatin in *Brca1* mutant mouse spermatocytes. The occasional normal XY body formation in *Brca1* mutant spermatocytes may occur in cells that manage to repair the (majority) of meiotic DSBs despite the lack of normally functional BRCA1. In this scenario, BRCA1 would not necessarily be upstream of ATR/ATM recruitment in meiotic cells.

Could there be another factor involved in recruiting ATR to XY body chromatin? In somatic cells, recruitment of ATR requires its interaction partner ATRIP, which binds to RPA filaments [280]. In order to activate ATR, the 9-1-1 complex and TOPBP1 are most likely also required. It might thus be suggested that a similar sequence of events occurs at persistent DSBs along the heterologous part of X (and Y). TOPBP1 and at least one component of the 9-1-1 complex, RAD1, also accumulate on the XY body [424,426,427]. RPA- and damage-independent recruitment of ATR to chromatin in somatic cells has also been reported. For example CDC6, a protein required for replication initiation, may recruit ATR to stalled replication forks [334]. In a similar manner, a yet unknown meiosis-specific protein that specifically localizes to unsynapsed axes may recruit ATR independent of DSB-repair.

### **Transcriptional silencing of unsynapsed chromatin**

When a homologous chromosome pair contains a large heterologous region, for example due to a translocation, such regions frequently remain unsynapsed. In analogy to MSCI, this also leads to transcriptional inactivation of this region during meiotic prophase, in males and females [435,436]. Surprisingly, such heterologous regions sometimes display heterologous synapsis (through synaptic adjustment, see above), providing an escape from silencing. Due to the tight coupling between asynapsis and silencing, this mechanism has been named meiotic silencing of unsynapsed chromatin (MSUC) [437]. MSCI and MSUC appear to be closely related; unsynapsed autosomal chromatin colocalizes with the XY body, and the presence of such silenced unsynapsed autosomal chromatin reduced the efficiency of XY body silencing [438]. In addition, similar to the XY body, silenced autosomal unsynapsed chromatin retains DSB-repair markers [406]. When heterologous synapsis and escape from silencing occur, these DSB-repair markers do not persist at the heterologous regions [406].

## **MEIOTIC SILENCING PRIOR TO SYNAPSIS AND DSB-REPAIR IN AVIAN SPECIES**

In birds, males have a ZZ sex chromosome constitution, whereas females are ZW. During oogenesis in chicken, the largely heterologous Z and W chromosome reach a state of complete synapsis [439]. Previously, it was suggested that this might “save” the heterologous sex chromosomes from transcriptional silencing during the lengthy prophase in oocytes [440]. Like the X chromosome in mammals, the Z chromosome is gene-rich, and it is to be expected that prolonged silencing of the Z chromosome would be detrimental to oocytes. We wondered how meiotic recombination between Z and W could be prevented during synapsis, and reasoned that the avian system could be a good model to discriminate between the roles of chromosome synapsis and meiotic recombination in the process of meiotic silencing. Surprisingly, we found that the chicken W chromosome is silenced immediately upon entrance in meiotic prophase [441]. The Z chromosome appears to be normally transcribed during leptotene and zygotene. However, when Z and W synapse in pachytene, the Z chromosome is also transcriptionally silenced. During this phase, repair of meiotic DSBs on the Z

chromosome appears to be postponed. This is based on the fact that no markers of DSB repair are detected on the synapsed ZW pair, but during ZW desynapsis, in late pachytene and early diplotene, the Z chromosome accumulates  $\gamma$ H2AX, and RAD51 foci reappear [441]. Subsequently, repair is completed,  $\gamma$ H2AX and RAD51 foci disappear and the Z chromosome is reactivated. More recently, we have also shown that the germ cell restricted single chromosome (GRC) that is present in zebra finch spermatocytes is also silenced upon entry into meiotic prophase [442]. Therefore, we have named this phenomenon meiotic silencing prior to synapsis (MSPS). We have proposed that MSC1 in chickens involves spreading of heterochromatin from Z onto W. In a second phase,  $\gamma$ H2AX formation may contribute to the maintenance of silencing of the Z chromosome until repair is completed [441]. These findings indicate that the initiation of MSPS in birds may be essentially different from the initiation of MSC1 in mammals. In birds this process is most likely independent of DSB repair and the final achievement of synapsis.

## CONCLUDING REMARKS

Persistent DSBs, present in heterologous regions, inhibit synapsis and may stimulate MSUC [406] (Figure 2). Progression of synapsis starting from homologous regions may generate a positive feedback system that facilitates further downstream synapsis. Such a system may overrule the inhibitory effect of DSBs that have not (yet) been repaired. This may even facilitate homology recognition at persistent DSBs that remain in regions that are actually homologous, because the chromosomes will be in permanent close proximity upon synapsis. In addition, repression of inter-sister repair may be relieved once synapsis has been accomplished.

Based upon the progressively decreasing size of the synapsed regions of X and Y during pachytene, the synapsis-inhibitory force on these chromosomes must be large enough to prevent heterologous synapsis and illegitimate recombination with almost 100% efficiency. For autosomal pairs that carry heterologous regions, the balance between synapsis promotion and inhibition may be dependent on the size of the homologous regions. Once synapsis has proceeded along a certain threshold length, it may proceed irrespective of the presence of persistent DSBs. Prevention of synapsis between X and Y also prevents completion of DSB-repair, most likely until the repression of intersister-recombination and/or the nonhomologous end-joining pathway are relieved during late pachytene or diplotene.

Persistent DSBs in yeast evoke specific changes in chromatin that can spread chromosome wide, such as sumoylation of H2A.Z [415]. Thus, persistent DSBs on the unsynapsed X (and Y) may be instrumental in the chromosome wide recruitment of  $\gamma$ H2AX and ubiquitylated H2A, and other downstream DSB-repair and checkpoint factors. Together, these modifications and factors could mediate transcriptional silencing of all X- and Y-chromosomal chromatin. Alternatively, asynapsis itself may somehow specifically allow recruitment of ATR, and subsequent formation of  $\gamma$ H2AX then triggers all downstream events that mediate silencing. In this scenario, the stalled DSB sites are not required for the initiation of MSC1, but may play a role in inhibition of synapsis.

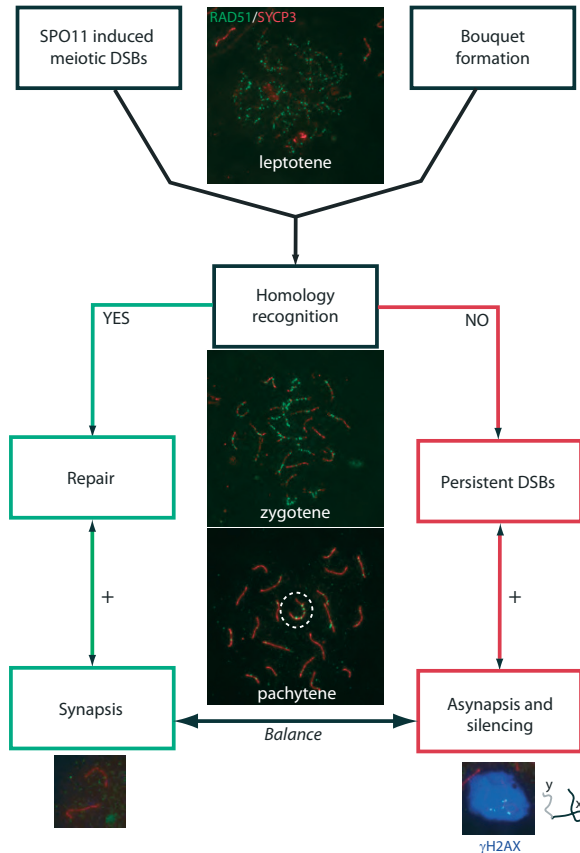


**Figure 2. Persistent meiotic DSBs homology recognition and transcriptional silencing of heterologous regions.** SPO11-induced DSBs and the bouquet configuration of the chromosomes both contribute to the homology recognition process. Numerous RAD51 foci in leptotene nuclei mark the initiation of the homology search. If homology recognition occurs, DSB repair proceeds and this is coupled to stimulation of progression of SC formation in zygotene nuclei (and SC formation may also help to complete the DSB repair process), leading to the complete SC with few remaining RAD51 foci in diplotene. If homology recognition does not occur, the DSB persists, additional DSB repair proteins accumulate, and spread along the chromatin, and progression of SC formation is inhibited (and lack of SC formation also inhibits invasion of the homologous template). This is associated with the recruitment of ATR to asynapsed regions, which induces a second wave of  $\gamma$ H2AX formation and transcriptional silencing. The balance between progression and inhibition of synapsis and DNA repair (black horizontal arrow) determines the final outcome in pachytene. The XY body in the pachytene nucleus is encircled. Spread mouse spermatocyte nuclei were stained with antibodies against RAD51 (green) and SYCP3 (red). The DNA was stained with DAPI (blue), with exception of the lower left and right images of synapsed autosomal chromosomes (left) and the XY body (right). Here, localization of  $\gamma$ H2AX is shown in blue, and the DNA is not stained.

At present it is not possible to determine whether the recruitment of ATR to XY body chromatin depends primarily on the presence of persistent DSBs, asynapsed chromosomal axes, or both. Once ATR has been recruited to the XY body chromatin, or to autosomal unsynapsed regions, the subsequent formation of  $\gamma$ H2AX is essential for the initiation of transcriptional silencing. The accumulation of ubiquitylated H2A(X)

and SUMOylated chromatin components that occur downstream of  $\gamma$ H2AX formation have been associated with transcriptional silencing in different contexts [435,443-446]. Therefore, it is tempting to speculate that  $\gamma$ H2AX formation and transcriptional silencing of the XY chromosome pair in meiosis evolved as a specialization of a general silencing mechanism that prevents ongoing RNA transcription from a damaged template when DSB repair is ongoing or blocked. Functional analyses of the initiating events in MSUC and MSCI will reveal the complex interplay between meiotic DSB repair, chromosome synapsis and silencing of chromatin that lacks a pairing partner.

## REFERENCES

1. P.R. Blier, A.J. Griffith, J. Craft, J.A. Hardin, Binding of Ku protein to DNA. Measurement of affinity for ends and demonstration of binding to nicks, *J Biol Chem* 268 (1993) 7594-7601.
2. A.J. Doherty, S.P. Jackson, DNA repair: how Ku makes ends meet, *Curr Biol* 11 (2001) R920-924.
3. M. Falzon, J.W. Fewell, E.L. Kuff, EBP-80, a transcription factor closely resembling the human autoantigen Ku, recognizes single- to double-strand transitions in DNA, *J Biol Chem* 268 (1993) 10546-10552.
4. T. Mimori, J.A. Hardin, Mechanism of interaction between Ku protein and DNA, *J Biol Chem* 261 (1986) 10375-10379.
5. T. Mimori, J.A. Hardin, J.A. Steitz, Characterization of the DNA-binding protein antigen Ku recognized by autoantibodies from patients with rheumatic disorders, *J Biol Chem* 261 (1986) 2274-2278.
6. M.R. Lieber, The Mechanism of Double-Strand DNA Break Repair by the Nonhomologous DNA End-Joining Pathway, *Annu Rev Biochem*.
7. R.B. West, M. Yaneva, M.R. Lieber, Productive and nonproductive complexes of Ku and DNA-dependent protein kinase at DNA termini, *Mol Cell Biol* 18 (1998) 5908-5920.
8. G. Chu, Double strand break repair, *J Biol Chem* 272 (1997) 24097-24100.
9. O. Hammarsten, L.G. DeFazio, G. Chu, Activation of DNA-dependent protein kinase by single-stranded DNA ends, *J Biol Chem* 275 (2000) 1541-1550.
10. S. Yoo, W.S. Dynan, Geometry of a complex formed by double strand break repair proteins at a single DNA end: recruitment of DNA-PKcs induces inward translocation of Ku protein, *Nucleic Acids Res* 27 (1999) 4679-4686.
11. S. Yoo, A. Kimzey, W.S. Dynan, Photocross-linking of an oriented DNA repair complex. Ku bound at a single DNA end, *J Biol Chem* 274 (1999) 20034-20039.
12. Y. Ma, M.R. Lieber, Binding of inositol hexakisphosphate (IP6) to Ku but not to DNA-PKcs, *J Biol Chem* 277 (2002) 10756-10759.
13. K. Meek, S. Gupta, D.A. Ramsden, S.P. Lees-Miller, The DNA-dependent protein kinase: the director at the end, *Immunol Rev* 200 (2004) 132-141.
14. D. Niewolik, U. Pannicke, H. Lu, Y. Ma, L.C. Wang, P. Kulesza, E. Zandi, M.R. Lieber, K. Schwarz, DNA-PKcs dependence of Artemis endonucleolytic activity, differences between hairpins and 5' or 3' overhangs, *J Biol Chem* 281 (2006) 33900-33909.
15. Y. Ma, K. Schwarz, M.R. Lieber, The Artemis:DNA-PKcs endonuclease cleaves DNA loops, flaps, and gaps, *DNA Repair (Amst)* 4 (2005) 845-851.
16. D. Moshous, I. Callebaut, R. de Chasseval, B. Corneo, M. Cavazzana-Calvo, F. Le Deist, I. Tezcan, O. Sanal, Y. Bertrand, N. Philippe, A. Fischer, J.P. de Villartay, Artemis, a novel DNA double-strand break repair/V(D)J recombination protein, is mutated in human severe combined immune deficiency, *Cell* 105 (2001) 177-186.
17. L. Chen, K. Trujillo, P. Sung, A.E. Tomkinson, Interactions of the DNA ligase IV-XRCC4 complex with DNA ends and the DNA-dependent protein kinase, *J Biol Chem* 275 (2000) 26196-26205.
18. L.G. DeFazio, R.M. Stansel, J.D. Griffith, G. Chu, Synapsis of DNA ends by DNA-dependent protein kinase, *Embo J* 21 (2002) 3192-3200.
19. M. Yaneva, T. Kowalewski, M.R. Lieber, Interaction of DNA-dependent protein kinase with DNA and with Ku: biochemical

- and atomic-force microscopy studies, *Embo J* 16 (1997) 5098-5112.
20. B. Bertocci, A. De Smet, J.C. Weill, C.A. Reynaud, Nonoverlapping functions of DNA polymerases  $\mu$ ,  $\lambda$ , and terminal deoxynucleotidyltransferase during immunoglobulin V(D)J recombination in vivo, *Immunity* 25 (2006) 31-41.
  21. Y. Ma, H. Lu, B. Tippin, M.F. Goodman, N. Shimazaki, O. Koiwai, C.L. Hsieh, K. Schwarz, M.R. Lieber, A biochemically defined system for mammalian nonhomologous DNA end joining, *Mol Cell* 16 (2004) 701-713.
  22. A.F. Moon, M. Garcia-Diaz, V.K. Batra, W.A. Beard, K. Bebenek, T.A. Kunkel, S.H. Wilson, L.C. Pedersen, The X family portrait: structural insights into biological functions of X family polymerases, *DNA Repair (Amst)* 6 (2007) 1709-1725.
  23. A.F. Moon, M. Garcia-Diaz, K. Bebenek, B.J. Davis, X. Zhong, D.A. Ramsden, T.A. Kunkel, L.C. Pedersen, Structural insight into the substrate specificity of DNA Polymerase  $\mu$ , *Nat Struct Mol Biol* 14 (2007) 45-53.
  24. S.A. Nick McElhinny, J.M. Havener, M. Garcia-Diaz, R. Juarez, K. Bebenek, B.L. Kee, L. Blanco, T.A. Kunkel, D.A. Ramsden, A gradient of template dependence defines distinct biological roles for family X polymerases in nonhomologous end joining, *Mol Cell* 19 (2005) 357-366.
  25. T.E. Wilson, M.R. Lieber, Efficient processing of DNA ends during yeast nonhomologous end joining. Evidence for a DNA polymerase  $\beta$  (Pol4)-dependent pathway, *J Biol Chem* 274 (1999) 23599-23609.
  26. T. Komori, A. Okada, V. Stewart, F.W. Alt, Lack of N regions in antigen receptor variable region genes of TdT-deficient lymphocytes, *Science* 261 (1993) 1171-1175.
  27. J. Gu, H. Lu, B. Tippin, N. Shimazaki, M.F. Goodman, M.R. Lieber, XRCC4:DNA ligase IV can ligate incompatible DNA ends and can ligate across gaps, *Embo J* 26 (2007) 1010-1023.
  28. J.W. Lee, L. Blanco, T. Zhou, M. Garcia-Diaz, K. Bebenek, T.A. Kunkel, Z. Wang, L.F. Povirk, Implication of DNA polymerase  $\lambda$  in alignment-based gap filling for nonhomologous DNA end joining in human nuclear extracts, *J Biol Chem* 279 (2004) 805-811.
  29. L.F. Povirk, Biochemical mechanisms of chromosomal translocations resulting from DNA double-strand breaks, *DNA Repair (Amst)* 5 (2006) 1199-1212.
  30. M.R. Lieber, The mechanism of human nonhomologous DNA end joining, *J Biol Chem* 283 (2008) 1-5.
  31. J. Gu, H. Lu, A.G. Tsai, K. Schwarz, M.R. Lieber, Single-stranded DNA ligation and XLF-stimulated incompatible DNA end ligation by the XRCC4-DNA ligase IV complex: influence of terminal DNA sequence, *Nucleic Acids Res* 35 (2007) 5755-5762.
  32. C.J. Tsai, S.A. Kim, G. Chu, Cernunnos/XLF promotes the ligation of mismatched and noncohesive DNA ends, *Proc Natl Acad Sci U S A* 104 (2007) 7851-7856.
  33. K.N. Mahajan, S.A. Nick McElhinny, B.S. Mitchell, D.A. Ramsden, Association of DNA polymerase  $\mu$  (pol  $\mu$ ) with Ku and ligase IV: role for pol  $\mu$  in end-joining double-strand break repair, *Mol Cell Biol* 22 (2002) 5194-5202.
  34. S.A. Nick McElhinny, C.M. Snowden, J. McCarville, D.A. Ramsden, Ku recruits the XRCC4-ligase IV complex to DNA ends, *Mol Cell Biol* 20 (2000) 2996-3003.
  35. J. San Filippo, P. Sung, H. Klein, Mechanism of eukaryotic homologous recombination, *Annu Rev Biochem* 77 (2008) 229-257.
  36. J.R. Lydeard, S. Jain, M. Yamaguchi, J.E. Haber, Break-induced replication and telomerase-independent telomere maintenance require Pol32, *Nature* 448 (2007) 820-823.
  37. A. Malkova, E.L. Ivanov, J.E. Haber, Double-strand break repair in the absence of RAD51 in yeast: a possible role for break-induced DNA replication, *Proc Natl Acad Sci U S A* 93 (1996) 7131-7136.
  38. M.S. Wold, Replication protein A: a heterotrimeric, single-stranded DNA-binding protein required for eukaryotic DNA metabolism, *Annu Rev Biochem* 66 (1997) 61-92.
  39. J. Buis, Y. Wu, Y. Deng, J. Leddon, G. Westfield, M. Eckersdorff, J.M. Sekiguchi, S. Chang, D.O. Ferguson, Mre11 nuclease activity has essential roles in DNA repair and genomic stability distinct from ATM activation, *Cell* 135 (2008) 85-96.
  40. L. Cao, E. Alani, N. Kleckner, A pathway for generation and processing of double-strand breaks during meiotic recombination in *S. cerevisiae*, *Cell* 61 (1990) 1089-1101.
  41. R. Shroff, A. Arbel-Eden, D. Pilch, G. Ira, W.M. Bonner, J.H. Petrini, J.E. Haber, M.

- Lichten, Distribution and dynamics of chromatin modification induced by a defined DNA double-strand break, *Curr Biol* 14 (2004) 1703-1711.
42. O. Limbo, C. Chahwan, Y. Yamada, R.A. de Bruin, C. Wittenberg, P. Russell, Ctp1 is a cell-cycle-regulated protein that functions with Mre11 complex to control double-strand break repair by homologous recombination, *Mol Cell* 28 (2007) 134-146.
  43. R.S. Williams, G.E. Dodson, O. Limbo, Y. Yamada, J.S. Williams, G. Guenther, S. Classen, J.N. Glover, H. Iwasaki, P. Russell, J.A. Tainer, Nbs1 flexibly tethers Ctp1 and Mre11-Rad50 to coordinate DNA double-strand break processing and repair, *Cell* 139 (2009) 87-99.
  44. R.S. Williams, G. Moncalian, J.S. Williams, Y. Yamada, O. Limbo, D.S. Shin, L.M. Groocock, D. Cahill, C. Hitomi, G. Guenther, D. Moiani, J.P. Carney, P. Russell, J.A. Tainer, Mre11 dimers coordinate DNA end bridging and nuclease processing in double-strand-break repair, *Cell* 135 (2008) 97-109.
  45. M. de Jager, J. van Noort, D.C. van Gent, C. Dekker, R. Kanaar, C. Wyman, Human Rad50/Mre11 is a flexible complex that can tether DNA ends, *Mol Cell* 8 (2001) 1129-1135.
  46. K.P. Hopfner, L. Craig, G. Moncalian, R.A. Zinkel, T. Usui, B.A. Owen, A. Karcher, B. Henderson, J.L. Bodmer, C.T. McMurray, J.P. Carney, J.H. Petrini, J.A. Tainer, The Rad50 zinc-hook is a structure joining Mre11 complexes in DNA recombination and repair, *Nature* 418 (2002) 562-566.
  47. J. van Noort, T. van Der Heijden, M. de Jager, C. Wyman, R. Kanaar, C. Dekker, The coiled-coil of the human Rad50 DNA repair protein contains specific segments of increased flexibility, *Proc Natl Acad Sci U S A* 100 (2003) 7581-7586.
  48. G. Luo, M.S. Yao, C.F. Bender, M. Mills, A.R. Bladl, A. Bradley, J.H. Petrini, Disruption of mRad50 causes embryonic stem cell lethality, abnormal embryonic development, and sensitivity to ionizing radiation, *Proc Natl Acad Sci U S A* 96 (1999) 7376-7381.
  49. J.H. Petrini, M.E. Walsh, C. DiMare, X.N. Chen, J.R. Korenberg, D.T. Weaver, Isolation and characterization of the human MRE11 homologue, *Genomics* 29 (1995) 80-86.
  50. J. Zhu, S. Petersen, L. Tessarollo, A. Nussenzweig, Targeted disruption of the Nijmegen breakage syndrome gene NBS1 leads to early embryonic lethality in mice, *Curr Biol* 11 (2001) 105-109.
  51. J.W. Theunissen, M.I. Kaplan, P.A. Hunt, B.R. Williams, D.O. Ferguson, F.W. Alt, J.H. Petrini, Checkpoint failure and chromosomal instability without lymphomagenesis in Mre11(ATLD1/ATLD1) mice, *Mol Cell* 12 (2003) 1511-1523.
  52. B.R. Williams, O.K. Mirzoeva, W.F. Morgan, J. Lin, W. Dunnick, J.H. Petrini, A murine model of Nijmegen breakage syndrome, *Curr Biol* 12 (2002) 648-653.
  53. Y. Xiao, D.T. Weaver, Conditional gene targeted deletion by Cre recombinase demonstrates the requirement for the double-strand break repair Mre11 protein in murine embryonic stem cells, *Nucleic Acids Res* 25 (1997) 2985-2991.
  54. P.T. Tran, N. Erdeniz, L.S. Symington, R.M. Liskay, EXO1-A multi-tasking eukaryotic nuclease, *DNA Repair (Amst)* 3 (2004) 1549-1559.
  55. M. Clerici, D. Mantiero, G. Lucchini, M.P. Longhese, The *Saccharomyces cerevisiae* Sae2 protein promotes resection and bridging of double strand break ends, *J Biol Chem* 280 (2005) 38631-38638.
  56. S. Gravel, J.R. Chapman, C. Magill, S.P. Jackson, DNA helicases Sgs1 and BLM promote DNA double-strand break resection, *Genes Dev* 22 (2008) 2767-2772.
  57. E.P. Mimitou, L.S. Symington, Sae2, Exo1 and Sgs1 collaborate in DNA double-strand break processing, *Nature* 455 (2008) 770-774.
  58. E.P. Mimitou, L.S. Symington, DNA end resection: many nucleases make light work, *DNA Repair (Amst)* 8 (2009) 983-995.
  59. Z. Zhu, W.H. Chung, E.Y. Shim, S.E. Lee, G. Ira, Sgs1 helicase and two nucleases Dna2 and Exo1 resect DNA double-strand break ends, *Cell* 134 (2008) 981-994.
  60. D.A. Bressan, H.A. Olivares, B.E. Nelms, J.H. Petrini, Alteration of N-terminal phosphoesterase signature motifs inactivates *Saccharomyces cerevisiae* Mre11, *Genetics* 150 (1998) 591-600.
  61. D. Mantiero, M. Clerici, G. Lucchini, M.P. Longhese, Dual role for *Saccharomyces cerevisiae* Tel1 in the checkpoint response to double-strand breaks, *EMBO Rep* 8 (2007) 380-387.
  62. S. Moreau, E.A. Morgan, L.S. Symington, Overlapping functions of the

- Saccharomyces cerevisiae* Mre11, Exo1 and Rad27 nucleases in DNA metabolism, *Genetics* 159 (2001) 1423-1433.
63. A.A. Sartori, C. Lukas, J. Coates, M. Mistrik, S. Fu, J. Bartek, R. Baer, J. Lukas, S.P. Jackson, Human CtIP promotes DNA end resection, *Nature* 450 (2007) 509-514.
  64. M.H. Yun, K. Hiom, CtIP-BRCA1 modulates the choice of DNA double-strand-break repair pathway throughout the cell cycle, *Nature* 459 (2009) 460-463.
  65. P. Huertas, S.P. Jackson, Human CtIP mediates cell cycle control of DNA end resection and double strand break repair, *J Biol Chem* 284 (2009) 9558-9565.
  66. C.Z. Bachrati, I.D. Hickson, RecQ helicases: suppressors of tumorigenesis and premature aging, *Biochem J* 374 (2003) 577-606.
  67. N.A. Ellis, D.J. Lennon, M. Proytcheva, B. Alhadeff, E.E. Henderson, J. German, Somatic intragenic recombination within the mutated locus BLM can correct the high sister-chromatid exchange phenotype of Bloom syndrome cells, *Am J Hum Genet* 57 (1995) 1019-1027.
  68. N.F. Neff, N.A. Ellis, T.Z. Ye, J. Noonan, K. Huang, M. Sanz, M. Proytcheva, The DNA helicase activity of BLM is necessary for the correction of the genomic instability of bloom syndrome cells, *Mol Biol Cell* 10 (1999) 665-676.
  69. J.H. Kim, H.D. Kim, G.H. Ryu, D.H. Kim, J. Hurwitz, Y.S. Seo, Isolation of human Dna2 endonuclease and characterization of its enzymatic properties, *Nucleic Acids Res* 34 (2006) 1854-1864.
  70. T. Masuda-Sasa, O. Imamura, J.L. Campbell, Biochemical analysis of human Dna2, *Nucleic Acids Res* 34 (2006) 1865-1875.
  71. J.P. Duxin, B. Dao, P. Martinsson, N. Rajala, L. Guittat, J.L. Campbell, J.N. Spelbrink, S.A. Stewart, Human Dna2 is a nuclear and mitochondrial DNA maintenance protein, *Mol Cell Biol* 29 (2009) 4274-4282.
  72. X. Yu, S. Fu, M. Lai, R. Baer, J. Chen, BRCA1 ubiquitinates its phosphorylation-dependent binding partner CtIP, *Genes Dev* 20 (2006) 1721-1726.
  73. L. Chen, C.J. Nievera, A.Y. Lee, X. Wu, Cell cycle-dependent complex formation of BRCA1.CtIP.MRN is important for DNA double-strand break repair, *J Biol Chem* 283 (2008) 7713-7720.
  74. T. Ogawa, A. Shinohara, A. Nabetani, T. Ikeya, X. Yu, E.H. Egelman, H. Ogawa, RecA-like recombination proteins in eukaryotes: functions and structures of RAD51 genes, *Cold Spring Harb Symp Quant Biol* 58 (1993) 567-576.
  75. P. Sung, D.L. Robberson, DNA strand exchange mediated by a RAD51-ssDNA nucleoprotein filament with polarity opposite to that of RecA, *Cell* 82 (1995) 453-461.
  76. X. Yu, S.A. Jacobs, S.C. West, T. Ogawa, E.H. Egelman, Domain structure and dynamics in the helical filaments formed by RecA and Rad51 on DNA, *Proc Natl Acad Sci U S A* 98 (2001) 8419-8424.
  77. A.L. Eggler, R.B. Inman, M.M. Cox, The Rad51-dependent pairing of long DNA substrates is stabilized by replication protein A, *J Biol Chem* 277 (2002) 39280-39288.
  78. T. Sugiyama, E.M. Zaitseva, S.C. Kowalczykowski, A single-stranded DNA-binding protein is needed for efficient presynaptic complex formation by the *Saccharomyces cerevisiae* Rad51 protein, *J Biol Chem* 272 (1997) 7940-7945.
  79. H.T. Beernink, S.W. Morriscal, RMPs: recombination/replication mediator proteins, *Trends Biochem Sci* 24 (1999) 385-389.
  80. P. Sung, Yeast Rad55 and Rad57 proteins form a heterodimer that functions with replication protein A to promote DNA strand exchange by Rad51 recombinase, *Genes Dev* 11 (1997) 1111-1121.
  81. P. Sung, Function of yeast Rad52 protein as a mediator between replication protein A and the Rad51 recombinase, *J Biol Chem* 272 (1997) 28194-28197.
  82. R. Cartwright, A.M. Dunn, P.J. Simpson, C.E. Tambini, J. Thacker, Isolation of novel human and mouse genes of the recA/RAD51 recombination-repair gene family, *Nucleic Acids Res* 26 (1998) 1653-1659.
  83. R. Cartwright, C.E. Tambini, P.J. Simpson, J. Thacker, The XRCC2 DNA repair gene from human and mouse encodes a novel member of the recA/RAD51 family, *Nucleic Acids Res* 26 (1998) 3084-3089.
  84. J. Thacker, A surfeit of RAD51-like genes?, *Trends Genet* 15 (1999) 166-168.
  85. L.S. Symington, Role of RAD52 epistasis group genes in homologous recombination and double-strand break

- repair, *Microbiol Mol Biol Rev* 66 (2002) 630-670, table of contents.
86. Y. Yonetani, H. Hochegger, E. Sonoda, S. Shinya, H. Yoshikawa, S. Takeda, M. Yamazoe, Differential and collaborative actions of Rad51 paralog proteins in cellular response to DNA damage, *Nucleic Acids Res* 33 (2005) 4544-4552.
  87. S. Sigurdsson, S. Van Komen, G. Petukhova, P. Sung, Homologous DNA pairing by human recombination factors Rad51 and Rad54, *J Biol Chem* 277 (2002) 42790-42794.
  88. Y.C. Lio, A.V. Mazin, S.C. Kowalczykowski, D.J. Chen, Complex formation by the human Rad51B and Rad51C DNA repair proteins and their activities in vitro, *J Biol Chem* 278 (2003) 2469-2478.
  89. M. Shinohara, E. Shita-Yamaguchi, J.M. Buerstedde, H. Shinagawa, H. Ogawa, A. Shinohara, Characterization of the roles of the *Saccharomyces cerevisiae* RAD54 gene and a homologue of RAD54, RDH54/TID1, in mitosis and meiosis, *Genetics* 147 (1997) 1545-1556.
  90. M.R. Singleton, L.M. Wentzell, Y. Liu, S.C. West, D.B. Wigley, Structure of the single-strand annealing domain of human RAD52 protein, *Proc Natl Acad Sci U S A* 99 (2002) 13492-13497.
  91. S.L. Hays, A.A. Firmenich, P. Massey, R. Banerjee, P. Berg, Studies of the interaction between Rad52 protein and the yeast single-stranded DNA binding protein RPA, *Mol Cell Biol* 18 (1998) 4400-4406.
  92. A. Shinohara, H. Ogawa, T. Ogawa, Rad51 protein involved in repair and recombination in *S. cerevisiae* is a RecA-like protein, *Cell* 69 (1992) 457-470.
  93. T. Sugiyama, S.C. Kowalczykowski, Rad52 protein associates with replication protein A (RPA)-single-stranded DNA to accelerate Rad51-mediated displacement of RPA and presynaptic complex formation, *J Biol Chem* 277 (2002) 31663-31672.
  94. J.H. New, T. Sugiyama, E. Zaitseva, S.C. Kowalczykowski, Rad52 protein stimulates DNA strand exchange by Rad51 and replication protein A, *Nature* 391 (1998) 407-410.
  95. A. Shinohara, T. Ogawa, Stimulation by Rad52 of yeast Rad51-mediated recombination, *Nature* 391 (1998) 404-407.
  96. T. Sugiyama, J.H. New, S.C. Kowalczykowski, DNA annealing by RAD52 protein is stimulated by specific interaction with the complex of replication protein A and single-stranded DNA, *Proc Natl Acad Sci U S A* 95 (1998) 6049-6054.
  97. M.J. McIlwraith, S.C. West, DNA repair synthesis facilitates RAD52-mediated second-end capture during DSB repair, *Mol Cell* 29 (2008) 510-516.
  98. T. Sugiyama, N. Kantake, Y. Wu, S.C. Kowalczykowski, Rad52-mediated DNA annealing after Rad51-mediated DNA strand exchange promotes second ssDNA capture, *Embo J* 25 (2006) 5539-5548.
  99. T. Rijkers, J. Van Den Ouweland, B. Morolli, A.G. Rolink, W.M. Baarends, P.P. Van Sloun, P.H. Lohman, A. Pastink, Targeted inactivation of mouse RAD52 reduces homologous recombination but not resistance to ionizing radiation, *Mol Cell Biol* 18 (1998) 6423-6429.
  100. M. Jasin, Homologous repair of DNA damage and tumorigenesis: the BRCA connection, *Oncogene* 21 (2002) 8981-8993.
  101. N. Siaud, E. Dray, I. Gy, E. Gerard, N. Takvorian, M.P. Doutriaux, Brca2 is involved in meiosis in *Arabidopsis thaliana* as suggested by its interaction with Dmc1, *Embo J* 23 (2004) 1392-1401.
  102. M. Tarsounas, A.A. Davies, S.C. West, RAD51 localization and activation following DNA damage, *Philos Trans R Soc Lond B Biol Sci* 359 (2004) 87-93.
  103. M. Tarsounas, D. Davies, S.C. West, BRCA2-dependent and independent formation of RAD51 nuclear foci, *Oncogene* 22 (2003) 1115-1123.
  104. P.L. Chen, C.F. Chen, Y. Chen, J. Xiao, Z.D. Sharp, W.H. Lee, The BRC repeats in BRCA2 are critical for RAD51 binding and resistance to methyl methanesulfonate treatment, *Proc Natl Acad Sci U S A* 95 (1998) 5287-5292.
  105. A.K. Wong, R. Pero, P.A. Ormonde, S.V. Tavtigian, P.L. Bartel, RAD51 interacts with the evolutionarily conserved BRC motifs in the human breast cancer susceptibility gene brca2, *J Biol Chem* 272 (1997) 31941-31944.
  106. R. Mizuta, J.M. LaSalle, H.L. Cheng, A. Shinohara, H. Ogawa, N. Copeland, N.A. Jenkins, M. Lalonde, F.W. Alt, RAB22 and RAB163/mouse BRCA2: proteins that specifically interact with the RAD51 protein, *Proc Natl Acad Sci U S A* 94 (1997) 6927-6932.
  107. S.K. Sharan, M. Morimatsu, U. Albrecht, D.S. Lim, E. Regel, C. Dinh, A. Sands, G.

- Eichele, P. Hasty, A. Bradley, Embryonic lethality and radiation hypersensitivity mediated by Rad51 in mice lacking Brca2, *Nature* 386 (1997) 804-810.
108. J.M. Wong, D. Ionescu, C.J. Ingles, Interaction between BRCA2 and replication protein A is compromised by a cancer-predisposing mutation in BRCA2, *Oncogene* 22 (2003) 28-33.
  109. W.D. Heyer, X. Li, M. Rolfmeier, X.P. Zhang, Rad54: the Swiss Army knife of homologous recombination?, *Nucleic Acids Res* 34 (2006) 4115-4125.
  110. E.I. Golub, O.V. Kovalenko, R.C. Gupta, D.C. Ward, C.M. Radding, Interaction of human recombination proteins Rad51 and Rad54, *Nucleic Acids Res* 25 (1997) 4106-4110.
  111. A.V. Mazin, A.A. Alexeev, S.C. Kowalczykowski, A novel function of Rad54 protein. Stabilization of the Rad51 nucleoprotein filament, *J Biol Chem* 278 (2003) 14029-14036.
  112. J.A. Solinger, K. Kiiianitsa, W.D. Heyer, Rad54, a Swi2/Snf2-like recombinational repair protein, disassembles Rad51:dsDNA filaments, *Mol Cell* 10 (2002) 1175-1188.
  113. S. Van Komen, G. Petukhova, S. Sigurdsson, P. Sung, Functional cross-talk among Rad51, Rad54, and replication protein A in heteroduplex DNA joint formation, *J Biol Chem* 277 (2002) 43578-43587.
  114. A.V. Mazin, C.J. Bornarth, J.A. Solinger, W.D. Heyer, S.C. Kowalczykowski, Rad54 protein is targeted to pairing loci by the Rad51 nucleoprotein filament, *Mol Cell* 6 (2000) 583-592.
  115. O.M. Mazina, A.V. Mazin, Human Rad54 protein stimulates DNA strand exchange activity of hRad51 protein in the presence of Ca<sup>2+</sup>, *J Biol Chem* 279 (2004) 52042-52051.
  116. G. Petukhova, S. Stratton, P. Sung, Catalysis of homologous DNA pairing by yeast Rad51 and Rad54 proteins, *Nature* 393 (1998) 91-94.
  117. S. Van Komen, G. Petukhova, S. Sigurdsson, S. Stratton, P. Sung, Superhelicity-driven homologous DNA pairing by yeast recombination factors Rad51 and Rad54, *Mol Cell* 6 (2000) 563-572.
  118. K. Miyagawa, T. Tsuruga, A. Kinomura, K. Usui, M. Katsura, S. Tashiro, H. Mishima, K. Tanaka, A role for RAD54B in homologous recombination in human cells, *Embo J* 21 (2002) 175-180.
  119. J. Wesoly, S. Agarwal, S. Sigurdsson, W. Bussen, S. Van Komen, J. Qin, H. van Steeg, J. van Benthem, E. Wassenaar, W.M. Baarends, M. Ghazvini, A.A. Tafel, H. Heath, N. Galjart, J. Essers, J.A. Grootegoed, N. Arnheim, O. Bezzubova, J.M. Buerstedde, P. Sung, R. Kanaar, Differential contributions of mammalian Rad54 paralogs to recombination, DNA damage repair, and meiosis, *Mol Cell Biol* 26 (2006) 976-989.
  120. Z. Zhang, H.Y. Fan, J.A. Goldman, R.E. Kingston, Homology-driven chromatin remodeling by human RAD54, *Nat Struct Mol Biol* 14 (2007) 397-405.
  121. K. Kiiianitsa, J.A. Solinger, W.D. Heyer, Terminal association of Rad54 protein with the Rad51-dsDNA filament, *Proc Natl Acad Sci U S A* 103 (2006) 9767-9772.
  122. X. Li, W.D. Heyer, RAD54 controls access to the invading 3'-OH end after RAD51-mediated DNA strand invasion in homologous recombination in *Saccharomyces cerevisiae*, *Nucleic Acids Res* 37 (2009) 638-646.
  123. F. Palladino, H.L. Klein, Analysis of mitotic and meiotic defects in *Saccharomyces cerevisiae* SRS2 DNA helicase mutants, *Genetics* 132 (1992) 23-37.
  124. L. Krejci, S. Van Komen, Y. Li, J. Villemain, M.S. Reddy, H. Klein, T. Ellenberger, P. Sung, DNA helicase Srs2 disrupts the Rad51 presynaptic filament, *Nature* 423 (2003) 305-309.
  125. X. Veaute, J. Jeusset, C. Soustelle, S.C. Kowalczykowski, E. Le Cam, F. Fabre, The Srs2 helicase prevents recombination by disrupting Rad51 nucleoprotein filaments, *Nature* 423 (2003) 309-312.
  126. M.J. McIlwraith, A. Vaisman, Y. Liu, E. Fanning, R. Woodgate, S.C. West, Human DNA polymerase  $\eta$  promotes DNA synthesis from strand invasion intermediates of homologous recombination, *Mol Cell* 20 (2005) 783-792.
  127. X. Li, C.M. Stith, P.M. Burgers, W.D. Heyer, PCNA is required for initiation of recombination-associated DNA synthesis by DNA polymerase  $\delta$ , *Mol Cell* 36 (2009) 704-713.
  128. L. Maloisel, F. Fabre, S. Gangloff, DNA polymerase  $\delta$  is preferentially recruited during homologous recombination to promote heteroduplex DNA extension, *Mol Cell Biol* 28 (2008) 1373-1382.

129. R. Holliday, The Induction of Mitotic Recombination by Mitomycin C in *Ustilago* and *Saccharomyces*, *Genetics* 50 (1964) 323-335.
130. Y. Liu, S.C. West, Happy Hollidays: 40th anniversary of the Holliday junction, *Nat Rev Mol Cell Biol* 5 (2004) 937-944.
131. D.V. Bugreev, O.M. Mazina, A.V. Mazin, Rad54 protein promotes branch migration of Holliday junctions, *Nature* 442 (2006) 590-593.
132. S.C. Ip, U. Rass, M.G. Blanco, H.R. Flynn, J.M. Skehel, S.C. West, Identification of Holliday junction resolvases from humans and yeast, *Nature* 456 (2008) 357-361.
133. L. Wu, C.Z. Bachrati, J. Ou, C. Xu, J. Yin, M. Chang, W. Wang, L. Li, G.W. Brown, I.D. Hickson, BLAP75/RM1 promotes the BLM-dependent dissolution of homologous recombination intermediates, *Proc Natl Acad Sci U S A* 103 (2006) 4068-4073.
134. L. Wu, I.D. Hickson, The Bloom's syndrome helicase suppresses crossing over during homologous recombination, *Nature* 426 (2003) 870-874.
135. X.B. Chen, R. Melchionna, C.M. Denis, P.H. Gaillard, A. Blasina, I. Van de Weyer, M.N. Boddy, P. Russell, J. Vialard, C.H. McGowan, Human Mus81-associated endonuclease cleaves Holliday junctions in vitro, *Mol Cell* 8 (2001) 1117-1127.
136. A. Ciccia, A. Constantinou, S.C. West, Identification and characterization of the human mus81-eme1 endonuclease, *J Biol Chem* 278 (2003) 25172-25178.
137. A. Constantinou, X.B. Chen, C.H. McGowan, S.C. West, Holliday junction resolution in human cells: two junction endonucleases with distinct substrate specificities, *Embo J* 21 (2002) 5577-5585.
138. E.R. Taylor, C.H. McGowan, Cleavage mechanism of human Mus81-Eme1 acting on Holliday-junction structures, *Proc Natl Acad Sci U S A* 105 (2008) 3757-3762.
139. F. Paques, J.E. Haber, Multiple pathways of recombination induced by double-strand breaks in *Saccharomyces cerevisiae*, *Microbiol Mol Biol Rev* 63 (1999) 349-404.
140. D.V. Bugreev, F. Hanaoka, A.V. Mazin, Rad54 dissociates homologous recombination intermediates by branch migration, *Nat Struct Mol Biol* 14 (2007) 746-753.
141. A.P. Davis, L.S. Symington, RAD51-dependent break-induced replication in yeast, *Mol Cell Biol* 24 (2004) 2344-2351.
142. E. Kraus, W.Y. Leung, J.E. Haber, Break-induced replication: a review and an example in budding yeast, *Proc Natl Acad Sci U S A* 98 (2001) 8255-8262.
143. A. Malkova, M.L. Naylor, M. Yamaguchi, G. Ira, J.E. Haber, RAD51-dependent break-induced replication differs in kinetics and checkpoint responses from RAD51-mediated gene conversion, *Mol Cell Biol* 25 (2005) 933-944.
144. M.J. McEachern, J.E. Haber, Break-induced replication and recombinational telomere elongation in yeast, *Annu Rev Biochem* 75 (2006) 111-135.
145. C.E. Smith, B. Llorente, L.S. Symington, Template switching during break-induced replication, *Nature* 447 (2007) 102-105.
146. J. Falck, J. Coates, S.P. Jackson, Conserved modes of recruitment of ATM, ATR and DNA-PKcs to sites of DNA damage, *Nature* 434 (2005) 605-611.
147. K. Cerosaletti, J. Wright, P. Concannon, Active role for nibrin in the kinetics of atm activation, *Mol Cell Biol* 26 (2006) 1691-1699.
148. E. Baroni, V. Viscardi, H. Cartagena-Lirola, G. Lucchini, M.P. Longhese, The functions of budding yeast Sae2 in the DNA damage response require Mec1- and Tel1-dependent phosphorylation, *Mol Cell Biol* 24 (2004) 4151-4165.
149. W.S. Dynan, S. Yoo, Interaction of Ku protein and DNA-dependent protein kinase catalytic subunit with nucleic acids, *Nucleic Acids Res* 26 (1998) 1551-1559.
150. M. Clerici, D. Mantiero, I. Guerini, G. Lucchini, M.P. Longhese, The Yku70-Yku80 complex contributes to regulate double-strand break processing and checkpoint activation during the cell cycle, *EMBO Rep* 9 (2008) 810-818.
151. C. Zierhut, J.F. Diffley, Break dosage, cell cycle stage and DNA replication influence DNA double strand break response, *Embo J* 27 (2008) 1875-1885.
152. Y. Aylon, B. Liefshitz, M. Kupiec, The CDK regulates repair of double-strand breaks by homologous recombination during the cell cycle, *Embo J* 23 (2004) 4868-4875.
153. P. Huertas, F. Cortes-Ledesma, A.A. Sartori, A. Aguilera, S.P. Jackson, CDK targets Sae2 to control DNA-end resection and homologous recombination, *Nature* 455 (2008) 689-692.

154. G. Ira, A. Pelliccioli, A. Balijja, X. Wang, S. Fiorani, W. Carotenuto, G. Liberi, D. Bressan, L. Wan, N.M. Hollingsworth, J.E. Haber, M. Foiani, DNA end resection, homologous recombination and DNA damage checkpoint activation require CDK1, *Nature* 431 (2004) 1011-1017.
155. A. Jazayeri, J. Falck, C. Lukas, J. Bartek, G.C. Smith, J. Lukas, S.P. Jackson, ATM- and cell cycle-dependent regulation of ATR in response to DNA double-strand breaks, *Nat Cell Biol* 8 (2006) 37-45.
156. F. Lazzaro, V. Sapountzi, M. Granata, A. Pelliccioli, M. Vaze, J.E. Haber, P. Plevani, D. Lydall, M. Muzi-Falconi, Histone methyltransferase Dot1 and Rad9 inhibit single-stranded DNA accumulation at DSBs and uncapped telomeres, *Embo J* 27 (2008) 1502-1512.
157. M. Grenon, T. Costelloe, S. Jimeno, A. O'Shaughnessy, J. Fitzgerald, O. Zgheib, L. Degerth, N.F. Lowndes, Docking onto chromatin via the *Saccharomyces cerevisiae* Rad9 Tudor domain, *Yeast* 24 (2007) 105-119.
158. R. Linding, L.J. Jensen, G.J. Ostheimer, M.A. van Vugt, C. Jorgensen, I.M. Miron, F. Diella, K. Colwill, L. Taylor, K. Elder, P. Metalnikov, V. Nguyen, A. Pasculescu, J. Jin, J.G. Park, L.D. Samson, J.R. Woodgett, R.B. Russell, P. Bork, M.B. Yaffe, T. Pawson, Systematic discovery of in vivo phosphorylation networks, *Cell* 129 (2007) 1415-1426.
159. X. Yu, J. Chen, DNA damage-induced cell cycle checkpoint control requires CtIP, a phosphorylation-dependent binding partner of BRCA1 C-terminal domains, *Mol Cell Biol* 24 (2004) 9478-9486.
160. S.F. Bunting, E. Callen, N. Wong, H.T. Chen, F. Polato, A. Gunn, A. Bothmer, N. Feldhahn, O. Fernandez-Capetillo, L. Cao, X. Xu, C.X. Deng, T. Finkel, M. Nussenzweig, J.M. Stark, A. Nussenzweig, 53BP1 inhibits homologous recombination in *Brc1*-deficient cells by blocking resection of DNA breaks, *Cell* 141 243-254.
161. P. Huertas, DNA resection in eukaryotes: deciding how to fix the break, *Nat Struct Mol Biol* 17 11-16.
162. H.D. Ulrich, The RAD6 pathway: control of DNA damage bypass and mutagenesis by ubiquitin and SUMO, *Chembiochem* 6 (2005) 1735-1743.
163. G.L. Moldovan, B. Pfander, S. Jentsch, PCNA, the maestro of the replication fork, *Cell* 129 (2007) 665-679.
164. S. Prakash, R.E. Johnson, L. Prakash, Eukaryotic translesion synthesis DNA polymerases: specificity of structure and function, *Annu Rev Biochem* 74 (2005) 317-353.
165. C. Lawrence, The RAD6 repair pathway in *Saccharomyces cerevisiae*: what does it do, and how does it do it?, *BioEssays* 16 (1994) 253-258.
166. C.M. Pickart, M.J. Eddins, Ubiquitin: structures, functions, mechanisms, *Biochim Biophys Acta* 1695 (2004) 55-72.
167. D. Voges, P. Zwickl, W. Baumeister, The 26S proteasome: a molecular machine designed for controlled proteolysis, *Annu Rev Biochem* 68 (1999) 1015-1068.
168. J.M. Galan, R. Haguenaer-Tsapis, Ubiquitin lys63 is involved in ubiquitination of a yeast plasma membrane protein, *Embo J* 16 (1997) 5847-5854.
169. J. Spence, R.R. Gali, G. Dittmar, F. Sherman, M. Karin, D. Finley, Cell cycle-regulated modification of the ribosome by a variant multiubiquitin chain, *Cell* 102 (2000) 67-76.
170. J. Spence, S. Sadis, A.L. Haas, D. Finley, A ubiquitin mutant with specific defects in DNA repair and multiubiquitination, *Mol Cell Biol* 15 (1995) 1265-1273.
171. M.S. Huen, R. Grant, I. Manke, K. Minn, X. Yu, M.B. Yaffe, J. Chen, RNF8 transduces the DNA-damage signal via histone ubiquitylation and checkpoint protein assembly, *Cell* 131 (2007) 901-914.
172. N.K. Kolas, J.R. Chapman, S. Nakada, J. Ylanko, R. Chahwan, F.D. Sweeney, S. Panier, M. Mendez, J. Wildenhain, T.M. Thomson, L. Pelletier, S.P. Jackson, D. Durocher, Orchestration of the DNA-damage response by the RNF8 ubiquitin ligase, *Science* 318 (2007) 1637-1640.
173. N. Mailand, S. Bekker-Jensen, H. Faustrup, F. Melander, J. Bartek, C. Lukas, J. Lukas, RNF8 ubiquitylates histones at DNA double-strand breaks and promotes assembly of repair proteins, *Cell* 131 (2007) 887-900.
174. R.J. Deshaies, C.A. Joazeiro, RING domain E3 ubiquitin ligases, *Annu Rev Biochem* 78 (2009) 399-434.
175. C. Hoege, B. Pfander, G.L. Moldovan, G. Pyrowolakis, S. Jentsch, RAD6-dependent DNA repair is linked to modification of PCNA by ubiquitin and SUMO, *Nature* 419 (2002) 135-141.
176. H. Xin, W. Lin, W. Sumanasekera, Y. Zhang, X. Wu, Z. Wang, The human

- RAD18 gene product interacts with HHR6A and HHR6B, *Nucleic Acids Res* 28 (2000) 2847-2854.
177. P.L. Kannouche, J. Wing, A.R. Lehmann, Interaction of human DNA polymerase  $\eta$  with monoubiquitinated PCNA: a possible mechanism for the polymerase switch in response to DNA damage, *Mol Cell* 14 (2004) 491-500.
  178. K. Watanabe, S. Tateishi, M. Kawasuji, T. Tsurimoto, H. Inoue, M. Yamaizumi, Rad18 guides  $\eta$  to replication stalling sites through physical interaction and PCNA monoubiquitination, *Embo J* 23 (2004) 3886-3896.
  179. A.R. Lehmann, A. Niimi, T. Ogi, S. Brown, S. Sabbioneda, J.F. Wing, P.L. Kannouche, C.M. Green, Translesion synthesis: Y-family polymerases and the polymerase switch, *DNA Repair (Amst)* 6 (2007) 891-899.
  180. W. Yang, R. Woodgate, What a difference a decade makes: insights into translesion DNA synthesis, *Proc Natl Acad Sci U S A* 104 (2007) 15591-15598.
  181. C. Masutani, R. Kusumoto, S. Iwai, F. Hanaoka, Mechanisms of accurate translesion synthesis by human DNA polymerase  $\eta$ , *Embo J* 19 (2000) 3100-3109.
  182. T. Matsuda, K. Bebenek, C. Masutani, F. Hanaoka, T.A. Kunkel, Low fidelity DNA synthesis by human DNA polymerase- $\eta$ , *Nature* 404 (2000) 1011-1013.
  183. J.P. McDonald, V. Ropic-Otrin, J.A. Epstein, B.C. Broughton, X. Wang, A.R. Lehmann, D.J. Wolgemuth, R. Woodgate, Novel human and mouse homologs of *Saccharomyces cerevisiae* DNA polymerase  $\eta$ , *Genomics* 60 (1999) 20-30.
  184. E. Ohashi, K. Bebenek, T. Matsuda, W.J. Feaver, V.L. Gerlach, E.C. Friedberg, H. Ohmori, T.A. Kunkel, Fidelity and processivity of DNA synthesis by DNA polymerase  $\kappa$ , the product of the human DINB1 gene, *J Biol Chem* 275 (2000) 39678-39684.
  185. R.E. Johnson, M.T. Washington, L. Haracska, S. Prakash, L. Prakash, Eukaryotic polymerases  $\iota$  and  $\zeta$  act sequentially to bypass DNA lesions, *Nature* 406 (2000) 1015-1019.
  186. A. Tissier, E.G. Frank, J.P. McDonald, S. Iwai, F. Hanaoka, R. Woodgate, Misinsertion and bypass of thymine-thymine dimers by human DNA polymerase  $\iota$ , *Embo J* 19 (2000) 5259-5266.
  187. W. Lin, H. Xin, Y. Zhang, X. Wu, F. Yuan, Z. Wang, The human REV1 gene codes for a DNA template-dependent dCMP transferase, *Nucleic Acids Res* 27 (1999) 4468-4475.
  188. P.E. Gibbs, W.G. McGregor, V.M. Maher, P. Nisson, C.W. Lawrence, A human homolog of the *Saccharomyces cerevisiae* REV3 gene, which encodes the catalytic subunit of DNA polymerase  $\zeta$ , *Proc Natl Acad Sci U S A* 95 (1998) 6876-6880.
  189. P.E. Gibbs, X.D. Wang, Z. Li, T.P. McManus, W.G. McGregor, C.W. Lawrence, V.M. Maher, The function of the human homolog of *Saccharomyces cerevisiae* REV1 is required for mutagenesis induced by UV light, *Proc Natl Acad Sci U S A* 97 (2000) 4186-4191.
  190. V. Khare, K.A. Eckert, The 3'  $\rightarrow$  5' exonuclease of T4 DNA polymerase removes premutagenic alkyl mispairs and contributes to futile cycling at O6-methylguanine lesions, *J Biol Chem* 276 (2001) 24286-24292.
  191. V. Khare, K.A. Eckert, The proofreading 3'  $\rightarrow$  5' exonuclease activity of DNA polymerases: a kinetic barrier to translesion DNA synthesis, *Mutat Res* 510 (2002) 45-54.
  192. D.J. Chang, K.A. Cimprich, DNA damage tolerance: when it's OK to make mistakes, *Nature chemical biology* 5 (2009) 82-90.
  193. M. Bienko, C.M. Green, N. Crosetto, F. Rudolf, G. Zapart, B. Coull, P. Kannouche, G. Wider, M. Peter, A.R. Lehmann, K. Hofmann, I. Dikic, Ubiquitin-binding domains in Y-family polymerases regulate translesion synthesis, *Science* 310 (2005) 1821-1824.
  194. W. Xiao, B.L. Chow, S. Broomfield, M. Hanna, The *Saccharomyces cerevisiae* RAD6 group is composed of an error-prone and two error-free postreplication repair pathways, *Genetics* 155 (2000) 1633-1641.
  195. A. Motegi, H.J. Liaw, K.Y. Lee, H.P. Roest, A. Maas, X. Wu, H. Moinova, S.D. Markowitz, H. Ding, J.H. Hoeijmakers, K. Myung, Polyubiquitination of proliferating cell nuclear antigen by HLTf and SHPRH prevents genomic instability from stalled replication forks, *Proc Natl Acad Sci U S A* 105 (2008) 12411-12416.
  196. A. Motegi, R. Sood, H. Moinova, S.D. Markowitz, P.P. Liu, K. Myung, Human SHPRH suppresses genomic instability through proliferating cell nuclear antigen polyubiquitination, *J Cell Biol* 175 (2006) 703-708.

197. I. Unk, I. Hajdu, K. Fatyol, J. Hurwitz, J.H. Yoon, L. Prakash, S. Prakash, L. Haracska, Human HLTf functions as a ubiquitin ligase for proliferating cell nuclear antigen polyubiquitination, *Proc Natl Acad Sci U S A* 105 (2008) 3768-3773.
198. I. Unk, I. Hajdu, K. Fatyol, B. Szakal, A. Blastyak, V. Bermudez, J. Hurwitz, L. Prakash, S. Prakash, L. Haracska, Human SHPRH is a ubiquitin ligase for Mms2-Ubc13-dependent polyubiquitylation of proliferating cell nuclear antigen, *Proc Natl Acad Sci U S A* 103 (2006) 18107-18112.
199. R.K. Chiu, J. Brun, C. Ramaekers, J. Theys, L. Weng, P. Lambin, D.A. Gray, B.G. Wouters, Lysine 63-polyubiquitination guards against translesion synthesis-induced mutations, *PLoS Genet* 2 (2006) e116.
200. S. Bergink, S. Jentsch, Principles of ubiquitin and SUMO modifications in DNA repair, *Nature* 458 (2009) 461-467.
201. E. Papouli, S. Chen, A.A. Davies, D. Huttner, L. Krejci, P. Sung, H.D. Ulrich, Crosstalk between SUMO and ubiquitin on PCNA is mediated by recruitment of the helicase Srs2p, *Mol Cell* 19 (2005) 123-133.
202. B. Pfander, G.L. Moldovan, M. Sacher, C. Hoege, S. Jentsch, SUMO-modified PCNA recruits Srs2 to prevent recombination during S phase, *Nature* 436 (2005) 428-433.
203. T. Robert, D. Dervins, F. Fabre, S. Gangloff, Mrc1 and Srs2 are major actors in the regulation of spontaneous crossover, *Embo J* 25 (2006) 2837-2846.
204. D. Branzei, F. Vanoli, M. Foiani, SUMOylation regulates Rad18-mediated template switch, *Nature* 456 (2008) 915-920.
205. S. Tateishi, H. Niwa, J. Miyazaki, S. Fujimoto, H. Inoue, M. Yamaizumi, Enhanced genomic instability and defective postreplication repair in RAD18 knockout mouse embryonic stem cells, *Mol Cell Biol* 23 (2003) 474-481.
206. I. Chiolo, M. Saponaro, A. Baryshnikova, J.H. Kim, Y.S. Seo, G. Liberi, The human F-Box DNA helicase FBH1 faces *Saccharomyces cerevisiae* Srs2 and postreplication repair pathway roles, *Mol Cell Biol* 27 (2007) 7439-7450.
207. K. Fugger, M. Mistrik, J.R. Danielsen, C. Dinant, J. Falck, J. Bartek, J. Lukas, N. Mailand, Human Fbh1 helicase contributes to genome maintenance via pro- and anti-recombinase activities, *J Cell Biol* 186 (2009) 655-663.
208. J. Kim, J.H. Kim, S.H. Lee, D.H. Kim, H.Y. Kang, S.H. Bae, Z.Q. Pan, Y.S. Seo, The novel human DNA helicase hFBH1 is an F-box protein, *J Biol Chem* 277 (2002) 24530-24537.
209. M. Kohzaki, A. Hatanaka, E. Sonoda, M. Yamazoe, K. Kikuchi, N. Vu Trung, D. Szuts, J.E. Sale, H. Shinagawa, M. Watanabe, S. Takeda, Cooperative roles of vertebrate Fbh1 and Blm DNA helicases in avoidance of crossovers during recombination initiated by replication fork collapse, *Mol Cell Biol* 27 (2007) 2812-2820.
210. C.Z. Bachrati, R.H. Borts, I.D. Hickson, Mobile D-loops are a preferred substrate for the Bloom's syndrome helicase, *Nucleic Acids Res* 34 (2006) 2269-2279.
211. C.Z. Bachrati, I.D. Hickson, Dissolution of double Holliday junctions by the concerted action of BLM and topoisomerase IIIalpha, *Methods Mol Biol* 582 (2009) 91-102.
212. D.V. Bugreev, R.M. Brosh, Jr., A.V. Mazin, RECQ1 possesses DNA branch migration activity, *J Biol Chem* 283 (2008) 20231-20242.
213. D.V. Bugreev, O.M. Mazina, A.V. Mazin, Bloom syndrome helicase stimulates RAD51 DNA strand exchange activity through a novel mechanism, *J Biol Chem* 284 (2009) 26349-26359.
214. D.V. Bugreev, X. Yu, E.H. Egelman, A.V. Mazin, Novel pro- and anti-recombination activities of the Bloom's syndrome helicase, *Genes Dev* 21 (2007) 3085-3094.
215. Y. Hu, X. Lu, E. Barnes, M. Yan, H. Lou, G. Luo, Recq15 and Blm RecQ DNA helicases have nonredundant roles in suppressing crossovers, *Mol Cell Biol* 25 (2005) 3431-3442.
216. Y. Hu, S. Raynard, M.G. Sehorn, X. Lu, W. Bussen, L. Zheng, J.M. Stark, E.L. Barnes, P. Chi, P. Janscak, M. Jasin, H. Vogel, P. Sung, G. Luo, RECQL5/Recq15 helicase regulates homologous recombination and suppresses tumor formation via disruption of Rad51 presynaptic filaments, *Genes Dev* 21 (2007) 3073-3084.
217. L.J. Barber, J.L. Youds, J.D. Ward, M.J. McIlwraith, N.J. O'Neil, M.I. Petalcorin, J.S. Martin, S.J. Collis, S.B. Cantor, M. Auclair, H. Tissenbaum, S.C. West, A.M. Rose, S.J. Boulton, RTEL1 maintains genomic stability by suppressing homologous recombination, *Cell* 135 (2008) 261-271.

218. R.T. Abraham, Cell cycle checkpoint signaling through the ATM and ATR kinases, *Genes Dev* 15 (2001) 2177-2196.
219. M.B. Kastan, J. Bartek, Cell-cycle checkpoints and cancer, *Nature* 432 (2004) 316-323.
220. Y. Shiloh, ATM and related protein kinases: safeguarding genome integrity, *Nat Rev Cancer* 3 (2003) 155-168.
221. J. Rouse, S.P. Jackson, Interfaces between the detection, signaling, and repair of DNA damage, *Science* 297 (2002) 547-551.
222. J. Melo, D. Toczyski, A unified view of the DNA-damage checkpoint, *Curr Opin Cell Biol* 14 (2002) 237-245.
223. J.A. Melo, J. Cohen, D.P. Toczyski, Two checkpoint complexes are independently recruited to sites of DNA damage in vivo, *Genes Dev* 15 (2001) 2809-2821.
224. B.B. Zhou, S.J. Elledge, The DNA damage response: putting checkpoints in perspective, *Nature* 408 (2000) 433-439.
225. M. Dinkelman, E. Spehalski, T. Stoneham, J. Buis, Y. Wu, J.M. Sekiguchi, D.O. Ferguson, Multiple functions of MRN in end-joining pathways during isotype class switching, *Nat Struct Mol Biol* 16 (2009) 808-813.
226. E. Rass, A. Grabarz, I. Plo, J. Gautier, P. Bertrand, B.S. Lopez, Role of Mre11 in chromosomal nonhomologous end joining in mammalian cells, *Nat Struct Mol Biol* 16 (2009) 819-824.
227. A. Xie, A. Kwok, R. Scully, Role of mammalian Mre11 in classical and alternative nonhomologous end joining, *Nat Struct Mol Biol* 16 (2009) 814-818.
228. E.R. Parrilla-Castellar, S.J. Arlander, L. Karnitz, Dial 9-1-1 for DNA damage: the Rad9-Hus1-Rad1 (9-1-1) clamp complex, *DNA Repair (Amst)* 3 (2004) 1009-1014.
229. H.L. Ball, M.R. Ehrhardt, D.A. Mordes, G.G. Glick, W.J. Chazin, D. Cortez, Function of a conserved checkpoint recruitment domain in ATRIP proteins, *Mol Cell Biol* 27 (2007) 3367-3377.
230. D. Cortez, S. Guntuku, J. Qin, S.J. Elledge, ATR and ATRIP: partners in checkpoint signaling, *Science* 294 (2001) 1713-1716.
231. G.C. Smith, F. d'Adda di Fagnana, N.D. Lakin, S.P. Jackson, Cleavage and inactivation of ATM during apoptosis, *Mol Cell Biol* 19 (1999) 6076-6084.
232. K. Unsal-Kacmaz, A.M. Makhov, J.D. Griffith, A. Sancar, Preferential binding of ATR protein to UV-damaged DNA, *Proc Natl Acad Sci U S A* 99 (2002) 6673-6678.
233. K.A. Cimprich, D. Cortez, ATR: an essential regulator of genome integrity, *Nat Rev Mol Cell Biol* 9 (2008) 616-627.
234. A. Sancar, L.A. Lindsey-Boltz, K. Unsal-Kacmaz, S. Linn, Molecular mechanisms of mammalian DNA repair and the DNA damage checkpoints, *Annu Rev Biochem* 73 (2004) 39-85.
235. C.J. Bakkenist, M.B. Kastan, DNA damage activates ATM through intermolecular autophosphorylation and dimer dissociation, *Nature* 421 (2003) 499-506.
236. C.T. Carson, R.A. Schwartz, T.H. Stracker, C.E. Lilley, D.V. Lee, M.D. Weitzman, The Mre11 complex is required for ATM activation and the G2/M checkpoint, *Embo J* 22 (2003) 6610-6620.
237. R. Kitagawa, C.J. Bakkenist, P.J. McKinnon, M.B. Kastan, Phosphorylation of SMC1 is a critical downstream event in the ATM-NBS1-BRCA1 pathway, *Genes Dev* 18 (2004) 1423-1438.
238. E.P. Rogakou, D.R. Pilch, A.H. Orr, V.S. Ivanova, W.M. Bonner, DNA double-stranded breaks induce histone H2AX phosphorylation on serine 139, *J Biol Chem* 273 (1998) 5858-5868.
239. M. Stucki, J.A. Clapperton, D. Mohammad, M.B. Yaffe, S.J. Smerdon, S.P. Jackson, MDC1 directly binds phosphorylated histone H2AX to regulate cellular responses to DNA double-strand breaks, *Cell* 123 (2005) 1213-1226.
240. K. Minter-Dykhouse, I. Ward, M.S. Huen, J. Chen, Z. Lou, Distinct versus overlapping functions of MDC1 and 53BP1 in DNA damage response and tumorigenesis, *J Cell Biol* 181 (2008) 727-735.
241. A. Xie, A. Hartlerode, M. Stucki, S. Odate, N. Puget, A. Kwok, G. Nagaraju, C. Yan, F.W. Alt, J. Chen, S.P. Jackson, R. Scully, Distinct roles of chromatin-associated proteins MDC1 and 53BP1 in mammalian double-strand break repair, *Mol Cell* 28 (2007) 1045-1057.
242. J.R. Chapman, S.P. Jackson, Phospho-dependent interactions between NBS1 and MDC1 mediate chromatin retention of the MRN complex at sites of DNA damage, *EMBO Rep* 9 (2008) 795-801.
243. M. Goldberg, M. Stucki, J. Falck, D. D'Amours, D. Rahman, D. Pappin, J. Bartek, S.P. Jackson, MDC1 is required for the intra-S-phase DNA damage checkpoint, *Nature* 421 (2003) 952-956.
244. F. Melander, S. Bekker-Jensen, J. Falck, J. Bartek, N. Mailand, J. Lukas,

- Phosphorylation of SDT repeats in the MDC1 N terminus triggers retention of NBS1 at the DNA damage-modified chromatin, *J Cell Biol* 181 (2008) 213-226.
245. C. Spycher, E.S. Miller, K. Townsend, L. Pavic, N.A. Morrice, P. Janscak, G.S. Stewart, M. Stucki, Constitutive phosphorylation of MDC1 physically links the MRE11-RAD50-NBS1 complex to damaged chromatin, *J Cell Biol* 181 (2008) 227-240.
246. Z. You, C. Chahwan, J. Bailis, T. Hunter, P. Russell, ATM activation and its recruitment to damaged DNA require binding to the C terminus of Nbs1, *Mol Cell Biol* 25 (2005) 5363-5379.
247. V. Plans, J. Scheper, M. Soler, N. Loukili, Y. Okano, T.M. Thomson, The RING finger protein RNF8 recruits UBC13 for lysine 63-based self polyubiquitylation, *J Cell Biochem* 97 (2006) 572-582.
248. G.S. Stewart, S. Panier, K. Townsend, A.K. Al-Hakim, N.K. Kolas, E.S. Miller, S. Nakada, J. Ylanko, S. Olivarius, M. Mendez, C. Oldreive, J. Wildenhain, A. Tagliaferro, L. Pelletier, N. Taubenheim, A. Durandy, P.J. Byrd, T. Stankovic, A.M. Taylor, D. Durocher, The RIDDLE syndrome protein mediates a ubiquitin-dependent signaling cascade at sites of DNA damage, *Cell* 136 (2009) 420-434.
249. G.S. Stewart, T. Stankovic, P.J. Byrd, T. Wechsler, E.S. Miller, A. Huissoon, M.T. Drayson, S.C. West, S.J. Elledge, A.M. Taylor, RIDDLE immunodeficiency syndrome is linked to defects in 53BP1-mediated DNA damage signaling, *Proc Natl Acad Sci U S A* 104 (2007) 16910-16915.
250. C. Doil, N. Mailand, S. Bekker-Jensen, P. Menard, D.H. Larsen, R. Pepperkok, J. Ellenberg, S. Panier, D. Durocher, J. Bartek, J. Lukas, C. Lukas, RNF168 binds and amplifies ubiquitin conjugates on damaged chromosomes to allow accumulation of repair proteins, *Cell* 136 (2009) 435-446.
251. H. Kim, J. Chen, X. Yu, Ubiquitin-binding protein RAP80 mediates BRCA1-dependent DNA damage response, *Science* 316 (2007) 1202-1205.
252. B. Sobhian, G. Shao, D.R. Lilli, A.C. Culhane, L.A. Moreau, B. Xia, D.M. Livingston, R.A. Greenberg, RAP80 targets BRCA1 to specific ubiquitin structures at DNA damage sites, *Science* 316 (2007) 1198-1202.
253. B. Wang, S. Matsuoka, B.A. Ballif, D. Zhang, A. Smogorzewska, S.P. Gygi, S.J. Elledge, Abraxas and RAP80 form a BRCA1 protein complex required for the DNA damage response, *Science* 316 (2007) 1194-1198.
254. J. Yan, Y.S. Kim, X.P. Yang, L.P. Li, G. Liao, F. Xia, A.M. Jetten, The ubiquitin-interacting motif containing protein RAP80 interacts with BRCA1 and functions in DNA damage repair response, *Cancer Res* 67 (2007) 6647-6656.
255. M.V. Botuyan, J. Lee, I.M. Ward, J.E. Kim, J.R. Thompson, J. Chen, G. Mer, Structural basis for the methylation state-specific recognition of histone H4-K20 by 53BP1 and Crb2 in DNA repair, *Cell* 127 (2006) 1361-1373.
256. Y. Huyen, O. Zgheib, R.A. Ditullio, Jr., V.G. Gorgoulis, P. Zacharatos, T.J. Petty, E.A. Sheston, H.S. Mellert, E.S. Stavridi, T.D. Halazonetis, Methylated lysine 79 of histone H3 targets 53BP1 to DNA double-strand breaks, *Nature* 432 (2004) 406-411.
257. G. Schotta, R. Sengupta, S. Kubicek, S. Malin, M. Kauer, E. Callen, A. Celeste, M. Pagani, S. Opravil, I.A. De La Rosa-Velazquez, A. Espejo, M.T. Bedford, A. Nussenzweig, M. Busslinger, T. Jenuwein, A chromatin-wide transition to H4K20 monomethylation impairs genome integrity and programmed DNA rearrangements in the mouse, *Genes Dev* 22 (2008) 2048-2061.
258. H. Yang, J.J. Pesavento, T.W. Starnes, D.E. Cryderman, L.L. Wallrath, N.L. Kelleher, C.A. Mizzen, Preferential dimethylation of histone H4 lysine 20 by Suv4-20, *J Biol Chem* 283 (2008) 12085-12092.
259. S.L. Sanders, M. Portoso, J. Mata, J. Bahler, R.C. Allshire, T. Kouzarides, Methylation of histone H4 lysine 20 controls recruitment of Crb2 to sites of DNA damage, *Cell* 119 (2004) 603-614.
260. B. Alpha-Bazin, A. Lorphelin, N. Nozerand, G. Charier, C. Marchetti, F. Berenguer, J. Couprie, B. Gilquin, S. Zinn-Justin, E. Quemeneur, Boundaries and physical characterization of a new domain shared between mammalian 53BP1 and yeast Rad9 checkpoint proteins, *Protein Sci* 14 (2005) 1827-1839.
261. G. Charier, J. Couprie, B. Alpha-Bazin, V. Meyer, E. Quemeneur, R. Guerois, I. Callebaut, B. Gilquin, S. Zinn-Justin, The Tudor tandem of 53BP1: a new structural motif involved in DNA and RG-rich peptide binding, *Structure* 12 (2004) 1551-1562.

262. N. Lancelot, G. Charier, J. Couprie, I. Duband-Goulet, B. Alpha-Bazin, E. Quemeneur, E. Ma, M.C. Marsolier-Kergoat, V. Ropars, J.B. Charbonnier, S. Miron, C.T. Craescu, I. Callebaut, B. Gilquin, S. Zinn-Justin, The checkpoint *Saccharomyces cerevisiae* Rad9 protein contains a tandem tudor domain that recognizes DNA, *Nucleic Acids Res* 35 (2007) 5898-5912.
263. O. Zgheib, K. Pataky, J. Brugger, T.D. Halazonetis, An oligomerized 53BP1 tudor domain suffices for recognition of DNA double-strand breaks, *Mol Cell Biol* 29 (2009) 1050-1058.
264. Y. Galanty, R. Belotserkovskaya, J. Coates, S. Polo, K.M. Miller, S.P. Jackson, Mammalian SUMO E3-ligases PIAS1 and PIAS4 promote responses to DNA double-strand breaks, *Nature* 462 (2009) 935-939.
265. J.R. Morris, C. Boutell, M. Keppler, R. Densham, D. Weekes, A. Alamshah, L. Butler, Y. Galanty, L. Pangon, T. Kiuchi, T. Ng, E. Solomon, The SUMO modification pathway is involved in the BRCA1 response to genotoxic stress, *Nature* 462 (2009) 886-890.
266. L. Anderson, C. Henderson, Y. Adachi, Phosphorylation and rapid relocalization of 53BP1 to nuclear foci upon DNA damage, *Mol Cell Biol* 21 (2001) 1719-1729.
267. R.A. DiTullio, Jr., T.A. Mochan, M. Venere, J. Bartkova, M. Sehested, J. Bartek, T.D. Halazonetis, 53BP1 functions in an ATM-dependent checkpoint pathway that is constitutively activated in human cancer, *Nat Cell Biol* 4 (2002) 998-1002.
268. O. Fernandez-Capetillo, H.T. Chen, A. Celeste, I. Ward, P.J. Romanienko, J.C. Morales, K. Naka, Z. Xia, R.D. Camerini-Otero, N. Motoyama, P.B. Carpenter, W.M. Bonner, J. Chen, A. Nussenzweig, DNA damage-induced G2-M checkpoint activation by histone H2AX and 53BP1, *Nat Cell Biol* 4 (2002) 993-997.
269. D. Cortez, Y. Wang, J. Qin, S.J. Elledge, Requirement of ATM-Dependent phosphorylation of *brca1* in the DNA damage response to double-strand breaks, *Science* 286 (1999) 1162-1166.
270. S. Okada, T. Ouchi, Cell cycle differences in DNA damage-induced BRCA1 phosphorylation affect its subcellular localization, *J Biol Chem* 278 (2003) 2015-2020.
271. J. Zhang, H. Willers, Z. Feng, J.C. Ghosh, S. Kim, D.T. Weaver, J.H. Chung, S.N. Powell, F. Xia, Chk2 phosphorylation of BRCA1 regulates DNA double-strand break repair, *Mol Cell Biol* 24 (2004) 708-718.
272. J. Silverman, H. Takai, S.B. Buonomo, F. Eisenhaber, T. de Lange, Human Rif1, ortholog of a yeast telomeric protein, is regulated by ATM and 53BP1 and functions in the S-phase checkpoint, *Genes Dev* 18 (2004) 2108-2119.
273. A. Celeste, O. Fernandez-Capetillo, M.J. Kruhlak, D.R. Pilch, D.W. Staudt, A. Lee, R.F. Bonner, W.M. Bonner, A. Nussenzweig, Histone H2AX phosphorylation is dispensable for the initial recognition of DNA breaks, *Nat Cell Biol* 5 (2003) 675-679.
274. A. Shibata, O. Barton, A.T. Noon, K. Dahm, D. Deckbar, A.A. Goodarzi, M. Lobrich, P.A. Jeggo, The role of ATM and the damage response mediator proteins, 53BP1 and MDC1, in the maintenance of G2/M checkpoint arrest, *Mol Cell Biol*.
275. B. Wang, S. Matsuoka, P.B. Carpenter, S.J. Elledge, 53BP1, a mediator of the DNA damage checkpoint, *Science* 298 (2002) 1435-1438.
276. J.C. Harrison, J.E. Haber, Surviving the breakup: the DNA damage checkpoint, *Annu Rev Genet* 40 (2006) 209-235.
277. X. Xu, W. Qiao, S.P. Linke, L. Cao, W.M. Li, P.A. Furth, C.C. Harris, C.X. Deng, Genetic interactions between tumor suppressors *Brcal* and *p53* in apoptosis, cell cycle and tumorigenesis, *Nat Genet* 28 (2001) 266-271.
278. L. Cao, S. Kim, C. Xiao, R.H. Wang, X. Coumoul, X. Wang, W.M. Li, X.L. Xu, J.A. De Soto, H. Takai, S. Mai, S.J. Elledge, N. Motoyama, C.X. Deng, ATM-Chk2-p53 activation prevents tumorigenesis at an expense of organ homeostasis upon *Brcal* deficiency, *Embo J* 25 (2006) 2167-2177.
279. L. Zou, D. Cortez, S.J. Elledge, Regulation of ATR substrate selection by Rad17-dependent loading of Rad9 complexes onto chromatin, *Genes Dev* 16 (2002) 198-208.
280. L. Zou, S.J. Elledge, Sensing DNA damage through ATRIP recognition of RPA-ssDNA complexes, *Science* 300 (2003) 1542-1548.
281. A. Maya-Mendoza, E. Petermann, D.A. Gillespie, K.W. Caldecott, D.A. Jackson, Chk1 regulates the density of active replication origins during the vertebrate S phase, *Embo J* 26 (2007) 2719-2731.

282. D. Shechter, V. Costanzo, J. Gautier, ATR and ATM regulate the timing of DNA replication origin firing, *Nat Cell Biol* 6 (2004) 648-655.
283. S.L. Davies, P.S. North, A. Dart, N.D. Lakin, I.D. Hickson, Phosphorylation of the Bloom's syndrome helicase and its role in recovery from S-phase arrest, *Mol Cell Biol* 24 (2004) 1279-1291.
284. W. Li, S.M. Kim, J. Lee, W.G. Dunphy, Absence of BLM leads to accumulation of chromosomal DNA breaks during both unperturbed and disrupted S phases, *J Cell Biol* 165 (2004) 801-812.
285. P. Pichierri, F. Rosselli, A. Franchitto, Werner's syndrome protein is phosphorylated in an ATR/ATM-dependent manner following replication arrest and DNA damage induced during the S phase of the cell cycle, *Oncogene* 22 (2003) 1491-1500.
286. R.S. Tibbetts, D. Cortez, K.M. Brumbaugh, R. Scully, D. Livingston, S.J. Elledge, R.T. Abraham, Functional interactions between BRCA1 and the checkpoint kinase ATR during genotoxic stress, *Genes Dev* 14 (2000) 2989-3002.
287. E. Fanning, V. Klimovich, A.R. Nager, A dynamic model for replication protein A (RPA) function in DNA processing pathways, *Nucleic Acids Res* 34 (2006) 4126-4137.
288. T.S. Byun, M. Pacek, M.C. Yee, J.C. Walter, K.A. Cimprich, Functional uncoupling of MCM helicase and DNA polymerase activities activates the ATR-dependent checkpoint, *Genes Dev* 19 (2005) 1040-1052.
289. C.A. MacDougall, T.S. Byun, C. Van, M.C. Yee, K.A. Cimprich, The structural determinants of checkpoint activation, *Genes Dev* 21 (2007) 898-903.
290. S. Yan, W.M. Michael, TopBP1 and DNA polymerase- $\alpha$  directly recruit the 9-1-1 complex to stalled DNA replication forks, *J Cell Biol* 184 (2009) 793-804.
291. S. Delacroix, J.M. Wagner, M. Kobayashi, K. Yamamoto, L.M. Karnitz, The Rad9-Hus1-Rad1 (9-1-1) clamp activates checkpoint signaling via TopBP1, *Genes Dev* 21 (2007) 1472-1477.
292. K. Furuya, M. Poitelea, L. Guo, T. Caspari, A.M. Carr, Chk1 activation requires Rad9 S/TQ-site phosphorylation to promote association with C-terminal BRCT domains of Rad4TOPBP1, *Genes Dev* 18 (2004) 1154-1164.
293. A. Kumagai, J. Lee, H.Y. Yoo, W.G. Dunphy, TopBP1 activates the ATR-ATRIP complex, *Cell* 124 (2006) 943-955.
294. J. Lee, A. Kumagai, W.G. Dunphy, The Rad9-Hus1-Rad1 checkpoint clamp regulates interaction of TopBP1 with ATR, *J Biol Chem* 282 (2007) 28036-28044.
295. H.Y. Yoo, A. Kumagai, A. Shevchenko, A. Shevchenko, W.G. Dunphy, Ataxia-telangiectasia mutated (ATM)-dependent activation of ATR occurs through phosphorylation of TopBP1 by ATM, *J Biol Chem* 282 (2007) 17501-17506.
296. E.J. Brown, D. Baltimore, ATR disruption leads to chromosomal fragmentation and early embryonic lethality, *Genes Dev* 14 (2000) 397-402.
297. A. de Klein, M. Muijtjens, R. van Os, Y. Verhoeven, B. Smit, A.M. Carr, A.R. Lehmann, J.H. Hoeijmakers, Targeted disruption of the cell-cycle checkpoint gene ATR leads to early embryonic lethality in mice, *Curr Biol* 10 (2000) 479-482.
298. K.M. Hopkins, W. Auerbach, X.Y. Wang, M.P. Hande, H. Hang, D.J. Wolgemuth, A.L. Joyner, H.B. Lieberman, Deletion of mouse rad9 causes abnormal cellular responses to DNA damage, genomic instability, and embryonic lethality, *Mol Cell Biol* 24 (2004) 7235-7248.
299. R.S. Weiss, T. Enoch, P. Leder, Inactivation of mouse Hus1 results in genomic instability and impaired responses to genotoxic stress, *Genes Dev* 14 (2000) 1886-1898.
300. T. Kondo, T. Wakayama, T. Naiki, K. Matsumoto, K. Sugimoto, Recruitment of Mec1 and Ddc1 checkpoint proteins to double-strand breaks through distinct mechanisms, *Science* 294 (2001) 867-870.
301. J. Lee, A. Kumagai, W.G. Dunphy, Claspin, a Chk1-regulatory protein, monitors DNA replication on chromatin independently of RPA, ATR, and Rad17, *Mol Cell* 11 (2003) 329-340.
302. Z. You, L. Kong, J. Newport, The role of single-stranded DNA and polymerase  $\alpha$  in establishing the ATR, Hus1 DNA replication checkpoint, *J Biol Chem* 277 (2002) 27088-27093.
303. A. Kumagai, W.G. Dunphy, Repeated phosphopeptide motifs in Claspin mediate the regulated binding of Chk1, *Nat Cell Biol* 5 (2003) 161-165.
304. S. Liu, S. Bekker-Jensen, N. Mailand, C. Lukas, J. Bartek, J. Lukas, Claspin operates downstream of TopBP1 to direct ATR

- signaling towards Chk1 activation, *Mol Cell Biol* 26 (2006) 6056-6064.
305. X. Wang, L. Zou, T. Lu, S. Bao, K.E. Hurov, W.N. Hittelman, S.J. Elledge, L. Li, Rad17 phosphorylation is required for caspase recruitment and Chk1 activation in response to replication stress, *Mol Cell* 23 (2006) 331-341.
  306. Q. Liu, S. Guntuku, X.S. Cui, S. Matsuoka, D. Cortez, K. Tamai, G. Luo, S. Carattini-Rivera, F. DeMayo, A. Bradley, L.A. Donehower, S.J. Elledge, Chk1 is an essential kinase that is regulated by Atr and required for the G(2)/M DNA damage checkpoint, *Genes Dev* 14 (2000) 1448-1459.
  307. A. Lopez-Girona, K. Tanaka, X.B. Chen, B.A. Baber, C.H. McGowan, P. Russell, Serine-345 is required for Rad3-dependent phosphorylation and function of checkpoint kinase Chk1 in fission yeast, *Proc Natl Acad Sci U S A* 98 (2001) 11289-11294.
  308. N.C. Walworth, R. Bernards, rad-dependent response of the chk1-encoded protein kinase at the DNA damage checkpoint, *Science* 271 (1996) 353-356.
  309. V.A. Smits, Spreading the signal: dissociation of Chk1 from chromatin, *Cell Cycle* 5 (2006) 1039-1043.
  310. V.A. Smits, P.M. Reaper, S.P. Jackson, Rapid PIKK-dependent release of Chk1 from chromatin promotes the DNA-damage checkpoint response, *Curr Biol* 16 (2006) 150-159.
  311. R. Boutros, C. Dozier, B. Ducommun, The when and where of CDC25 phosphatases, *Curr Opin Cell Biol* 18 (2006) 185-191.
  312. C. Karlsson-Rosenthal, J.B. Millar, Cdc25: mechanisms of checkpoint inhibition and recovery, *Trends Cell Biol* 16 (2006) 285-292.
  313. M. Donzelli, G.F. Draetta, Regulating mammalian checkpoints through Cdc25 inactivation, *EMBO Rep* 4 (2003) 671-677.
  314. J. Ahn, M. Urist, C. Prives, The Chk2 protein kinase, *DNA Repair (Amst)* 3 (2004) 1039-1047.
  315. C.M. Lovly, L. Yan, C.E. Ryan, S. Takada, H. Piwnica-Worms, Regulation of Chk2 ubiquitination and signaling through autophosphorylation of serine 379, *Mol Cell Biol* 28 (2008) 5874-5885.
  316. J. Bartek, J. Lukas, Chk1 and Chk2 kinases in checkpoint control and cancer, *Cancer Cell* 3 (2003) 421-429.
  317. J. Jin, T. Shirogane, L. Xu, G. Nalepa, J. Qin, S.J. Elledge, J.W. Harper, SCFbeta-TRCP links Chk1 signaling to degradation of the Cdc25A protein phosphatase, *Genes Dev* 17 (2003) 3062-3074.
  318. C.Y. Peng, P.R. Graves, R.S. Thoma, Z. Wu, A.S. Shaw, H. Piwnica-Worms, Mitotic and G2 checkpoint control: regulation of 14-3-3 protein binding by phosphorylation of Cdc25C on serine-216, *Science* 277 (1997) 1501-1505.
  319. Y. Kanemori, K. Uto, N. Sagata, Beta-TrCP recognizes a previously undescribed nonphosphorylated destruction motif in Cdc25A and Cdc25B phosphatases, *Proc Natl Acad Sci U S A* 102 (2005) 6279-6284.
  320. L. Busino, M. Donzelli, M. Chiesa, D. Guardavaccaro, D. Ganoth, N.V. Dorrello, A. Hershko, M. Pagano, G.F. Draetta, Degradation of Cdc25A by beta-TrCP during S phase and in response to DNA damage, *Nature* 426 (2003) 87-91.
  321. A. Hirao, A. Cheung, G. Duncan, P.M. Girard, A.J. Elia, A. Wakeham, H. Okada, T. Sarkissian, J.A. Wong, T. Sakai, E. De Stanchina, R.G. Bristow, T. Suda, S.W. Lowe, P.A. Jeggo, S.J. Elledge, T.W. Mak, Chk2 is a tumor suppressor that regulates apoptosis in both an ataxia telangiectasia mutated (ATM)-dependent and an ATM-independent manner, *Mol Cell Biol* 22 (2002) 6521-6532.
  322. H. Takai, K. Naka, Y. Okada, M. Watanabe, N. Harada, S. Saito, C.W. Anderson, E. Appella, M. Nakanishi, H. Suzuki, K. Nagashima, H. Sawa, K. Ikeda, N. Motoyama, Chk2-deficient mice exhibit radioresistance and defective p53-mediated transcription, *Embo J* 21 (2002) 5195-5205.
  323. L. Chen, D.M. Gilkes, Y. Pan, W.S. Lane, J. Chen, ATM and Chk2-dependent phosphorylation of MDMX contribute to p53 activation after DNA damage, *Embo J* 24 (2005) 3411-3422.
  324. C. LeBron, L. Chen, D.M. Gilkes, J. Chen, Regulation of MDMX nuclear import and degradation by Chk2 and 14-3-3, *Embo J* 25 (2006) 1196-1206.
  325. Y. Pereg, S. Lam, A. Teunisse, S. Biton, E. Meulmeester, L. Mittelman, G. Buscemi, K. Okamoto, Y. Taya, Y. Shiloh, A.G. Jochemsen, Differential roles of ATM- and Chk2-mediated phosphorylations of Hdmx in response to DNA damage, *Mol Cell Biol* 26 (2006) 6819-6831.
  326. P. Sung, H. Klein, Mechanism of homologous recombination: mediators

- and helicases take on regulatory functions, *Nat Rev Mol Cell Biol* 7 (2006) 739-750.
327. S.C. West, The search for a human Holliday junction resolvase, *Biochemical Society transactions* 37 (2009) 519-526.
328. S. Panier, D. Durocher, Regulatory ubiquitylation in response to DNA double-strand breaks, *DNA Repair (Amst)* 8 (2009) 436-443.
329. J.C. Fung, B. Rockmill, M. Odell, G.S. Roeder, Imposition of crossover interference through the nonrandom distribution of synapsis initiation complexes, *Cell* 116 (2004) 795-802.
330. P.W. Brown, L. Judis, E.R. Chan, S. Schwartz, A. Seftel, A. Thomas, T.J. Hassold, Meiotic synapsis proceeds from a limited number of subtelomeric sites in the human male, *Am J Hum Genet* 77 (2005) 556-566.
331. X. Ding, R. Xu, J. Yu, T. Xu, Y. Zhuang, M. Han, SUN1 is required for telomere attachment to nuclear envelope and gametogenesis in mice, *Dev Cell* 12 (2007) 863-872.
332. S. Kuznetsov, M. Pellegrini, K. Shuda, O. Fernandez-Capetillo, Y. Liu, B.K. Martin, S. Burkett, E. Southon, D. Pati, L. Tessarollo, S.C. West, P.J. Donovan, A. Nussenzweig, S.K. Sharan, RAD51C deficiency in mice results in early prophase I arrest in males and sister chromatid separation at metaphase II in females, *J Cell Biol* 176 (2007) 581-592.
333. D.L. Pittman, J. Cobb, K.J. Schimenti, L.A. Wilson, D.M. Cooper, E. Brignull, M.A. Handel, J.C. Schimenti, Meiotic prophase arrest with failure of chromosome synapsis in mice deficient for Dmc1, a germline-specific RecA homolog, *Mol. Cell* 1 (1998) 697-705.
334. K. Yoshida, G. Kondoh, Y. Matsuda, T. Habu, Y. Nishimune, T. Morita, The mouse RecA-like gene Dmc1 is required for homologous chromosome synapsis during meiosis, *Mol. Cell* 1 (1998) 707-718.
335. F. Yang, P.J. Wang, The Mammalian synaptonemal complex: a scaffold and beyond, *Genome dynamics* 5 (2009) 69-80.
336. F.A. de Vries, E. de Boer, M. van den Bosch, W.M. Baarends, M. Ooms, L. Yuan, J.G. Liu, A.A. van Zeeland, C. Heyting, A. Pastink, Mouse Sycp1 functions in synaptonemal complex assembly, meiotic recombination, and XY body formation, *Genes Dev* 19 (2005) 1376-1389.
337. E. Bolcun-Filas, Y. Costa, R. Speed, M. Taggart, R. Benavente, D.G. De Rooij, H.J. Cooke, SYCE2 is required for synaptonemal complex assembly, double strand break repair, and homologous recombination, *J Cell Biol* 176 (2007) 741-747.
338. G. Hamer, H. Wang, E. Bolcun-Filas, H.J. Cooke, R. Benavente, C. Hoog, Progression of meiotic recombination requires structural maturation of the central element of the synaptonemal complex, *J Cell Sci* 121 (2008) 2445-2451.
339. E. Bolcun-Filas, E. Hall, R. Speed, M. Taggart, C. Grey, B. de Massy, R. Benavente, H.J. Cooke, Mutation of the mouse Sycp1 gene disrupts synapsis and suggests a link between synaptonemal complex structural components and DNA repair, *PLoS Genet* 5 (2009) e1000393.
340. L. Yuan, J.G. Liu, J. Zhao, E. Brundell, B. Daneholt, C. Hoog, The murine SCP3 gene is required for synaptonemal complex assembly, chromosome synapsis, and male fertility, *Mol Cell* 5 (2000) 73-83.
341. A. Kouznetsova, I. Novak, R. Jessberger, C. Hoog, SYCP2 and SYCP3 are required for cohesin core integrity at diplotene but not for centromere cohesion at the first meiotic division, *J Cell Sci* 118 (2005) 2271-2278.
342. F. Yang, R. De La Fuente, N.A. Leu, C. Baumann, K.J. McLaughlin, P.J. Wang, Mouse SYCP2 is required for synaptonemal complex assembly and chromosomal synapsis during male meiosis, *J Cell Biol* 173 (2006) 497-507.
343. T. Ashley, A.P. Gaeth, L.B. Creemers, A.M. Hack, D.G. de Rooij, Correlation of meiotic events in testis sections and microspreads of mouse spermatocytes relative to the mid-pachytene checkpoint, *Chromosoma* 113 (2004) 126-136.
344. L. Yuan, J.G. Liu, M.R. Hoja, J. Wilbertz, K. Nordqvist, C. Hoog, Female germ cell aneuploidy and embryo death in mice lacking the meiosis-specific protein SCP3, *Science* 296 (2002) 1115-1118.
345. P.A. Hunt, T.J. Hassold, Sex matters in meiosis, *Science* 296 (2002) 2181-2183.
346. H. Wang, C. Hoog, Structural damage to meiotic chromosomes impairs DNA recombination and checkpoint control in mammalian oocytes, *J Cell Biol* 173 (2006) 485-495.
347. V. Borde, A.S. Goldman, M. Lichten, Direct coupling between meiotic DNA replication and recombination initiation, *Science* 290 (2000) 806-809.

348. S. Keeney, M.J. Neale, Initiation of meiotic recombination by formation of DNA double-strand breaks: mechanism and regulation, *Biochemical Society transactions* 34 (2006) 523-525.
349. V. Borde, N. Robine, W. Lin, S. Bonfils, V. Geli, A. Nicolas, Histone H3 lysine 4 trimethylation marks meiotic recombination initiation sites, *Embo J* 28 (2009) 99-111.
350. J.A. Farah, G.A. Cromie, G.R. Smith, Ctp1 and Exonuclease 1, alternative nucleases regulated by the MRN complex, are required for efficient meiotic recombination, *Proc Natl Acad Sci U S A* 106 (2009) 9356-9361.
351. E. Hartsuiker, K. Mizuno, M. Molnar, J. Kohli, K. Ohta, A.M. Carr, Ctp1CtIP and Rad32Mre11 nuclease activity are required for Rec12Spo11 removal, but Rec12Spo11 removal is dispensable for other MRN-dependent meiotic functions, *Mol Cell Biol* 29 (2009) 1671-1681.
352. N. Milman, E. Higuchi, G.R. Smith, Meiotic DNA double-strand break repair requires two nucleases, MRN and Ctp1, to produce a single size class of Rec12 (Spo11)-oligonucleotide complexes, *Mol Cell Biol* 29 (2009) 5998-6005.
353. M. Rothenberg, J. Kohli, K. Ludin, Ctp1 and the MRN-complex are required for endonucleolytic Rec12 removal with release of a single class of oligonucleotides in fission yeast, *PLoS Genet* 5 (2009) e1000722.
354. S. Burma, B.P. Chen, M. Murphy, A. Kurimasa, D.J. Chen, ATM phosphorylates histone H2AX in response to DNA double-strand breaks, *J Biol Chem* 276 (2001) 42462-42467.
355. T. Uziel, Y. Lerenthal, L. Moyal, Y. Andegeko, L. Mittelman, Y. Shiloh, Requirement of the MRN complex for ATM activation by DNA damage, *Embo J* 22 (2003) 5612-5621.
356. J.H. Lee, T.T. Paull, Direct activation of the ATM protein kinase by the Mre11/Rad50/Nbs1 complex, *Science* 304 (2004) 93-96.
357. W. Goedecke, M. Eijpe, H.H. Offenberg, M. van Aalderen, C. Heyting, Mre11 and Ku70 interact in somatic cells, but are differentially expressed in early meiosis, *Nat Genet* 23 (1999) 194-198.
358. P. Sung, L. Krejci, S. Van Komen, M.G. Sehorn, Rad51 recombinase and recombination mediators, *J Biol Chem* 278 (2003) 42729-42732.
359. A.W. Plug, A.H. Peters, Y. Xu, K.S. Keegan, M.F. Hoekstra, D. Baltimore, P. de Boer, T. Ashley, ATM and RPA in meiotic chromosome synapsis and recombination, *Nat. Genet.* 17 (1997) 457-461.
360. P.B. Moens, N.K. Kolas, M. Tarsounas, E. Marcon, P.E. Cohen, B. Spyropoulos, The time course and chromosomal localization of recombination-related proteins at meiosis in the mouse are compatible with models that can resolve the early DNA-DNA interactions without reciprocal recombination, *J. Cell. Sci.* 115 (2002) 1611-1622.
361. N.K. Kolas, E. Marcon, M.A. Crackower, C. Hoog, J.M. Penninger, B. Spyropoulos, P.B. Moens, Mutant meiotic chromosome core components in mice can cause apparent sexual dimorphic endpoints at prophase or X-Y defective male-specific sterility, *Chromosoma* 114 (2005) 92-102.
362. L.A. Bannister, J.C. Schimenti, Homologous recombinational repair proteins in mouse meiosis, *Cytogenet Genome Res* 107 (2004) 191-200.
363. E. Marcon, P.B. Moens, The evolution of meiosis: recruitment and modification of somatic DNA-repair proteins, *Bioessays* 27 (2005) 795-808.
364. S.K. Sharan, A. Pyle, V. Coppola, J. Babus, S. Swaminathan, J. Benedict, D. Swing, B.K. Martin, L. Tessarollo, J.P. Evans, J.A. Flaws, M.A. Handel, BRCA2 deficiency in mice leads to meiotic impairment and infertility, *Development* 131 (2004) 131-142.
365. F. Yang, S. Eckardt, N.A. Leu, K.J. McLaughlin, P.J. Wang, Mouse TEX15 is essential for DNA double-strand break repair and chromosomal synapsis during male meiosis, *J Cell Biol* 180 (2008) 673-679.
366. K. Treuner, M. Findeisen, U. Strausfeld, R. Knippers, Phosphorylation of replication protein A middle subunit (RPA32) leads to a disassembly of the RPA heterotrimer, *J Biol Chem* 274 (1999) 15556-15561.
367. X. Xu, O. Aprelikova, P. Moens, C.X. Deng, P.A. Furth, Impaired meiotic DNA-damage repair and lack of crossing-over during spermatogenesis in BRCA1 full-length isoform deficient mice, *Development* 130 (2003) 2001-2012.
368. V.L. Cressman, D.C. Backlund, A.V. Avrutskaya, S.A. Leadon, V. Godfrey, B.H. Koller, Growth retardation, DNA repair defects, and lack of spermatogenesis in BRCA1-deficient mice, *Mol Cell Biol* 19 (1999) 7061-7075.

369. P.B. Moens, D.J. Chen, Z. Shen, N. Kolas, M. Tarsounas, H.H. Heng, B. Spyropoulos, Rad51 immunocytology in rat and mouse spermatocytes and oocytes, *Chromosoma* 106 (1997) 207-215.
370. H. Niu, L. Wan, B. Baumgartner, D. Schaefer, J. Loidl, N.M. Hollingsworth, Partner choice during meiosis is regulated by Hop1-promoted dimerization of Mek1, *Mol Biol Cell* 16 (2005) 5804-5818.
371. H. Niu, L. Wan, V. Busygina, Y. Kwon, J.A. Allen, X. Li, R.C. Kunz, K. Kubota, B. Wang, P. Sung, K.M. Shokat, S.P. Gygi, N.M. Hollingsworth, Regulation of meiotic recombination via Mek1-mediated Rad54 phosphorylation, *Mol Cell* 36 (2009) 393-404.
372. V. Busygina, M.G. Sehorn, I.Y. Shi, H. Tsubouchi, G.S. Roeder, P. Sung, Hed1 regulates Rad51-mediated recombination via a novel mechanism, *Genes Dev* 22 (2008) 786-795.
373. H. Niu, X. Li, E. Job, C. Park, D. Moazed, S.P. Gygi, N.M. Hollingsworth, Mek1 kinase is regulated to suppress double-strand break repair between sister chromatids during budding yeast meiosis, *Mol Cell Biol* 27 (2007) 5456-5467.
374. P. Chi, Y. Kwon, D.N. Moses, C. Seong, M.G. Sehorn, A.K. Singh, H. Tsubouchi, E.C. Greene, H.L. Klein, P. Sung, Functional interactions of meiotic recombination factors Rdh54 and Dmc1, *DNA Repair (Amst)* 8 (2009) 279-284.
375. R.J. Pezza, O.N. Voloshin, F. Vanevski, R.D. Camerini-Otero, Hop2/Mnd1 acts on two critical steps in Dmc1-promoted homologous pairing, *Genes Dev* 21 (2007) 1758-1766.
376. T. Habu, T. Taki, A. West, Y. Nishimune, T. Morita, The mouse and human homologs of DMC1, the yeast meiosis-specific homologous recombination gene, have a common unique form of exon-skipped transcript in meiosis, *Nucleic Acids Res* 24 (1996) 470-477.
377. G.V. Petukhova, P.J. Romanienko, R.D. Camerini-Otero, The Hop2 protein has a direct role in promoting interhomolog interactions during mouse meiosis, *Dev Cell* 5 (2003) 927-936.
378. R. Kanaar, C. Troelstra, S.M.A. Swagemakers, J. Essers, B. Smit, J.-H. Franssen, A. Pastink, O.Y. Bezzubova, J.-M. Buerstedde, B. Clever, W.-D. Heyer, J.H.J. Hoeijmakers, Human and mouse homologs of the *Saccharomyces cerevisiae* RAD54 DNA repair gene: evidence for functional conservation., *Current Biol.* 6 (1996) 828-838.
379. J. Essers, R.W. Hendriks, S.M. Swagemakers, C. Troelstra, J. de Wit, D. Bootsma, J.H. Hoeijmakers, R. Kanaar, Disruption of mouse RAD54 reduces ionizing radiation resistance and homologous recombination, *Cell* 89 (1997) 195-204.
380. T. Allers, M. Lichten, Differential timing and control of noncrossover and crossover recombination during meiosis, *Cell* 106 (2001) 47-57.
381. G.A. Cromie, G.R. Smith, Branching out: meiotic recombination and its regulation, *Trends Cell Biol* 17 (2007) 448-455.
382. J.K. Holloway, J. Booth, W. Edelmann, C.H. McGowan, P.E. Cohen, MUS81 generates a subset of MLH1-MLH3-independent crossovers in mammalian meiosis, *PLoS Genet* 4 (2008) e1000186.
383. N. Kleckner, A. Storlazzi, D. Zickler, Coordinate variation in meiotic pachytene SC length and total crossover/chiasma frequency under conditions of constant DNA length, *Trends Genet* 19 (2003) 623-628.
384. E. de Boer, P. Stam, A.J. Dietrich, A. Pastink, C. Heyting, Two levels of interference in mouse meiotic recombination, *Proc Natl Acad Sci U S A* 103 (2006) 9607-9612.
385. M. Barchi, I. Roig, M. Di Giacomo, D.G. de Rooij, S. Keeney, M. Jasin, ATM promotes the obligate XY crossover and both crossover control and chromosome axis integrity on autosomes, *PLoS Genet* 4 (2008) e1000076.
386. S.M. Cherry, C.A. Adelman, J.W. Theunissen, T.J. Hassold, P.A. Hunt, J.H. Petrini, The Mre11 complex influences DNA repair, synapsis, and crossing over in murine meiosis, *Curr Biol* 17 (2007) 373-378.
387. A.J. Bartrand, D. Iyasu, S.M. Marinco, G.S. Brush, Evidence of meiotic crossover control in *Saccharomyces cerevisiae* through Mec1-mediated phosphorylation of replication protein A, *Genetics* 172 (2006) 27-39.
388. W.M. Baarends, E. Wassenaar, J.W. Hoogerbrugge, G. van Cappellen, H.P. Roest, J. Vreeburg, M. Ooms, J.H. Hoeijmakers, J.A. Grootegoed, Loss of HR6B ubiquitin-conjugating activity results in damaged synaptonemal complex structure and increased crossing-over frequency during the male

- meiotic prophase, *Mol Cell Biol* 23 (2003) 1151-1162.
389. K. Robzyk, J. Recht, M.A. Osley, Rad6-dependent ubiquitination of histone H2B in yeast, *Science* 287 (2000) 501-504.
390. J. Kim, M. Guermah, R.K. McGinty, J.S. Lee, Z. Tang, T.A. Milne, A. Shilatifard, T.W. Muir, R.G. Roeder, RAD6-Mediated transcription-coupled H2B ubiquitylation directly stimulates H3K4 methylation in human cells, *Cell* 137 (2009) 459-471.
391. H.P. Roest, J. Klaveren van, J. Wit de, C.G. Gulp van, M.H.M. Koken, M. Vermey, J.H. Roijen van, J.T.M. Vreeburg, W.M. Baarends, D. Bootsma, J.A. Grootegoed, J.H.J. Hoeijmakers, Inactivation of the HR6B ubiquitin-conjugating DNA repair enzyme in mice causes a defect in spermatogenesis associated with chromatin modification, *Cell* 86 (1996) 799-810.
392. W.M. Baarends, E. Wassenaar, J.W. Hoogerbrugge, S. Schoenmakers, Z.W. Sun, J.A. Grootegoed, Increased phosphorylation and dimethylation of XY body histones in the Hr6b-knockout mouse is associated with depression of the X chromosome, *J Cell Sci* 120 (2007) 1841-1851.
393. E. de Boer, A.J. Dietrich, C. Hoog, P. Stam, C. Heyting, Meiotic interference among MLH1 foci requires neither an intact axial element structure nor full synapsis, *J Cell Sci* 120 (2007) 731-736.
394. K. Yamashita, M. Shinohara, A. Shinohara, Rad6-Bre1-mediated histone H2B ubiquitylation modulates the formation of double-strand breaks during meiosis, *Proc Natl Acad Sci U S A* 101 (2004) 11380-11385.
395. D.G. Mets, B.J. Meyer, Condensins regulate meiotic DNA break distribution, thus crossover frequency, by controlling chromosome structure, *Cell* 139 (2009) 73-86.
396. A. Sato, B. Isaac, C.M. Phillips, R. Rillo, P.M. Carlton, D.J. Wynne, R.A. Kasad, A.F. Dernburg, Cytoskeletal forces span the nuclear envelope to coordinate meiotic chromosome pairing and synapsis, *Cell* 139 (2009) 907-919.
397. A.M. Penkner, A. Fridkin, J. Gloggnitzer, A. Baudrimont, T. Machacek, A. Woglar, E. Csaszar, P. Pasierbek, G. Ammerer, Y. Gruenbaum, V. Jantsch, Meiotic chromosome homology search involves modifications of the nuclear envelope protein Matefin/SUN-1, *Cell* 139 (2009) 920-933.
398. A.F. Dernburg, K. McDonald, G. Moulder, R. Barstead, M. Dresser, A.M. Villeneuve, Meiotic recombination in *C. elegans* initiates by a conserved mechanism and is dispensable for homologous chromosome synapsis, *Cell* 94 (1998) 387-398.
399. F. Baudat, K. Manova, J.P. Yuen, M. Jasin, S. Keeney, Chromosome synapsis defects and sexually dimorphic meiotic progression in mice lacking Spo11, *Mol Cell* 6 (2000) 989-998.
400. P.J. Romanienko, R.D. Camerini-Otero, The mouse Spo11 gene is required for meiotic chromosome synapsis, *Mol Cell* 6 (2000) 975-987.
401. W. Edelmann, P.E. Cohen, B. Kneitz, N. Winand, M. Lia, J. Heyer, R. Kolodner, J.W. Pollard, R. Kucherlapati, Mammalian MutS homologue 5 is required for chromosome pairing in meiosis, *Nat Genet* 21 (1999) 123-127.
402. S.S. de Vries, E.B. Baart, M. Dekker, A. Siezen, D.G. de Rooij, P. de Boer, H. te Riele, Mouse MutS-like protein Msh5 is required for proper chromosome synapsis in male and female meiosis, *Genes Dev* 13 (1999) 523-531.
403. B. Kneitz, P.E. Cohen, E. Avdievich, L. Zhu, M.F. Kane, H. Hou, Jr., R.D. Kolodner, R. Kucherlapati, J.W. Pollard, W. Edelmann, MutS homolog 4 localization to meiotic chromosomes is required for chromosome pairing during meiosis in male and female mice, *Genes Dev* 14 (2000) 1085-1097.
404. L.L. Tres, Extensive pairing of the XY bivalent in mouse spermatocytes as visualized by whole-mount electron microscopy, *J Cell Sci* 25 (1977) 1-15.
405. A.H. Peters, A.W. Plug, P. de Boer, Meiosis in carriers of heteromorphic bivalents: sex differences and implications for male fertility, *Chromosome Res.* 5 (1997) 313-324.
406. S. Schoenmakers, E. Wassenaar, W.A. van Cappellen, A.A. Derijck, P. de Boer, J.S. Laven, J.A. Grootegoed, W.M. Baarends, Increased frequency of asynapsis and associated meiotic silencing of heterologous chromatin in the presence of irradiation-induced extra DNA double strand breaks, *Dev Biol* 317 (2008) 270-281.
407. V. Monesi, Differential rate of ribonucleic acid synthesis in the autosomes and sex chromosomes during male meiosis in the mouse, *Chromosoma* 17 (1965) 11-21.
408. D. Motzkus, P.B. Singh, S. Hoyer-Fender, M31, a murine homolog of *Drosophila*

- HP1, is concentrated in the XY body during spermatogenesis, *Cytogenet Cell Genet* 86 (1999) 83-88.
409. J.M. Turner, S.K. Mahadevaiah, P.J. Ellis, M.J. Mitchell, P.S. Burgoyne, Pachytene asynapsis drives meiotic sex chromosome inactivation and leads to substantial postmeiotic repression in spermatids, *Dev Cell* 10 (2006) 521-529.
  410. G.W. van der Heijden, A.A. Derijck, E. Posfai, M. Giele, P. Pelczar, L. Ramos, D.G. Wansink, J. van der Vlag, A.H. Peters, P. de Boer, Chromosome-wide nucleosome replacement and H3.3 incorporation during mammalian meiotic sex chromosome inactivation, *Nat Genet* 39 (2007) 251-258.
  411. S.K. Mahadevaiah, J.M. Turner, F. Baudat, E.P. Rogakou, P. de Boer, J. Blanco-Rodriguez, M. Jasin, S. Keeney, W.M. Bonner, P.S. Burgoyne, Recombinational DNA double-strand breaks in mice precede synapsis, *Nat Genet* 27 (2001) 271-276.
  412. O. Fernandez-Capetillo, S.K. Mahadevaiah, A. Celeste, P.J. Romanienko, R.D. Camerini-Otero, W.M. Bonner, K. Manova, P. Burgoyne, A. Nussenzweig, H2AX is required for chromatin remodeling and inactivation of sex chromosomes in male mouse meiosis, *Dev Cell* 4 (2003) 497-508.
  413. W.M. Baarends, J.W. Hoogerbrugge, H.P. Roest, M. Ooms, J. Vreeburg, J.H. Hoeijmakers, J.A. Grootegoed, Histone ubiquitination and chromatin remodeling in mouse spermatogenesis, *Dev Biol* 207 (1999) 322-333.
  414. R.S. Rogers, A. Inselman, M.A. Handel, M.J. Matunis, SUMO modified proteins localize to the XY body of pachytene spermatocytes, *Chromosoma* 113 (2004) 233-243.
  415. M. Kalocsay, N.J. Hiller, S. Jentsch, Chromosome-wide Rad51 spreading and SUMO-H2A.Z-dependent chromosome fixation in response to a persistent DNA double-strand break, *Mol Cell* 33 (2009) 335-343.
  416. P.J.M. Hendriksen, J.W. Hoogerbrugge, A.P.N. Themmen, M.H.M. Koken, J.H.J. Hoeijmakers, B.A. Oostra, T. Van der Lende, J.A. Grootegoed, Postmeiotic transcription of X and Y chromosomal genes during spermatogenesis in the mouse., *Dev. Biol.* 170 (1995) 730-733.
  417. J.L. Mueller, S.K. Mahadevaiah, P.J. Park, P.E. Warburton, D.C. Page, J.M. Turner, The mouse X chromosome is enriched for multicopy testis genes showing postmeiotic expression, *Nat Genet* 40 (2008) 794-799.
  418. S.H. Namekawa, P.J. Park, L.F. Zhang, J.E. Shima, J.R. McCarrey, M.D. Griswold, J.T. Lee, Postmeiotic sex chromatin in the male germline of mice, *Curr Biol* 16 (2006) 660-667.
  419. J. Cocquet, P.J. Ellis, Y. Yamauchi, S.K. Mahadevaiah, N.A. Affara, M.A. Ward, P.S. Burgoyne, The multicopy gene *Sly* represses the sex chromosomes in the male mouse germline after meiosis, *PLoS biology* 7 (2009) e1000244.
  420. M.A. Bellani, P.J. Romanienko, D.A. Cairatti, R.D. Camerini-Otero, SPO11 is required for sex-body formation, and Spo11 heterozygosity rescues the prophase arrest of *Atm*<sup>-/-</sup> spermatocytes, *J Cell Sci* 118 (2005) 3233-3245.
  421. A.W. Plug, A.H. Peters, K.S. Keegan, M.F. Hoekstra, P. de Boer, T. Ashley, Changes in protein composition of meiotic nodules during mammalian meiosis, *J Cell Sci* 111 (1998) 413-423.
  422. R. Scully, J. Chen, A. Plug, Y. Xiao, D. Weaver, J. Feunteun, T. Ashley, D.M. Livingston, Association of BRCA1 with Rad51 in mitotic and meiotic cells, *Cell* 88 (1997) 265-275.
  423. J. Chen, D.P. Silver, D. Walpita, S.B. Cantor, A.F. Gazdar, G. Tomlinson, F.J. Couch, B.L. Weber, T. Ashley, D.M. Livingston, R. Scully, Stable interaction between the products of the BRCA1 and BRCA2 tumor suppressor genes in mitotic and meiotic cells, *Mol Cell* 2 (1998) 317-328.
  424. R. Freire, J.R. Murguia, M. Tarsounas, N.F. Lowndes, P.B. Moens, S.P. Jackson, Human and mouse homologs of *Schizosaccharomyces pombe rad1(+)* and *Saccharomyces cerevisiae RAD17*: linkage to checkpoint control and mammalian meiosis, *Genes Dev* 12 (1998) 2560-2573.
  425. D. Walpita, A.W. Plug, N.F. Neff, J. German, T. Ashley, Bloom's syndrome protein, BLM, colocalizes with replication protein A in meiotic prophase nuclei of mammalian spermatocytes, *Proc Natl Acad Sci U S A* 96 (1999) 5622-5627.
  426. K. Reini, L. Uitto, D. Perera, P.B. Moens, R. Freire, J.E. Syvaoja, TopBP1 localises to centrosomes in mitosis and to chromosome cores in meiosis, *Chromosoma* 112 (2004) 323-330.
  427. D. Perera, L. Perez-Hidalgo, P.B. Moens, K. Reini, N. Lakin, J.E. Syvaoja, P.A. San-Segundo, R. Freire, TopBP1 and ATR colocalization at meiotic chromosomes:

- role of TopBP1/Cut5 in the meiotic recombination checkpoint, *Mol Biol Cell* 15 (2004) 1568-1579.
428. E.A. Ahmed, A. van der Vaart, A. Barten, H.B. Kal, J. Chen, Z. Lou, K. Minter-Dykhouse, J. Bartkova, J. Bartek, P. de Boer, D.G. de Rooij, Differences in DNA double strand breaks repair in male germ cell types: lessons learned from a differential expression of Mdc1 and 53BP1, *DNA Repair (Amst)* 6 (2007) 1243-1254.
429. R. van der Laan, E.J. Uringa, E. Wassenaar, J.W. Hoogerbrugge, E. Sleddens, H. Odijk, H.P. Roest, P. de Boer, J.H. Hoeijmakers, J.A. Grootegoed, W.M. Baarends, Ubiquitin ligase Rad18Sc localizes to the XY body and to other chromosomal regions that are unpaired and transcriptionally silenced during male meiotic prophase, *J Cell Sci* 117 (2004) 5023-5033.
430. P. Karmakar, M. Seki, M. Kanamori, K. Hashiguchi, M. Ohtsuki, E. Murata, E. Inoue, S. Tada, L. Lan, A. Yasui, T. Enomoto, BLM is an early responder to DNA double-strand breaks, *Biochem Biophys Res Commun* 348 (2006) 62-69.
431. N. Chester, F. Kuo, C. Kozak, C.D. O'Hara, P. Leder, Stage-specific apoptosis, developmental delay, and embryonic lethality in mice homozygous for a targeted disruption in the murine Bloom's syndrome gene, *Genes Dev* 12 (1998) 3382-3393.
432. A.L. Barlow, M.A. Hulten, Crossing over analysis at pachytene in man, *Eur J Hum Genet* 6 (1998) 350-358.
433. S.K. Mahadevaiah, D. Bourc'his, D.G. de Rooij, T.H. Bestor, J.M. Turner, P.S. Burgoyne, Extensive meiotic asynapsis in mice antagonises meiotic silencing of unsynapsed chromatin and consequently disrupts meiotic sex chromosome inactivation, *J Cell Biol* 182 (2008) 263-276.
434. J.M. Turner, O. Aprelikova, X. Xu, R. Wang, S. Kim, G.V. Chandramouli, J.C. Barrett, P.S. Burgoyne, C.X. Deng, BRCA1, histone H2AX phosphorylation, and male meiotic sex chromosome inactivation, *Curr Biol* 14 (2004) 2135-2142.
435. W.M. Baarends, E. Wassenaar, R. van der Laan, J.W. Hoogerbrugge, E. Sleddens-Linkels, J.H. Hoeijmakers, P. de Boer, J.A. Grootegoed, Silencing of unpaired chromatin and histone H2A ubiquitination in mammalian meiosis, *Mol Cell Biol* 25 (2005) 1041-1053.
436. J.M. Turner, S.K. Mahadevaiah, O. Fernandez-Capetillo, A. Nussenzweig, X. Xu, C.X. Deng, P.S. Burgoyne, Silencing of unsynapsed meiotic chromosomes in the mouse, *Nat Genet* 37 (2005) 41-47.
437. J. Schimenti, Synapsis or silence, *Nat Genet* 37 (2005) 11-13.
438. D. Homolka, R. Ivanek, J. Capkova, P. Jansa, J. Forejt, Chromosomal rearrangement interferes with meiotic X chromosome inactivation, *Genome Res* 17 (2007) 1431-1437.
439. A.J. Solari, Equalization of Z and W axes in chicken and quail oocytes, *Cytogenet Cell Genet* 59 (1992) 52-56.
440. E. Jablonka, M.J. Lamb, Meiotic pairing constraints and the activity of sex chromosomes, *J Theor Biol* 133 (1988) 23-36.
441. S. Schoenmakers, E. Wassenaar, J.W. Hoogerbrugge, J.S. Laven, J.A. Grootegoed, W.M. Baarends, Female meiotic sex chromosome inactivation in chicken, *PLoS Genet* 5 (2009) e1000466.
442. S. Schoenmakers, E. Wassenaar, J.S. Laven, J.A. Grootegoed, W.M. Baarends, Meiotic silencing and fragmentation of the male germline restricted chromosome in zebra finch, *Chromosoma In Press* (2010).
443. J. Fang, T. Chen, B. Chadwick, E. Li, Y. Zhang, Ring1b-mediated H2A ubiquitination associates with inactive X chromosomes and is involved in initiation of X-inactivation, *J Biol Chem* (2004).
444. M. de Napoles, J.E. Mermoud, R. Wakao, Y.A. Tang, M. Endoh, R. Appanah, T.B. Nesterova, J. Silva, A.P. Otte, M. Vidal, H. Koseki, N. Brockdorff, Polycomb group proteins Ring1A/B link ubiquitylation of histone H2A to heritable gene silencing and X inactivation, *Dev Cell* 7 (2004) 663-676.
445. D. Nathan, K. Ingvarsdottir, D.E. Sterner, G.R. Bylebyl, M. Dokmanovic, J.A. Dorsey, K.A. Whelan, M. Krzmanovic, W.S. Lane, P.B. Meluh, E.S. Johnson, S.L. Berger, Histone sumoylation is a negative regulator in *Saccharomyces cerevisiae* and shows dynamic interplay with positive-acting histone modifications, *Genes Dev* 20 (2006) 966-976.
446. B. Stielow, A. Sapetschnig, I. Kruger, N. Kunert, A. Brehm, M. Boutros, G. Suske, Identification of SUMO-dependent chromatin-associated transcriptional repression components by a genome-wide RNAi screen, *Mol Cell* 29 (2008) 742-754.

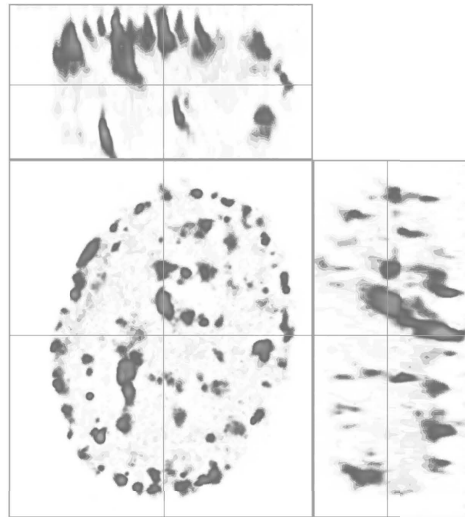
2

# DYNAMIC LOCALIZATION OF HUMAN RAD18 DURING THE CELL CYCLE AND A FUNCTIONAL CONNECTION WITH DNA DOUBLE-STRAND BREAK REPAIR

DNA repair, February 2009, Volume 8, Issue 2, 1 Pages 190-201

Akiko Inagaki, Wiggert A. van Cappellen, Roald van der Laan<sup>1</sup>,  
Adriaan B. Houtsmuller<sup>2</sup>, Jan H. J. Hoeijmakers<sup>1</sup>,  
J. Anton Grootegoed, and Willy M. Baarends\*

\* Corresponding author



Department of Reproduction and Development, <sup>1</sup>Department of Cell Biology and Genetics, Erasmus MC - University Medical Center and <sup>2</sup>Department of Pathology, Josephine Nefkens Institute Erasmus MC - University Medical Center, Rotterdam, The Netherlands

**ABSTRACT**

The ubiquitin ligase RAD18 is involved in different DNA repair processes. Here, we show that in G1 phase, human RAD18 accumulates in a few relatively large spontaneous foci that contain proteins involved in double-strand break (DSB) repair. These foci persist until cells enter S phase, when numerous small foci appear. At these sites, only 20% of RAD18 colocalizes with PCNA, a known RAD18 substrate. In late G2 phase, RAD18 relocates to nucleoli. After UVC irradiation, PCNA accumulates at the damaged site, followed by RAD18, independent of the cell cycle phase. After induction of DSBs, using low-power multi photon laser, RAD18 accumulated at the DSB sites, but no PCNA accumulation was observed. Our data show that RAD18 accumulates on DSBs independent of the cell cycle phase. DSBs marked by RAD18 and RAD51 are also positive for RPA in G1 phase, and these DSBs persist until S phase. In addition, we show that DSBs generated in G2 phase are not all repaired, and are observed again in the next G1 phase. We conclude that repair of induced and spontaneous DSBs that accumulate RAD18 and RAD51 in G1 phase cells is delayed until S phase.

**Key words:** RAD18, DNA double-strand break repair, PCNA, cell cycle

## 1. INTRODUCTION

Cells are constantly exposed to internal and external factors that may cause DNA damage. Various DNA repair pathways are essential for progress through the cell cycle and long-term survival. During DNA replication, the presence of unrepaired DNA lesions threatens to block progression of the replication machinery. Replicative damage bypass (RDB) is a special pathway that allows progression of DNA replication in the presence of DNA damage (reviewed in [1]). In *Saccharomyces cerevisiae*, the E2 ubiquitin-conjugating enzyme Rad6 is essential for this pathway. Depending on interactions with downstream components, error-free or error-prone sub-pathways can be activated. The first step in both pathways involves mono-ubiquitylation of PCNA by the Rad6-Rad18 complex, in which Rad18 acts as an ubiquitin ligase (E3 enzyme) [2]. PCNA forms a homo-trimer that encircles double-stranded DNA, and operates as a sliding clamp to keep the DNA polymerase machinery firmly on the DNA during DNA replication (reviewed in [3]). Mono-ubiquitylation of PCNA by the Rad6-Rad18 complex recruits specific translesion synthesis polymerases that can incorporate nucleotides in the strand opposite the site of the DNA lesions. Depending on which polymerase is recruited, this process may be error-prone or error-free (reviewed in [4,5]). Alternatively, mono-ubiquitylation by the Rad6-Rad18 complex may be followed by Rad5-Mms2-Ubc13-mediated poly-ubiquitylation [2]. The ubiquitin ligase Rad5 interacts with both the Rad6-Rad18 and the Mms2-Ubc13 complexes to stimulate poly-ubiquitination of PCNA. Subsequently, Rad5 is involved in error-free bypass of the damage.

In mammalian cells, RAD18 complexes with the RAD6 homologs HR6A (UBE2A) and HR6B (UBE2B) [6], and regulates PCNA mono-ubiquitylation [7,8]. *RAD18*-knockout cells are sensitive to UVC light exposure [9,10], camptothecin, and ionizing radiation (IR) [11], that induce distortions of DNA geometry, single-strand breaks (SSBs), and double-strand breaks (DSBs), respectively. Thus, in mammalian cells, RAD18 is required for survival after the induction of almost any type of DNA damage, and this appears to be associated with novel RAD18 functions outside the context of RDB. However, the nature of these functions is still unclear. Nakajima et al. [12] showed that RAD18 accumulates at sites of SSBs, in an S-phase-independent manner. Shiomi et al. [11] also provided evidence for RAD18 functions at sites of SSBs, but restricted to S phase and PCNA independent. In addition, at DSB repair sites during S phase, RAD18 may facilitate homologous recombination (HR), independent of PCNA, by suppressing non-homologous end-joining (NHEJ) at DSBs that result from blockage of replication [13,14].

Here, we show that RAD18 has a dynamic localization pattern during the cell cycle, which is mostly different from that of PCNA but similar to DSB repair-associated proteins, RAD51 and  $\gamma$ H2AX. We conclude that RAD18 accumulates at sites of DSBs, throughout the cell cycle, in the absence of a detectable increase in local PCNA concentration. Furthermore, we show that spontaneous and induced DSBs in G1 persist until the cells enter S phase.

## 2. MATERIALS AND METHODS

### 2.1 DNA constructs, transfection and cell culture

YFP-tagged RAD18 was generated by cloning a cDNA fragment encoding the entire human *RAD18* gene, except the start codon, into pEYFP-C1 (Clontech). The *RAD18* fragment was amplified using primer set (fw/5'CCGGAATTCTGACTCCCTGGCCGAGTCTC3' and rev/5'CGCGATCCTTAATTCCTGTTTCGTTTATTTCTTGGTTCAATCTCA GCA3'), digested at the introduced *Eco*RI and *Bam*HI sites (underlined) and inserted into the pEYFP-C1 vector. To prevent downregulation of YFP-RAD18 by siRNA treatment, four silent mutations were inserted in the 3' region of the cDNA (italic). To generate HeLa cells stably expressing YFP-RAD18, cells were transfected with 2  $\mu$ g of the pEYFP-RAD18 plasmid using FuGene6 (Roche). Cells were cultured for 7 days after transfection with medium containing 1.0 mg/ml of G418. Colonies containing cells showing YFP signal in the nuclei were selected, and immunoblot analysis was used to further select cell lines that showed the appropriate level of YFP-RAD18.

A mCherry-PCNA construct was created by cloning a cDNA fragment encoding the entire human PCNA [15] into mCherry-C1 (kindly provided by Dr. Roger Y. Tsien, University of California, San Diego, USA). The entire *PCNA* gene, except the start codon, was amplified by using primer set (fw/5'CCCAAGCTTCGTTTCGAGGC GCGCCTGGTC3' and rev/5'CCCGATCCCTAAGATCCTTCTTCATCCTCG3'), digested at the introduced *Hind*III and *Bam*HI sites (underlined) and inserted into the mCherry-C1 vector. Transient and stable expression of mCherry-PCNA was obtained as described above for YFP-RAD18.

HeLa cells were cultured at 37°C in DMEM/F12 (GIBCO) supplemented with 5% v/v fetal calf serum, streptomycin sulfate and penicillin, under 5% CO<sub>2</sub> in air.

### 2.2 RNA interference

$2 \times 10^5$  cells were plated into six-well culture dishes. After 24 hours, cells were transfected with siRNA and incubated for 48 hours. Each transfection mixture contained 9  $\mu$ l HiPerFect Transfection Reagent (Qiagen) and 2  $\mu$ M siRNA (Ambion) in 400  $\mu$ l serum-free DMEM/F12. siRNA132977 (Ambion) was used to downregulate both YFP-RAD18 and endogenous RAD18 expressions. siRNA28198 (Ambion) was used to downregulate only endogenous RAD18. siRNA (Ambion) does not target any gene, and was used as a control.

### 2.3 Global $\gamma$ -ray irradiation

To induce global ionizing damage, cultured cells were irradiated with  $\gamma$ -rays from a <sup>137</sup>Cs source (0.71 Gy/minute).

### 2.4 Global UVC irradiation

To induce global UVC damage, cultured cells were irradiated with a Philips TUV lamp (254 nm) at a dose of 20 J/m<sup>2</sup>. For colocalization analyses, cells were cultured for 1 hour following UVC irradiation, and living cell images were captured with a Zeiss LSM510NLO confocal microscope (Carl Zeiss, Jena). For immunoblot analysis, cells were cultured for another 8 hours and whole-cell extracts were prepared.

## 2.5 Immunoblot analysis

Whole-cell extracts were prepared from cultured cells collected in a buffer (50 mM Tris-HCl pH 6.8, 2% w/v SDS, 0.1% w/v bromophenol blue, 10% v/v glycerol and 100 mM dithiothreitol), and sonicated. After 5 minutes incubation at 100°C, the cell extracts were separated by sodium dodecyl sulfate 10% polyacrylamide gel electrophoresis and transferred to nitrocellulose membranes. The membranes were incubated with antibodies to analyse expression of target proteins. The expression was detected using enhanced chemiluminescence (PerkinElmer).

## 2.6 Immunocytochemistry

Cells were cultured on 24 mm round coverslips, washed with PBS and fixed in 2% w/v paraformaldehyde in PBS for 15 minutes. For RAD18 and PCNA detection, cells were fixed in ice-cold MeOH at -20°C for 10 minutes. Cells were permeabilized for 20 minutes with 0.2% v/v Triton X-100 in PBS. For detection of cyclobutane pyrimidine dimers (CPDs), cells were subsequently treated with 0.07 M NaOH in PBS for 5 minutes and permeabilized again for 20 minutes with 0.2% Triton X-100 in PBS. Cells were blocked with PBS<sup>+</sup> (PBS containing 0.5% w/v BSA and 0.15% w/v glycine) for 30 minutes, incubated with primary antibody for 2 hours, and washed with 0.2% Triton X-100 in PBS. Subsequently, cells were incubated with secondary antibody for 1 hour, washed with 0.2% Triton X-100 in PBS. Coverslips were placed on a slide, mounted with the Prolong Gold reagent (Invitrogen).

## 2.7 Antibodies

For primary antibodies, we used mouse monoclonal antibodies anti-CPD (Bioconnect), anti-fibrillarin 38F3 (Abcam), anti-GAPDH (Chemicon), anti-GFP (Roche), anti-phosphorylated H2AX (Upstate), anti-XRCC1 (Abcam), anti-PCNA PC10 (Abcam), anti-RPA/p34 Ab-1 (Thermo scientific), and rabbit polyclonal antibodies anti-RAD18 [16], anti-RAD51 [17], anti-XPA [18], and a goat polyclonal anti-Ku86 (Santa Cruz). For secondary antibodies, we used a goat anti-rabbit/mouse IgG-peroxidase (SIGMA), goat anti-rabbit alexa 488/564/633, donkey anti-rabbit 488/564, goat anti-mouse alexa 488/564/633, donkey anti-mouse 488/564, or donkey anti-goat alexa 488/555 (Molecular Probes).

## 2.8 Confocal and time-lapse microscopy

Images of living cells expressing YFP-tagged and mCherry-tagged proteins were obtained using a Zeiss LSM510NLO microscope (Carl Zeiss, Jena) with a 63×/1.40 NA oil immersion lens. Cells were maintained at 37°C in a mixture of air with 5% CO<sub>2</sub>. YFP-tagged proteins were detected by exciting YFP with a 488 nm Argon gas laser and monitoring YFP emission through a 500-550 band-pass filter. mCherry-tagged proteins were detected by exciting mCherry with a 543 nm Helium Neon laser and monitoring mCherry emission through a long-pass 560 filter. To minimize the effect of photobleaching, images were taken with 10 μW for a 488 nm laser, and with 20 μW for a 543 nm laser. For time-lapse experiments, cell images of 6 confocal planes at 1.5 μm intervals were taken every 10 minutes for 38 hours. All images were captured with a line average of 2. Time-lapse images were analysed using the AIM software (Carl Zeiss, Jena).

## 2.9 Foci analysis

A maximum projection of cell images of 6 confocal planes was made using the AIM software. A single nucleus was selected, aligned, and pixel intensities were measured with the ImageJ software (Rasband, W.S., ImageJ, U.S. National Institutes of Health, Bethesda, Maryland, USA [<http://rsb.info.nih.gov/ij/>]). On the basis of the pixel intensities, mean ( $\mu$ ) and standard deviation ( $\sigma$ ) were calculated, and the number and average size of foci were measured with the ImageJ software. We defined a region where Pixel intensity (I) is higher than the sum of the mean, and 1.5 times the standard deviation ( $I > \mu + 1.5 * \sigma$ ) as a focus [19]. For colocalization analysis, the AIM software was used for data analysis.

## 2.10 Local UV laser DNA damage induction

Local DNA damage induction using ZSI-A200 (Rapp Optoelectronic, Hamburg) connected to a Zeiss LSM510Meta confocal microscope (Carl Zeiss, Jena) has been described elsewhere [20]. Cells were locally irradiated with UVC for 0.49 seconds and images were monitored at 5 seconds intervals for 10 minutes immediately after irradiation. All images were captured with a line average of 4.

## 2.11 Local multi-photon DNA damage induction

A Coherent Mira modelocked Ti:Sapphire laser (multi-photon laser, MPL) (Coherent) connected to the Zeiss LSM510NLO confocal microscope was used at 800 nm with a pulse length of 200 fs and repetition rate of 76 MHz. For local DNA damage induction, an area of irradiation was set at  $4 \mu\text{m}^2$  ( $40 \times 40$  pixels), and the output of laser power was set at either 75 mW or 40 mW at pixel-dwell time 1.6  $\mu\text{s}$  with 5 iterations. Two images were taken before MPL irradiation and monitored at 10 seconds intervals for 10 minutes immediately after MPL irradiation. All images were captured with a line average of 1.

To detect accumulation of endogenous proteins at irradiated sites in fixed cells, etched grid coverslips (Bellco Biotechnology) were used to mark the position of irradiated cells.

## 2.12 Data analyses following local DNA damage induction

To analyse the data, fluorescence intensity of the irradiated area was measured at each time point using the AIM software. The data were normalized to obtain the fold induction of fluorescence intensity by setting the intensity of the area before irradiation at 1.0. The relative accumulation was normalized by setting the fluorescence intensity of the irradiated area before damage at 0, and the maximum fluorescence intensity at 1.0.

## 2.13 Inverse fluorescence recovery after photo-bleaching (iFRAP)

Local damage was applied in a selected region using MPL as described above. Outside this region, approximately 70% of nuclear area was bleached using the Zeiss LSM510NLO confocal microscope with a Helium Neon 543 nm laser with 158  $\mu\text{W}$  with 100 iterations. Cells were bleached 10 minutes after DNA damage had been induced with MPL irradiation. Cell images were taken before and after bleaching. For data analysis, the AIM software was used to measure the fluorescence intensity of the region of interest (1: irradiated with MPL and non-bleached; 2: non-irradiated

and non-bleached; 3: non-irradiated and bleached region). At each region, the loss of fluorescence intensity was calculated as  $I_{(area)} = I_a / I_b$ , ( $I_{(area)}$  is the loss of fluorescence intensity,  $I_a$  is the fluorescence intensity after bleaching, and  $I_b$  is the fluorescence intensity before bleaching).

### 3. RESULTS

#### 3.1 Functional analysis of YFP-RAD18 and mCherry-PCNA

We generated a HeLa cell line that stably expresses human RAD18 tagged with YFP at the N-terminus. On immunoblot, the expression level of YFP-RAD18 was equivalent to that of endogenous RAD18, and no free YFP or breakdown products of YFP-RAD18 were detected (Fig. 1A). Next, we tested the capability of YFP-RAD18 to mono-ubiquitylate PCNA in UVC-irradiated cells. Wild-type cells and cells stably expressing YFP-RAD18 were treated with siRNA targeting both endogenous RAD18 and YFP-RAD18, siRNA targeting only endogenous RAD18, or non-targeting siRNA. Subsequently, these cells were irradiated with UVC to induce PCNA mono-ubiquitylation. The basal as well as UV-induced PCNA mono-ubiquitylation in cells expressing both YFP-RAD18 and endogenous RAD18 were slightly higher than the level in wild-type cells or in cells expressing only YFP-RAD18 (Fig. 1B). After downregulation of both endogenous RAD18 and YFP-RAD18, UV-induced PCNA mono-ubiquitylation was strongly reduced. When we specifically downregulated only endogenous RAD18 in YFP-RAD18 cells, UV-induced PCNA mono-ubiquitylation was maintained at the wild-type level (Fig. 1B). Together, these results show that the addition of the YFP tag does not interfere with ubiquitylation of PCNA.

We also generated a HeLa cell line stably expressing human PCNA tagged with mCherry at the N-terminus. On immunoblot, the expression level of mCherry-PCNA was equivalent to that of endogenous PCNA (Fig. 1C). Both endogenous PCNA and mCherry-PCNA were mono-ubiquitylated after UVC irradiation, and their levels of mono-ubiquitylation were similar (Fig. 1D). This indicates that mCherry-PCNA can be incorporated into trimeric PCNA rings and ubiquitylated. Together, these results validate the use of fluorescent-tagged RAD18 and PCNA to study the behavior of these two proteins in living cells.

#### 3.2 Subnuclear localization of YFP-RAD18 during the cell cycle in living cells

We first characterized the localization pattern of YFP-RAD18 throughout the cell cycle. To identify the different phases of the cell cycle, mCherry-PCNA was transiently co-expressed and monitored. The subnuclear localization pattern of PCNA has been described [15] and we found the same localization for mCherry-PCNA. Images of living cells with 6 confocal planes were captured every 10 min for 38 h (Fig. 2A). In addition, the number and size of YFP-RAD18 and mCherry-PCNA foci were determined using maximal projection of the 6 confocal planes for each image (Fig. 2B, C). In G1 phase, YFP-RAD18 was excluded from nucleoli, but otherwise homogeneously distributed in the nuclei, with the exception of one or two relatively large and bright foci in approximately 84% (94/112) of the cells. These G1 foci are often localized adjacent to

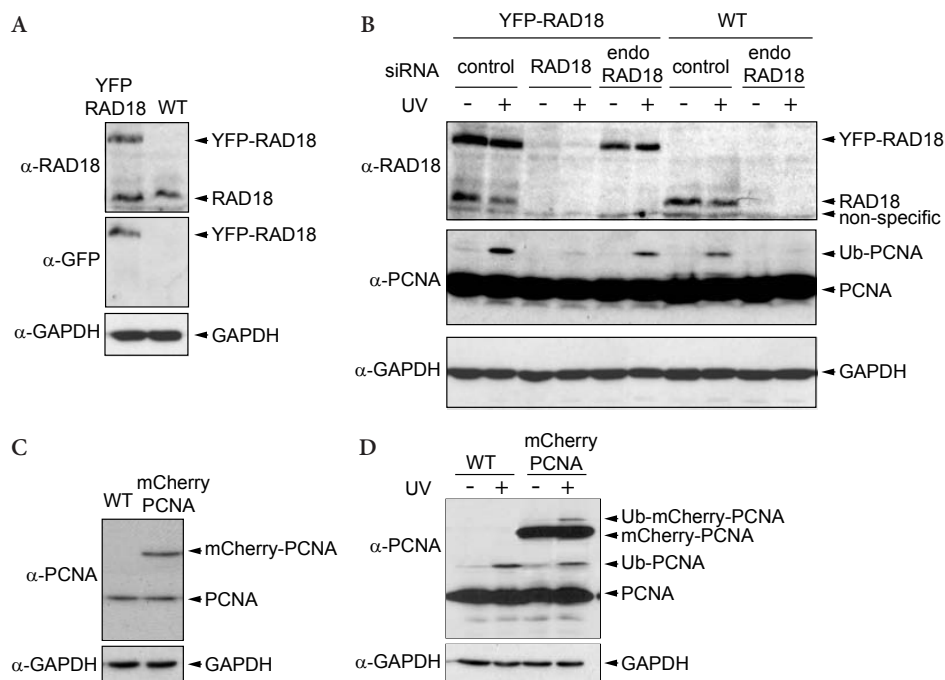


**Figure 1.** HeLa cells stably expressing either YFP-RAD18 or mCherry-PCNA. (A) Expression levels of endogenous RAD18 and overexpressed YFP-RAD18 were analysed in wild-type HeLa cells and HeLa cells stably expressing YFP-RAD18, on immunoblots with  $\alpha$ -RAD18,  $\alpha$ -GFP and  $\alpha$ -GAPDH. (B) Wild-type HeLa cells and HeLa cells stably expressing YFP-RAD18 were transfected with siRNA targeting both YFP-RAD18 and endogenous RAD18 (endoRAD18), only endogenous RAD18 (endoRAD18) or non-targeting siRNA (control). Forty-eight hours after addition of the si-RNAs, cells were irradiated with UVC and whole-cell extracts were prepared 8 hours later. Expression levels of YFP-RAD18, endogenous RAD18 and mono-ubiquitylated PCNA were analysed on immunoblots with  $\alpha$ -RAD18 and  $\alpha$ -PCNA, using  $\alpha$ -GAPDH as control. (C) Expression levels of endogenous PCNA and overexpressed mCherry-PCNA were analysed in wild-type HeLa cells and HeLa cells stably expressing mCherry-PCNA on immunoblots with  $\alpha$ -PCNA, using  $\alpha$ -GAPDH as control. (D) Wild-type HeLa cells and HeLa cells stably expressing mCherry-PCNA were irradiated with UVC as described above. Expression levels of endogenous PCNA, mono-ubiquitylated PCNA, mCherry-PCNA and mono-ubiquitylated mCherry-PCNA were analysed on immunoblots with  $\alpha$ -PCNA, using  $\alpha$ -GAPDH as control.

the nucleoli (181/200) (Fig. S1 in supplementary material). When cells entered S phase, more YFP-RAD18 foci appeared and the size of the foci decreased (Fig. 2B, C). At this stage, it was not possible to determine whether the G1 foci disappeared or decreased in size and brightness. The number of the foci increased until mid S phase, while the average size remained constant (Fig. 2B, C). YFP-RAD18 foci were still present during early G2 phase when mCherry-PCNA foci were no longer detected. At the end of G2 phase, YFP-RAD18 relocated into the nucleoli.

Next, we measured the total intensity of YFP-RAD18 signal throughout the cell cycle, relative to the level at the beginning of G1 phase. This signal increased two-fold during G1 and remained constant until cells underwent mitosis. After cell division, the YFP-RAD18 signal in the two daughter cells was similar to that of the mother cell at

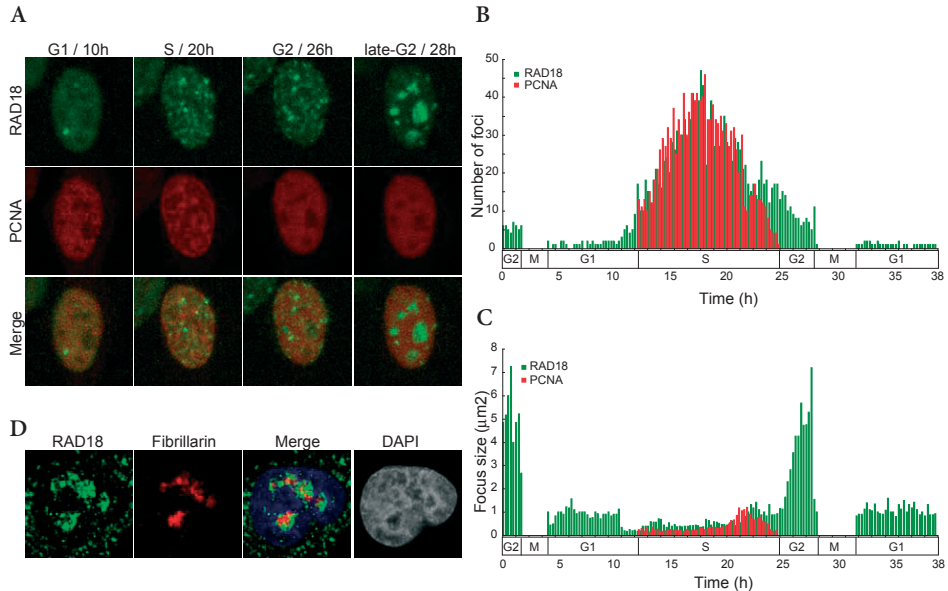


**Figure 2. Dynamics of RAD18 during the cell cycle.** (A) Images from time-lapse analysis of a living HeLa cell stably expressing YFP-RAD18 and transiently co-expressed mCherry-PCNA. To analyse YFP-RAD18 throughout the cell cycle, a cell in G2 phase was selected and this time point of the beginning of the analysis was set at 0. Subsequently, images were captured every 10 minutes for 38 hours. The time points indicated above the pictures correspond to the time points shown in B and C. (B, C) The number (B) and average size (C) of nuclear foci for YFP-RAD18 (green) and mCherry-PCNA (red). (D) Wild-type HeLa cells were fixed and RAD18 was visualized using the antibody in late G2 phase. Nucleoli were visualized using an antibody against fibrillarin.

the beginning of G1 (data not shown). This indicates that the dynamic changes in the number and size of YFP-RAD18 foci during S and G2 phases are not related to either synthesis or degradation of YFP-RAD18.

We confirmed that the specific distribution pattern of YFP-RAD18 represents the behavior of endogenous RAD18 by immunostaining for endogenous RAD18 and PCNA in fixed wild-type HeLa cells (Fig. S2 in supplementary material). The localization of endogenous RAD18 in the nucleoli at late G2 was verified by co-immunostaining for the nucleolar protein fibrillarin (Fig. 2D). Fibrillarin is known to localize to the dense fibrillar component of the nucleolus. The RAD18 immunostaining immediately surrounded the fibrillarin-positive area, indicating that RAD18 localizes to the granular component of the nucleolus.

### 3.3. Limited colocalization of YFP-RAD18 foci with mCherry-PCNA foci in S phase

The function of PCNA during DNA replication is thought to be visualized by the numerous PCNA foci that form only in S phase [15]. Since we found that YFP-RAD18 forms many foci in S phase (Fig. 2A), we reasoned that the majority of these YFP-RAD18 foci might reflect sites of PCNA ubiquitylation at stalled replication forks. Surprisingly, we observed that only a minority of the YFP-RAD18 foci overlapped

with the mCherry-PCNA foci in early, mid and late S phases (Fig. 3A). In mid and late S, YFP-RAD18 and mCherry-PCNA obviously displayed different localization patterns, but in early S, the distribution patterns were more similar (Fig. 3A). At this stage, approximately 20% of YFP-RAD18 colocalized with mCherry-PCNA. This colocalization percentage increased to approximately 50% following UVC irradiation (Fig. 3D). The partial colocalization was visualized with nuclear line scans in a single focal plane (Fig. 3B for non-irradiated cells, Fig. 3C for UVC-irradiated cells). This indicates that in S phase, the majority of RAD18 functions separately from PCNA. However, it is clear that RAD18 cooperates more frequently with PCNA following UVC irradiation.

### **3.4. Kinetics of YFP-RAD18 and mCherry-PCNA accumulation at UVC-irradiated sites in living cells**

It has been reported that RAD18 [12] and PCNA [21,22] accumulate at UVC-induced DNA damage. Here we analysed the kinetics of these accumulations at UVC-irradiated sites during all cell-cycle phases in living cells. UVC light is known to directly induce helix-distorting lesions such as cyclobutane pyrimidine dimers (CPDs) and 6-4 photoproducts [23,24]. It is important to note that the UVC laser was set to induce only NER-specific lesions and no SSBs or DSBs [20]. Cells in G1 phase showed accumulation of mCherry-PCNA at the irradiated site, followed by YFP-RAD18 (Fig. 3E arrowhead and lower graph). Maximal levels of accumulation were reached around 10 minutes after irradiation, and the fluorescence intensities of YFP-RAD18 and mCherry-PCNA at the irradiated site increased 3.5-fold and 2-fold, respectively (Fig. 3E, upper graph). Intriguingly, similar accumulation patterns were observed in S and G2 cells (Fig. S3 in supplementary material). The accumulation of RAD18 at these DNA repair sites throughout the cell cycle may indicate that translesion polymerases are required for DNA synthesis at these sites. We performed the same experiments using cells stably expressing mCherry-PCNA and transiently co-expressing YFP-RAD18, and obtained similar results (data not shown).

### **3.5. Spontaneous YFP-RAD18 foci in G1 and S phases colocalize with proteins involved in double-strand break repair**

Next, we investigated the colocalization of spontaneous RAD18 foci with repair-associated proteins. We fixed wild-type HeLa cells, and visualized RAD51, Ku86 and  $\gamma$ H2AX (associated with DSB repair), RPA (single-stranded DNA binding protein involved in DNA replication and other DNA processing pathways), XRCC1 (associated with SSB repair), or XPA (associated with nucleotide excision repair (NER)), with immunofluorescence. In RAD18-positive G1 foci, neither SSB repair nor NER-associated proteins accumulated. Intriguingly, we found colocalization of the DSB repair-associated proteins and RPA with RAD18 foci in G1 phase (Fig. 4A). 44% (41/94), 47% (72/153), 26% (39/138), and 63% (78/123) of RAD18 G1 foci colocalized with foci of RAD51, RPA, Ku86, and  $\gamma$ H2AX, respectively. Triple staining of RAD18, RPA and RAD51 indicated that the majority of RAD18 foci that were positive for RAD51 also contained RPA (91% (98/105)). In addition, RPA-positive RAD18 foci without RAD51

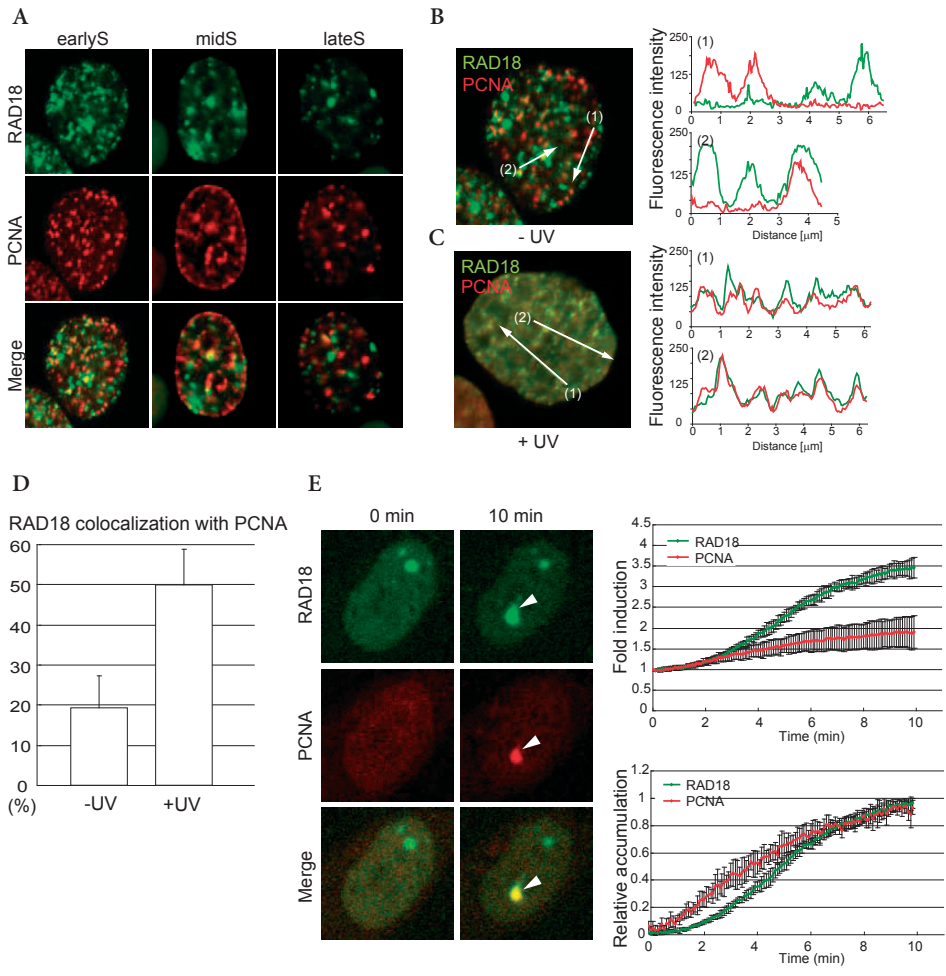


**Figure 3. Differential distribution of YFP-RAD18 and mCherry-PCNA during S phase, and accumulation of both proteins following local UVC irradiation.** (A) Confocal images of living HeLa cells stably expressing YFP-RAD18 and transiently co-expressing mCherry-PCNA in early, mid, and late S phases. (B) A confocal image of YFP-RAD18 and mCherry-PCNA in an early S phase nucleus. White lines correspond to the line scans (line 1; upper graph, line 2; lower graph). The signal intensities of YFP-RAD18 (green) and mCherry-PCNA (red) were measured using ImageJ software. (C) HeLa cells stably expressing YFP-RAD18 and transiently co-expressing mCherry-PCNA were globally irradiated with UVC and the confocal image was captured after 1 hour. White lines correspond to the line scans as described above. (D) The percentage of YFP-RAD18 foci that overlapped with mCherry-PCNA foci in control and globally irradiated nuclei with UVC; 45 nuclei for control cells and 45 nuclei for UVC-irradiated cells were measured from three independent experiments. The error bars represent the standard deviation. (E) Nuclei of living HeLa cells stably expressing YFP-RAD18 and transiently co-expressing mCherry-PCNA were locally irradiated with a UVC laser, and the fluorescence intensities of YFP-RAD18 and mCherry-PCNA at the irradiated site were measured every 5 seconds for 10 minutes. The fold induction is shown upper graph and the relative accumulation is shown in lower graph. The error bars in the graphs represent the standard deviation for 20 nuclei.

were not observed. When we analysed the RAD51 and RPA positive RAD18 foci in more detail, we found that RAD51 and RPA were concentrated in the center of the more diffuse RAD18 signal. Occasionally, RAD18 foci contained multiple RAD51 and RPA foci (Fig. 4B). Together, these data suggest that the G1 foci may contain either Ku86 or RAD51, the latter often together with RPA. In addition, it appears that RAD18 does not bind directly to the site of DNA damage but localizes to the surrounding chromatin area.

In S and G2 phases, RAD51 and  $\gamma$ H2AX accumulated in a large number of spontaneous foci, and the majority of these colocalized with RAD18 foci (Fig. 4C, D). These data show that spontaneous RAD18 foci in S and G2 frequently colocalize with DSB repair-associated proteins. We did not detect any Ku86 foci formation in S/G2 phase nuclei (data not shown). In S phase, DSBs are often generated at sites where the replication machinery has collapsed, and RAD51 may be recruited to such sites. To study this, we investigated the colocalization of spontaneous RAD51 and PCNA foci in

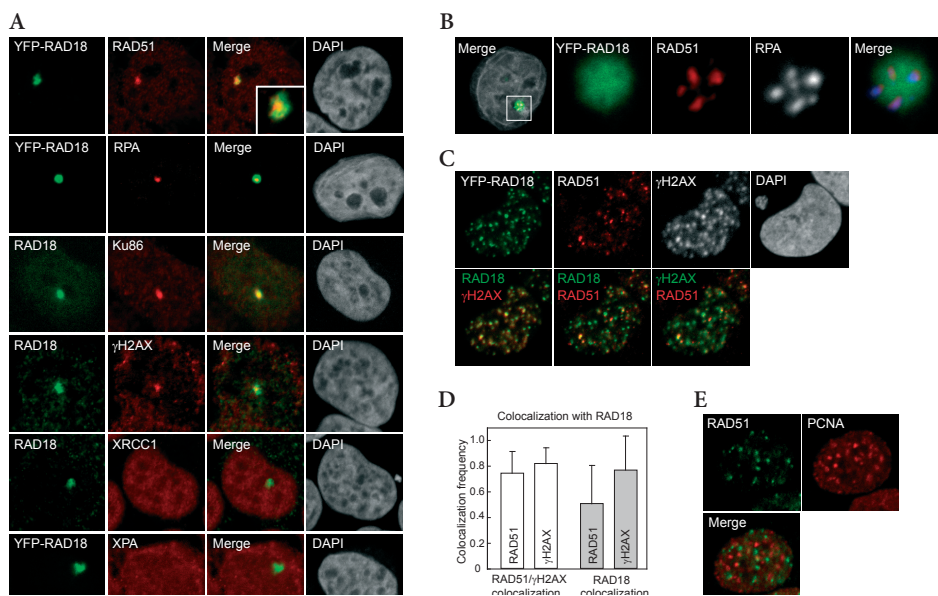


**Figure 4. Localization of RAD18 in relation to endogenous repair associated proteins at different cell cycle phases.** Wild-type HeLa cells or HeLa cells stably expressing YFP-RAD18 were fixed, and proteins were visualized using the antibodies indicated in the pictures. Endogenous RAD51 and XPA were detected in HeLa cells stably expressing YFP-RAD18. The other endogenous proteins were detected in wild-type cells, together with endogenous RAD18. (A) Colocalization of the RAD18 G1 focus with RAD51, RPA,  $\gamma$ H2AX, and Ku86, but not with XRCC1 and XPA. Inset in the merge of RAD51 and YFP-RAD18 shows a magnification of the RAD51-positive RAD18 focus, to visualize the diffuse RAD18 and more concentrated RAD51 signals. (B) Colocalization of G1 phase RAD18 focus with RAD51 and RPA. Multiple RAD51/RPA foci of different intensities localize within a single diffuse RAD18 focus. (C) Colocalization of the S phase foci of YFP-RAD18 with RAD51 and  $\gamma$ H2AX. (D) Colocalization frequency of RAD51 and  $\gamma$ H2AX with RAD18 foci in S/G2 phase (white bars), and colocalization frequency of RAD18 foci with RAD51 and  $\gamma$ H2AX (grey bars). The error bars in the graph represent the standard deviation for 50 nuclei. (E) Colocalization of RAD51 foci with PCNA in S phase. Colocalization frequency of RAD51 with PCNA was 8%, obtained from the analysis of 30 nuclei.

S phase. Similar to Tashiro et al. [25], we found that only a few RAD51 foci colocalized with PCNA (8%) (Fig. 4E).

To investigate whether the formation of RAD51 and  $\gamma$ H2AX foci depends on RAD18, we downregulated RAD18 by siRNA and examined foci formation of DSB repair-associated proteins throughout the cell cycle. Knockdown of YFP-RAD18 and endogenous RAD18 did not affect the formation of spontaneous RAD51 and  $\gamma$ H2AX foci at any of the cell cycle phases (Fig. S4 in supplementary material).

### **3.6. Dynamic analysis of YFP-RAD18 foci induced by global ionizing radiation in living cells**

The RAD18 foci in G1 phase could represent genuine DSB repair sites. To analyse the dynamics of these spontaneous G1 foci in the presence of (additional) exogenously induced DSBs, we globally exposed HeLa cells stably expressing YFP-RAD18 to IR (2.5 Gy) during G1, and performed time-lapse experiments. Upon irradiation, numerous extra RAD18 foci appeared. The number of IR-induced RAD18 foci was dose-dependent (data not shown). Analyses of fixed cells showed that the vast majority of induced RAD18 foci contain  $\gamma$ H2AX, and a subpopulation is positive for RAD51, indicating that DSBs were generated (Fig. 5A). In accordance with a previous study [26], global  $\gamma$ -irradiation did not induce visible Ku86 accumulation with different doses (0.5 - 10 Gy) at different time points (0.5 - 4 hours) in all cell-cycle phases (data not shown). To repair a single DSB site by NHEJ, most likely only a few molecules of Ku heterodimers are required [26], and the accumulation of such a small number of molecules could remain below the level of detection with immunofluorescence. Most of the IR-induced RAD18 foci gradually disappeared, but a few foci persisted and increased in size (Fig. 5B). Notably, the persisting RAD18 G1 foci included spontaneous G1 foci (Fig. 5B, arrowhead), and colocalized with RAD51 (Fig. 5C, arrowhead). Upon entrance of S phase, multiple foci appeared, in a pattern that was similar to what was observed in non-irradiated S phase cells (Fig. 2A for non-irradiated cells). IR irradiation produces more SSBs than DSBs [27,28]. Possibly, the IR-induced SSBs are represented by the RAD18 foci that disappear rapidly, whereas the persistent foci mark DSBs.

Upon irradiation with 2.5 Gy in late G2, RAD18 was recruited from the nucleoli and formed a large number of foci (Fig. 5A, D), and the majority of IR-induced RAD18 contained RAD51 and  $\gamma$ H2AX (Fig. 5A). After a prolonged G2 phase, the IR-induced RAD18 foci disappeared, and RAD18 relocated into the nucleoli before cells entered M phase (Fig. 5D). These cells still contain several  $\gamma$ H2AX foci (data not shown). After cell division, the daughter cells contained more spontaneous RAD18 foci than non-irradiated cells (Fig. 5D), and these foci persisted until cells entered S phase (data not shown).

### **3.7. Response of DSB repair associated proteins to DNA damage induced by low-power MPL irradiation**

To be able to study RAD18 accumulation at DSBs in more detail during all cell cycle phases, we optimized a pulsed 800 nm laser (multi-photon laser, MPL) to induce local DSBs. A pulsed 800 nm laser with three-photon excitation is able to excite molecules at 266 nm, which is the same wavelength with the UVC laser described above [29].

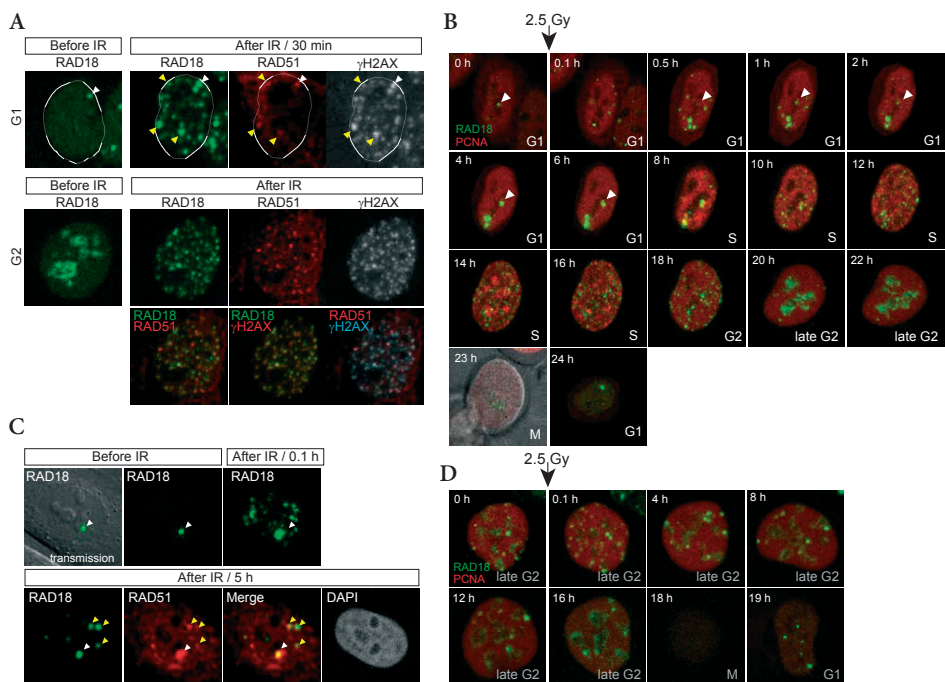


**Figure 5.** YFP-RAD18 accumulation following global IR. HeLa cells stably expressing YFP-RAD18 were imaged and, subsequently irradiated with IR (2.5 Gy). White and yellow arrowheads represent endogenous G1 focus and IR-induced DSB sites, respectively. (A) Confocal images of living HeLa cells stably expressing YFP-RAD18 in G1 and in late G2. 30 minutes after IR irradiation, the same nuclei were fixed and endogenous RAD51 and  $\gamma$ H2AX were visualized using the antibodies. The nucleus is outlined. (B, D) Time-lapse experiments of living cells were performed after IR irradiation in G1 (B) or late G2 (D). Maximum projections of 6 confocal planes are shown. Time after IR irradiation (left-top) and cell-cycle phases (right-bottom) are shown in the pictures. Different phases of the cell cycle were identified by subnuclear localization of transiently co-expressed mCherry-PCNA. (C) Confocal images of living HeLa cells stably expressing YFP-RAD18 in G1 before and 6 minutes after IR irradiation. The same nuclei were fixed 5 hours after IR irradiation and endogenous RAD51 was visualized using the antibodies.

The laser also likely excites molecules with one or two-photon. The MPL at high power output is known to induce many types of DNA lesions such as helix-distorting lesions [20,29], SSBs and DSBs (Fig. S5A in supplementary material). Damage induction with low output power is a new application of this tool. We characterized the accumulation of different DNA repair proteins using the MPL with output power at 40 mW. Although the DSB repair-associated proteins RAD51, Ku86 and  $\gamma$ H2AX accumulated at the irradiated site, there was no apparent accumulation of CPDs, XPA (involved in NER), and XRCC1 (involved in SSB repair) (Table 1, Fig. S5B in supplementary material). Accumulation of CPDs, XPA, and XRCC1 was still detected at sites of high-power MPL irradiation on the same coverslips, providing a positive control for the immunostaining method (Fig. S5A in supplementary material). This indicates that low-power laser output preferentially generates DSBs, whereas high-power laser output induces various additional types of damage.

**Table I.** Accumulation of repair-associated proteins after MPL irradiation (40mW/75mW)

	RAD18	RAD51	Ku86	$\gamma$ H2AX	XRCC1	CPD	XPA
40 mW	+ <sup>a)</sup>	+	+	+	-	-	-
75 mW	+	+	+	+	+	+	+

<sup>a)</sup> Positive and negative accumulations of indicated proteins at MPL irradiated sites are presented with + and -, respectively

### 3.8. Kinetic analysis of YFP-RAD18 and mCherry-PCNA accumulation in response to MPL irradiation

To further investigate the damage response of RAD18 and PCNA, we induced DNA damage using a MPL with either high-power (75 mW) or low-power (40 mW). Cells stably expressing YFP-RAD18 and transiently co-expressing mCherry-PCNA were locally irradiated, and images were captured every 10 seconds for 10 minutes. Cells irradiated with high-power MPL showed accumulation of YFP-RAD18 and mCherry-PCNA at the irradiated site at all cell-cycle phases (Fig. 6A and Fig. S6 in supplementary material). mCherry-PCNA accumulated first, reaching plateau level within 3 minutes, whereas YFP-RAD18 started to accumulate later, with the signal increasing continuously until 6-8 minutes after damage induction (Fig. 6C, E, F). Downregulation of RAD18 did not have any effect on PCNA accumulation at high-power MPL irradiated sites (data not shown), indicating that PCNA accumulates independent of RAD18. Surprisingly, the low-power MPL irradiation did not induce detectable mCherry-PCNA accumulation at the damaged site at any cell cycle phases, in contrast to YFP-RAD18 that did accumulate (Fig. 6B, D and Fig. S6 in supplementary material).

The maximum accumulation of YFP-RAD18 at high-power MPL exposure was similar throughout the cell cycle (approximately 9-fold). Using low-power MPL irradiation, the maximum accumulation of RAD18 was 5-6-fold in G1 and S (Fig. 6D, E), and 2-3-fold in G2 (Fig. 6F). The relative accumulation in the different situations show that PCNA exhibited a similar fast accumulation at sites of high-power MPL damage at all cell-cycle phases. Note that with low-power MPL irradiation, PCNA accumulation was not detectable. RAD18 accumulated with fast kinetics in G1 after high-power MPL irradiation, and in S after low- and high-power MPL irradiation. Slow accumulation of RAD18 was observed in G1 after low-power MPL irradiation, and in G2 after low and high-power MPL irradiation (Fig. 6G). For cells stably expressing mCherry-PCNA and transiently co-expressing YFP-RAD18, MPL irradiation showed the same results as described above (data not shown).

To study whether the accumulation of RAD51 and  $\gamma$ H2AX at MPL-induced damage sites functionally depends on expression of RAD18, we downregulated RAD18 by siRNA, and checked damage-induced accumulation of RAD51 and  $\gamma$ H2AX. Knockdown of YFP-RAD18 and endogenous RAD18 did not affect the accumulation of RAD51 and  $\gamma$ H2AX at the damaged sites (Fig. S7 in supplementary material), indicating that these process can occur independent of normal amount of RAD18.

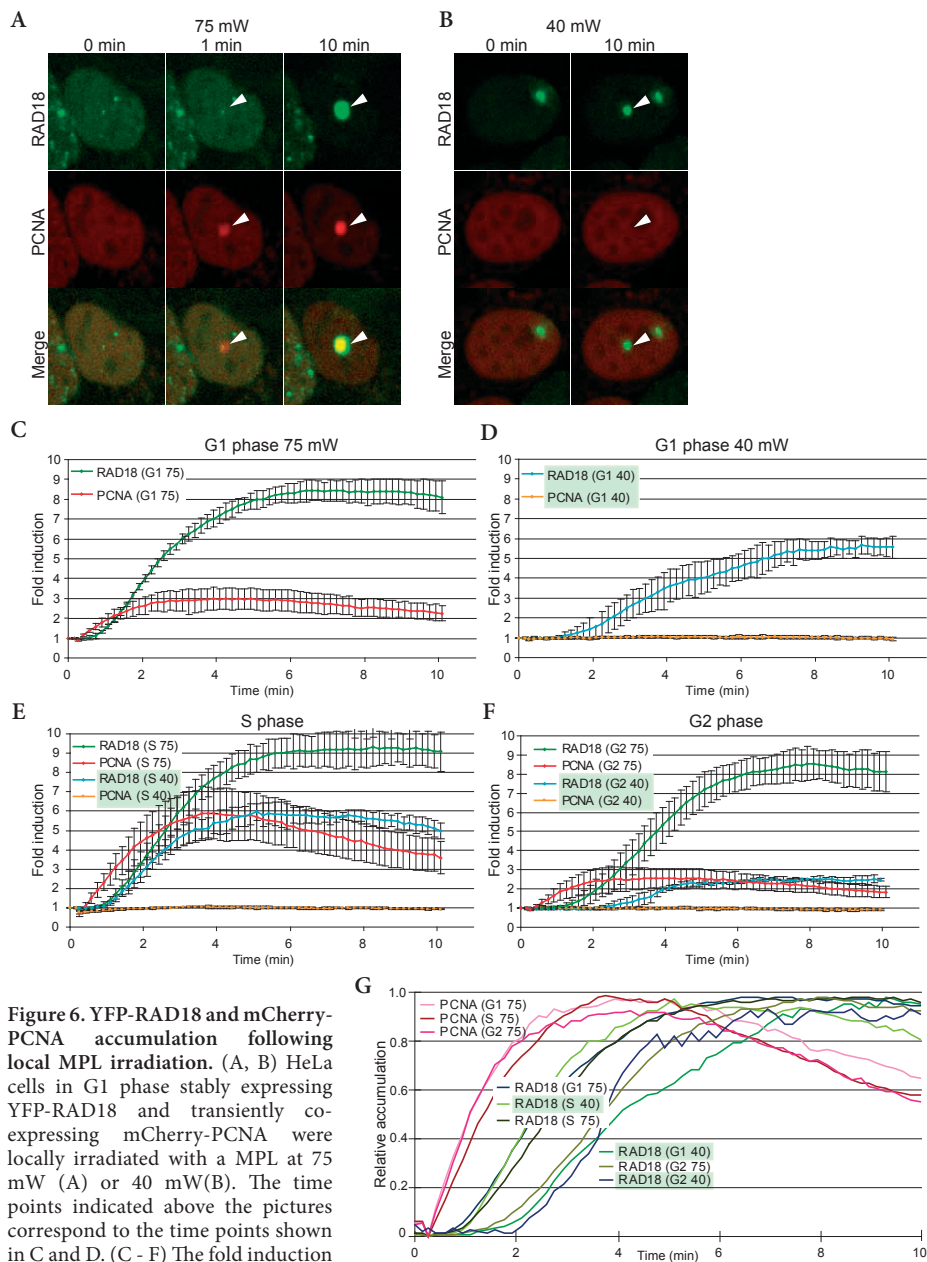


**Figure 6. YFP-RAD18 and mCherry-PCNA accumulation following local MPL irradiation.** (A, B) HeLa cells in G1 phase stably expressing YFP-RAD18 and transiently co-expressing mCherry-PCNA were locally irradiated with a MPL at 75 mW (A) or 40 mW (B). The time points indicated above the pictures correspond to the time points shown in C and D. (C - F) The fold induction of YFP-RAD18 and mCherry-PCNA at irradiated sites is shown. The error bars in the graphs represent the standard deviation for 10 nuclei. (A - D) Cells in G1 phase. (E) Cells in S phase. (F) Cells in G2 phase. (G) The relative accumulation of YFP-RAD18 and mCherry-PCNA at irradiated sites for all experimental conditions tested.

### 3.9. Analysis of mCherry-PCNA accumulation at locally damaged sites using inverse fluorescent recovery after photo-bleaching

No accumulation of mCherry-PCNA was observed after low-power MPL irradiation (Fig. 6B). The amount of accumulated mCherry-PCNA may remain below the level of detection, due to the large total amount of PCNA relative to the number of available binding sites. Accumulated mCherry-PCNA at the damaged site may become visible after the free fraction of mCherry-PCNA has been bleached. To test this, we first applied local damage, using MPL with either low or high power in G1 cells, and subsequently bleached the mCherry signal (Fig. 7A). The intensity of mCherry-PCNA was measured at the locally damaged site, and in bleached and non-bleached control sites (Fig. 7B, C). Following photo-bleaching, the fluorescence intensity at the irradiated site with high-power MPL decreased only 2% (Fig. 7B, region 1), whereas the intensity level at the non-irradiated area decreased 31% (Fig. 7B, region 2). This indicates that mCherry-PCNA is less mobile at the irradiated site than at the non-irradiated site. In contrast, the intensity level at the irradiated site with low-power MPL decreased 38% following photo-bleaching (Fig. 7C, region 1) and this was similar to the decrease of 39% at the non-irradiated site (Fig. 7C, region 2). This confirms that mCherry-PCNA does not specifically accumulate at the irradiated site with low-power MPL.

We next studied the accumulation of endogenous PCNA at MPL irradiated sites using fixed cells. Corresponding to the observations for mCherry-PCNA accumulation in living cells, endogenous PCNA accumulated at the irradiated site when high-power MPL was used, but not with low power (Fig. 7D).

## 4. DISCUSSION

### 4.1 RAD18 functions throughout the cell cycle

In the present work, the use of cells expressing both mCherry-PCNA and YFP-RAD18 provided a powerful tool to study individual living cells at defined phases of the cell cycle, without the need for cell synchronization.

We found that RAD18 accumulates at multiple types of DNA damage throughout the cell cycle, but with different kinetics depending on the type of damage and the cell cycle phases. The kinetic analysis of PCNA and RAD18 at locally UVC-induced sites showed that PCNA accumulated first at these sites followed by RAD18. This observation supports the current notion that the RAD18-RAD6 complex is recruited to the stalled DNA polymerase machinery to mono-ubiquitylate PCNA in S phase [7]. Surprisingly, the kinetics of PCNA and RAD18 accumulation is similar throughout the cell cycle, and thus independent of ongoing DNA replication. Previously, Essers et al. [15] have shown that recruitment of PCNA to local UVC damage is independent of the cell cycle, and requires an intact NER pathway. In contrast, RAD18 has been shown to accumulate at sites of local UVC damage in XPA and XPC mutant cells [12]. This indicates that the recruitment of PCNA and RAD18 to local UV damage occurs independently. Surprisingly, RAD18 showed only very limited colocalization with PCNA throughout the cell cycle, indicating that a large fraction of RAD18 functions

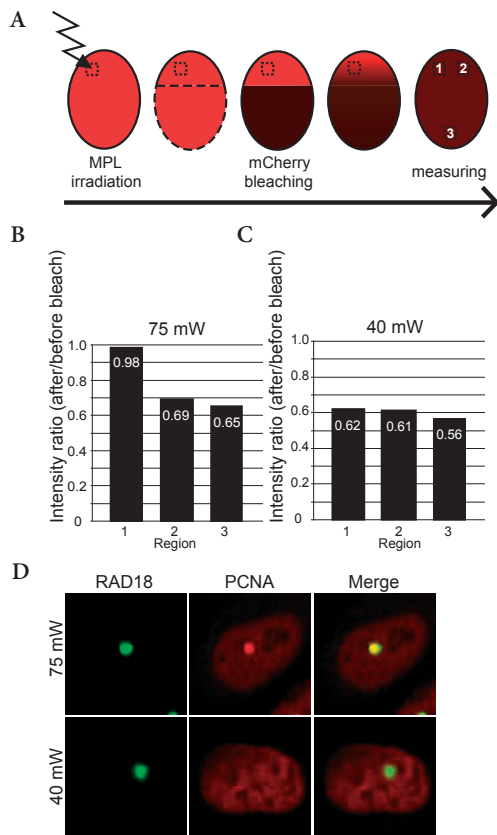


**Figure 7. iFRAP analysis and response of endogenous PCNA to local MPL damage.** (A) Schematic presentation of the iFRAP experiment. HeLa cells expressing YFP-RAD18 and mCherry-PCNA were locally irradiated with MPL either at (B) 75 mW or (C) 40 mW. Subsequently, mCherry-PCNA were locally bleached in the indicated area. Nuclear images of mCherry-PCNA were captured and fluorescence intensity was measured before and after bleaching at region 1 (irradiated with MPL and non-bleached), at region 2 (non-irradiated and non-bleached), and at region 3 (non-irradiated and bleached). (B, C) The loss of fluorescence intensity for mCherry-PCNA in each region. Five independent experiments were performed and representative results are shown. (D) Cells stably expressing YFP-RAD18 were irradiated with MPL either at 75 mW or at 40 mW. Subsequently, cells were fixed and endogenous PCNA was visualized using anti-PCNA.

independently of PCNA, and most likely outside the context of the RDB pathway. Previously, RAD18 has been shown to accumulate at SSB repair sites throughout the cell cycle [12]. Herein we provide evidence for RAD18 functions at DSB repair sites.

#### 4.2 RAD18 and DSB-repair in G1 phase

RAD18 forms 1 or 2 spontaneous G1 foci that colocalize with either RAD51 (and RPA) or Ku86 and that are also positive for  $\gamma$ H2AX. We suggest that the Ku86-positive RAD18 G1 foci are sites of ongoing NHEJ repair, and when the NHEJ process has completed, these foci may disappear. Single IR-induced DSBs are not expected to show visible Ku heterodimer accumulation, since the number of molecules that bind to the ends of a single DSB has been estimated to remain below 50 [26]. This suggests that spontaneous Ku86-positive RAD18 foci may contain multiple DSBs. The presence of multiple RAD51/RPA foci in some RAD18 foci also indicates that more than one DSB can be present in a single G1 focus. RAD18 G1 foci that contain RAD51 often colocalize with RPA, indicating that these DSBs have undergone strand resection and formation of RPA filaments on the single-stranded DNA, precluding repair by NHEJ. These sites may not be able to complete repair during G1, due to the absence of the

sister chromatid as repair template. To support this hypothesis, we induced extra DSBs in G1 phase cells by  $\gamma$ -irradiation and analysed repair of these induced DSBs. Global  $\gamma$ -irradiation of G1 cells induced the formation of multiple RAD18 foci, and a few of these persisted into S phase. These persisting foci partially corresponded to the spontaneous foci that were present prior to irradiation. The increased size of these foci compared to the size of the foci shortly after irradiation is most likely caused by the establishment of a new equilibrium between the amount of free YFP-RAD18 and bound YFP-RAD18, depending on the number of high affinity binding sites. This phenomenon is reciprocal to the decreased intensity of the spontaneous G1 focus upon local damage induction (Fig. 3E, 6A, B). A large fraction of these persisting RAD18 foci are RAD51 and RPA positive. This indicates that both the spontaneous and induced G1 foci reflect DSB repair sites, and that these breaks remain present until the cells enter S phase. These observations are in accordance with the findings described by Barlow et al. [30] who suggested that IR-induced DSBs in G1 persist until entry into S phase in yeast. Zierhut and Diffley [31] have shown that DSB resection, which is required in HR, is suppressed by NHEJ, but not absent during G1 in yeast. It is not clear whether and/or how DSBs generated in G1 can be repaired by HR in S/G2 because DSBs interfere with DNA replication. Taken together, we suggest that in G1 phase, RAD18 binds to sites containing DSBs that may be recognized by the NHEJ or HR pathway. Depending on the chosen pathway, the DSBs are either repaired (NHEJ) or persist until S phase (HR). All the proteins analysed in this study still accumulate at DSBs in the absence of RAD18, and therefore, RAD18 most likely functions downstream from the actual damage recognition components. Since RAD18 recognizes multiple types of DNA damage, and localizes in a diffuse region surrounding the site of damage, we suggest that RAD18 does not function as an actual repair protein, but may signal in the checkpoint pathway or is necessary for DNA repair associated chromatin remodeling. Identification of the specific ubiquitylation substrates at damaged sites will help to define this function in more detail.

#### 4.3 RAD18 and DSB-repair in S phase

Recently, different groups have provided evidence for RAD18 functions in DSB repair. For RAD18-deficient human HCT116 cells, gene integration frequency is ten times higher than that of control cells [11]. Similarly, gene recombination and sister chromatid exchange are enhanced in *Rad18*-knockout mouse ES cells [9]. In RAD18-deficient cells, DNA lesions may be channeled from disabled RDB into HR. This idea is supported by the fact that *rad18/rad54* double-knockout DT40 chicken cells are not viable. However, RAD18 may also play a direct role in HR, since DSB-induced gene conversion frequencies in human and DT40 cells without RAD18 are lower [14,32]. Saberi et al. [14] showed that this phenotype depends on an intact NHEJ pathway, and suggest that RAD18 may suppress toxic effects of NHEJ during HR on DSBs induced at stalled replication forks. In this study, we found that RAD18 formed multiple spontaneous foci in S and early G2 phases of which only a minority colocalizes with the known substrate PCNA. Based on recent data obtained in yeast, another candidate substrate is the 9-1-1 (RAD9-RAD1-HUS1) checkpoint clamp [33]. However, one of

the 9-1-1 components, RAD9, does not form spontaneous foci in S phase (data not shown). Intriguingly, we found that many of the RAD18 foci in S and early G2 contain RAD51 and  $\gamma$ H2AX, and only 8% of RAD51 foci colocalized with PCNA foci in S phase. In accordance with our observations, previous studies reported the occurrence of spontaneous RAD51 foci during S phase in asynchronous cells [25,34-37], where the RAD51 foci colocalize with proteins involved in HR, such as BRCA1 but not with PCNA [37]. Together with our data, this indicates that RAD18 foci that colocalize with PCNA in S phase mark sites of RDB, whereas RAD18 foci that colocalize with RAD51 in S and early G2 phases mark sites of HR repair. RAD18 foci that colocalize with both PCNA and RAD51 might mark sites of DSBs caused by collapsed DNA replication forks in S phase. In addition, the results obtained with low-power MPL irradiation reveal that RAD18 always accumulates at sites of DSBs, independent of DNA replication.

#### **4.4 RAD18 moves from persisting DSBs into the nucleolus in late G2 phase, and reappears at these sites in G1**

Near the end of G2 phase, RAD18 relocates into the granular component of the nucleoli. Notably, we do not find accumulation of either  $\gamma$ H2AX or RAD51 in the nucleoli. The primary function of the nucleolus is ribosome biogenesis, which is maximal in S and G2 phases. However, possible additional functions of the nucleolus have been suggested. A number of DNA repair-associated proteins have been reported to localize in the nucleolus. Upon induction of DNA damage, most of these proteins move out of the nucleolus and disperse into the rest of the nucleus, or accumulate in DNA repair foci. On the basis of these observations, the nucleolus may act both as a sensor of DNA damage, and as a storage site in damage response pathways (reviewed by [38]). RAD18 localizes in the nucleoli only in late G2 phase. From there, it can still be recruited to sites of local and global DNA damage although the relative accumulation was slowest in G2 phase after MPL irradiation. This indicates that RAD18 is relatively immobile in the nucleoli. Surprisingly, RAD18 recruited from the nucleoli to the IR-induced damaged sites relocates again to the nucleoli before the cell reaches M phase. Furthermore, the daughter cells subsequently show a higher number of spontaneous G1 foci. This indicates that RAD18 is released from unrepaired DSB sites before cells enter mitosis, and relocates to these sites after cell division, in early G1 phase. Recently, Deckbar et al. [39] showed that there is a threshold below which cells are released from the G2/M checkpoint and are able to enter M phase in the presence of DSBs. Our time-lapse data confirm and strengthen the notion that mammalian cells can enter M phase in the presence of unrepaired DSBs. Furthermore, we show that such DSBs are recognized by proteins involved in the HR repair pathway and RAD18 in the next G1 phase. The relocation of RAD18 to the nucleoli before the G2/M transition may be required to pass the G2/M checkpoint. It is unclear why RAD18 localizes to the nucleoli only in late G2 phase. Little is known about the mechanisms that regulate cell-cycle-specific storage of proteins in the nucleolus, and the relevance of RAD18 relocation to the nucleolus, selectively in G2 phase remains to be determined.

#### 4.5 RAD18 and DSBs-repair in meiotic prophase

RAD18 is highly expressed during meiotic prophase in mouse spermatocytes [16], in which approximately 400 DSBs are induced by the topoisomerase-like enzyme SPO11 [40,41]. Normally, a non-sister chromatid on the homologous chromosome is used for repair, since repair via the sister chromatid is repressed. This creates a problem for the X and Y chromosomes that are largely heterologous. SPO11-induced DSBs, marked by RAD51 foci, persist on the XY pair [42]. This is associated with the accumulation of RAD18,  $\gamma$ H2AX [16,40] and other repair-associated proteins. On the basis of our study, we suggest that the presence of RAD18 on the XY body might be functionally linked to the persistence of DSBs.

#### ACKNOWLEDGEMENTS

We thank Dr. R.Y. Tsien (University of California, San Diego, USA) for kindly providing the mCherry-C1 vector.

This work was supported by the Netherlands Organisation for Scientific Research (NWO) through ALW (VIDI 864.05.003).

#### CONFLICT OF INTEREST STATEMENT

The authors declare that there are no conflicts of interest.

#### REFERENCES

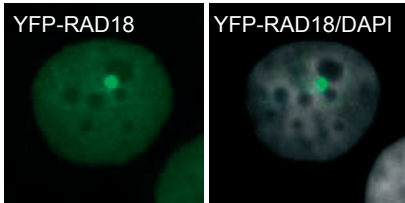
1. H.D. Ulrich, The RAD6 pathway: control of DNA damage bypass and mutagenesis by ubiquitin and SUMO, *Chembiochem* 6 (2005) 1735-1743.
2. C. Hoege, B. Pfander, G.L. Moldovan, G. Pyrowolakis, S. Jentsch, RAD6-dependent DNA repair is linked to modification of PCNA by ubiquitin and SUMO, *Nature* 419 (2002) 135-141.
3. G.L. Moldovan, B. Pfander, S. Jentsch, PCNA, the maestro of the replication fork, *Cell* 129 (2007) 665-679.
4. A.R. Lehmann, A. Niimi, T. Ogi, S. Brown, S. Sabbioneda, J.F. Wing, P.L. Kannouche, C.M. Green, Translesion synthesis: Y-family polymerases and the polymerase switch, *DNA Repair (Amst)* 6 (2007) 891-899.
5. W. Yang, R. Woodgate, What a difference a decade makes: insights into translesion DNA synthesis, *Proc Natl Acad Sci U S A* 104 (2007) 15591-15598.
6. H. Xin, W. Lin, W. Sumanasekera, Y. Zhang, X. Wu, Z. Wang, The human RAD18 gene product interacts with HHR6A and HHR6B, *Nucleic Acids Res.* 28 (2000) 2847-2854.
7. P.L. Kannouche, J. Wing, A.R. Lehmann, Interaction of human DNA polymerase  $\eta$  with monoubiquitinated PCNA: a possible mechanism for the polymerase switch in response to DNA damage, *Mol Cell* 14 (2004) 491-500.
8. K. Watanabe, S. Tateishi, M. Kawasuji, T. Tsurimoto, H. Inoue, M. Yamaizumi, Rad18 guides pol $\eta$  to replication stalling sites through physical interaction and PCNA monoubiquitination, *Embo J* 23 (2004) 3886-3896.
9. S. Tateishi, H. Niwa, J. Miyazaki, S. Fujimoto, H. Inoue, M. Yamaizumi, Enhanced genomic instability and defective postreplication repair in RAD18 knockout mouse embryonic stem cells, *Mol Cell Biol* 23 (2003) 474-481.
10. S. Miyase, S. Tateishi, K. Watanabe, K. Tomita, K. Suzuki, H. Inoue, M. Yamaizumi, Differential regulation of Rad18 through Rad6-dependent mono- and polyubiquitination, *J Biol Chem* 280 (2005) 515-524.

11. N. Shiomi, M. Mori, H. Tsuji, T. Imai, H. Inoue, S. Tateishi, M. Yamaizumi, T. Shiomi, Human RAD18 is involved in S phase-specific single-strand break repair without PCNA monoubiquitination, *Nucleic Acids Res* 35 (2007) e9.
12. S. Nakajima, L. Lan, S. Kanno, N. Usami, K. Kobayashi, M. Mori, T. Shiomi, A. Yasui, Replication-dependent and -independent responses of RAD18 to DNA damage in human cells, *J Biol Chem* 281 (2006) 34687-34695.
13. E. Sonoda, H. Hohegger, A. Saberi, Y. Taniguchi, S. Takeda, Differential usage of non-homologous end-joining and homologous recombination in double strand break repair, *DNA Repair (Amst)* 5 (2006) 1021-1029.
14. A. Saberi, H. Hohegger, D. Szuts, L. Lan, A. Yasui, J.E. Sale, Y. Taniguchi, Y. Murakawa, W. Zeng, K. Yokomori, T. Helleday, H. Teraoka, H. Arakawa, J.M. Buerstedde, S. Takeda, RAD18 and poly(ADP-ribose) polymerase independently suppress the access of nonhomologous end joining to double-strand breaks and facilitate homologous recombination-mediated repair, *Mol Cell Biol* 27 (2007) 2562-2571.
15. J. Essers, A.F. Theil, C. Baldeyron, W.A. van Cappellen, A.B. Houtsmuller, R. Kanaar, W. Vermeulen, Nuclear dynamics of PCNA in DNA replication and repair, *Mol Cell Biol* 25 (2005) 9350-9359.
16. R. van der Laan, E.J. Uringa, E. Wassenaar, J.W. Hoogerbrugge, E. Sleddens, H. Odijk, H.P. Roest, P. de Boer, J.H. Hoeijmakers, J.A. Grootegeod, W.M. Baarends, Ubiquitin ligase Rad18Sc localizes to the XY body and to other chromosomal regions that are unpaired and transcriptionally silenced during male meiotic prophase, *J Cell Sci* 117 (2004) 5023-5033.
17. J. Essers, R.W. Hendriks, J. Wesoly, C.E. Beerens, B. Smit, J.H. Hoeijmakers, C. Wyman, M.L. Dronkert, R. Kanaar, Analysis of mouse Rad54 expression and its implications for homologous recombination, *DNA Repair (Amst)* 1 (2002) 779-793.
18. N. Miura, I. Miyamoto, H. Asahina, I. Satokata, K. Tanaka, Y. Okada, Identification and characterization of xpac protein, the gene product of the human XPAC (xeroderma pigmentosum group A complementing) gene, *J Biol Chem* 266 (1991) 19786-19789.
19. M.E. van Royen, S.M. Cunha, M.C. Brink, K.A. Mattern, A.L. Nigg, H.J. Dubbink, P.J. Verschure, J. Trapman, A.B. Houtsmuller, Compartmentalization of androgen receptor protein-protein interactions in living cells, *J Cell Biol* 177 (2007) 63-72.
20. C. Dinant, M. de Jager, J. Essers, W.A. van Cappellen, R. Kanaar, A.B. Houtsmuller, W. Vermeulen, Activation of multiple DNA repair pathways by sub-nuclear damage induction methods, *J Cell Sci* 120 (2007) 2731-2740.
21. J. Essers, W.A. van Cappellen, A.F. Theil, E. van Drunen, N.G. Jaspers, J.H. Hoeijmakers, C. Wyman, W. Vermeulen, R. Kanaar, Dynamics of relative chromosome position during the cell cycle, *Mol Biol Cell* 16 (2005) 769-775.
22. O. Mortusewicz, H. Leonhardt, XRCC1 and PCNA are loading platforms with distinct kinetic properties and different capacities to respond to multiple DNA lesions, *BMC Mol Biol* 8 (2007) 81.
23. D. Perdiz, P. Grof, M. Mezzina, O. Nikaido, E. Moustacchi, E. Sage, Distribution and repair of bipyrimidine photoproducts in solar UV-irradiated mammalian cells. Possible role of Dewar photoproducts in solar mutagenesis, *J Biol Chem* 275 (2000) 26732-26742.
24. G. Rodrigo, S. Roumagnac, M.S. Wold, B. Salles, P. Calsou, DNA replication but not nucleotide excision repair is required for UVC-induced replication protein A phosphorylation in mammalian cells, *Mol Cell Biol* 20 (2000) 2696-2705.
25. S. Tashiro, J. Walter, A. Shinohara, N. Kamada, T. Cremer, Rad51 accumulation at sites of DNA damage and in postreplicative chromatin, *J Cell Biol* 150 (2000) 283-291.
26. P.O. Mari, B.I. Florea, S.P. Persengiev, N.S. Verkaik, H.T. Bruggenwirth, M. Modesti, G. Giglia-Mari, K. Bezstarosti, J.A. Demmers, T.M. Luider, A.B. Houtsmuller, D.C. van Gent, Dynamic assembly of end-joining complexes requires interaction between Ku70/80 and XRCC4, *Proc Natl Acad Sci U S A* 103 (2006) 18597-18602.
27. J. Fulford, H. Nikjoo, D.T. Goodhead, P. O'Neill, Yields of SSB and DSB induced in DNA by Al(K) ultrasoft X-rays and alpha-particles: comparison of experimental and simulated yields, *Int J Radiat Biol* 77 (2001) 1053-1066.
28. D.E. Charlton, H. Nikjoo, J.L. Humm, Calculation of initial yields of single- and double-strand breaks in cell nuclei from electrons, protons and alpha particles, *Int J Radiat Biol* 56 (1989) 1-19.

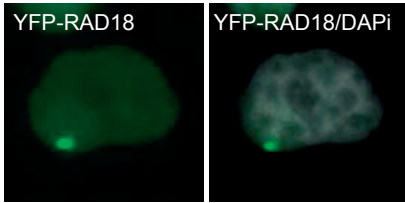
29. R.A. Meldrum, S.W. Botchway, C.W. Wharton, G.J. Hirst, Nanoscale spatial induction of ultraviolet photoproducts in cellular DNA by three-photon near-infrared absorption, *EMBO Rep* 4 (2003) 1144-1149.
30. J.H. Barlow, M. Lisby, R. Rothstein, Differential regulation of the cellular response to DNA double-strand breaks in G1, *Mol Cell* 30 (2008) 73-85.
31. C. Zierhut, J.F. Diffley, Break dosage, cell cycle stage and DNA replication influence DNA double strand break response, *Embo J* 27 (2008) 1875-1885.
32. D. Szuts, L.J. Simpson, S. Kabani, M. Yamazoe, J.E. Sale, Role for RAD18 in homologous recombination in DT40 cells, *Mol Cell Biol* 26 (2006) 8032-8041.
33. Y. Fu, Y. Zhu, K. Zhang, M. Yeung, D. Durocher, W. Xiao, Rad6-Rad18 mediates a eukaryotic SOS response by ubiquitinating the 9-1-1 checkpoint clamp, *Cell* 133 (2008) 601-611.
34. M. Tarsounas, D. Davies, S.C. West, BRCA2-dependent and independent formation of RAD51 nuclear foci, *Oncogene* 22 (2003) 1115-1123.
35. M. Tarsounas, A.A. Davies, S.C. West, RAD51 localization and activation following DNA damage, *Philos Trans R Soc Lond B Biol Sci* 359 (2004) 87-93.
36. T. Taniguchi, I. Garcia-Higuera, P.R. Andreassen, R.C. Gregory, M. Grompe, A.D. D'Andrea, S-phase-specific interaction of the Fanconi anemia protein, FANCD2, with BRCA1 and RAD51, *Blood* 100 (2002) 2414-2420.
37. R. Scully, J. Chen, R.L. Ochs, K. Keegan, M. Hoekstra, J. Feunteun, D.M. Livingston, Dynamic changes of BRCA1 subnuclear location and phosphorylation state are initiated by DNA damage, *Cell* 90 (1997) 425-435.
38. V. Tembe, B.R. Henderson, Protein trafficking in response to DNA damage, *Cell Signal* 19 (2007) 1113-1120.
39. D. Deckbar, J. Birraux, A. Krempler, L. Tchouandong, A. Beucher, S. Walker, T. Stiff, P. Jeggo, M. Lobrich, Chromosome breakage after G2 checkpoint release, *J Cell Biol* 176 (2007) 749-755.
40. S.K. Mahadevaiah, J.M. Turner, F. Baudat, E.P. Rogakou, P. de Boer, J. Blanco-Rodriguez, M. Jasin, S. Keeney, W.M. Bonner, P.S. Burgoyne, Recombinational DNA double-strand breaks in mice precede synapsis, *Nat Genet* 27 (2001) 271-276.
41. F.A. de Vries, E. de Boer, M. van den Bosch, W.M. Baarends, M. Ooms, L. Yuan, J.G. Liu, A.A. van Zeeland, C. Heyting, A. Pastink, Mouse Sycp1 functions in synaptonemal complex assembly, meiotic recombination, and XY body formation, *Genes Dev* 19 (2005) 1376-1389.
42. P.B. Moens, D.J. Chen, Z. Shen, N. Kolas, M. Tarsounas, H.H. Heng, B. Spyropoulos, Rad51 immunocytology in rat and mouse spermatocytes and oocytes, *Chromosoma* 106 (1997) 207-215.

## SUPPLEMENTARY MATERIALS

2

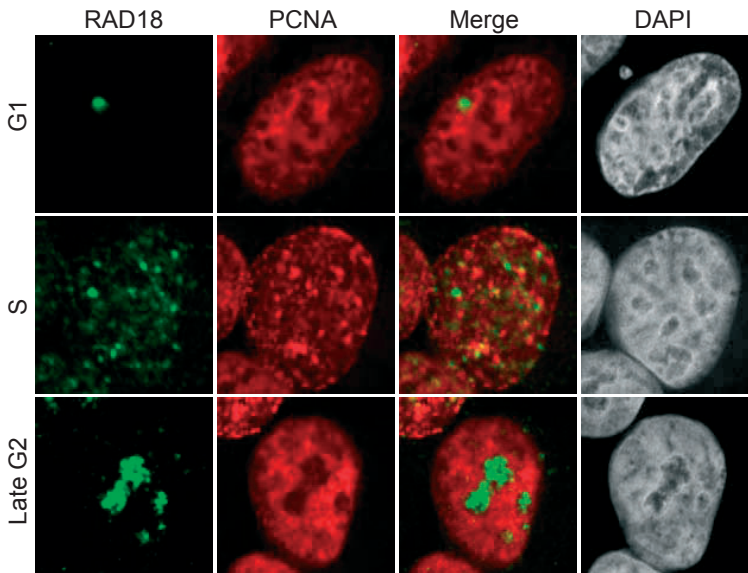


Adjacent to the nucleoli (181 / 200)

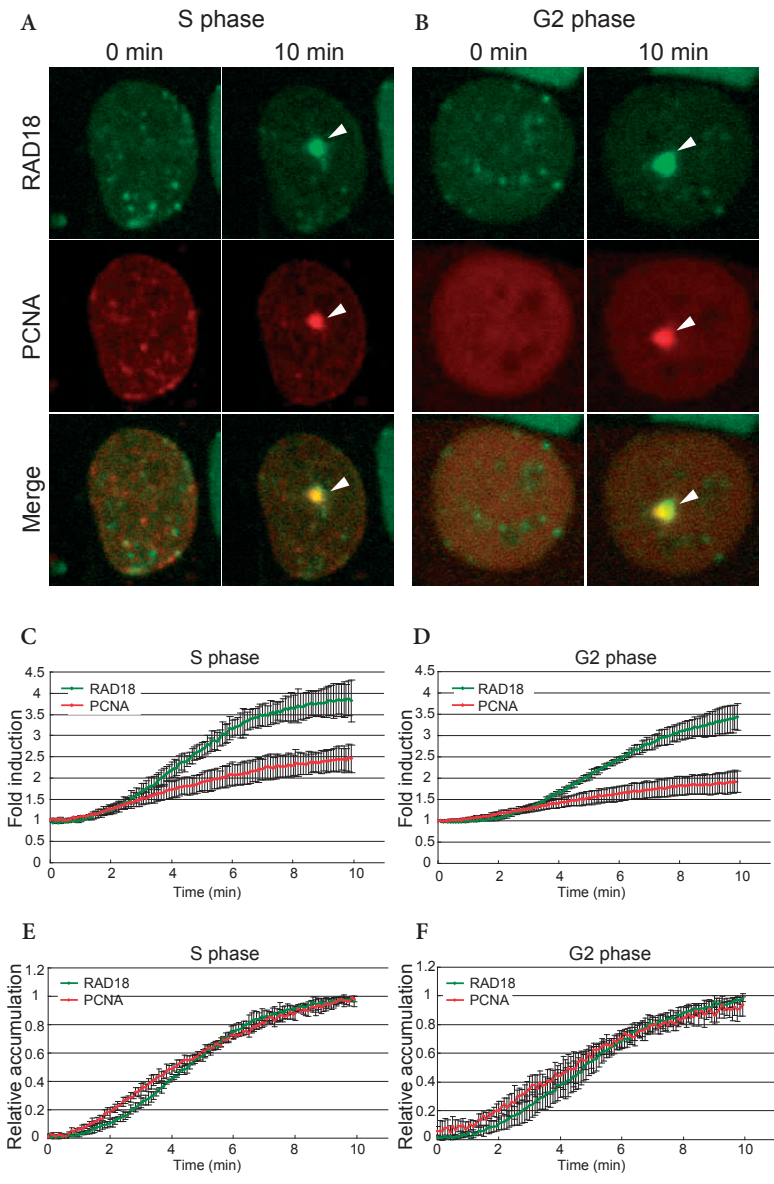


Not adjacent to the nucleoli (19 / 200)

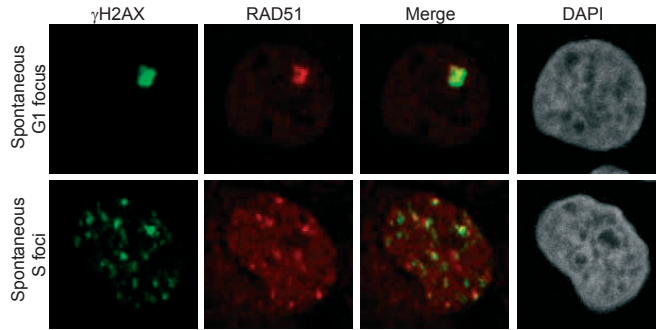
Supplemental figure 1. Sub-nuclear localization of spontaneous RAD18 focus in G1 phase. Confocal images of HeLa cells in G1 stably expressing YFP-RAD18 were captured and localization of spontaneous RAD18 G1 focus was analyzed. Approximately 91% of the RAD18 foci in G1 phase were localized adjacent to the nucleoli (181/200), visualized by the DAPI-negative areas in the merged images.



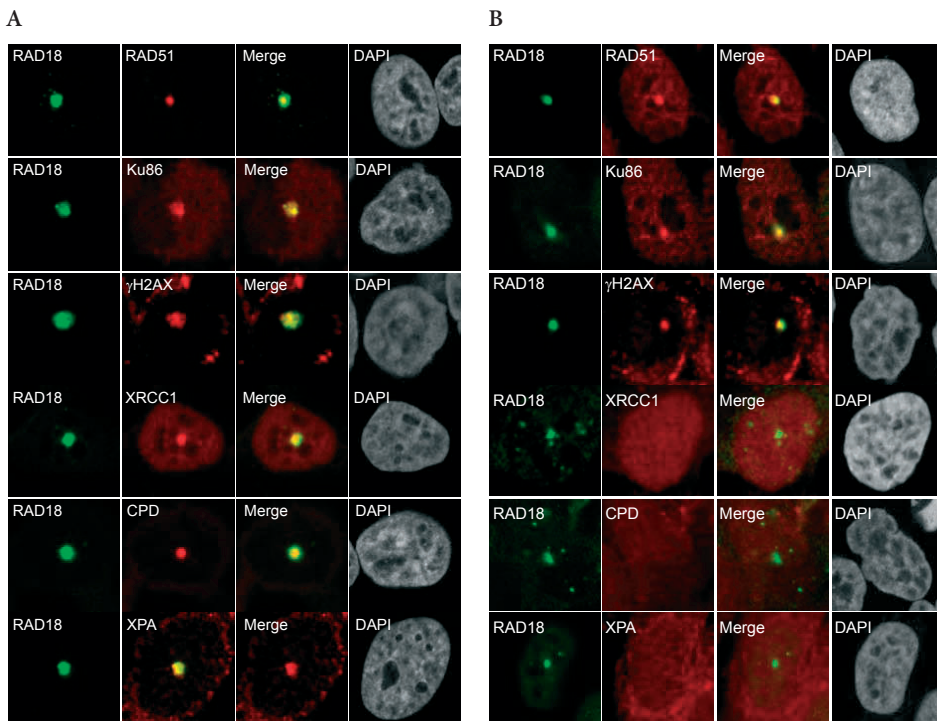
Supplemental figure 2. The subnuclear localization of endogenous RAD18 in wild-type HeLa cells was visualized by immunostaining using anti-RAD18. The different cell cycle stages were identified based on the subnuclear localization of endogenous PCNA.



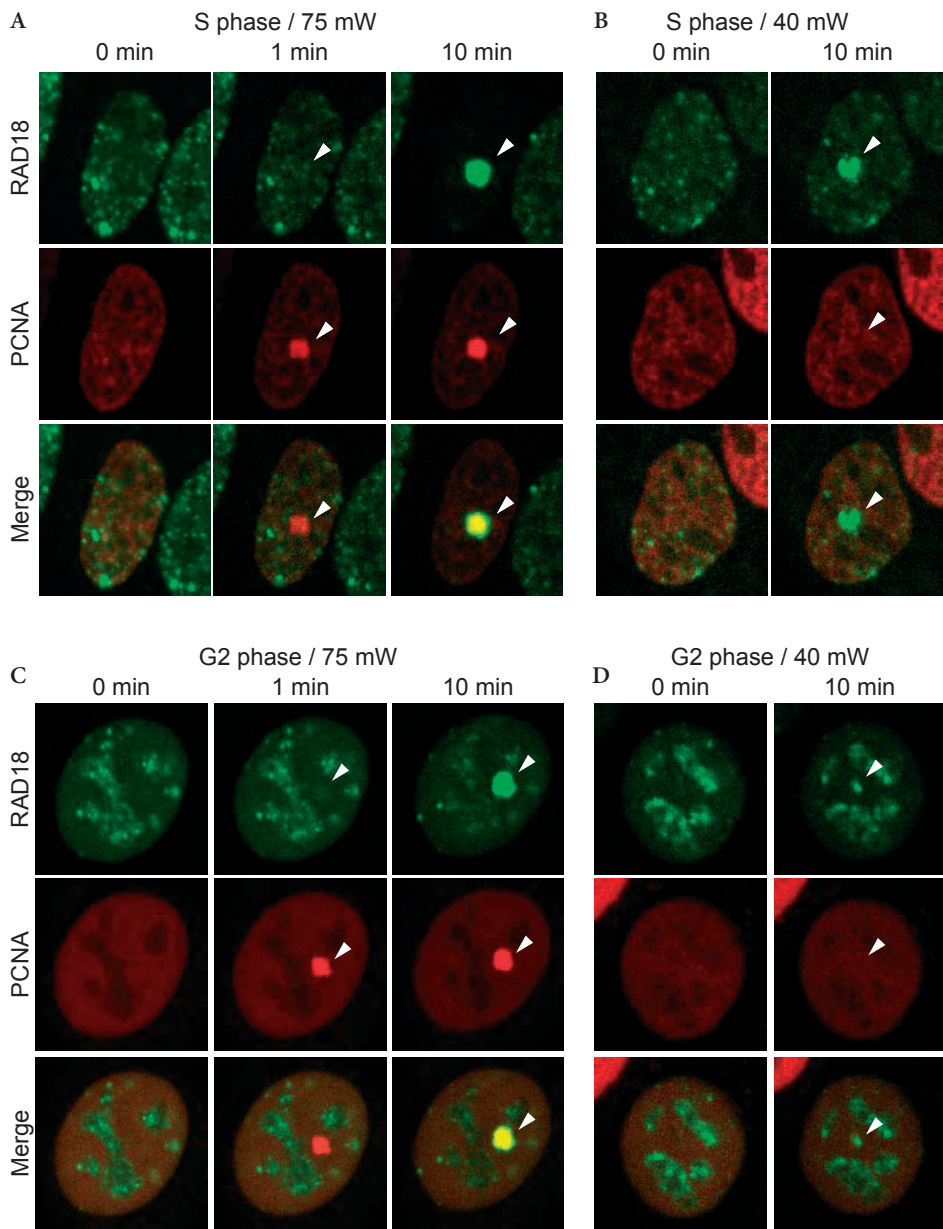
**Supplemental figure 3. YFP-RAD18 and mCherry-PCNA accumulation following local UVC irradiation.** Nuclei of living HeLa cells stably expressing YFP-RAD18 and transiently co-expressing mCherry-PCNA were locally irradiated with a UVC laser for 0.49 seconds, and the fluorescence intensities of YFP-RAD18 and mCherry-PCNA at the irradiated site were measured immediately thereafter every 5 seconds for 10 minutes. The signal intensity at the irradiated region prior to UVC irradiation was set at 1.0, and the fold induction is shown in graphs C and D. The signal intensities at the irradiated region before and 10 minutes after irradiation were set at 0 and 1.0, respectively, and the relative accumulation is shown in graphs E and F. (A, C, E) Cells in S phase. (B, D, F) Cells in G2 phase. The Error bars in the graphs represent the standard deviation for 20 nuclei.



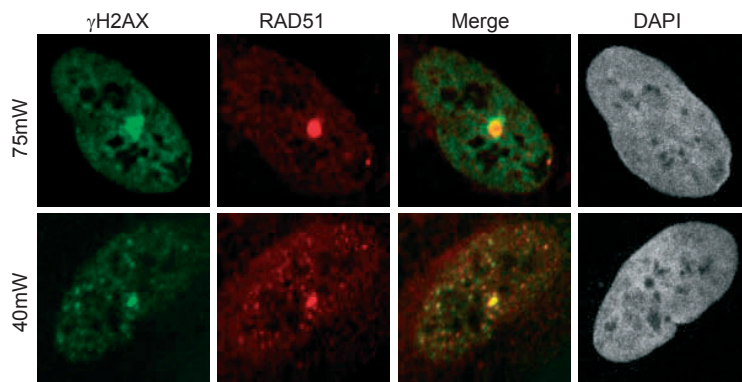
Supplemental figure 4. HeLa cells stably expressing YFP-RAD18 were treated with siRNA against both endogenous RAD18 and YFP-RAD18, and spontaneous RAD51 and  $\gamma$ H2AX foci formation were detected.



Supplemental figure 5. Characterization of damage induction following MPL irradiation. HeLa cells stably expressing YFP-RAD18 were locally irradiated using a multi-photon laser either at 75 mW (A) or at 40 mW (B) of laser power. 15 minutes after irradiation, cells were fixed and endogenous proteins and CPD, as indicated in the pictures, were visualized with antibodies. At least 60 nuclei were studied for each protein and representative images are shown.



**Supplemental figure 6. YFP-RAD18 and mCherry-PCNA accumulation following local MPL irradiation in S and G2 phase cells.** Living HeLa cells stably expressing YFP-RAD18 and transiently co-expressing mCherry-PCNA in S phase (A, B) or G2 phase (C, D) were locally irradiated with a multi-photon laser with 75 mW (A, C) or 40 mW (B, D) of laser power. The pictures show representative images of cells at time points 0, 1, and 10 minutes after MPL irradiation. Arrowheads indicate sites of MPL irradiation.



**Supplemental figure 7. RAD18 does not affect accumulation of RAD51 and  $\gamma$ H2AX at MPL-irradiated sites.** HeLa cells stably expressing YFP-RAD18 were treated with siRNA targeting both endogenous RAD18 and YFP-RAD18 for 48 h. Subsequently, cells were locally irradiated with high or low-power MPL, and accumulation of RAD51 and  $\gamma$ H2AX at irradiated sites were detected with immunostaining using antibody against RAD51 and  $\gamma$ H2AX.



3

# HUMAN RAD18 INTERACTS WITH UBIQUITYLATED CHROMATIN COMPONENTS AND FACILITATES RAD9 RECRUITMENT TO DNA DOUBLE STRAND BREAKS

Submitted

Akiko Inagaki<sup>1</sup>, Esther Sleddens-Linkels<sup>1</sup>, Wiggert A. van Cappellen<sup>1</sup>,  
Richard G. Hibbert<sup>3</sup>, Titia K. Sixma<sup>3</sup>, Jan H. J. Hoeijmakers<sup>2</sup>,  
J. Anton Grootegoed<sup>1</sup>, and Willy M. Baarends<sup>1\*</sup>

\* Corresponding author



<sup>1</sup>Department of Reproduction and Development, and <sup>2</sup>Department of Cell Biology and Genetics, Erasmus MC - University Medical Center, Rotterdam, The Netherlands,

<sup>3</sup>Division of Biochemistry and Center for Biomedical Genetics, Netherlands Cancer Institute, Amsterdam, The Netherlands

**ABSTRACT**

RAD18 is an ubiquitin ligase involved in replicative damage bypass and DNA double-strand break (DSB) repair processes. We performed functional analyses of human RAD18 by analyzing mutations in its RING finger, Zinc finger, SAP domain, and HR6A/B binding domain. Interaction of RAD18 with the ubiquitin-conjugating enzyme HR6A/B requires not only an intact RING finger and HR6A/B-binding domain, but also the SAP domain. Surprisingly, and in contrast to the ubiquitylation of PCNA, mono-ubiquitylation of RAD18 itself occurs independent of its RING finger, but requires an intact Zinc finger. The RAD18 Zinc finger that interacts with ubiquitin is also essential for recruitment of RAD18 to chromatin surrounding DSBs. In addition, we found that RPA is also required for RAD18 accumulation at sites of spontaneous and  $\gamma$ -irradiation-induced DNA damage. In accordance with its ubiquitin-binding property, RAD18 colocalizes with chromatin-associated conjugated ubiquitin throughout the cell cycle and following irradiation. We found that RAD18 directly binds to ubiquitylated H2A and several other unknown ubiquitylated chromatin components, and this interaction depends on the RAD18 Zinc finger. Regarding the functional relevance of RAD18 localization at DSBs, we found that RAD18 is required for recruitment of RAD9, one of the components of the 9-1-1 checkpoint complex, to these sites. Recruitment of RAD9 requires the RING and Zinc finger domains of RAD18. Together, our data indicate that association of RAD18 with DSBs through ubiquitylated H2A and other ubiquitylated chromatin components allows recruitment of RAD9, which may function directly in DSB repair, independent of downstream activation of the checkpoint kinases CHK1 and CHK2.

**Keywords:** RAD18, HR6A/B, ubiquitylated H2A, DNA double-strand break repair, RPA, RAD9

## 1. INTRODUCTION

Mammalian cells require the E3 ubiquitin ligase RAD18 for survival after the induction of various types of DNA damage. *RAD18* knockout cells are sensitive to UVC light exposure [1-3], camptothecin [1,4], and ionizing radiation (IR) [1,4,5], that induce distortions of DNA geometry, single strand breaks (SSBs), and double strand breaks (DSBs), respectively. RAD18 complexes with the two mammalian orthologs of the yeast E2 ubiquitin-conjugating enzyme Rad6; HR6A (UBE2A) and HR6B (UBE2B) [6]. Rad6 is most well known for its role in replicative damage bypass (RDB) that allows progression of DNA replication in the presence of DNA damage (reviewed in [7]). The first step in the RDB pathway involves mono-ubiquitylation of PCNA by the RAD18-HR6A/B complex [8]. PCNA forms a homotrimer that encircles double-stranded DNA, and operates as a sliding clamp to keep the DNA polymerase machinery firmly on the DNA during DNA replication (reviewed in [9]). Mono-ubiquitylation of PCNA by the RAD18-HR6A/B complex recruits specific translesion synthesis polymerases that can incorporate nucleotides in the strand opposite the site of the DNA lesions [10]. RAD18 contains a RING finger that has been shown to be required for ubiquitylation of PCNA [1,10]. In addition to this domain, HR6A/B interacting domains [11-13], and a so-called SAP domain that shows binding affinity to single-stranded DNA (ssDNA) *in vitro* [14] have been identified. The SAP domain is also required for PCNA ubiquitylation [1]. Finally, it was recently described that RAD18 also contains a Zinc finger that functions as an ubiquitin binding domain [14-17].

In addition to the RDB pathway, RAD18 also functions in DSB repair. DSBs may arise from exogenous factors such as ionizing radiation. In addition, DSBs can arise when the replication fork collapses during S phase. Two distinct DSB repair pathways have been identified in mammalian cells; non-homologous end-joining (NHEJ), and homologous recombination (HR). NHEJ is an error-prone form of DSB repair, in which the two ends of the broken DNA are processed for direct ligation. This mechanism is thought to be operative mainly during the G1 phase. In contrast, HR is an error-free mechanism, in which a homologous sequence of the sister chromatid is used as a template to process repair in S and G2 phases. All HR pathways are initiated by 5'-3' degradation of one strand at both sides of the break; the so-called DNA-end resection, generating stretches of ssDNA, that are subsequently coated by the ssDNA binding protein complex RPA (reviewed in [18]). RPA is a heterotrimeric protein complex composed of RPA1, RPA2 and RPA3, and is essential for DNA replication and various DNA repair pathways [18-23]. RPA is subsequently replaced by RAD51 on the single stranded tails, which allows efficient RAD51-mediated recombination [24]. Previous analyses in *S. cerevisiae* and human cells have shown that RAD18 interacts directly with RPA [25,26]. Furthermore, it has been suggested that exposure of ssDNA at stalled replication forks results in accumulation of RPA, which is essential for PCNA ubiquitylation both in *S. cerevisiae* and mammalian cells [25,27], followed by recruitment of RAD18 [26].

RAD18 accumulates at DSBs at all cell cycle phases [1,5,28], and this was found to be independent of PCNA [28]. During S phase, RAD18 may facilitate HR independent

of PCNA, by suppressing NHEJ at DSB repair sites that result from blockage of replication [29,30]. Recently, two novel interaction partners of RAD18, RAD51C and 53BP1, were discovered that might be involved in possible functions of RAD18 at DSB repair sites [1,5].

The chromatin surrounding DSBs undergoes various modifications. One of the first modifications is phosphorylation of histone H2A variant H2AX ( $\gamma$ H2AX) [31]. Subsequently, histone H2AX and H2A are highly ubiquitylated by the E3 ligases RNF8 [32] and RNF168 [33,34]. Concomitantly, a number of DNA damage response factors, including RAD18, associate with chromatin enriched in  $\gamma$ H2AX and ubiquitylated H2A/H2AX [32,35-39]. The 9-1-1 complex, which consists of RAD9, RAD1 and HUS1, forms a PCNA-like heterotrimer [40-42], and functions as checkpoint protein. Cell cycle arrest is imposed by the activation of two downstream effector kinases, CHK1 and CHK2 [43]. It has been shown that the 9-1-1 complex is required to activate CHK1 to mediate UV-induced S phase arrest [44-47]. The 9-1-1 complex is also loaded at DSBs after IR [45,48,49], and depletion of RAD9 induces hypersensitivity to IR [45,50,51]. In contrast to 9-1-1 complex-dependent CHK1 phosphorylation following UV, depletion of any of the 9-1-1 components does not cause impairment of either G2/M checkpoint activation [44,46,51] or CHK2 phosphorylation [44,45,47,51] following IR, suggesting that the role of the 9-1-1 complex in DSB repair may involve a function outside the context of checkpoint activation [45,51]. In *S. cerevisiae*, Rad18 was reported to interact with Rad17, a component of the 9-1-1 complex (an ortholog of mammalian RAD1), and to mediate its ubiquitylation [52]. However, more recent results indicate that all components of the 9-1-1 complex are ubiquitylated, but independent of RAD18, and without any effect on the DNA damage response [53].

Herein, we aim to determine how RAD18 is recruited to DSBs, and the downstream effects of RAD18 functions at DSBs. We report that RAD18 requires its Zinc finger domain to bind to ubiquitylated H2A and other ubiquitylated chromatin components that are enriched in the regions surrounding DSBs, and colocalize with RAD18 throughout the cell cycle. Furthermore, we reveal that RAD18 facilitates the accumulation of RAD9 at DSBs.

## 2. MATERIALS AND METHODS

### 2.1. DNA constructs, transfection and cell culture

Design of the YFP-RAD18 construct containing four silent mutations, and generation of the HeLa cell line stably expressing YFP-RAD18 were described elsewhere [28]. All mutant RAD18 constructs were generated by PCR reactions (30 sec at 90 °C, 1 min at 55 °C, and 12 min at 68 °C for 25 cycles) with primers carrying mutations (Supplementary Table I). The YFP-RAD18 construct was used as template DNA. 50  $\mu$ l of the PCR products were mixed with 2  $\mu$ l of *DpnI* (Bio England) for 2 hours at 37 °C. XL1-blue (Stratagene) was transformed with 2  $\mu$ l of the *DpnI* digested PCR products. Plasmids containing appropriate mutants were digested with *EcoRI* and *BamHI* and sub-cloned into pEYFP-C1 (Clontech) and mCherry-C1 (Clontech). pEGFP-RAD9 construct was kindly provided by Daniel Warmerdam [54].

For yeast two-hybrid assays, open reading frames of human *RAD18*, *PCNA*, *RAD9*, *HUS1* and *RAD1*, and mouse *Hr6a* and *Hr6b* genes were amplified using primer sets (Supplementary Table II) from cDNA and sub-cloned into pGADT7 and pGBKT7 plasmids (Clontech).

To stably downregulate *RAD18*, two complementary nucleotides (Supplementary Table III) containing a hairpin loop structure which targets endogenous *RAD18* (sh*RAD18*) were annealed (1 min at 94 °C, 4 min at 65 °C, 5 min at 30 °C and 2 h at 4 °C) and sub-cloned into pSuper-puro vector (OligoEngine). To generate HeLa cells stably expressing pSuper-sh*RAD18*, cells were transfected with 2 µg of the pSuper-sh*RAD18* plasmid using FuGene6 (Roche). Cells were cultured for 7 days after transfection with medium containing 0.1 mM of puromycin. Surviving colonies were selected, and RT-PCR and immunoblot analysis were used to further select cell lines that showed downregulation of *RAD18*. As a control, the empty pSuper-puro vector was transfected followed by the same selection procedure. In order to transfect mutant *RAD18* in the *RAD18* knockdown cell line, five silent mutations were introduced in the *RAD18* gene in the region that is targeted by pSuper-sh*RAD18* (Supplementary Table I), and this construct was subcloned into pEYFP-C1 and mCherry-C1. All constructs were verified by sequencing (Base Clear, The Netherlands). HeLa cell line stably expressing H2A-GFP was described elsewhere [55,56].

To express YFP-tagged mutant *RAD18*, cells were transfected with 2 µg of the pEYFP-mutant*RAD18* plasmids using FuGene6 (Roche)

HeLa cells were cultured at 37°C in DMEM/F12 (GIBCO) supplemented with 5% v/v fetal calf serum, streptomycin sulfate and penicillin, under 5% CO<sub>2</sub> in air. Female human primary fibroblast was cultured at 37 °C in DMEM/F12 (GIBCO) supplemented with 15% v/v fetal calf serum, 1% non essential amino acid (GIBCO), 0.1 mM β-mercaptoethanol, and penicillin, under 5% CO<sub>2</sub> in air.

## 2.2. Antibodies

For primary antibodies, we used mouse monoclonal antibodies anti-GAPDH (Chemicon), anti-GFP (Roche), anti-RPA2 (Thermo Scientific), anti-FK2 (Millipore, #04-263), anti-PCNA PC10 (Abcam), anti-ubiquitylated histone H2A (Millipore, #05-678), and rabbit polyclonal antibodies anti-*RAD18* [28], anti-GFP (Abcam), anti-phosphorylated CHK1 Ser-345 (Cell Signaling), anti-phosphorylated CHK2 at Tyr-68 (Cell Signaling), and anti-HR6A/B [57]. For secondary antibodies, we used a goat anti-rabbit/mouse IgG-peroxidase (Sigma), IgM-peroxidase (Sigma), IRDye680 goat-anti-rabbit/mouse IgG (Li-cor), IRDye800 goat-anti-rabbit/mouse IgG (Li-cor), goat anti-rabbit alexa 488/564, or goat anti-mouse alexa 488/564 (Molecular Probes). The antibody anti-GFP (Abcam) was also used to detect YFP, and was described in the text and figures as anti-YFP to avoid the confusion.

## 2.3. RNA interference

Portions of  $2 \times 10^5$  cells were plated into six-well culture dishes. After 24 hours, cells were transfected with siRNA and incubated for 72 hours. Each transfection mixture contained 9 µl HiPerFect Transfection Reagent (Qiagen) and 2 µM siRNA (Ambion) in

400  $\mu$ l serum-free DMEM/F12. siRNA28198 (si-endoRAD18) (Ambion) was used to downregulate only endogenous RAD18 but not YFP-RAD18 or mutant YFP-RAD18. siRPA1 (Ambion) [22] and siRPA2 (Ambion) were used to downregulate RPA70, and RPA34, respectively. The sequences of all siRNAs are shown in Supplementary Table IV. A si-control (Ambion) which does not target any gene, was used as a control.

#### 2.4. Real-time RT-PCR

For real-time RT-PCR, RNA was prepared by Trizol from HeLa cells stably expressing shRAD18 or non-targeting shRNA, DNase-treated and reverse transcribed using random hexamer primers and Superscript II reverse transcriptase (Invitrogen). PCR was carried out with the iQ SYBR green PCR mastermix (Applied Biosystems) in the DNA engine Opticon 2 real-time PCR detection system (Bio-Rad) with RAD18 primer; forward/ TCTGTATGCATGGGACAGGA, reverse/ TCAGGTTCCAATTCCTCTGG. PCR of  $\beta$ -actin mRNA was included in each reaction and used to normalize the data. Three independent experiments were performed and each real-time PCR was performed in duplicate. All  $-RT$  reactions were negative.

#### 2.5. Global $\gamma$ -ray irradiation

To induce global ionizing damage, cultured cells were irradiated with  $\gamma$ -rays from a  $^{137}\text{Cs}$  source (0.71 Gy/minutes).

#### 2.6. Global UVC irradiation

To induce global UVC damage, cultured cells were irradiated with a Philips TUV lamp (254 nm) at a dose of 20 J/m<sup>2</sup>. For immunoblot analysis, cells were cultured for another 6 hours and whole-cell extracts were prepared.

#### 2.7. Protein immunoprecipitation analysis

HeLa cells expressing either wild type or mutant YFP-RAD18 were lysed in 2.0 ml Lysis buffer 1 (50 mM Tris-HCl pH 8.0, 450 mM NaCl, 5 mM MgCl<sub>2</sub>, 0.5 mM EDTA, 0.2% Nonidet P-40, 10% (v/v) glycerol, 0.5 mM dithiothreitol, and protease inhibitors (Roche)). The cell suspension was left on ice for 1 h, sonicated 5 times for 5 sec. Subsequently the lysate was treated with 0.125 U/ $\mu$ l of benzonase nuclease (Novagen) for 2 h, and centrifuged for 30 min (full speed at 4°C). The efficiency of nuclease was checked by DNA precipitation. The cell lysate was diluted with Lysis buffer 2 (50 mM Tris-HCl pH 8.0, 5 mM MgCl<sub>2</sub>, 0.5 mM EDTA, 0.2% Nonidet P-40, 10% (v/v) glycerol, 0.5 mM dithiothreitol, and protease inhibitors (Roche)) to decrease the concentration of NaCl to 150 mM. The cell lysate was pre-cleared with 20  $\mu$ l of protein A-agarose beads (GE Healthcare) for 2 hours at 4°C. To cross-link antibodies with beads, antibodies (1  $\mu$ g) were first incubated with 20  $\mu$ l of beads for 2 hours at 4°C. The beads were washed three times with lysis buffer and subsequently incubated with borate buffer pH 8.0 containing 20  $\mu$ M dimethyl pimelimidate (Sigma) for 1 hour at RT. The beads were washed once with ethanol amine pH 8.0 and incubated for 1 hour at RT. The beads were washed three times with lysis buffer and incubated with lysis buffer containing 5% BSA for 2 hours at 4°C. Subsequently, the beads were used for immunoprecipitation analysis. Each immunoprecipitation analysis contained 2 mg of soluble lysate and 25  $\mu$ l

of protein A-agarose, and the mixture was incubated overnight at 4 °C. After washing three times with 500 µl of Lysis buffer, bound proteins were analyzed by SDS-PAGE and immunoblots.

### 2.8. Immunoblot analysis

Whole-cell extracts were prepared from cultured cells collected in a Tris buffer (50 mM Tris-HCl pH 6.8, 2% w/v SDS, 0.1% w/v bromophenol blue, 10% v/v glycerol and 100 mM dithiothreitol), and sonicated. After 5 minutes incubation at 100 °C, the cell extracts were separated by SDS 10% polyacrylamide gel electrophoresis and transferred to nitrocellulose membranes. The membranes were incubated with antibodies to analyze expression of target proteins. The expression was detected using enhanced chemiluminescence (PerkinElmer). The target proteins detected using IRDye680 or IRDye800 were quantified with Odyssey (Li-cor).

### 2.9. Immunocytochemistry

Cells were cultured on 24 mm round coverslips, washed with PBS and fixed in 2% w/v paraformaldehyde in PBS for 15 minutes. To detect ubiquitylation of histone H2A, cells were pretreated with 0.2% v/v Triton X-100 in PBS for 30 seconds before the fixation step. Cells were permeabilized for 20 minutes with 0.2% v/v Triton X-100 in PBS. Cells were blocked with PBS<sup>+</sup> (PBS containing 0.5% w/v BSA and 0.15% w/v glycine) for 30 minutes, incubated with primary antibody for 2 hours, and washed with 0.2% Triton X-100 in PBS. Subsequently, cells were incubated with secondary antibody for 1 hour, washed with 0.2% Triton X-100 in PBS. Coverslips were placed on a slide, mounted with Prolong Gold reagent (Invitrogen).

### 2.10. Confocal and time-lapse microscopy

Images of living cells expressing YFP-tagged and mCherry-tagged proteins were obtained using a Zeiss LSM510NLO microscope (Carl Zeiss) with a 63 × /1.40 NA oil immersion lens. Cells were maintained at 37 °C in a mixture of air with 5% CO<sub>2</sub>. YFP-tagged proteins were detected by exciting YFP with a 488 nm Argon gas laser and monitoring YFP emission through a 500-550 band-pass filter. mCherry-tagged proteins were detected by exciting mCherry with a 543 nm helium neon laser and monitoring mCherry emission through a long-pass 560 filter. To minimize the effect of photo-bleaching, images were taken with 10 µW for a 488 nm laser, and with 20 µW for a 543 nm laser. For time-lapse experiments, cell images of 6 confocal planes at 1.5 µm intervals were taken every 20 minutes for 27 hours. All images were captured with a line average of 2. Time-lapse images were analysed using the ImageJ software (Rasband, W.S., ImageJ, U.S. National Institutes of Health, Bethesda, Maryland, USA [<http://rsb.info.nih.gov/ij/>]).

### 2.11. Local multi-photon DNA damage induction

A Coherent Mira mode-locked Ti:Sapphire laser (multi-photon laser, MPL) (Coherent) connected to a Zeiss LSM510NLO confocal microscope was used at 800 nm with a pulse length of 200 fs and repetition rate of 76 MHz. For local DNA damage induction, an area of irradiation was set at 4 µm<sup>2</sup> (40 × 40 pixels), and the output of laser power was

set at 75 mW at pixel-dwell time 1.6  $\mu$ s with 5 iterations. Two images were taken before MPL irradiation and monitored at 10 seconds intervals for 10 minutes immediately after MPL irradiation. All images were captured with a line average of 1.

### 2.12. Yeast two-hybrid analysis

*Saccharomyces cerevisiae* AH109 (Clontech) were cultured in YPD medium (1% (w/v) yeast extract (Difco), 2% peptone (w/v) 2% glucose (w/v)) at 30 °C. When the density of the medium was 1.0, cells were harvested and washed twice with distilled water, mixed with transformation buffer (240  $\mu$ l 50% v/v PEG1500, 36  $\mu$ l 1M LiAc), 5  $\mu$ l 10 mM salmon sperm DNA (Clontech), 50  $\mu$ l H<sub>2</sub>O, 4  $\mu$ g of pGADT7 vector carrying target DNA with Gal4 activation domain, and 4  $\mu$ g of pGBKT7 carrying target DNA with Gal4 binding domain), incubated 30 min at 30 °C, and subsequently 30 min at 42 °C. The transformation buffer was discarded and 10% of transformed cells were spread onto the selection drop medium SD-L-W (Clontech). Interactions were determined by spot assay on SD-L-W-H (Clontech) and SD-L-W-H-A (Clontech) indicator plates.

## 3. RESULTS

### 3.1. Ubiquitylation of human RAD18 is independent of its own RING finger domain

We performed functional analyses of human RAD18 mutants to discriminate which domains are required for interaction with HR6A/B, RAD18 ubiquitylation, PCNA ubiquitylation, and localization at DSB repair sites. RAD18 contains several distinct functional domains; a C3HC4 type RING finger, a C2HC type Zinc finger, a SAP domain, and a HR6A/B binding domain (HR6BD) (Fig. 1A) [14]. We generated several mutations in human RAD18 tagged with YFP at the N-terminus, as shown in Fig. 1A.

In the analysis of the immunoblots, HeLa cells stably expressing YFP-RAD18 at a level similar to endogenous RAD18 (Fig. 1B) [28] were used as a control. It has been shown that RAD18 is monoubiquitylated [2,14] in a HR6A/B-dependent manner [14]. In agreement with these findings, both endogenous and overexpressed wild-type YFP-RAD18 appeared as a double band separated by 7 kDa on immunoblots (Fig. 1B), and the upper band was recognized by an antibody against conjugated ubiquitin (FK2) (Fig. 1C). In the experiments presented in Fig. 1D, endogenous RAD18 was downregulated by siRNAs in HeLa cells as previously described [28]. The knockdown of RAD18 is very efficient, and the protein was no longer detectable on immunoblots; suggesting >90% downregulation [18]. For YFP-RAD18, a RAD18 double band was still formed for both RING finger mutants (Fig. 1D, input), but not for the Zinc finger or HR6BD mutants. These findings suggest that the ubiquitylation of RAD18 is independent of the RING domain, but does depend on the Zinc finger and the HR6BD. A mutant carrying mutations in all putative autoubiquitylation sites (K161R/K261R/K309R/K318R) ( $\Delta$ ubi) [14] still appeared as a doublet that was identical to the doublet observed for wild type RAD18 (Supplementary Fig. S1A). In addition, based upon evolutionary conservation of lysines between species, we induced single mutations at 4 additional candidate lysines (K197R, K230R, K241R, and K245R) that might represent autoubiquitylation sites. The results suggest that none of these sites is

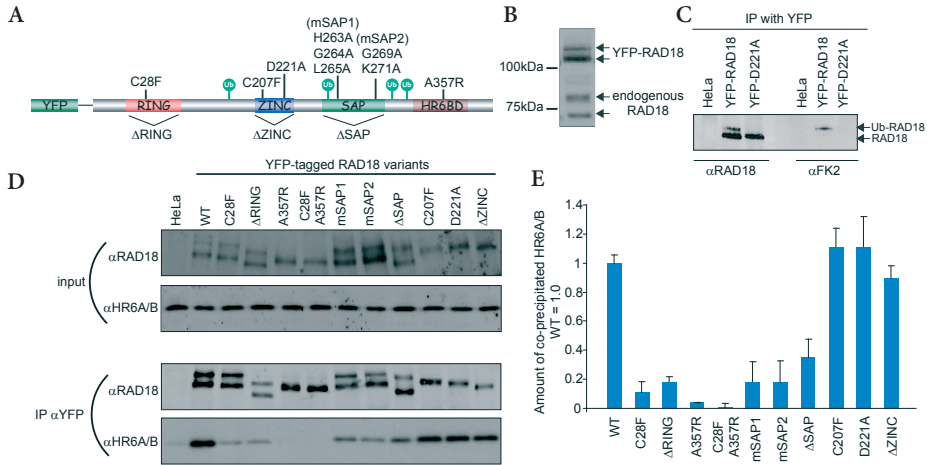


**Figure 1. Functional analyses of human RAD18.** (A) Schematic primary structure of human RAD18. All four putative ubiquitylation sites indicated with green circles were mutated in the Aubi construct. In the RING finger, C28 was mutated to phenylalanine (C28F), to abolish the E3 ligase activity [2]. In addition, a complete RING finger deletion mutant ( $\Delta$ RING, aa25-63) was generated. Two different point mutations were generated in the Zinc finger; C207 was mutated to phenylalanine (C207F) [2], and a conserved aspartic acid D221, present in all Zinc finger domains that have been shown to bind to ubiquitin to date, was mutated to alanine (D221A). The whole Zinc finger (aa201-225) was also deleted ( $\Delta$ ZINC). In the SAP domain we generated combined mutations that have been shown to have a reduced binding activity for single-stranded and double-stranded DNA *in vitro* [14]. mSAP1 contained mutations at H263, G264, and L265, and mSAP2 was mutated at G269 and K271; all these residues were mutated to an alanine residue. The entire SAP domain (aa248-282) was also deleted ( $\Delta$ SAP). In the HR6BD, A357 was mutated to arginine (A357R) to disrupt the binding to HR6A/B. Finally, a double mutation in the RING finger and the HR6A/B binding domain (C28F/A357R) was also generated. (B) Expression levels detected on immunoblots with  $\alpha$ RAD18, for endogenous RAD18 and stably expressed YFP-RAD18 in HeLa cells. (C) HeLa cells stably expressing YFP-RAD18 or transiently expressing YFP-mutant RAD18, and wild-type HeLa cells were lysed and immunoprecipitation with YFP antibody (IP  $\alpha$ YFP) was performed. The results of immunoprecipitation of RAD18 ( $\alpha$ RAD18) or ubiquitylated RAD18 ( $\alpha$ FK2) were detected on immunoblots. (D) HeLa cells stably expressing YFP-RAD18 or transiently expressing YFP-mutant RAD18, and wild-type HeLa cells were transfected with siRNA targeting endogenous RAD18 (si-endoRAD18). Forty-eight hours later, cells were lysed (input) and immunoprecipitation with YFP antibody (IP  $\alpha$ YFP) was performed. The expression levels of RAD18 and HR6A/B in the lysate, detected with  $\alpha$ RAD18 and  $\alpha$ HR6A/B, are shown as input. (E) Quantification of the amount of co-immunoprecipitated HR6A/B in the IP results of (D). The amount of HR6A/B that co-precipitated with wild-type RAD18 was set at 1.0. The error bars in the graph represent the standard deviation of three independent experiments.

required for RAD18 ubiquitylation (Supplementary Fig. S1B), indicating the presence of another unknown putative ubiquitylation site in RAD18 that is required for mono-ubiquitylation *in vivo*. However, it cannot be excluded that the autoubiquitylation site changes when the preferred lysine is mutated.

### 3.2. Binding of HR6A/B to RAD18 requires not only an intact RING finger and HR6A/B binding domain, but also the SAP domain *in vivo*

In *Saccharomyces cerevisiae*, Rad6 binds to Rad18 via the C-terminal domain of Rad18, as shown in a yeast two-hybrid assay [13]. In addition to the C-terminal domain, the

RING finger seems to be also essential for binding of mammalian RAD18 to HR6A/B, as found in an *in vitro* assay [14] and yeast two-hybrid assay [58]. In the present study, we performed pull-down assays using HeLa cells expressing YFP-tagged RAD18 carrying different mutations, while endogenous RAD18 was downregulated by siRNAs (Fig. 1D), and analyzed the interaction between RAD18 and HR6A/B (Fig. 1E). A 40-fold reduction in amount of co-precipitated HR6A/B was observed for the RAD18 A357R mutant (HR6BD), compared with wild-type. In addition, the RING finger mutants also showed a 5-10 fold decreased efficiency of HR6A/B co-precipitation (Fig. 1D and 1E), suggesting that both the RING finger and HR6BD mediate interaction with HR6A/B *in vivo*. Indeed, a double mutant RAD18 (C28F/A357R) completely failed to co-precipitate HR6A/B, confirming that HR6A/B interacts with RAD18 via both the HR6BD and the RING finger domains *in vivo* (Fig. 1D and 1E). SAP domain mutants also showed a reduced co-precipitation efficiency for HR6A/B, whereas the Zinc finger mutants and  $\Delta$ ubi mutant behaved similar to the wild type protein with respect to co-immunoprecipitation of HR6A/B (Fig. 1D and 1E, Supplementary Fig. S1 for  $\Delta$ ubi).

To analyze the E3 ligase function of RAD18, we examined the ability of RAD18 mutants to ubiquitylate PCNA, which is a well known substrate of RAD18 [10,59]. In accordance with the findings of Huang et al. (2009) [1], mutations in the SAP domain precluded PCNA ubiquitylation as well as mutations in the RING finger or the HR6BD (Supplementary Fig. S3). Together with the data obtained for co-immunoprecipitation of RAD18 mutants with HR6A/B, this suggests that interaction of HR6A/B with RAD18 is crucial for PCNA ubiquitylation, since the level of PCNA ubiquitylation correlated with the amount of HR6A/B that coprecipitated with the different YFP-RAD18 mutants.

We next examined which domains of RAD18 are essential for RAD18 foci formation during the cell cycle. In accordance with the results of Huang et al. (2009) [1], we found that accumulation of RAD18 in foci depends on its Zinc finger, and is independent of its RING finger domain, the SAP domain, or the HR6BD (Supplementary Fig. S2). To analyze the localization of the Zinc finger mutant of RAD18 throughout the cell cycle, we performed time lapse analyses (images of living cells with six confocal planes were captured every 30 min for 27 hours), and found no foci at any cell cycle stage (Supplementary Movie 1 for wild type and Supplementary Movies 2 and 3 for Zinc finger mutant D221A). These results indicate that neither the E3-ligase function nor the DNA binding function of RAD18 is required to accumulate at damaged sites or replication foci.

### 3.3. RAD18 accumulation at DSBs depends on RPA

Having established that the Zinc finger domain of RAD18 is required for the formation of RAD18 foci throughout the cell cycle and upon irradiation, we next investigated which proteins are required for RAD18 recruitment to chromatin. It has been suggested that exposure of ssDNA at stalled replication forks results in accumulation of RPA followed by recruitment of RAD18 [26].

In order to examine whether RPA is required for RAD18 accumulation at sites of  $\gamma$ -irradiation-induced DNA damage, RPA2 was depleted using siRNA, and foci

formation of RAD18 was analyzed. Downregulation of RPA2 expression (Fig. 2A) also reduced the expression level of RPA1, and no PCNA mono-ubiquitylation was detected following UV irradiation. It needs to be taken into account that RPA-deficient cells are very likely blocked in G1 phase, since RPA is essential for DNA replication. In these RPA-deficient cells, we were no longer able to detect spontaneous or IR-induced foci formation of RAD18 (Fig. 2B), although the expression level of RAD18 did not change (Fig. 2A). Note that RAD18 is able to form IR-induced foci in G1 phase of wild type cells [28]. Since downregulation of RAD18 did not influence either RPA expression (Fig. 2C) or localization (Fig. 2D), RPA most likely acts upstream of RAD18 at IR-induced DSBs. It probably functions at a very early stage of the DNA damage response signaling pathway, since accumulation of conjugated ubiquitins, a known early step in the DNA damage response [32], was also RPA dependent (Fig. 2E).

These results, together with the mutation analyses, and the fact that RAD18 did not show exact colocalization with RPA (Fig. 2D) [28], prompted us to examine the localization pattern of conjugated ubiquitins in comparison with that of RAD18. We found an overall colocalization of RAD18 with conjugated ubiquitins at all cell cycle phases, and after IR (Fig. 2F). This localization pattern of conjugated ubiquitins was independent of RAD18 expression (Fig. 2F). These observations suggest that the localization of RAD18 to chromatin is preceded by ubiquitylation of an unknown chromatin component.

### 3.4. RAD18 binds to ubiquitylated chromatin components including histone H2A

Following induction of DSBs, the surrounding chromatin at the break sites undergoes various modifications. One of the first modifications is phosphorylation of histone H2A variant H2AX ( $\gamma$ H2AX) by ATM (serine/threonine protein kinase ataxia telangiectasia mutated) [31]. MDC1, a mediator protein, is immediately recruited to sites of DSBs, interacts directly with  $\gamma$ H2AX via its BRCT domains [60], and plays a crucial role in the DNA damage response pathway [39,61]. Subsequently, histone H2A and H2AX are ubiquitylated in the chromatin surrounding DSBs by the E3 ubiquitin ligases RNF8 and RNF168 in a MDC1-dependent manner [32-34]. Since RAD18 carrying a mutation in its ubiquitin-binding Zinc finger did not form any DSB-associated foci (Fig. S2, Supplementary Fig. S2, and Supplementary Movies 2 and 3), we hypothesized that RAD18 is recruited to the chromatin surrounding a DSB through binding to ubiquitylated H2A and/or H2AX. This idea is supported by the recent finding that the accumulation of RAD18 at sites of DSBs is dependent on RNF8 [1]. To investigate this hypothesis, we examined the physical interaction of wild-type RAD18 with ubiquitylated H2A by an immunoprecipitation assay in HeLa cells with and without IR exposure. Cell lysates were pretreated with nuclease (Fig. 3A), to exclude that any co-immunoprecipitation observed resulted from indirect interactions via DNA. On immunoblots, we did not observe a clear increase in the amount of either ubiquitylated H2A or conjugated ubiquitin recognized by the FK2 antibody in cells treated with IR compared to controls (Fig. 3B and 3E, input). This might be due to the abundant amounts of ubiquitylated H2A that localize to silenced genomic regions, independent of DNA damage, and has also been observed by others [62]. Upon immunoprecipitation

of YFP-RAD18, we could clearly co-immunoprecipitate ubiquitylated H2A (Fig. 3B, IP  $\alpha$ YFP), and the amount was somewhat increased after IR (Fig. 3B, IP  $\alpha$ YFP). This suggests that RAD18 is recruited to DSB repair sites at least in part via interaction with mono-ubiquitylated H2A. Note that FK2 antibody recognizes not only ubiquitylated H2A but also other ubiquitylated proteins, indicating that RAD18 interacts with many additional ubiquitylated proteins (Fig. 3B). Non-ubiquitylated H2A was not specifically co-precipitated (Fig 3B, IP  $\alpha$ YFP). The H2A antibody detected ubiquitylated H2A only upon overexposure in the input fraction (Fig. 3C), and not in the IP, most likely because the low molecular weight of IgG band co-migrated with the ubiquitylated H2A band (Fig. 3B, IP  $\alpha$ YFP). Using a HeLa cell line that overexpresses H2A-GFP [55,56], we detected increased ubiquitylation upon irradiation (Fig 3D, input), as well as increased co-immunoprecipitation of endogenous RAD18 (Fig. 3D, IP  $\alpha$ GFP). Intriguingly,

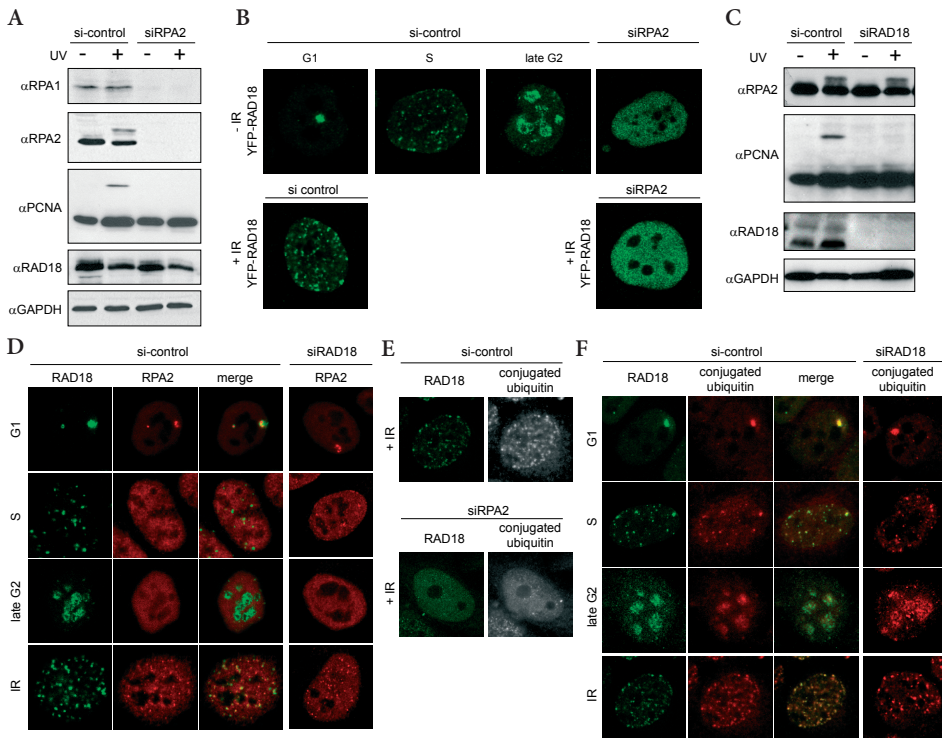


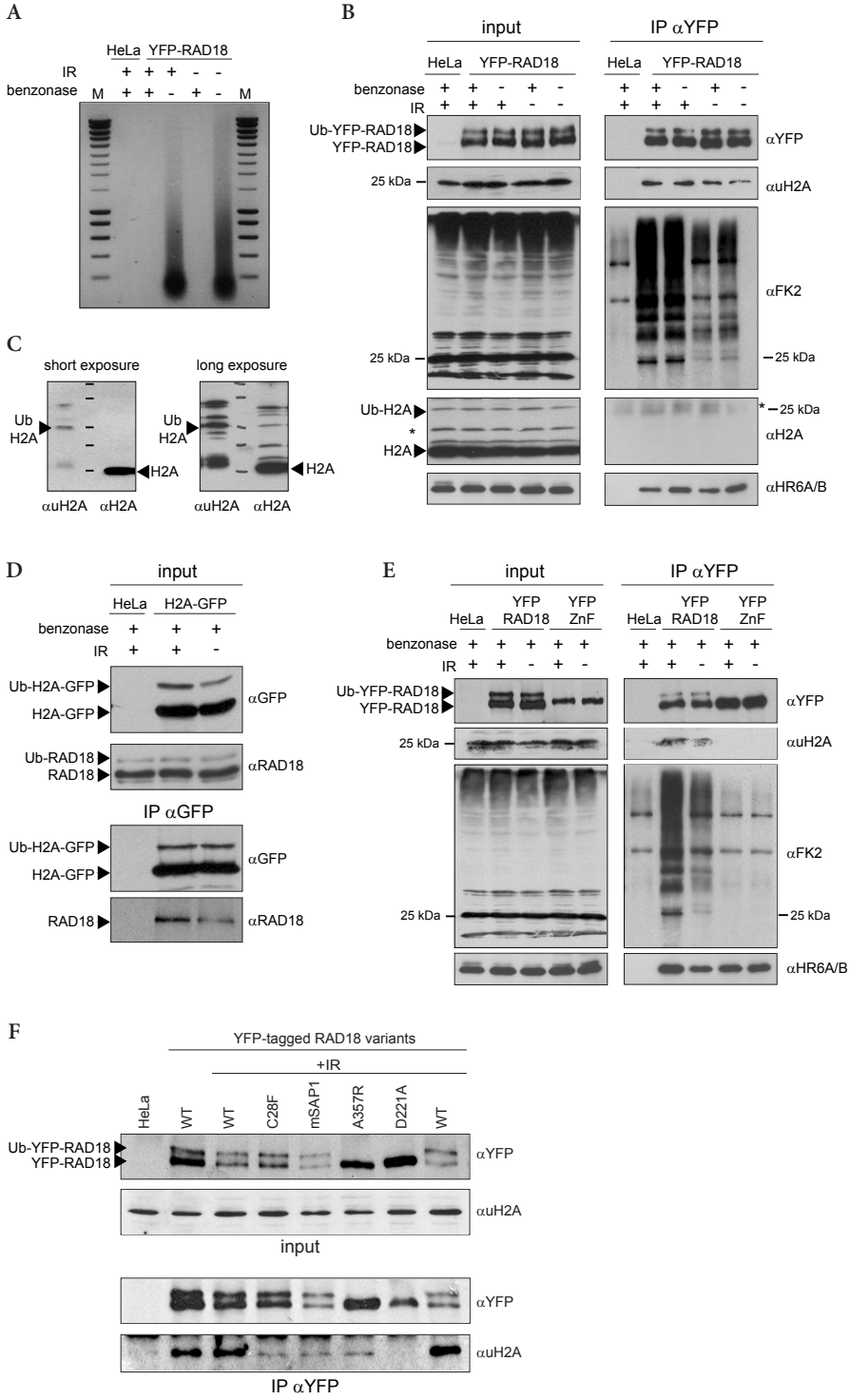
**Figure 2.** RPA2-dependent RAD18 accumulation at sites of DNA damage. HeLa cells stably expressing YFP-RAD18 were transfected with siRNA against RPA2 (siRPA2) (A, B, E), or RAD18 (siRAD18) (C, D, F) for 48 hours. Non-targeting siRNA (si-control) was used as a control. (A, C) Cells were irradiated with 20 J/m<sup>2</sup> UV-C and whole-cell extracts were prepared 8 h later. Expression levels of RPA1, RPA2, mono-ubiquitylated PCNA, and RAD18 were analyzed with immunoblots using different antibodies as indicated. GAPDH was used as a loading control. (B) Confocal images of living YFP-RAD18 HeLa cells in all cell cycle phases as indicated above the pictures. For cells treated with siRPA2, it was not possible to determine the cell cycle phase. Subsequently, cells were exposed to IR (5 Gy), and living cell nuclear images were captured 30 min after IR. (D, E, F) Cells were exposed to IR (5 Gy), and fixed 30 min later. Antibodies recognizing RPA and RAD18 were used to visualize the proteins as indicated. Anti-FK2 was used to visualize conjugated ubiquitins. Cell cycle phases are indicated on the left of each panel.

ubiquitylated H2A-GFP interacted only with the non-ubiquitylated form of RAD18 (Fig. 3D, IP  $\alpha$ GFP). In order to analyse whether RAD18 interacts with ubiquitylated H2A through the Zinc finger of RAD18, we performed co-immunoprecipitation assays using HeLa cells in which endogenous RAD18 was stably downregulated via shRNA expression (see Material and Methods and Fig. 5F and 5G), and that transiently expressed either wild-type or Zinc finger mutant YFP-RAD18 (Fig. 3E). Ubiquitylated H2A was only co-precipitated by wild type YFP-RAD18 and not by the RAD18 Zinc finger mutant D221A, and the amount of co-precipitated ubiquitylated H2A was increased in cells treated with IR (Fig. 3E, IP $\alpha$ YFP). Another RAD18 Zinc finger mutant (C207F) also did not show any interaction with ubiquitylated H2A (data not shown). In addition to the interaction of RAD18 with ubiquitylated H2A, our immunoprecipitation results also indicate that RAD18 interacts with many additional ubiquitylated proteins, in a Zinc finger-dependent way, making it highly likely that apart from H2A and H2AX, other ubiquitylated chromatin components will also be used by RAD18 to bind to chromatin near DSB repair sites. Note that these unknown ubiquitylated proteins which interact with RAD18 show distinct banding patterns on immunoblots compared to the input materials, indicating that RAD18 does not randomly bind to any ubiquitylated protein (Fig. 3B). As a control for the assay, co-immunoprecipitation of HR6A/B was checked, and both wild-type RAD18 and the Zinc finger mutant were able to co-precipitate HR6A/B (Fig. 4D, IP  $\alpha$ YFP). RAD18 carrying mutations in either the RING finger, SAP domain, or HR6BD was still capable to interact with ubiquitylated H2A, although these RAD18 mutants showed considerably reduced amounts of co-precipitated ubiquitylated H2A (Fig. 4F). Taken together, these data support the notion that the accumulation of RAD18 at damaged sites depends on interaction between the Zinc finger domain of RAD18 and ubiquitylated chromatin components, including ubiquitylated H2A.

### **3.5. RAD18 always colocalizes with ubiquitylated H2A during the cell cycle in HeLa cells, but rarely with ubiquitylated H2A at the Barr body in human female fibroblasts**

The immunocytochemical analyses of conjugated ubiquitin in relation to the localization of RAD18 in HeLa cells indicate that RAD18 localization to chromatin is dependent on the presence of ubiquitylated chromatin components (Fig. 2F). The immunoprecipitation analyses indicate that RAD18 interacts with mono-ubiquitylated H2A as well as other ubiquitylated substrates in a RAD18 Zinc finger-dependent manner (Fig. 3E). To examine whether RAD18 localizes with ubiquitylated H2A or some other ubiquitylated substrates recognized by FK2 antibody, we examined the localization of RAD18 and ubiquitylated H2A during the cell cycle and after IR in HeLa cells (Fig. 4A). Throughout the cell cycle and following IR, we detected the colocalization of RAD18 with ubiquitylated H2A (Fig. 4A). These results confirm that ubiquitylated H2A is one of the main ubiquitylated chromatin components.

Next, to analyze whether RAD18 always colocalizes with regions that show enhanced H2A ubiquitylation, we analyzed human female primary fibroblast cultures. In these cells, dosage compensation has resulted in the inactivation of one of the two



X chromosomes, and the inactivated chromosome, forming the Barr body, is known to be enriched for ubiquitylated H2A and trimethylation of histone H3 at lysine 27 (H3K27me3). Immunocytochemical analyses of ubiquitylated H2A, conjugated ubiquitins, H3K27me3, and RAD18 signals in these cells revealed that the Barr body, visible by dense DAPI staining, and H3K27me3 (data not shown) was mostly not enriched for RAD18, even if uH2A staining was enhanced in this region. In a small percentage of the nuclei (6%), RAD18 enrichment was detected at the Barr body (Fig. 4B). Sometimes, the cells displayed accumulation of uH2A in two separated areas; one representing the Barr body, and the other positive for RAD18 (Fig. 4B, the lowest panels), suggesting that the interaction between RAD18 and uH2A depends on the context; i.e. the presence or absence of specific chromatin-associated factors.

### 3.6. RAD18-dependent accumulation of RAD9 at damaged sites

Next, we attempted to analyze the downstream effects of RAD18 localization to DSB repair sites. In eukaryotes, RAD9, RAD1 and HUS1 form the PCNA-like heterotrimeric 9-1-1 checkpoint complex, which plays a crucial role in cell cycle checkpoint signaling following endogenous and exogenous DNA damage [63,64]. The 9-1-1 complex is known to be activated by replication fork stalling and to initiate checkpoint signaling cascade during S phase [22], whereas RAD18 facilitates the RDB pathway at stalled replication sites [10,59]. It has been shown that both RAD18 and the 9-1-1 clamp loader directly interact with the RPA complex [25,65,71], suggesting a functional interaction at stalled replication sites. However, a possible functional interaction between the 9-1-1 complex and RAD18 at DSBs has not been studied. One of the components of the 9-1-1 complex, RAD9, is known to associate with chromatin at sites of DSBs in human cells [48,66]. Therefore we investigated the possible functional interaction between RAD9 and RAD18 in mammalian cells. First, their dynamic localization was examined by

- ◁ **Figure 3. Interaction of RAD18 with ubiquitylated histone H2A via its Zinc finger following IR.** (A) Cell lysates from wild type HeLa cells and HeLa cells stably expressing YFP-RAD18 were treated with or without benzonase nuclease for 2h on ice. In the presence of benzonase, DNA was absent from the cell lysates that were used for the immunoprecipitation assay shown in (B). M in the figure indicates DNA ladder. (B) HeLa cells stably expressing YFP-RAD18 were exposed to IR (10 Gy). One hour later, cells were lysed and immunoprecipitation (IP) was performed using an YFP antibody. Subsequently, co-precipitation of ubiquitylated histone H2A (uH2A), conjugated ubiquitin (FK2), histone H2A, and HR6A/B was detected on immunoblots using antibodies as indicated. The expression level of YFP-RAD18, ubiquitylated H2A, FK2, H2A, and HR6A/B in the input samples is shown in the left panel. Wild-type HeLa cells were used as a control. The asterisk indicates the presence of a nonspecific band (light chain of IgG in IP  $\alpha$ YFP,  $\alpha$ H2A). (C) Expression level of H2A and ubiquitylated H2A was analysed in HeLa cells using two different antibodies as shown in the figures. Detection of ubiquitylated H2A with the antibody directed against H2A requires a long exposure. (D) Under the same experimental conditions as in (B), HeLa cells stably expressing H2A-GFP were analyzed for their interaction with endogenous RAD18. (E) Wild type or Zinc finger mutant (D221A;YFP-ZnF) YFP-RAD18 were expressed in HeLa cells in which endogenous RAD18 was stably downregulated (see Materials and Methods and Fig. 5F and 5G). Both wild type and mutant YFP-RAD18 contain 5 silent mutations at the shRNA target site to prevent downregulation. Under the same experimental condition as in (B), interaction of either YFP-RAD18 or YFP-ZnF with ubiquitylated H2A was analyzed by immunoprecipitation. Subsequently, co-precipitation of uH2A, conjugated ubiquitin, and HR6A/B was detected on immunoblots using antibodies as indicated. The expression level of YFP-RAD18, YFP-ZnF, uH2A, conjugated ubiquitin, and HR6A/B in the input samples is shown in the left panel. Wild-type HeLa cells were used as a control. (F) Under the same experimental conditions as in (B) but without benzonase treatment, several RAD18 mutants as indicated were analyzed for their interaction with ubiquitylated H2A.

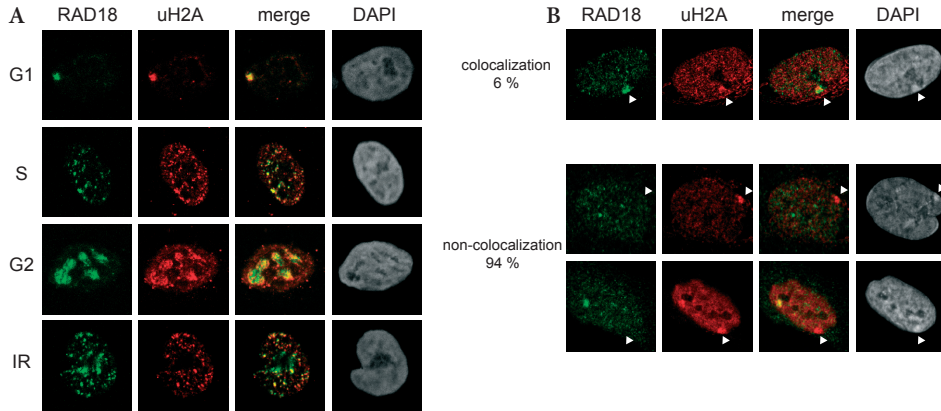
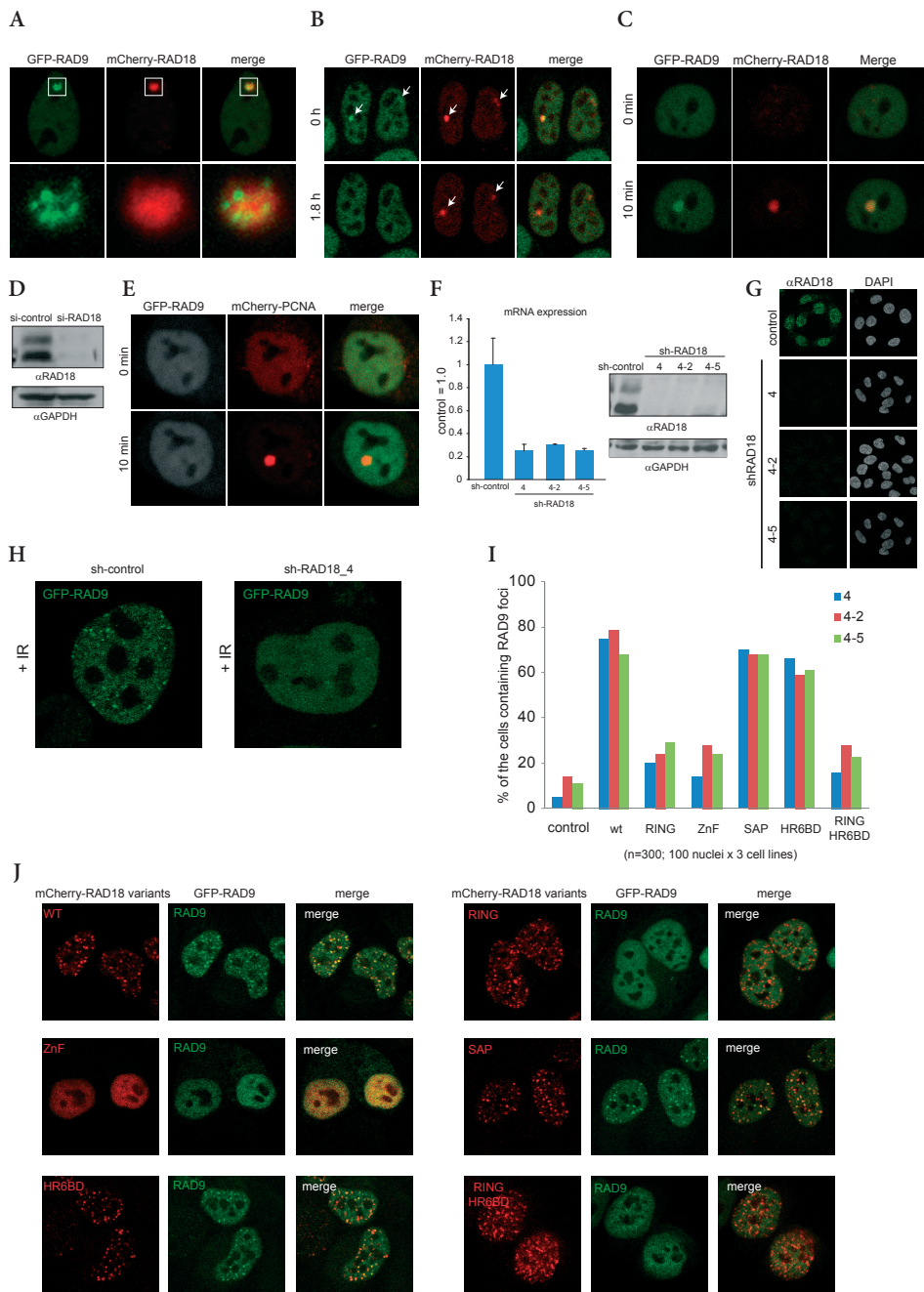


**Figure 4.** RAD18 always colocalizes with uH2A in HeLa cells throughout the cell cycle and after IR, but only very rarely with the uH2A-enriched Barr body. (A) Localization of RAD18 and uH2A was visualized using the indicated antibodies. Cell phases were determined by the subnuclear distribution pattern of RAD18. To induce DSBs, HeLa cells were exposed to IR (5 Gy) and fixed 30 min later. Cell cycle phases are indicated on the left of the pictures. (B) Localization of RAD18 and uH2A in human primary female fibroblast cells. Arrowheads indicate the Barr body, based on the intense DAPI staining.

**Figure 5.** RAD18 facilitates RAD9 localization at induced damaged sites. (A) A confocal image of a living HeLa cell expressing GFP-RAD9 and mCherry-RAD18 in G1 phase. The enlarged G1 foci are shown in the lower panels. (B) Images from time-lapse analysis of living HeLa cells expressing GFP-RAD9 and mCherry-RAD18 in G1 phase. The first moment at which RAD18 was found to colocalize with RAD9 was set at time 0. Arrows in the pictures indicate the G1 foci. (C) HeLa cells expressing GFP-RAD9 and mCherry-RAD18 were locally irradiated with a multi-photon laser (MPL) at 75 mW. (D, E) The expression of RAD18 was downregulated with siRNA against RAD18 (si-RAD18) in HeLa cells stably expressing GFP-RAD9 and transiently co-expressing mCherry-PCNA. Subsequently, the cells were locally irradiated with MPL at 75 mW. As a control, mCherry-PCNA was also analyzed. (F) The level of RAD18 mRNA and protein expression in three different HeLa cell lines stably expressing shRNA targeting *RAD18*. The control level, in HeLa cells stably expressing non-targeting shRNA, was set at 1.0. (G) Expression of endogenous RAD18 was detected by immunostaining using antibody against RAD18 in control and RAD18 knockdown cell lines (shRAD18). Cells were irradiated with IR at 5 Gy, and fixed after 1 hour. (H) GFP-RAD9 was overexpressed in HeLa cells stably expressing either shRNA against RAD18 or non-targeting shRNA. Subsequently, cells were irradiated with IR (5 Gy) and confocal images of living cells were captured 2 hours later. (I) mCherry-tagged RAD18 variants and GFP-RAD9 were co-expressed in RAD18 knockdown cell lines. Subsequently, cells were irradiated with IR at 5 Gy and fixed 2 hours later. Nuclei expressing both mCherry-RAD18 variants and GFP-RAD9 were analyzed and the number of nuclei containing IR-induced RAD9 foci is shown in the graph. 100 nuclei in each mutant and in each *RAD18* knockdown cell line were counted (300 nuclei per mutant). RAD18 mutations shown in the graph are RING = C28F, ZnF = D221A, SAP = mSAP1, HR6BD = A357R, and RING/HR6BD = C28F/A357R. (J) Representative pictures of nuclei expressing both mCherry-RAD18 variants and GFP-RAD9 examined in (I) are shown.



time-lapse experiments in living cells. In G1 phase, RAD18 forms a few foci which also contain RAD51, RPA and  $\gamma$ H2AX [28]. In these so-called G1 foci, we observed RAD9 accumulation (Fig. 5A). The higher magnification in the lower panels of Fig. 5A shows that RAD9 accumulates as multiple foci, whereas RAD18 shows a more diffuse accumulation, surrounding RAD9 foci. This pattern of RAD9 localization in G1 is very similar to what has been observed for RPA and RAD51 [28]. This might reflect the previously reported interaction between RAD18 and RPA [65] and RAD51 [51], and or direct binding of RAD9 to DNA. The localization of RAD9 foci within the RAD18-positive chromatin area in G1 was found for only a few hours (1-2h). Subsequently, RAD9 foci disappeared (Fig. 5B), although the RAD18 foci remained present until the cell entered S phase [28]. In S and G2 phases, RAD9 showed a homogeneous distribution in the nucleus and did not form any foci. In contrast, RAD18 accumulates in many foci in S and G2 phases [28]. To further analyze the functional relation between RAD18 and RAD9 at damaged sites, local damage was induced with a multi-photon laser (MPL) [28]. This revealed that both RAD18 and RAD9 accumulated at the damaged sites (Fig. 5C). Interestingly, using HeLa cells in which RAD18 was transiently downregulated with siRNA (Fig. 5D) or stably downregulated with shRNA (Fig. 5F and 5G), RAD9 no longer accumulated at damaged sites following MPL (Fig. 5E) or IR exposure (Fig. 5H). To analyze the ability of different RAD18 mutants to recruit RAD9 following IR, wild type and mutant RAD18 (mutation in either the RING finger, Zinc finger, SAP domain, or HR6BD, and a double mutant in the RING finger and HR6BD) were transiently co-expressed with GFP-RAD9 in three different *RAD18* knockdown HeLa cell lines (Fig. 5I and 5J). Wild type RAD18 was able to rescue foci formation of RAD9 after IR in approximately 80% of the cells (Fig. 5I and 5J). Expression of RAD18 containing the SAP domain mutation (mSAP1) or a mutation in the HR6BD (A357R) also rescued RAD9 accumulation, RAD18 carrying a point mutation in the RING finger (C28F), or the Zinc finger (D221A), and the double mutant in the RING finger and the HR6BD (C28F/A357R) showed severely reduced IR-induced RAD9 accumulation compared to the wild type (Fig. 5I and 5J). In control experiments, we observed RAD9 accumulation in approximately 5-10% of *RAD18* knockdown cells (Fig. 5I), in accordance with a more than 90% downregulation of RAD18 expression in the *RAD18* knockdown cell lines (Fig. 5F). In addition, *RAD18* knockdown HeLa cells expressing RAD18 mutants used in this experiment showed an equivalent cell growth rate and time span of the cell cycle compared to *RAD18* knockdown HeLa cells expressing wild-type RAD18 (data not shown). Taken together, these data suggest that recruitment of RAD9 to IR-induced DSBs requires the Zinc finger domain of RAD18 and its E3 ligase activity. To analyze this further, we studied physical interactions between RAD18 and components of the 9-1-1 complex by the yeast two-hybrid assay in the absence and presence of DNA damage (HU, CPT, MMS, and IR). In accordance with recent data concerning yeast RAD18 and the 9-1-1 complex [53], no direct interaction between human RAD18 and the 9-1-1 complex was detected (Supplementary Fig. S3A), although interactions among the 9-1-1 complex components (Supplementary Fig. S3B), between RAD18 and HR6A/B, and also between RAD18 and PCNA (Supplementary Fig. S3C) were detected. These results suggest that RAD18 might not interact stably or directly with the 9-1-1

complex. Next, we investigated whether knockdown of RAD18 and the subsequent lack of foci formation of RAD9 upon IR also affected activation of the downstream checkpoint kinases CHK1 and CHK2, but the response to 10 Gy IR was identical in control and *Rad18* knockdown cells (Supplementary Fig. S4).

## 4. DISCUSSION

### 4.1. RPA is required for RAD18 foci formation, and PCNA ubiquitylation occurs independent of the Zinc finger domain of RAD18

Two distinct manners of recruitment of RAD18 to sites of DNA damage can be observed. First, RAD18 has a direct DNA binding ability mediated by the SAP domain, and/or RPA bound to ssDNA mediates recruitment of RAD18 to the ssDNA. RPA and the SAP domain of RAD18 are both required for PCNA ubiquitylation in the RDB pathway [25]. Second, recruitment of RAD18 to the chromatin surrounding DSB sites depends on the ubiquitin-binding Zinc finger domain of RAD18. This type of RAD18 recruitment also requires RPA, but perhaps more indirectly, since RAD18 shows a more diffuse localization compared to RPA at DSB sites, and RPA and RAD18 show relatively little colocalization during the cell cycle.

RPA is a single-stranded DNA (ssDNA) binding protein, essential for both DNA replication and recombination [18-23]. According to current models [25,26], stalled replication forks expose ssDNA covered by RPA which is required for PCNA ubiquitylation [25,27] and the recruitment of RAD18 [25,26]. Once RAD18 is bound to RPA, or to ssDNA, or to both, it may ubiquitylate PCNA. RAD18 (complexed with HR6A/B) carrying mutations in the Zinc finger most likely is still capable of binding to ssDNA via the SAP domain, and could be present at stalled replication forks, perhaps undetectable due to the small number of molecules present, below the threshold for foci formation. Since the interaction between RAD18 and HR6A/B partially depends on an intact SAP domain, we were unable to determine whether the SAP domain functions in PCNA ubiquitylation by mediating RAD18 binding to DNA *in vivo*, or as a third domain required for RAD18-HR6A/B interaction, or both. Our observations on the differential requirement of the Zinc finger and the SAP domain in mediating PCNA ubiquitylation nicely mirror the results described by Nakajima et al. (2006) who found that the Zinc finger domain of RAD18 is required for focal localization of RAD18 in undamaged cells and at damaged sites in cells irradiated with an UVA or UVC laser. In addition, RAD18 carrying a mutation in the Zinc finger domain could restore Pol $\eta$  foci formation at sites of stalled replication, whereas a SAP domain mutant could not [67].

### 4.2. RAD18 is recruited to sites of DSB-repair via binding to ubiquitylated H2A and other ubiquitylated chromatin components

In a previous study, we have shown that RAD18 colocalizes with  $\gamma$ H2AX in G1, S and early G2 phase cells and also following damage induction by IR [28]. Kinetics studies of a number of DNA-damage response proteins including mediator and repair proteins revealed that RNF8, NBS1, and MDC1 show fast accumulation at DSBs, followed by 53BP1 and BRCA1 [32]. RNF8 depletion did not affect accumulation of MDC1 and

NBS1, indicating that these are among the first proteins that recognize DNA damaged sites following IR [32]. In the present study, we found a physical interaction between RAD18 and ubiquitylated H2A via its Zinc finger. In addition to the interaction of RAD18 with ubiquitylated H2A, the immunoprecipitation results also indicate that RAD18 interacts with additional ubiquitylated proteins in a Zinc finger-dependent manner, suggesting that other ubiquitylated chromatin components will also be used by RAD18 to bind to chromatin near DSB repair sites. The distribution pattern of conjugated ubiquitin during the cell cycle was identical to that of RAD18. This finding is substantiated by the evidence that RAD18 foci formation is dependent on H2AX, MDC1, and RNF8, but not on BRCA1, or 53BP1 [1]. Ubiquitylation of histones occurs in an RNF8/RNF168-dependent manner, and depletion of RNF8/RNF168 ablates the formation of conjugated ubiquitin on chromatin, even after IR [32-34]. Since RNF8 functions upstream of RNF168, it might be interesting to study whether RAD18 recruitment at DSBs also depends on RNF168.

Taken together, RAD18 interacts with ubiquitylated chromatin components in an RNF8-dependent manner, and one of these components is ubiquitylated H2A. Intriguingly, immunocytochemical analyses in human female primary fibroblast cells revealed that the Barr body, known to be marked with uH2A, was mostly not enriched for RAD18, even if uH2A and FK2 staining was enhanced in this region. These data indicate that the interaction of RAD18 with ubiquitylated chromatin components including uH2A is related to DNA damage, and possibly regulated. Such regulation might occur via phosphorylation of RAD18 by ATM kinase, similar to what occurs for many other proteins involved in the DNA damage response pathway.

#### **4.3. Autoubiquitylation of RAD18 depends on the Zinc finger domain, but does not require the RING finger domain**

Previous work has shown that ubiquitylated RAD18 is found mainly in the soluble fraction, and not in the chromatin-associated fraction of cell extracts [25]. It is, therefore, intriguing that the Zinc finger, that was found to be required for localization of RAD18 to chromatin, is also essential for mono-ubiquitylation of RAD18 *in vivo*. In *RNF8*-knockdown cells, in which RAD18 is no longer recruited to DSB repair sites, RAD18 ubiquitylation is still observed [1], indicating that it is unlikely that it is the aberrant localization of the Zinc finger mutant that causes the lack of ubiquitylation of RAD18.

Surprisingly, the RING finger is not required for RAD18 ubiquitylation [2] (and present results). It might be suggested that ubiquitylation of RAD18 is performed by a different E3 ligase, but this would then also depend on interaction of RAD18 with HR6A/B. Alternatively, the residual interaction between RAD18 and HR6A/B through the HR6BD domain in the RING finger mutant may still allow RAD18 ubiquitylation, independent of E3 activity, in a mechanism described by Hoeller et al. (2007) [68] for ubiquitin binding domain (UBD) containing proteins. In this mechanism, the UBD can directly cooperate with the Ub-charged E2 enzyme, and allow ubiquitylation of the host protein, in the absence of an E3 ligase [68]. In RAD18, the Zinc finger represents a UBD [14], and is required for RAD18 ubiquitylation. Thus, interaction

of RAD18 with Ub-charged HR6A/B, via the HR6BD and the Zinc finger UBD, most likely allows RAD18 ubiquitylation even if the E3-ligase function of RAD18 is absent. In accordance with this notion, RAD18 mutants that are unable to bind HR6A/B are not ubiquitylated. This E3-independent ubiquitylation of UBD-containing proteins is thought to lead to their inactivation due to intra- or inter-molecular association of the covalently attached ubiquitin moiety with the UBD (reviewed in [69]). This would fit with the idea that mono-ubiquitylation of RAD18 occurs when it is not functionally engaged in the ubiquitylation of a substrate, for example when it is freely diffusing in the nucleoplasm. It is also in accordance with our observation that precipitation of (ubiquitylated) H2A co-precipitates only the non-ubiquitylated form of RAD18.

#### 4.4. RAD18 facilitates RAD9 recruitment selectively to G1 foci and DSB repair sites

In the present study, we showed that human RAD9 localizes at IR-induced damaged sites in a RAD18-dependent manner. This function depends on the Zinc finger and ubiquitin ligase activity of RAD18. In accordance with our findings, Huang et al. [1] also showed that the role of RAD18 in HR requires the Zinc finger and RING finger domains of RAD18, although their data indicated that the E3 ligase activity of RAD18 is not required to promote HR [1]. RAD18 may play several roles in DSB repair, some of which may be dependent on or independent from its E3 ligase activity. In this context, it is also somewhat surprising that the HR6BD is not required for RAD9 recruitment to DSBs. This may point to a structural requirement for the RING finger domain instead of a functional requirement, although it is not very likely that RAD18 structure is severely disrupted by the C28F mutation. Alternatively, in the absence of the HR6BD, the RING finger could still be sufficient to maintain the RAD18-HR6A/B interaction in this context. At present, it is not possible to distinguish between these two possibilities. We have not detected a direct stable interaction between RAD18 and the 9-1-1 complex (Supplementary Fig. S3A), and could not obtain evidence for RAD18-dependent ubiquitylation of the 9-1-1 complex (data not shown).

Earlier reports have also shown association of human RAD9 with chromatin after DNA damage [49], and depletion of mammalian RAD9 leads to IR sensitivity [45,50,51] in particular in the S and G2 phase of the cell cycle [51]. Loading of the 9-1-1 complex to damaged sites depends on the mammalian clamp loader RAD17, but occurs independent of ATM/ATR localization [70]. One of the known functions of the 9-1-1 complex is to activate CHK1, a kinase which is involved in the checkpoint signaling pathway [44-47]. Surprisingly, RAD9 deficient cells are not defective in activating S [45] or G2 checkpoints [45,51] following IR exposure. Since hRAD9 function does not influence IR-induced ATM phosphorylation [51] or ATM-mediated CHK2 phosphorylation at Tyr68 [45,51], it was suggested that RAD9 has a direct role in DNA damage repair rather than cell cycle checkpoint control following IR [45,51]. However, Hopkins et al. (2004) find a mild defect in IR-induced G2 checkpoint control in RAD9 deficient ES cells, but their data also indicate that RAD9 performs additional, checkpoint independent functions, that promote ionizing-radiation resistance [50]. We have shown in the present study that depletion of RAD18, and thereby of RAD9 from the damaged site, does not cause any deficiency in phosphorylation of CHK1 or CHK2,

also suggesting a role for RAD18 and RAD9 at IR-induced DNA damage, independent from the function of cell cycle checkpoint control by the 9-1-1 complex. RAD9 might function directly in HR repair through interaction with hRAD51 [51] and/or RPA [65,71]. Based upon our data, it is likely that RAD18 somehow (via ubiquitylation of an unknown substrate) facilitates the interaction of RAD9 with RPA and/or RAD51. Thereafter, they may stimulate HR at damage-induced DSBs throughout the cell cycle, and in G1 foci in the absence of damage. Previously, we have shown that part of these RAD18-positive G1 sites represent DSBs that have been processed for HR, based on the colocalization with RAD51 and RPA. Most likely, these DSBs persist because no template for repair is available [28]. Other RAD18-positive G1 foci colocalize with KU86, which is involved in NHEJ, and these sites may reach complete repair before entry into S phase [28]. The localization pattern of RAD9 within the RAD18-positive area in G1 shows a striking resemblance to the RPA and RAD51 pattern, indicating that RAD9 localizes to the G1 foci that are attempting to perform HR, where it may interact with RPA and/or RAD51. In addition, Warmerdam et al. [48] have shown that IR-induced RAD9 foci depend on the presence of CTIP, which stimulates DSB-resection, again pointing to a role of RAD9 in HR instead of NHEJ.

## CONCLUSION

Taken together, our data suggest that RPA is required for RAD18 localisation at DSBs. This most likely occurs through indirect recruitment of RNF8/RNF168 to DSBs, and subsequent ubiquitylation of H2A and other chromatin components. RAD18 binds to ubiquitylated H2A and other ubiquitylated chromatin components via its Zinc finger domain and this facilitates RAD9 recruitment via the ubiquitin ligase activity of RAD18. The role of RAD18 in stimulating HR may thus be mediated in part through direct actions of RAD9 interacting with RAD51 and/or RPA.

## CONFLICT OF INTEREST STATEMENT

The authors declare that there are no conflicts of interest.

## ACKNOWLEDGEMENTS

We thank Jurgen A. Marteijn (Erasmus MC, Rotterdam, The Netherlands) for the H2A-GFP cell line, Daniël O. Warmerdam (Erasmus MC, Rotterdam, The Netherlands) for the GFP-RAD9 construct, and Annelies de Klein (Erasmus MC, Rotterdam, The Netherlands) and Stefan Barakat (Erasmus MC, Rotterdam, The Netherlands) for the female primary fibroblast.

This work was supported by the Netherlands Organization for Scientific Research (NWO) through ALW (VIDI 864.05.003).

## REFERENCES

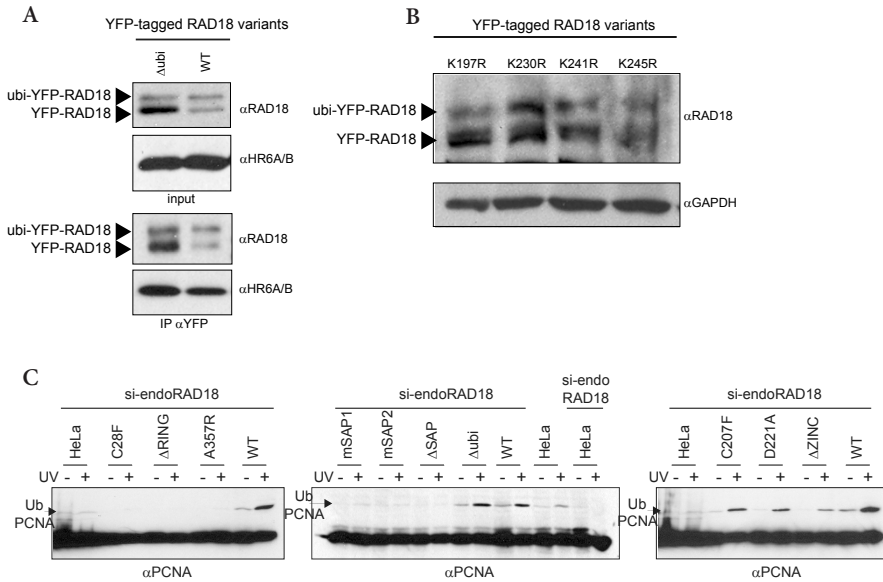
1. J. Huang, M.S. Huen, H. Kim, C.C. Leung, J.N. Glover, X. Yu, J. Chen, RAD18 transmits DNA damage signalling to elicit homologous recombination repair, *Nat Cell Biol* 11 (2009) 592-603.
2. S. Miyase, S. Tateishi, K. Watanabe, K. Tomita, K. Suzuki, H. Inoue, M. Yamaizumi, Differential regulation of Rad18 through Rad6-dependent mono- and polyubiquitination, *J Biol Chem* 280 (2005) 515-524.
3. S. Tateishi, H. Niwa, J. Miyazaki, S. Fujimoto, H. Inoue, M. Yamaizumi, Enhanced genomic instability and defective postreplication repair in RAD18 knockout mouse embryonic stem cells, *Mol Cell Biol* 23 (2003) 474-481.
4. N. Shiomi, M. Mori, H. Tsuji, T. Imai, H. Inoue, S. Tateishi, M. Yamaizumi, T. Shiomi, Human RAD18 is involved in S phase-specific single-strand break repair without PCNA monoubiquitination, *Nucleic Acids Res* 35 (2007) e9.
5. K. Watanabe, K. Iwabuchi, J. Sun, Y. Tsuji, T. Tani, K. Tokunaga, T. Date, M. Hashimoto, M. Yamaizumi, S. Tateishi, RAD18 promotes DNA double-strand break repair during G1 phase through chromatin retention of 53BP1, *Nucleic Acids Res* (2009).
6. H. Xin, W. Lin, W. Sumanasekera, Y. Zhang, X. Wu, Z. Wang, The human RAD18 gene product interacts with HHR6A and HHR6B, *Nucleic Acids Res* 28 (2000) 2847-2854.
7. H.D. Ulrich, The RAD6 pathway: control of DNA damage bypass and mutagenesis by ubiquitin and SUMO, *Chembiochem* 6 (2005) 1735-1743.
8. C. Hoege, B. Pfander, G.L. Moldovan, G. Pyrowolakis, S. Jentsch, RAD6-dependent DNA repair is linked to modification of PCNA by ubiquitin and SUMO, *Nature* 419 (2002) 135-141.
9. G.L. Moldovan, B. Pfander, S. Jentsch, PCNA, the maestro of the replication fork, *Cell* 129 (2007) 665-679.
10. P.L. Kannouche, J. Wing, A.R. Lehmann, Interaction of human DNA polymerase  $\epsilon$  with monoubiquitinated PCNA: a possible mechanism for the polymerase switch in response to DNA damage, *Mol Cell* 14 (2004) 491-500.
11. V. Bailly, J. Lamb, P. Sung, S. Prakash, L. Prakash, Specific complex formation between yeast RAD6 and RAD18 proteins: a potential mechanism for targeting RAD6 ubiquitin-conjugating activity to DNA damage sites, *Genes Dev* 8 (1994) 811-820.
12. V. Bailly, S. Lauder, S. Prakash, L. Prakash, Yeast DNA repair proteins Rad6 and Rad18 form a heterodimer that has ubiquitin conjugating, DNA binding, and ATP hydrolytic activities, *J Biol Chem* 272 (1997) 23360-23365.
13. V. Bailly, S. Prakash, L. Prakash, Domains required for dimerization of yeast RAD6 ubiquitin-conjugating enzyme and Rad18 DNA binding protein, *Mol Cell Biol* 17 (1997) 4536-4543.
14. V. Notenboom, R.G. Hibbert, S.E. van Rossum-Fikkert, J.V. Olsen, M. Mann, T.K. Sixma, Functional characterization of Rad18 domains for Rad6, ubiquitin, DNA binding and PCNA modification, *Nucleic Acids Res* 35 (2007) 5819-5830.
15. R.A. Bish, M.P. Myers, Werner helicase interacting protein 1 (WRNIP1) binds polyubiquitin via its zinc finger domain, *J Biol Chem* (2007).
16. M.G. Bomar, M.T. Pai, S.R. Tzeng, S.S. Li, P. Zhou, Structure of the ubiquitin-binding zinc finger domain of human DNA Y-polymerase  $\epsilon$ , *EMBO Rep* 8 (2007) 247-251.
17. J.H. Hurley, S. Lee, G. Prag, Ubiquitin-binding domains, *Biochem J* 399 (2006) 361-372.
18. M.S. Wold, Replication protein A: a heterotrimeric, single-stranded DNA-binding protein required for eukaryotic DNA metabolism, *Annu Rev Biochem* 66 (1997) 61-92.
19. C. Iftode, Y. Daniely, J.A. Borowiec, Replication protein A (RPA): the eukaryotic SSB, *Crit Rev Biochem Mol Biol* 34 (1999) 141-180.
20. Y. Wang, C.D. Putnam, M.F. Kane, W. Zhang, L. Edelmann, R. Russell, D.V. Carrion, L. Chin, R. Kucherlapati, R.D. Kolodner, W. Edelmann, Mutation in Rpa1 results in defective DNA double-strand break repair, chromosomal instability and cancer in mice, *Nat Genet* 37 (2005) 750-755.
21. M.S. Wold, T. Kelly, Purification and characterization of replication protein A, a cellular protein required for in vitro replication of simian virus 40 DNA, *Proc Natl Acad Sci U S A* 85 (1988) 2523-2527.
22. L. Zou, S.J. Elledge, Sensing DNA damage through ATRIP recognition of RPA-

- ssDNA complexes, *Science* 300 (2003) 1542-1548.
23. Y. Zou, Y. Liu, X. Wu, S.M. Shell, Functions of human replication protein A (RPA): from DNA replication to DNA damage and stress responses, *J Cell Physiol* 208 (2006) 267-273.
  24. S. Sigurdsson, S. Van Komen, W. Bussen, D. Schild, J.S. Alcala, P. Sung, Mediator function of the human Rad51B-Rad51C complex in Rad51/RPA-catalyzed DNA strand exchange, *Genes Dev* 15 (2001) 3308-3318.
  25. A.A. Davies, D. Huttner, Y. Daigaku, S. Chen, H.D. Ulrich, Activation of ubiquitin-dependent DNA damage bypass is mediated by replication protein a, *Mol Cell* 29 (2008) 625-636.
  26. D. Huttner, H.D. Ulrich, Cooperation of replication protein A with the ubiquitin ligase Rad18 in DNA damage bypass, *Cell Cycle* 7 (2008) 3629-3633.
  27. A. Niimi, S. Brown, S. Sabbioneda, P.L. Kannouche, A. Scott, A. Yasui, C.M. Green, A.R. Lehmann, Regulation of proliferating cell nuclear antigen ubiquitination in mammalian cells, *Proc Natl Acad Sci U S A* 105 (2008) 16125-16130.
  28. A. Inagaki, W.A. van Cappellen, R. van der Laan, A.B. Houtsmuller, J.H. Hoeijmakers, J.A. Grootegoed, W.M. Baarends, Dynamic localization of human RAD18 during the cell cycle and a functional connection with DNA double-strand break repair, *DNA Repair (Amst)* 8 (2009) 190-201.
  29. E. Sonoda, H. Hohegger, A. Saberi, Y. Taniguchi, S. Takeda, Differential usage of non-homologous end-joining and homologous recombination in double strand break repair, *DNA Repair (Amst)* 5 (2006) 1021-1029.
  30. A. Saberi, H. Hohegger, D. Szuts, L. Lan, A. Yasui, J.E. Sale, Y. Taniguchi, Y. Murakawa, W. Zeng, K. Yokomori, T. Helleday, H. Teraoka, H. Arakawa, J.M. Buerstedde, S. Takeda, RAD18 and poly(ADP-ribose) polymerase independently suppress the access of nonhomologous end joining to double-strand breaks and facilitate homologous recombination-mediated repair, *Mol Cell Biol* 27 (2007) 2562-2571.
  31. E.P. Rogakou, D.R. Pilch, A.H. Orr, V.S. Ivanova, W.M. Bonner, DNA double-stranded breaks induce histone H2AX phosphorylation on serine 139, *J Biol Chem* 273 (1998) 5858-5868.
  32. N. Mailand, S. Bekker-Jensen, H. Fastrup, F. Melander, J. Bartek, C. Lukas, J. Lukas, RNF8 ubiquitylates histones at DNA double-strand breaks and promotes assembly of repair proteins, *Cell* 131 (2007) 887-900.
  33. C. Doil, N. Mailand, S. Bekker-Jensen, P. Menard, D.H. Larsen, R. Pepperkok, J. Ellenberg, S. Panier, D. Durocher, J. Bartek, J. Lukas, C. Lukas, RNF168 binds and amplifies ubiquitin conjugates on damaged chromosomes to allow accumulation of repair proteins, *Cell* 136 (2009) 435-446.
  34. G.S. Stewart, Solving the RIDDLE of 53BP1 recruitment to sites of damage, *Cell Cycle* 8 (2009) 1532-1538.
  35. A. Celeste, O. Fernandez-Capetillo, M.J. Kruhlak, D.R. Pilch, D.W. Staudt, A. Lee, R.F. Bonner, W.M. Bonner, A. Nussenzweig, Histone H2AX phosphorylation is dispensable for the initial recognition of DNA breaks, *Nat Cell Biol* 5 (2003) 675-679.
  36. M.S. Huen, R. Grant, I. Manke, K. Minn, X. Yu, M.B. Yaffe, J. Chen, RNF8 transduces the DNA-damage signal via histone ubiquitylation and checkpoint protein assembly, *Cell* 131 (2007) 901-914.
  37. N.K. Kolas, J.R. Chapman, S. Nakada, J. Ylanko, R. Chahwan, F.D. Sweeney, S. Panier, M. Mendez, J. Wildenhain, T.M. Thomson, L. Pelletier, S.P. Jackson, D. Durocher, Orchestration of the DNA-damage response by the RNF8 ubiquitin ligase, *Science* 318 (2007) 1637-1640.
  38. G.S. Stewart, B. Wang, C.R. Bignell, A.M. Taylor, S.J. Elledge, MDC1 is a mediator of the mammalian DNA damage checkpoint, *Nature* 421 (2003) 961-966.
  39. A. Xie, A. Hartlerode, M. Stucki, S. Odate, N. Puget, A. Kwok, G. Nagaraju, C. Yan, F.W. Alt, J. Chen, S.P. Jackson, R. Scully, Distinct roles of chromatin-associated proteins MDC1 and 53BP1 in mammalian double-strand break repair, *Mol Cell* 28 (2007) 1045-1057.
  40. M.A. Burtelow, P.M. Roos-Mattjus, M. Rauen, J.R. Babendure, L.M. Karnitz, Reconstitution and molecular analysis of the hRad9-hHus1-hRad1 (9-1-1) DNA damage responsive checkpoint complex, *J Biol Chem* 276 (2001) 25903-25909.
  41. C. Venclovas, M.P. Thelen, Structure-based predictions of Rad1, Rad9, Hus1 and Rad17 participation in sliding clamp and clamp-loading complexes, *Nucleic Acids Res* 28 (2000) 2481-2493.

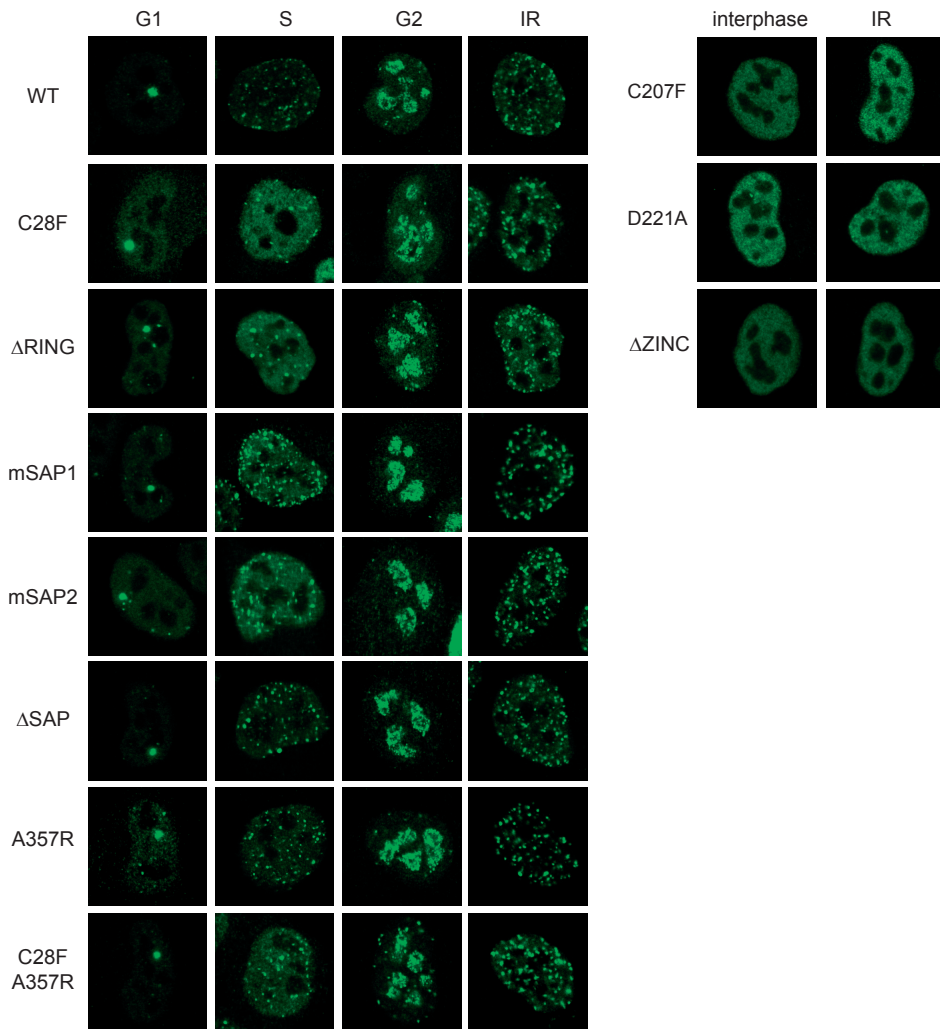
42. E. Volkmer, L.M. Karnitz, Human homologs of *Schizosaccharomyces pombe* rad1, hus1, and rad9 form a DNA damage-responsive protein complex, *J Biol Chem* 274 (1999) 567-570.
43. A. Sancar, L.A. Lindsey-Boltz, K. Unsal-Kacmaz, S. Linn, Molecular mechanisms of mammalian DNA repair and the DNA damage checkpoints, *Annu Rev Biochem* 73 (2004) 39-85.
44. S. Bao, T. Lu, X. Wang, H. Zheng, L.E. Wang, Q. Wei, W.N. Hittelman, L. Li, Disruption of the Rad9/Rad1/Hus1 (9-1-1) complex leads to checkpoint signaling and replication defects, *Oncogene* 23 (2004) 5586-5593.
45. P. Roos-Mattjus, K.M. Hopkins, A.J. Oestreich, B.T. Vroman, K.L. Johnson, S. Naylor, H.B. Lieberman, L.M. Karnitz, Phosphorylation of human Rad9 is required for genotoxin-activated checkpoint signaling, *J Biol Chem* 278 (2003) 24428-24437.
46. R.S. Weiss, P. Leder, C. Vaziri, Critical role for mouse Hus1 in an S-phase DNA damage cell cycle checkpoint, *Mol Cell Biol* 23 (2003) 791-803.
47. R.S. Weiss, S. Matsuoka, S.J. Elledge, P. Leder, Hus1 acts upstream of chk1 in a mammalian DNA damage response pathway, *Curr Biol* 12 (2002) 73-77.
48. D.O. Warmerdam, R. Freire, R. Kanaar, V.A. Smits, Cell cycle-dependent processing of DNA lesions controls localization of Rad9 to sites of genotoxic stress, *Cell Cycle* 8 (2009) 1765-1774.
49. M.A. Burtelow, S.H. Kaufmann, L.M. Karnitz, Retention of the human Rad9 checkpoint complex in extraction-resistant nuclear complexes after DNA damage, *J Biol Chem* 275 (2000) 26343-26348.
50. K.M. Hopkins, W. Auerbach, X.Y. Wang, M.P. Hande, H. Hang, D.J. Wolgemuth, A.L. Joyner, H.B. Lieberman, Deletion of mouse rad9 causes abnormal cellular responses to DNA damage, genomic instability, and embryonic lethality, *Mol Cell Biol* 24 (2004) 7235-7248.
51. R.K. Pandita, G.G. Sharma, A. Laszlo, K.M. Hopkins, S. Davey, M. Chakhparonian, A. Gupta, R.J. Wellinger, J. Zhang, S.N. Powell, J.L. Roti Roti, H.B. Lieberman, T.K. Pandita, Mammalian Rad9 plays a role in telomere stability, S- and G<sub>2</sub>-phase-specific cell survival, and homologous recombinational repair, *Mol Cell Biol* 26 (2006) 1850-1864.
52. Y. Fu, Y. Zhu, K. Zhang, M. Yeung, D. Durocher, W. Xiao, Rad6-Rad18 mediates a eukaryotic SOS response by ubiquitinating the 9-1-1 checkpoint clamp, *Cell* 133 (2008) 601-611.
53. A.A. Davies, A. Neiss, H.D. Ulrich, Ubiquitylation of the 9-1-1 checkpoint clamp is independent of rad6-rad18 and DNA damage, *Cell* 141 1080-1087.
54. A.L. Medhurst, D.O. Warmerdam, I. Akerman, E.H. Verwayen, R. Kanaar, V.A. Smits, N.D. Lakin, ATR and Rad17 collaborate in modulating Rad9 localisation at sites of DNA damage, *J Cell Sci* 121 (2008) 3933-3940.
55. H. Kimura, N. Takizawa, E. Allemand, T. Hori, F.J. Iborra, N. Nozaki, M. Muraki, M. Hagiwara, A.R. Krainer, T. Fukagawa, K. Okawa, A novel histone exchange factor, protein phosphatase 2C $\gamma$ , mediates the exchange and dephosphorylation of H2A-H2B, *J Cell Biol* 175 (2006) 389-400.
56. J.A. Martejijn, S. Bekker-Jensen, N. Mailand, H. Lans, P. Schwertman, A.M. Gourdin, N.P. Dantuma, J. Lukas, W. Vermeulen, Nucleotide excision repair-induced H2A ubiquitination is dependent on MDC1 and RNF8 and reveals a universal DNA damage response, *J Cell Biol* 186 (2009) 835-847.
57. W.M. Baarends, E. Wassenaar, J.W. Hoogerbrugge, G. van Cappellen, H.P. Roest, J. Vreeburg, M. Ooms, J.H. Hoeijmakers, J.A. Grootegoed, Loss of HR6B ubiquitin-conjugating activity results in damaged synaptonemal complex structure and increased crossing-over frequency during the male meiotic prophase, *Mol Cell Biol* 23 (2003) 1151-1162.
58. S. Tateishi, Y. Sakuraba, S. Masuyama, H. Inoue, M. Yamaizumi, Dysfunction of human Rad18 results in defective postreplication repair and hypersensitivity to multiple mutagens, *Proc Natl Acad Sci U S A* 97 (2000) 7927-7932.
59. K. Watanabe, S. Tateishi, M. Kawasuji, T. Tsurimoto, H. Inoue, M. Yamaizumi, Rad18 guides poleta to replication stalling sites through physical interaction and PCNA monoubiquitination, *Embo J* 23 (2004) 3886-3896.
60. M. Stucki, J.A. Clapperton, D. Mohammad, M.B. Yaffe, S.J. Smerdon, S.P. Jackson, MDC1 directly binds phosphorylated histone H2AX to regulate cellular responses to DNA double-strand breaks, *Cell* 123 (2005) 1213-1226.

61. K. Minter-Dykhouse, I. Ward, M.S. Huen, J. Chen, Z. Lou, Distinct versus overlapping functions of MDC1 and 53BP1 in DNA damage response and tumorigenesis, *J Cell Biol* 181 (2008) 727-735.
62. G.S. Stewart, S. Panier, K. Townsend, A.K. Al-Hakim, N.K. Kolas, E.S. Miller, S. Nakada, J. Ylanko, S. Olivarius, M. Mendez, C. Oldreive, J. Wildenhain, A. Tagliaferro, L. Pelletier, N. Taubenheim, A. Durandy, P.J. Byrd, T. Stankovic, A.M. Taylor, D. Durocher, The RIDDLE syndrome protein mediates a ubiquitin-dependent signaling cascade at sites of DNA damage, *Cell* 136 (2009) 420-434.
63. T. Kondo, T. Wakayama, T. Naiki, K. Matsumoto, K. Sugimoto, Recruitment of Mec1 and Ddc1 checkpoint proteins to double-strand breaks through distinct mechanisms, *Science* 294 (2001) 867-870.
64. J.A. Melo, J. Cohen, D.P. Toczyski, Two checkpoint complexes are independently recruited to sites of DNA damage in vivo, *Genes Dev* 15 (2001) 2809-2821.
65. X. Wu, S.M. Shell, Y. Zou, Interaction and colocalization of Rad9/Rad1/Hus1 checkpoint complex with replication protein A in human cells, *Oncogene* 24 (2005) 4728-4735.
66. D.A. Greer, B.D. Besley, K.B. Kennedy, S. Davey, hRad9 rapidly binds DNA containing double-strand breaks and is required for damage-dependent topoisomerase II beta binding protein 1 focus formation, *Cancer Res* 63 (2003) 4829-4835.
67. S. Nakajima, L. Lan, S. Kanno, N. Usami, K. Kobayashi, M. Mori, T. Shiomi, A. Yasui, Replication-dependent and -independent responses of RAD18 to DNA damage in human cells, *J Biol Chem* 281 (2006) 34687-34695.
68. D. Hoeller, C.M. Hecker, S. Wagner, V. Rogov, V. Dotsch, I. Dikic, E3-independent monoubiquitination of ubiquitin-binding proteins, *Mol Cell* 26 (2007) 891-898.
69. A. Sorkin, Ubiquitination without E3, *Mol Cell* 26 (2007) 771-773.
70. L. Zou, D. Cortez, S.J. Elledge, Regulation of ATR substrate selection by Rad17-dependent loading of Rad9 complexes onto chromatin, *Genes Dev* 16 (2002) 198-208.
71. X. Xu, S. Vaithiyalingam, G.G. Glick, D.A. Mordes, W.J. Chazin, D. Cortez, The basic cleft of RPA70N binds multiple checkpoint proteins, including RAD9, to regulate ATR signaling, *Mol Cell Biol* 28 (2008) 7345-7353.

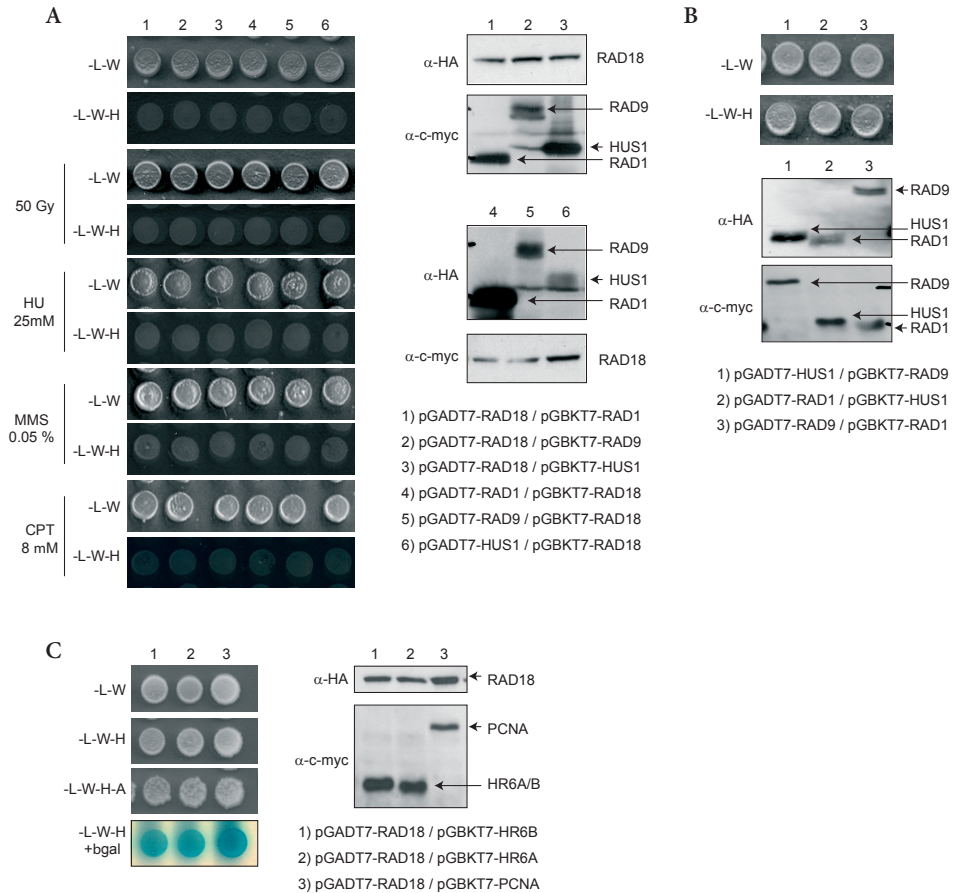
## SUPPLEMENTARY MATERIALS



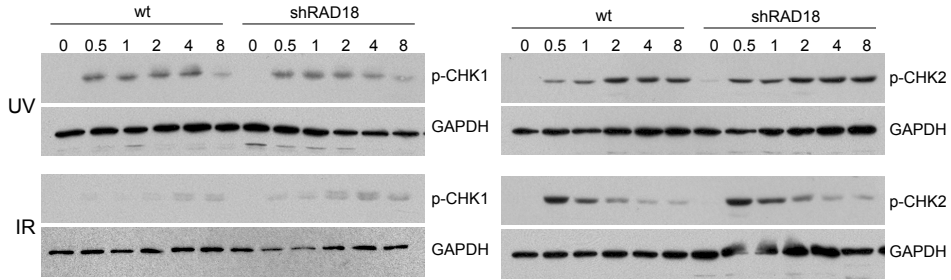
**Supplementary Figure 1.** (A) HeLa cells stably expressing YFP-RAD18 or transiently expressing YFP- $\Delta$ ubi were transfected with siRNA against endogenous RAD18. Forty-eight hours later, cells were lysed (input) and immunoprecipitation with YFP antibody (IP  $\alpha$ YFP) was performed. The expression levels of RAD18 and HR6A/B in the lysate are shown as input. Immunoprecipitated RAD18 and co-immunoprecipitated HR6A/B were detected on immunoblots (IP  $\alpha$ YFP). (B) HeLa cells transiently expressing YFP-mutant RAD18 in putative auto-ubiquitylation sites were transfected with siRNA against endogenous RAD18 (si-endoRAD18). Forty-eight hours later, auto-ubiquitylations of YFP-RAD18 was analyzed on immunoblots. GAPDH was used as a loading control. (C) HeLa cells stably expressing YFP-RAD18 or transiently expressing YFP-mutant RAD18 (the different mutations are explained in A), and wild-type HeLa cells were transfected with siRNA against endogenous RAD18 (si-endoRAD18). The expression level of wild-type and mutant RAD18 (not shown) was similar to that in Fig. 1C (input). Forty-eight hours later, cells were irradiated with 20 J/m<sup>2</sup> UV-C, and whole-cell extracts were prepared 8 h after irradiation. Expression levels of mono-ubiquitylated PCNA were analyzed on immunoblots using  $\alpha$ PCNA. Arrows point at mono-ubiquitylated PCNA (ubi-PCNA). The panels show the results of a representative experiment, where three independent experiments yielded similar results.



**Supplementary Figure 2. Subnuclear localization of wild type and mutant YFP-RAD18 during the cell cycle and after irradiation.** Confocal images of living HeLa cells expressing wild-type or mutant YFP-RAD18 in G1, S, and late G2 phases, and after irradiation with IR (5 Gy). Endogenous RAD18 was downregulated by siRNA (si-endoRAD18). RAD18 carrying mutations in its Zinc finger (C207F, D221A) and a deletion of the Zinc finger (ΔZINC) showed no cell cycle specific localization. In contrast, RAD18 carrying either mutations of the RING finger (C28F, ΔRING) or SAP domain (mSAP1, mSAP2, ΔSAP) showed a localization pattern identical to that of wild-type RAD 18 (WT).



**Supplementary Figure 3. Yeast two-hybrid assay.** Yeast carrying both pGADT7-target DNA and pGBKT7-target DNA were spotted on SD-L-W plates to confirm the yeast transformation. The interaction was confirmed by growth on selective medium plates, SD-L-W+X-Gal, SD-L-W-H and SD-L-W-H-A. The protein expression of transformed plasmids was examined on immunoblots by different antibodies as indicated. pGADT7 vector contains a HA-epitope tag, and the pGBKT7 vector contains a c-myc epitope tag. Three independent experiments were performed and representative results are shown. (A) Yeast two hybrid assay between RAD18 and all 9-1-1 components. Various types of DNA damage were induced by irradiation with 50 Gy, or growth on the selective medium plates containing 25 mM HU, 0.05% MMS, or 8  $\mu$ M CPT. Different concentrations of HU (6.25 mM, 12.5 mM, 50 mM, 100mM), MMS (0.005% ,0.01%, 0.1%, 0.2%), CPT (2  $\mu$ M, 4  $\mu$ M, 16  $\mu$ M, 32  $\mu$ M) were examined and showed similar results (data not shown). (B) Yeast two hybrid assay between the 9-1-1 components. (C) Yeast two hybrid assay between RAD18, and HR6A, HR6B or PCNA.



**Supplementary Figure 4.** HeLa cells stably expressing non-targeting shRNA or shRNA targeting RAD18 were exposed either with UV at 20 J/m<sup>2</sup> or IR at 10 Gy. Prior to irradiation, and after certain time points indicated in the figure, phosphorylation of CHK1 at Ser 354 and CHK2 at Tyr 68 was analyzed on immunoblots. GAPDH was used as a loading control.

**Supplementary Table I.** Designed primers to create mutant RAD18

RING finger aa 25-63	
C28F	
forward	GATTTGCTGCGGTGTGGAATTT <b>TTC</b> TTCGAGTATTTCAACATTGC*
reverse	GCAATGTTGAAATACTCGAAGAAAATTCCACACCGCAGCAAATC
Deletion	
forward	CAATAGATGATTTGCTGCGGTGTGTGACTGTCACAGAG
reverse	CTCTGTGACAGTCACACACCGCAGCAAATCATCTATTG
Zinc finger aa 201-225	
C207F	
forward	CTAAAGTGGATTGTCTCTGTT <b>TTC</b> GGGGTTAACATTCCAGAAAG
reverse	CTTTCGTGGAATGTTAACCCCGAAAACAGGACAATCCACTTTAG
D221A	
forward	GTCACATTAATAAGCATTTA <b>GCC</b> AGCTGTTTATCACGCGAAGA
reverse	TCTTCGCGTGATAAACAGCTGGCTAAATGCTTATTAATGTGAC
Deletion	
forward	CCACTTTGAAACAAGTTACTCGCGAAGAGAAGAAGGAAAG
reverse	CTTTCCTTCTCTCTTCGAGTAACTTGTTTCAAAGTGG
SAP domain aa 248-282	
G269A+K271A (mSAP1)	
forward	GCATGGATTATCTATTCAAG <b>GCAAATGC</b> ACAACAGCTCATTAAGGCG
reverse	GCCTTTTAATGAGCTGTTGTGCATTTGCTTGAATAGATAATCCATGC
H263A+G264A+L265 (mSAP2)	
forward	GAAAAAGCTAAAAGAG <b>GCTGCAGCA</b> TCTATTCAAGGAAATAAACACAGC
reverse	GCTGTTGTTTATTTCTTGAATAGATGCTGCAGCCTCTTTTAGCTTTTTC
Deletion	
forward	GCTGCCCAAACTGTACACATGTACAATGCCCAATG
reverse	CATTGGGCATTGTACATGTGTACAGTTTGGGCAGC
Auto-ubiquitylation sites	
K161R	
forward	CAAATTCAGCCCTCAA <b>AGA</b> GAGGGCGAGCCCTGCTG
reverse	CAGCAGGGCTCGCCTCTCTTTGAGGGCTGAATTTG
K197R	
forward	CACCCTCGACATCCACTTT <b>AGA</b> CAAGTTACTAAAGTGGATTG
reverse	CAATCCACTTTAGTAACCTGTCTCAAAGTGGATGTGCGAGGGTG
K230R	
forward	GTTTATCACGCGAAGAGAAG <b>AGG</b> GAAAGCCTCAGAAGTTCTG

reverse	CAGAACTTCTGAGGCTTTCCTCTTCTCTTCGCGTGATAAAC
K241R	
forward	GAAGTTCGTTCACAAAAGG <b>AGG</b> CCGCTGCCCAAACTG
reverse	CAGTTTTGGGCAGCGGCCTCCTTTTGTGAACAGAACTTC
K245R	
forward	CAAAAGGAAGCCGCTGCC <b>CA</b> ACTGTATATAATTTGCTCTC
reverse	GAGAGCAAATTATATACAGTTCTGGGCAGCGGCTTCCTTTTG
K261R	
forward	CGTGATTTAAAGAAAAAGCTA <b>AG</b> AGAGCATGGATTATCTATTCAAG
reverse	CTTGAATAGATAATCCATGCTCTCTTAGCTTTTTCTTTAAATCAGC
K309R	
forward	GAAATCGAAAATATAGAG <b>AGG</b> ACTAGGATGCGTCTTGAAGC
reverse	GCTTCAAGACGCATCCTAGTCCTCTCTATATTTTCGATTC
K318R	
forward	GGATGCGTCTTGAAGCTAGT <b>AGA</b> CTCAATGAAAGTGTAAATGG
reverse	CCATTACACTTTCATTGAGTCTACTAGCTTCAAGACGCATCC
HR6A/B binding domain	
A357R	
forward	GAATTCAGCTTCTGGTGGATCAG <b>CGT</b> AGAAAAGGATACAAGAAAATTG
reverse	CAATTTTCTTGTATCCTTTTCTACGCTGATCCACCAGAAGCTGAAATTC
Silent mutation against shRAD18	
forward	CACGCGAAGAGAAGAAGGAG <b>AGT</b> CTGAGGAGCTCTGTTCAAAAAGGAAGCCG
reverse	CGGCTTCCTTTTGTGAACAGAGCTCCTCAGACTCTCCTTCTTCTTCGCGTG

\* Mutated amino acid codons are shown in bold, and the introduced mutations are underlined.

### Supplementary Table II. Primers used to generate Y2H vectors

RAD18	
forward	<u>GAATTC</u> GACTCCCTGGCCGAGTCTC ( <i>EcoRI</i> )*
reverse	<u>GGATCC</u> TTAATTCCTATTACGCTGTTTCT ( <i>BamHI</i> )
PCNA	
forward	<u>CATATG</u> TTCGAGGCGGCCTGG ( <i>NdeI</i> )
reverse	<u>GGATCC</u> CTAAGATCCTTCTTCATCCTCG ( <i>BamHI</i> )
RAD9	
forward	<u>CATATG</u> AAGTGCTGGTCACGGGCG ( <i>NdeI</i> )
reverse	<u>GGATCC</u> TCAGCCTTCACCCTCACTGT ( <i>BamHI</i> )
HUS1	
forward	<u>CATATG</u> AAGTTTCGGGCCAAGATCGTG ( <i>NdeI</i> )
reverse	<u>GGATCC</u> CTAGGACAGCGCAGGGATGA ( <i>BamHI</i> )
RAD1	
forward	<u>CATATG</u> CCCCTTCTGACCCAACAGAT ( <i>NdeI</i> )
reverse	<u>GGATCC</u> CTCAAGACTCAGATTCAGGAACTT ( <i>BamHI</i> )
Hr6a	
forward	<u>CATATG</u> TTCGACCCCGGCCGG ( <i>NdeI</i> )
reverse	<u>GGATCC</u> TCAACAGTCGCGCCAGCTTT ( <i>BamHI</i> )
Hr6b	
forward	<u>GAATTC</u> CATGTTCGACCCCGGCCCGT ( <i>EcoRI</i> )
reverse	<u>GGATCC</u> TTATGAATCATTCAGCTTTGC ( <i>BamHI</i> )

\* Restriction enzyme sites used for subcloning are underlined

### Supplementary Table III. Primers used to generate a vector carrying shRAD18

---

shRAD18	
forward	GATCCCCGGAAAAGCCTCAGAAGTTCTTTCAAGAGAAGAAGCTTCTGAGGCTTTCCTTTTTC
reverse	TCGAGAAAAAGGAAAAGCCTCAGAAGTTCTTCTCTTGAAGAAGCTTCTGAGGCTTTCGGG

---

3

### Supplementary Table IV. siRNAs used in this study

---

endoRAD18	GGAAAUAGAUGAAAUCCAC
RPA1	CACUCUAUCCUCUUUCAUG
RPA2	CCUAGUUUCACAAUCUGU

---

**Supplementary Movies 1-3.** Time lapse images of nuclei expressing (1) wild type YFP-RAD18 or (2, 3) mutant YFP-RAD18 in its Zinc finger (D221A). Images were captured every 30 min for 27 hours, a single nucleus was selected, aligned, and 5 frames of the images are shown per second. Endogenous RAD18 was downregulated by siRNA. (1) Analyses began in S phase, and the cell went through G2, M and G1 phases. (2) Analyses started in G1 phase, and the cell went through S, and most likely G2 phases. (3) Analyses began in G2 phase and the cell went through, M, G1, and most likely S phases. The cell cycle phases of mutant YFP-D221A were inferred from the time passed since the previous M-phase or the time span until the next M-phase, and the duration of G1, S, G2 and M phase in wild type cells. The growth rates of wild type and mutant cells were not different (data not shown).



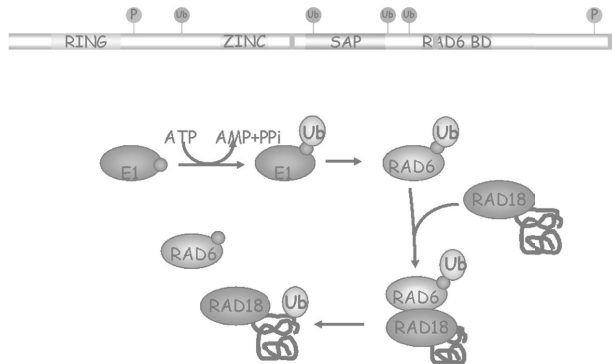
4

# MEIOTIC FUNCTIONS OF RAD18

Submitted

Akiko Inagaki, Esther Sleddens-Linkels, Evelyne Wassenaar, Marja Ooms,  
Wiggert A. van Cappellen, Jan H. J. Hoeijmakers<sup>1</sup>, Jost Seibler<sup>2</sup>,  
Thomas F. Vogt<sup>3</sup>, Myung K. Shin<sup>3</sup>, J. Anton Grootegoed, and Willy M. Baarends\*

\* Corresponding author



Department of Reproduction and Development,  
Erasmus MC, University Medical Center, Rotterdam, The Netherlands

<sup>1</sup>Department of Cell Biology and Genetics, Erasmus MC,  
University Medical Center, Rotterdam, The Netherlands

<sup>2</sup>Taconic Artemis GmbH, Cologne, Germany,

<sup>3</sup>Merck & Co., Inc., Merck Research Laboratories, Rahway, NJ USA

**ABSTRACT**

RAD18 is an ubiquitin ligase involved in replicative damage bypass and DNA double strand break (DSB) repair processes in mitotic cells. Herein, we investigated the testicular phenotype of *Rad18* knockdown mice to determine the function of RAD18 in meiosis. We found that RAD18 is recruited to persistent meiotic DSBs, induced by the meiosis-specific topoisomerase-like enzyme SPO11. In addition, RAD18 is recruited to the chromatin of the XY chromosome pair, that forms the transcriptionally silent XY body. At the XY body, RAD18 mediates the chromatin association of its interaction partners, the ubiquitin-conjugating enzymes HR6A and HR6B. Moreover, RAD18 was found to regulate the level of dimethylation of histone H3 at lysine 4 and the maintenance of meiotic sex chromosome inactivation, in a manner similar to what was previously observed for HR6B. In addition, we show that RAD18 and HR6B are required for the efficient repair of a small subset of meiotic DSBs. Our data suggest that RAD18 may function to stimulate inter-sister-mediated repair of meiotic DSBs at synapsed autosomal regions.

**Key words:** RAD18, HR6B, meiosis, DNA double-strand break repair, XY body

## INTRODUCTION

The E3 ubiquitin ligase RAD18 is crucial for cell survival after induction of various types of DNA damage in mammalian somatic cells [1-5]. RAD18 functions in complex with HR6A (UBE2A) and HR6B (UBE2B), the two mammalian orthologs of the *Saccharomyces cerevisiae* E2 ubiquitin-conjugating enzyme Rad6 [6]. In *S. cerevisiae*, Rad6 and Rad18 are most well known for their role in replicative damage bypass (RDB). This pathway allows progression of DNA replication by translesion synthesis polymerases in the presence of DNA damage (reviewed in [7]). Functional orthologs of proteins involved in the RDB pathway have been identified in mammals, implying that this pathway is generally well conserved. In addition to its function in the RDB pathway, RAD18 also acts at double-strand break (DSB) repair sites in mammalian mitotic cells [1,5]. The exact function of RAD18 in DSB repair in mammalian cells is not fully clear. Recent data indicate that RAD18 may facilitate homologous recombination through binding of RAD51C, a RAD51 paralogue, via the RING finger of RAD18 at ssDNAs [1]. RAD18 is expressed in multiple tissues, but the highest level is found in spermatocytes, developing germ cells in meiotic prophase in the testis [8], suggesting that RAD18 may function in meiosis. In *S. cerevisiae*, the *RAD18* gene expression increases during meiosis, also suggesting a specific function in this process [9], although the *rad18* deletion does not affect either meiosis or meiotic recombination [10-12]. However, double mutants of *rad18* and various excision-repair-involved genes show drastic reduction in spore viability, compared to the single mutants [10], suggesting that Rad18 does perform a specific function during meiosis in yeast.

Meiotic DSBs are induced by the meiosis-specific topoisomerase II-like enzyme SPO11 in prophase [13,14], and are required for proper homologous chromosome pairing and meiotic recombination in yeast and mammals [15-17]. The chromatin surrounding mitotic and meiotic DSBs undergoes a series of orchestrated modifications. One of the first modifications is phosphorylation of histone H2A variant H2AX ( $\gamma$ H2AX) [18,19], which is accompanied by the formation of RAD51 foci on chromatin [20,21]. In mitotic cells, DSBs can be repaired via two distinct repair pathways; homologous recombination (HR) and non-homologous DNA end-joining (NHEJ). HR is an error-free mechanism, in which a homologous sequence of the sister chromatid is used as a template to process repair. NHEJ is an error-prone form of DSB repair, in which the two ends of the broken DNA are processed for direct ligation, with increased chance of small deletions or insertions. In meiotic cells, this NHEJ-repair mechanism is repressed [22], leaving HR as the only available pathway for repair. In meiotic prophase, HR has been specially adapted to stimulate the use of one of the chromatids of the homologous chromosome as the template for repair; the use of the sister chromatid as a template to process repair is most likely repressed [23,24]. HR may lead to the formation of crossovers, although repair of most meiotic DSBs generates noncrossovers. Each chromosome pair forms at least one crossover, and this is required to ensure correct segregation of homologous chromosomes during the first meiotic division. The repair of meiotic DSBs is accompanied by progression of synapsis, which is achieved by the formation of the synaptonemal complex (SC) between the chromosomal axes of the paired homologous chromosomes (reviewed in [25]).

During meiotic prophase, all homologous chromosomes initiate pairing and synapsis in zygotene. In pachytene nuclei, all chromosomes have completely synapsed, and this can be visualized using antibodies that recognize components of the SC. SYCP3, a major protein component of the SC, is present in the axial and lateral elements of the SC, and it can be used to distinguish the substages of meiotic prophase in nuclear spread preparations of primary spermatocytes [26]. The X and Y chromosomes are largely heterologous, and during midpachytene in mouse, synapsis is observed only along the short homologous pseudoautosomal regions. The rest of the chromosomal arms remains unsynapsed, and form a subnuclear region called XY body (or sex body), which is first seen around early pachytene and persists into diplotene [27]. XY body formation is associated with meiotic sex chromosome inactivation (MSCI) [28]. The chromatin surrounding the XY body undergoes various modifications reminiscent of DSB repair in mitotic cells, such as phosphorylation of H2AX [19], and ubiquitylation of histone H2A at lysine 119 [29]. In addition, many DSB-related factors accumulate specifically on the XY body (reviewed in [25]). The RDB enzyme HR6A/B and its E3 ligase partner RAD18 also accumulate on the XY body [30]. Single HR6A and HR6B knockout mice are viable, while double knockout mice are embryonic lethal [31]. Spermatogenesis of *Hr6b* knockout mice is markedly affected during postmeiotic steps, leading to male infertility. In addition, *Hr6b* knockout spermatocytes show an increased rate of apoptosis, longer synaptonemal complexes, and an increased frequency of crossover formation [32]. HR6B exerts control over different histone modifications in spermatocytes and spermatids. In *Hr6b* knockout spermatocytes, the level of H3K4 dimethylation increases on the X and Y chromosomes in diplotene, and this persists in postmeiotic round spermatids. This function contributes to the postmeiotic maintenance of X chromosome silencing [33,34]. It is not known which E3 enzymes are required for the different functions of HR6B in meiotic and postmeiotic germ cell development. Herein, we investigated the function of the well-known HR6A and HR6B interaction partner, RAD18 in mammalian meiosis using *Rad18* knockdown mice.

## MATERIALS AND METHODS

### Mice

#### *Generation of Rad18 knockdown and control mice*

The recombinase mediated cassette exchange (RMCE) for the efficient generation of targeted transgenes has been previously described [35]. Into the exchange vector for RMCE (pRMCE-U6) the following oligonucleotides representing the shRNA sequence against the *Rad18* mRNA were cloned using the restriction endonucleases Bbs1/Asc1: (20-1 s:CCGCTGAAACAGTATGGCTTATTCAAGAGATAAGCCATACTGTTTCAGCTTTTTTGG) and (20-1 as:CGCCAAAAAGCTGAAACAGTATGGCTTATCTCTTGAATAAGCCATACTGTTTCAG). The resulting vector is called pshRad18 and contains the following elements in 5' to 3' direction: a synthetic polyA signal, an F3-site, a neomycin-resistance gene lacking the start ATG, the P<sub>gk</sub> polyadenylation signal, the human U6-promoter, shRNA-20-1 and an FRT-site.

A control plasmid, called empty vector, contains the following elements in 5' to 3' direction: a synthetic polyA signal, an F3-site, a neomycin-resistance gene lacking the start ATG, the P<sub>gk</sub> polyadenylation signal and an FRT-site. ES cell culture was carried out as described before [36]. The generation of ES cells carrying the RMCE configuration at the *Rosa26* locus with the *Rad18* shRNA expression vector or the control vector was performed as described [35].

Mice heterozygote for the targeted allele with the *Rad18* shRNA and mice heterozygote for the control vector at the *Rosa26* locus were generated via tetraploid embryo complementation as described [35]. Founder mice were backcrossed to C57/Bl6 mice. Mice were genotyped using specific primers for the targeted control sequence and *Rad18* shRNA; forward: CATCAGAAGCTGACTCTAGATGGC, reverse: CTTGTCCCTCCAATTTTACACC with condition of 95 °C 5 min, 35 cycle of 95 °C 30 sec, 60°C 30 sec, 72 °C 1 sec, and 72°C 5 min. Amplification of DNA from *Rad18* shRNA mice resulted in a 688 bp PCR fragment and from the targeted control in a 250 bp PCR fragment

#### *Spo11 mutant mice*

We used a *Spo11* knockin mouse model in which the catalytically active Tyr 100 residue is replaced by a Phe (A. Inagaki, unpublished). Identical to the *Spo11* knockout [37], male and female double-knockin mice (ki) are infertile, and meiotic prophase is blocked, with spermatocytes and oocytes reaching a zygotene-like stage with variable degrees of (heterologous) synapsis (data not shown).

#### *Sycp1 knockout mice and Rad54 knockout mice*

*Sycp1* knockout mice were generated and described previously [38] and *Rad54* knockout mice have also been described [39].

#### *Analyses of fertility*

Adult heterozygous male and female control and *Rad18* knockdown (kd) mice were bred with control females and males, respectively for a maximum of 6 weeks. Litter number and litter size were recorded. To analyse spermatogenesis, adult males were sacrificed by cervical dislocation, and testes and epididymides were isolated and weighed. To obtain sperm for assessment of morphology, the epididymides were transferred into a plastic Petri dish (Greiner bio-one) containing 0.5 ml Dulbecco's medium (Gibco) with 0.5 % w/v BSA, and carefully cut to allow sperm to move out of the tissue. After 10-20 minutes, the medium was carefully stirred, and aliquots were removed for sperm morphology analysis in smears stained by hematoxylin/eosin. Then, the epididymides were transferred into a small glass Potter and homogenized by hand. The total number of sperm present in the epididymides was counted using an improved Neubauer hemocytometer and a phase contrast microscope at a magnification of 400 times. At least 200 sperm in 2 different samples from three animals were counted.

#### **Irradiation of mice**

Adult wild type mice were subjected to whole body  $\gamma$ -irradiation with Elekta linear accelerator (Crawley). Mice received a total dose of 5 Gy and were sacrificed at 3 h

after irradiation. Testes were collected and used to prepare spread nuclei preparations as described below.

### **Antibodies**

For primary antibodies, we used mouse monoclonal antibodies anti-phosphorylated H2AX (Upstate), anti-ubiquitylated histone H2A (Millipore, #05-678), and anti-MLH1 (Becton and Dickinson), rabbit polyclonal antibodies anti-RAD18 [40], anti-RAD51 [41], anti-HR6A/B [32], anti-SYCP3 (gift from C. Heyting), and anti-H3K4me2 (Upstate), and rat polyclonal antibody anti-SYCP3 [33]. For secondary antibodies, we used a goat anti-rabbit/mouse IgG-peroxidase (Sigma), goat anti-rabbit IgG Alexa 488/564, goat anti-mouse Alexa IgG 488/564, or goat anti-mouse IgM Alexa 564 (Molecular Probes).

### **Protein isolation and immunoblot analysis**

Cell lysates from testes were prepared in 2.0 ml lysis buffer (50 mM Tris-HCl pH 8.0, 150 mM NaCl, 5 mM MgCl<sub>2</sub>, 0.5 mM EDTA, 0.2% v/v Nonidet P-40, 10% v/v glycerol, 0.5 mM dithiothreitol, and protease inhibitors (Roche)). Testis tissue was homogenized, and the cell suspension was left on ice for 30 min and sonicated. The expression level of protein from whole cell lysate was analyzed by SDS-PAGE and immunoblots. Cell extracts were mixed with 4x SDS sample buffer (200 mM Tris-HCl pH 6.8, 8% w/v SDS, 0.4% w/v bromophenol blue, and 40% v/v glycerol), added dithiothreitol to a final concentration of 100 mM, and sonicated. After 5 minutes incubation at 100 °C, the cell extracts were separated by sodium dodecyl sulfate 10% polyacrylamide gel electrophoresis and transferred to nitrocellulose membranes. The membranes were incubated with antibodies to analyse expression of target proteins. The expression was detected using enhanced chemiluminescence (PerkinElmer).

### **Meiotic spread nuclei preparations and immunocytochemistry**

Testis tissues were processed to obtain spread nuclei for immunocytochemistry as described by Peters et al [42]. Spread nuclei of spermatocytes were stained with antibodies mentioned above. Before incubation with antibodies, slides were washed in PBS (3x10 min), and non-specific sites were blocked with 0.5% w/v BSA and 0.5% w/v milk powder in PBS. Primary antibodies were diluted in 10% w/v BSA in PBS, and incubations were overnight at room temperature in a humid chamber. Subsequently, slides were washed (3x10 min) in PBS, blocked in 10% v/v normal goat serum (Sigma) in blocking buffer (supernatant of 5% w/v milk powder in PBS centrifuged at 14,000 rpm for 10 min), and incubated with secondary antibodies in 10% normal goat serum in blocking buffer at room temperature for 2 hours. Finally, slides were washed (3x10 min) in PBS (in the dark) and embedded in Prolong Gold with DAPI (invitrogen).

### **Histological analysis**

Testes were isolated from control and heterozygous *Rad18* kd mice that were 4 and 19 weeks old. Testes were fixed in Bouin's fixative for morphological analysis, and embedded in paraffin according to standard procedures. Mounted sections were deparaffinized, rehydrated, and stained with hematoxylin and eosin.

### Confocal microscopy

Images of cells were obtained using a Zeiss LSM510NLO microscope (Carl Zeiss) with a  $63 \times /1.40$  NA oil immersion lens. Proteins stained with Alexa 488 were detected by exciting the probes with a 488 nm Argon gas laser and monitoring the emission through a 500-550 band-pass filter. Proteins stained with Alexa 564 were detected by exciting the probes with a 543 nm helium neon laser and monitoring the emission through a long-pass 560 filter. To minimize the effect of photo-bleaching, images were taken with 10  $\mu$ W for a 488 nm laser, and with 20  $\mu$ W for a 543 nm laser. For quantification of immunofluorescent signal, slides were analyzed on the same day. Fluorescent images were taken under identical conditions for all slides, and images were analysed using the ImageJ software

(Rasband, W.S., ImageJ, U.S. National Institutes of Health, Bethesda, Maryland, USA [<http://rsb.info.nih.gov/ij/>]). Nuclei were selected and the mean ( $\mu$ ) and standard deviation ( $\sigma$ ) was calculated by Image J software, and the threshold was determined [43]. To select the HR6A/B or H3K4me2 positive area on the XY body, threshold was set by using the formula;  $\mu + 1.5 \cdot \sigma$ . The intensity of selected area was measured by Image J. To count the number of RAD51 foci, threshold was set by using the formula;  $\mu + 2.5 \cdot \sigma$ . To further prevent counting non-specific background as RAD51 foci, areas with a signal above the threshold that was less than 2 pixels in size were not counted. The number of foci was counted using Image J.

### Real-time RT-PCR

For real-time RT-PCR, RNA was prepared from testes by Trizol, DNase-treated and reverse transcribed using random hexamer primers and Superscript II reverse transcriptase (Invitrogen). PCR was carried out with the iQ SYBR green PCR mastermix (Applied Biosystems) in the DNA engine Opticon 2 real-time PCR detection system (Bio-Rad). The names of examined genes, primer sequences, and annealing temperatures are shown in supplementary Table S1. PCR of  $\beta$ -actin mRNA was included in each reaction and used to normalize the data. Three independent experiments were performed and each real-time PCR was performed in duplicate. All -RT reactions were negative.

### Statistics

The Mann–Whitney *U* test or Chi-squared test was used for the significance tests.

## RESULTS

### RAD18 expression is efficiently downregulated following transgenic expression of shRNA

*Rad18* knockdown (kd) and control mice were generated through targeted insertion of a *Rad18* specific and shRNA construct, and a control construct not encoding shRNA, respectively, driven by the U6 promoter in the *Rosa26* locus (see Materials and Methods) [35]. It is important to note that in these animals, only one allele of the *Rosa26* locus is targeted. We first investigated the expression level of *Rad18* mRNA in

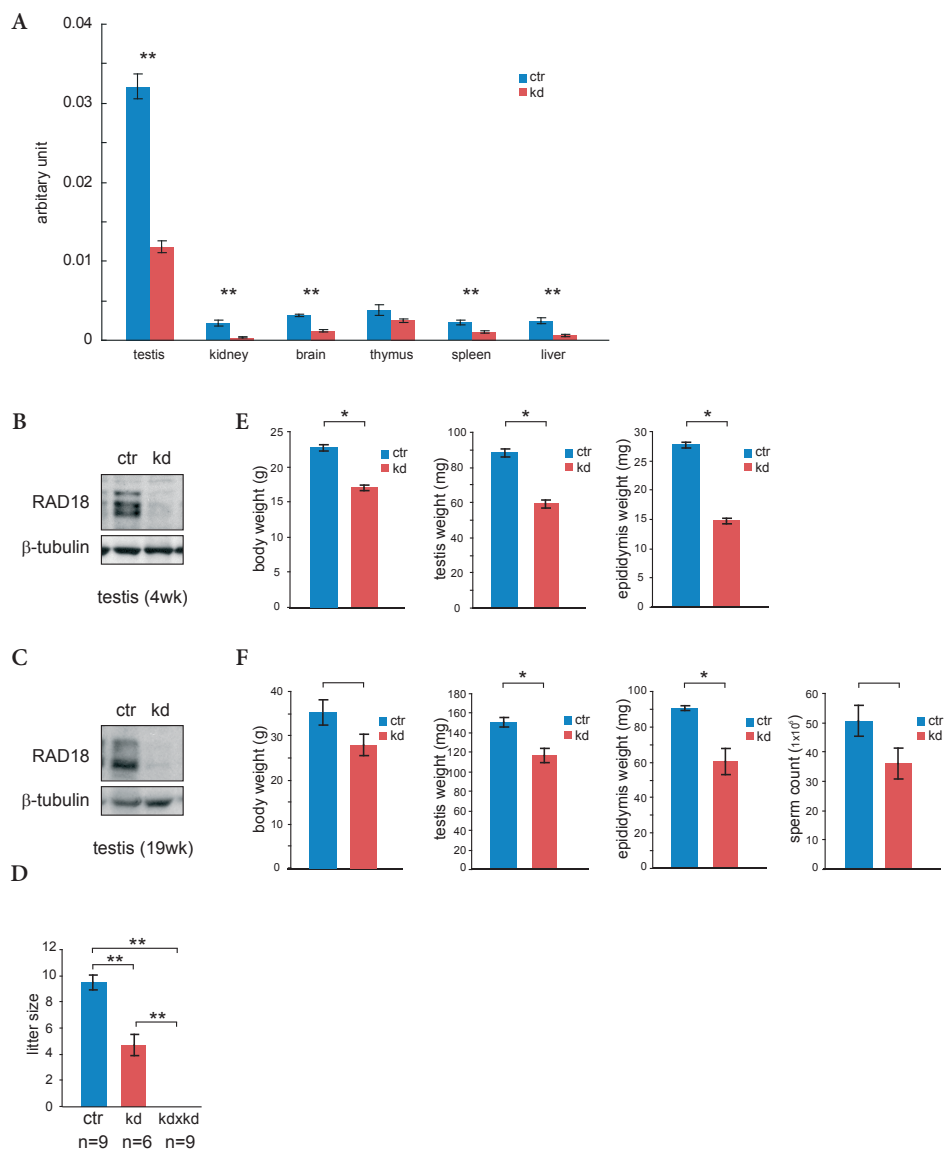


**Figure 1. Characterization of *Rad18* knockdown mice.** (A) *Rad18* mRNA expression in testis, kidney, brain, thymus, spleen and liver of 3 control mice and 3 *Rad18* knockdown mice. Error bars indicate standard error of the mean (SEM) for 3 mice of 3 independent experiments with duplicate measurements. Blue and red bars indicate control and *Rad18* knockdown, respectively. (B, C) RAD18 expression in total cell extracts from testis of 4-week-old (B) and 19-week-old (C) from control (ctr) and *Rad18* knockdown mice (kd) was detected on immunoblots.  $\beta$ -tubulin was used as loading control. (D) Average litter size obtained from matings between control and wild type (ctr), knockdown and wild type (kd), and two knockdowns (kd x kd). Error bars indicate SEM from 6, 9 and 6 independent breedings of ctr x wt, kd x wt, and kd x kd, respectively. (E, F) Body, testis and epididymis weights (E, F) and the number of sperm (F) from 4-week-old (E) and 19-week-old (F) control and *Rad18* kd mice. Error bars indicate SEM from 3 control and 3 knockdown mice. Blue and red bars indicate control and *Rad18* knockdown, respectively. (A, D, E, F) Single and double asterisks indicate  $p < 0.05$  and  $p < 0.01$ , respectively (Mann-Whitney *U* test).

testis, brain, kidney, liver, spleen and thymus from 4-week-old mice (4 kd and 3 control mice). *Rad18* mRNA was most highly expressed in testis (Fig. 1A) in agreement with previous analyses [30], and the expression was significantly downregulated in kd mice, although the efficiency of downregulation varied between tissues. In *Rad18* kd testis, RAD18 protein expression appeared to be even more efficiently downregulated than the mRNA (Fig. 1B and C). In the rest of the tissues mentioned above, we were not able to detect RAD18 expression on immunoblots in both control and *Rad18* kd samples (data not shown).

### **Subfertility and reduced testis and body weights of *Rad18* kd mice**

Repeated breeding experiments to obtain homozygous *Rad18* kd mice were so far unsuccessful (Fig. 1D). Breeding experiments using the heterozygous *Rad18* kd males and females in combination with wild-type C57/bl6 females and males, respectively, revealed that *Rad18* kd mice are subfertile. The average litter size of *Rad18* kd males and females was smaller than that of control (kd: 4.7 +/- SD (standard deviation) 2.9; control: 9.5 +/- SD 1.3;  $p = 0.004$ ) (Fig. 1D), although there was no significant difference in the litter size born from female or male *Rad18* kd mice (female: 3.8 +/- SD 3.0; male: 5.4 +/- SD 2.9;  $p=0.5$ ). To further analyze the possible role of RAD18 in spermatogenesis, we first compared the weights of reproductive organs in *Rad18* kd and control mice. On average, testis weights were 33% reduced in 4-week-old *Rad18* kd mice, and the epididymis weight was even 50% reduced. Since the body weight of the *Rad18* kd mice was also reduced compared to controls, these effects might be caused by delayed testicular development (Fig. 1E). However, when we examined adult (19-week-old) mice, *Rad18* kd testis, epididymis and body weight were also reduced compared to controls (Fig. 1F). In addition, the number of sperm was 29% reduced, which corresponds to the 22% reduced testis weight in *Rad18* kd males, although the differences were not statistically significant (Fig. 1F).

### **RAD18 deficient mice produced aberrant elongating spermatid heads**

Histological analysis of cross-sections of control and *Rad18* kd testes, revealed no overall differences (Fig. 2A for control, 2B for *Rad18* kd). Complete spermatogenesis was apparent in both genotypes. However, in *Rad18* kd mice, elongating spermatids frequently showed an aberrant head shape (Fig. 2B, arrows and enlarged insets). This was quantified on spread nuclei preparations (Fig. 2C, D, and G). In 19-week-old animals, the overall frequency of aberrant spermatid heads was highly reduced (Fig. 2E and F), but still significantly increased in *Rad18* kd mice versus controls (Fig. 2G).

### **Reduced XY synopsis in *Rad18* kd mice**

The X and Y chromosomes are largely heterologous, but they share a small homologous region, called the pseudo-autosomal region (PAR), where X and Y synapse during pachytene (Fig. 3A, arrow in the enlarged panel). RAD18 associates with the largely unpaired X and Y chromosomes, that form the transcriptionally inactive so-called XY body in pachytene and diplotene spermatocytes [28] (Fig. 3A), but the exact role of RAD18 on the XY body remains unclear. In spermatocytes of *Rad18* kd mice, the RAD18 expression was considerably decreased (Fig. 3B), with a level of RAD18 staining on the

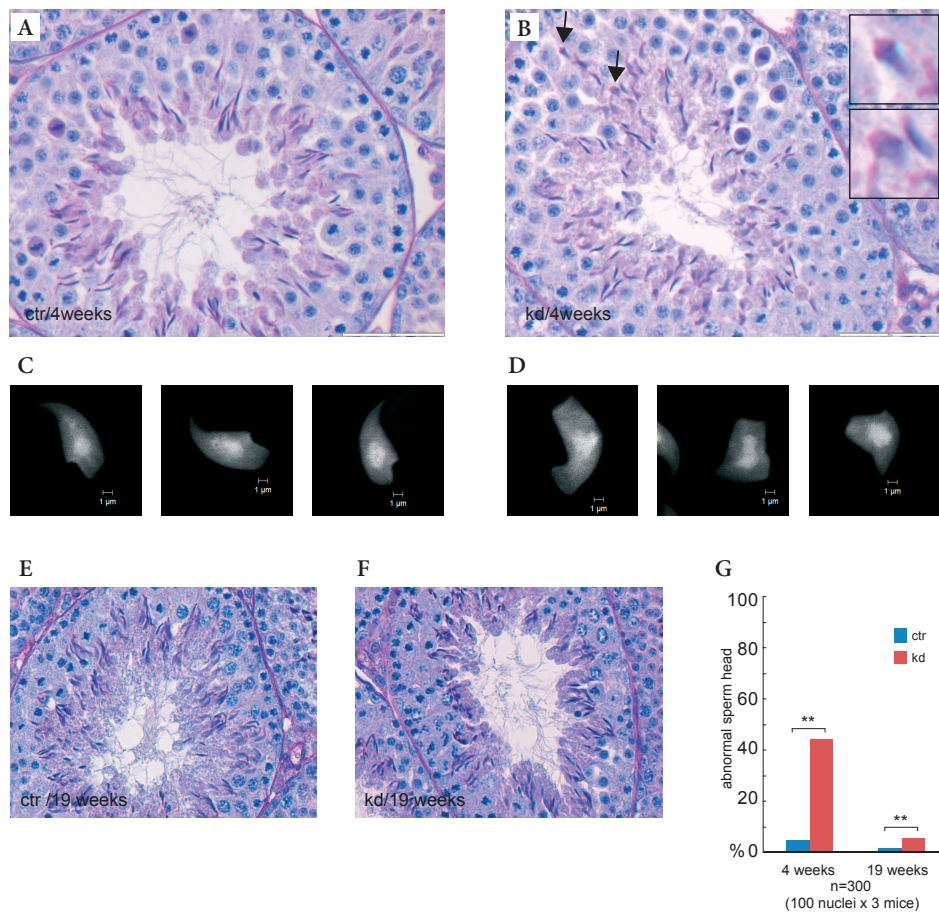


**Figure 2. Morphological analysis of testes from *Rad18* knockdown mice and controls.** (A, B, E, F) Histological sections of 4-week-old (A, B) and 19-week-old (E, F) control (A, E) and *Rad18* kd (B, F) testes were stained with hematoxylin and eosin. (B) Elongated spermatids indicated with arrows are shown in enlarged pictures in the inserts. (C, D) DAPI staining of spread nuclei from elongated spermatids of control (C) and *Rad18* kd (D). (G) Graph depicts the percentage of elongated spermatids with aberrant shape in control and *Rad18* kd mice. Blue and red bars indicate control and *Rad18* knockdown, respectively. 300 nuclei from 3 different mice were examined. Double asterisks indicate  $p < 0.01$  (Chi-squared test).

XY body that was approximately 80% lower than in control mice (Fig. 3C). An increased frequency of XY asynapsis was found in pachytene spermatocyte of *Rad18* kd mice (Fig. 3D). When X and Y were not synapsed, they were still adjacent to each other in 66% of these nuclei (Fig. 3E), whereas in the rest of the nuclei that displayed asynapsed X and Y chromosomes, they were at a larger distance (Fig. 3F). The asynapsed X and Y chromosomes did not lead to increased frequency of XY aneuploidies in spermatids in the *Rad18* kd mice, as verified using DNA FISH with X and Y painting probes (data not shown). To examine whether this function is dependent on HR6B, we examined XY synapsis in spermatocytes of *Hr6b* knockout mice. However, the frequency of XY

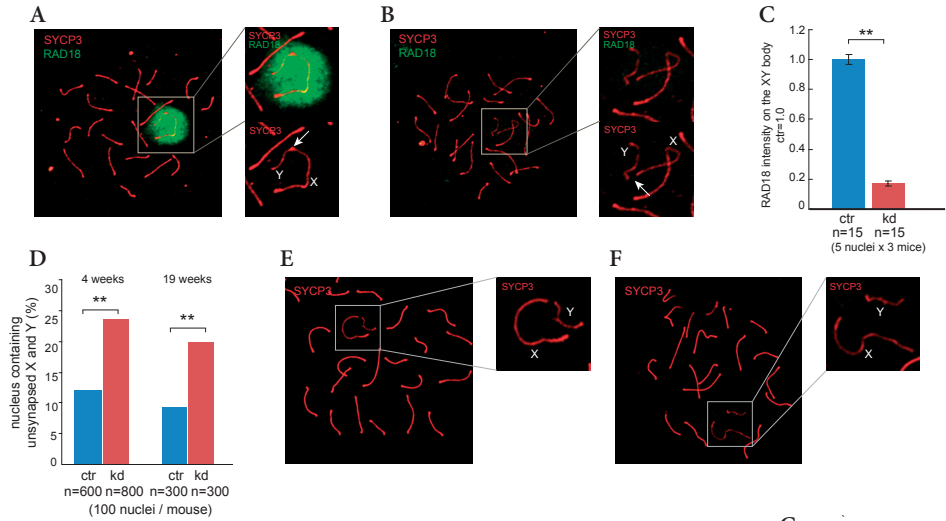


**Figure 3. Efficient knockdown of RAD18 in spermatocytes from *Rad18* knockdown mice, and increased frequency of XY asynapsis.** (A, B) Double immunostaining of pachytene spermatocyte nuclei of control (A) and *Rad18* kd mice (B) with anti-SYCP3 (red) and anti-RAD18 (green). The insert shows a larger magnification of the area containing the XY body. Arrows point to the pseudoautosomal synapsed region (A) and unsynapsed region. (C) RAD18 intensity on the XY body was measured with Image J software. The intensity of RAD18 in control nuclei was set at 1.0. Error bars indicate SEM from 45 nuclei in 3 independent mice. Blue and red bars indicate control (ctr) and *Rad18* knockdown (kd), respectively. Double asterisks indicate  $p < 0.01$  (Mann-Whitney *U* test). (D) The percentage of unsynapsed X and Y chromosomes in mid-pachytene of 4-week-old and 19-week-old mice. Blue and red bars represent control (ctr) and *Rad18* knockdown (kd) mice, respectively. 600 nuclei from 3 independent mice for 4-week-old mice, and 300 nuclei from 3 independent mice for 19-week-old mice were examined. Double asterisks indicate  $p < 0.01$  (Chi-squared test). (E, F) Immunostaining of *Rad18* kd pachytene spermatocyte nuclei with anti-SYCP3 (red). The insert shows a larger magnification of the area containing the XY body. X and Y chromosomes are indicated in the enlarged pictures. (G) As mentioned in (D) in 4-week-old wild-type and *Hr6b* knockout mice. 200 nuclei in 2 independent mice were examined.

asynapsis in *Hr6b* knockout pachytene spermatocytes was not different from that of controls (Fig. 3G).

### RAD18-dependent HR6A/B localization at the XY body

We previously found that the ubiquitin-conjugating enzymes HR6A and HR6B associate with the XY body in pachytene and diplotene spermatocytes [30,34]. In mitotic cells, the mammalian RAD18-HR6A/B complex is known to ubiquitylate PCNA during replication damage bypass [44,45]. This complex is highly stable, even under high salt conditions (1 M NaCl) (data not shown). We examined whether the association of HR6A/B with the XY body depends on RAD18. In *Rad18* kd mice, a decreased level of HR6A/B was detected in whole nuclei and on the XY body (Fig. 4A and B), although the expression level of HR6A/B in *Rad18* kd testis extracts was similar to that of control extracts (Fig. 4C), indicating that RAD18 mediates the chromatin association of

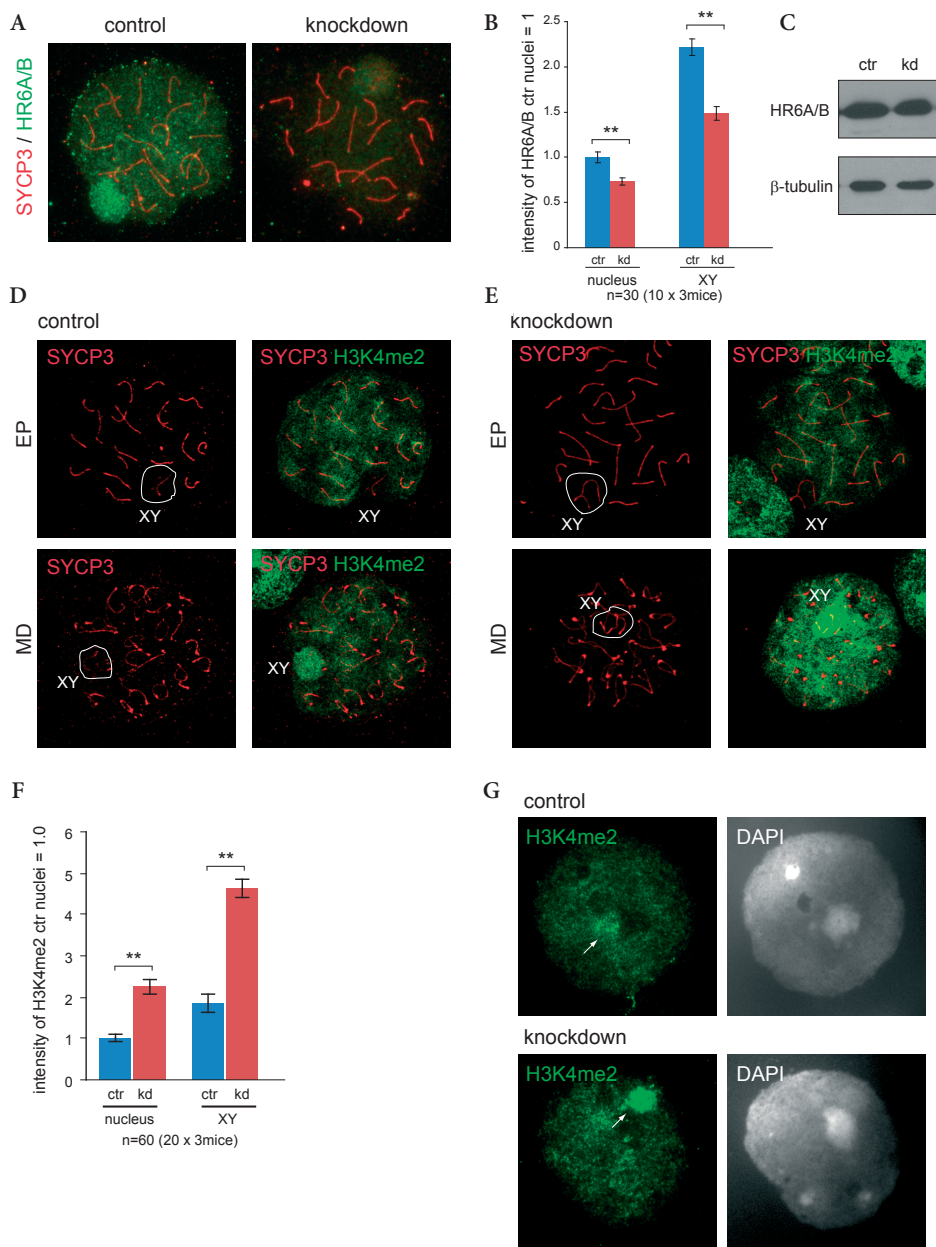


**Figure 4. Reduced HR6A/B and increased dimethylation of histone H3 at lysine 4 in *Rad18* knockdown spermatocytes.** (A) Double immunostaining of control and *Rad18* knockdown pachytene spermatocyte nuclei with anti-SYCP3 (red) and anti-HR6A/B (green). (B) The intensities of HR6A/B in the nucleus and on the XY body were measured with Image J software. The intensity of HR6A/B in control nuclei was set to 1.0. Error bars indicate SEM for 10 nuclei from 3 independent mice. Blue and red bars indicate control (ctr) and *Rad18* knockdown (kd), respectively. Double asterisks indicate  $p < 0.01$  (Mann-Whitney  $U$  test). (C) HR6A/HR6B expression in total cell extracts from testis of 4-week-old from control (ctr) and *Rad18* knockdown mice (kd) was detected on immunoblots.  $\beta$ -tubulin was used as loading control.  $\triangleright$

HR6A/B in meiosis. The residual binding of HR6A/B to the XY body may result from the residual amount of RAD18 that is still present, or may be RAD18-independent.

### Overall increased di-methylation of histone H3 lysine 4 in *Rad18* kd mice

The reduced level of HR6A/B in *Rad18* kd spermatocytes prompted us to analyze several aspects of meiotic prophase that were found to be aberrant in *Hr6b* knockout mouse spermatocytes, to investigate which meiotic HR6B functions depend on RAD18. In *Hr6b* knockout mice, increased dimethylation of histone H3 at lysine 4 (H3K4me2) was found on the XY body of diplotene spermatocytes and round spermatids [33]. In addition, increased histone H2A phosphorylation at tyrosine 120 (H2AT120p) was also found on the XY body [33]. In control mice, H3K4me2 was more or less evenly distributed in the nucleus in zygotene (data not shown), in accordance with previous observations [33]. In early-mid pachytene, this modification disappeared from the XY body but remained present in the rest of the nucleus (Fig. 4D and E in EP). In diplotene, H3K4me2 reappeared on the XY body and became enhanced in comparison to the rest of the nucleus (Fig. 4D in MD). In *Rad18* kd mice, the H3K4me2 signal was increased on the XY body as well as in the rest of the nucleus in diplotene nuclei, compared with controls (Fig. 4E in MD, and 4F). In haploid round spermatids, either the X or the Y chromosome is located adjacent to the chromocenter, and localization of H3K4me2 on the X or Y chromosomes has been verified using FISH [33]. In round spermatids of *Rad18* kd males, H3K4me2 levels were increased on the sex chromosomes, compared to controls (Fig. 4G). The expression level and pattern of H2AT120p did not show any significant differences between *Rad18* kd and control mice (data not shown).

### De-repression of X-linked genes

An increased level of H3K4me2 on the sex chromosomes of *Hr6b* knockout spermatocytes and spermatids is associated with an overall increase in X-linked gene expression in spermatids, indicating that the post-meiotic maintenance of meiotic sex chromosome inactivation (MSCI) is disturbed in *Hr6b* knockout mice [33,34]. To analyze whether this function of HR6B also depends on RAD18, the gene expression level of selected X-, Y-, and autosome-linked genes was examined by using mRNA isolated from total testes of 19-week-old control and *Rad18* kd mice. Genes were selected based on our previous observations made in mRNA preparations of isolated spermatocytes and spermatids from *Hr6b* knockout and control mice [33,34]. We selected two Y-linked genes that were reported to be expressed only in postmeiotic spermatids. In addition, we analysed seven X-linked genes; one of these is expressed in meiotic and postmeiotic cells (*4930408F14Rik*), three of these are expressed in

- ▷ (D, E) Double immunostaining of spermatocyte nuclei with anti-SYCP3 (red) and anti- H3 dimethylated at lysine 4 (H3K4Me2) (green) in control (D) and *Rad18* knockdown mice (E). EP; early-pachytene. MD; mid-diplotene. The XY body is shown in the white circle. (F) The intensities of H3K4me2 in the nucleus and on the XY body from 4-week-old and 19-week-old mice were measured using Image J software. The intensity of H3K4me2 in control nuclei was set at 1.0. Error bars indicate SEM from 60 nuclei in 3 independent mice. Blue and red bars indicate control (ctr) and *Rad18* knockdown (kd), respectively. Double asterisks indicate  $p < 0.01$  (Mann–Whitney *U* test). (G) Immunostaining of spermatid nuclei with anti-H3K4me2 (green) in *Rad18* kd and control mice. Arrows indicate sites of the accumulation of H3K4me2.

premeiotic cells but repressed in meiotic and postmeiotic cells (*Atp7a*, *Gla* and *Hprt*), two of these genes show postmeiotic reactivation (*Eif1ay* and *Gm614*), and one gene is mainly expressed in Sertoli and peritubular myoid cells (*Pgk1*) [46] (Mammalian Reproductive Genetics database). We also selected six autosomal genes that are expressed in peritubular myoid cells (*Lzp-s*), or at premeiotic (*Cd24a*), meiotic (*Spo11* and *Sycp3*) and postmeiotic (*Hils* and *Creb3l4*) spermatogenic developmental steps [46] (Mammalian Reproductive Genetics database). Both analyzed Y-linked genes *Sly* and *Ssty* showed increased expression in *Rad18* kd testes compared with the control (Fig. 5). Three X-linked genes, *Gm614*, *F14Rik*, and *Eif1ay*, expressed at meiotic and postmeiotic stages also showed increased expression in *Rad18* kd testes. However, for four other X-linked genes, *Atp7a*, *Hprt*, *Gla*, and *Pgk1*, expressed highly in premeiotic or somatic cells, we did not observe an effect of RAD18 depletion, except a decreased expression of *Gla*. Thus, in *Rad18* kd total testes, only X- and Y-linked genes that are normally induced during postmeiotic germ cell development, showed increased expression. Note that for genes that are also expressed in premeiotic and somatic cells, a selective effect on the expression in meiotic and postmeiotic cells, may be not apparent if the expression in premeiotic cells and somatic cells is also high, since all these cells are present in the total testis samples. For the autosomal genes, all five genes that were analysed did not show any significant differences between control and *Rad18* kd cells.

#### Normal formation of meiotic crossover sites in *Rad18* knockdown mice

Another major meiotic phenotype previously observed in *Hr6b* knockout spermatocytes is an increased number of MLH1 foci, and resultant crossovers [32]. In *Rad18* kd mice, the average number of MLH1 spots was 23.5 (n=120), which was not significantly

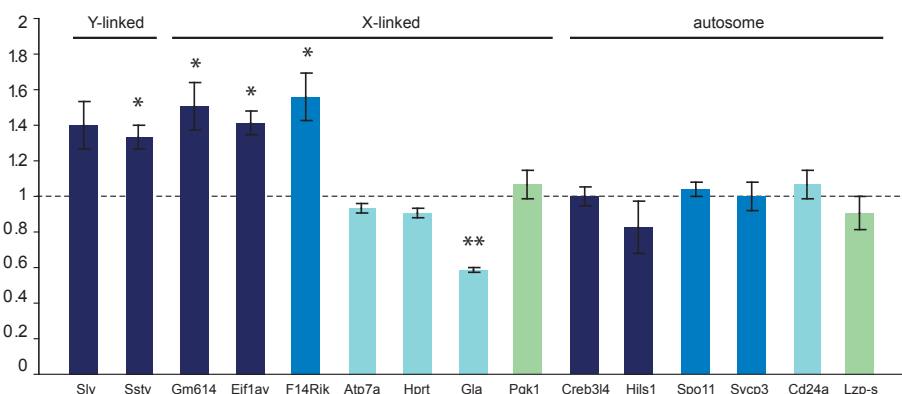


**Figure 5. Derepression of X- and Y-linked genes in *Rad18* knockdown mice.** Real-time RT-PCR quantification of mRNA levels of X-, Y-, and autosome-linked genes in total testes from *Rad18* kd mice. The amount of PCR products was normalized to *Actb* ( $\beta$ -actin) mRNA. The level of mRNA expression in control is set as 1.0, and mRNA expression levels of indicated genes in *Rad18* kd testes relative to the control are shown in the graph. Error bars show SEM for two independent experiments from 3 mice. Dark blue bars indicate genes mainly expressed in postmeiotic cells, blue bars indicate genes mainly expressed in meiotic prophase cells, light blue bars represent premeiotic genes, and the light green bars that are mainly expressed in somatic cells. Single asterisk indicates  $p < 0.05$  (Mann–Whitney *U* test).

different from control mice (24.0, n=90), indicating that knockdown of *Rad18* does not influence the number of crossover sites (not shown).

### **RAD51 localization to meiotic DSBs does not depend on RAD18**

During meiotic prophase, DSBs are induced by the topoisomerase II-like protein SPO11 in leptotene nuclei [13,14], and these DSBs can be visualized as RAD51 foci. RAD51 is an essential DSB repair protein involved in mitotic and meiotic HR. In leptotene nuclei of control mice, many RAD51 foci accumulated at meiotic DSB sites, and the number of foci gradually decreased through zygotene and pachytene ([47], and Supplementary Fig. S1A). In mid-pachytene, the majority of RAD51 foci had disappeared from autosomes, while RAD51 foci persisted on the axial elements of the unsynapsed X chromosomal arms (Supplementary Fig. S1A, enlarged picture in pachytene). In *Rad18* deficient mitotic MEF cells, Huang et al. [1] found that the number of IR-induced RAD51 foci depends on intact RAD18. To examine whether RAD18 influences the number of SPO11-induced RAD51 foci in meiosis, we counted the number of RAD51 foci in *Rad18* kd leptotene nuclei. We observed similar numbers of the SPO11-induced RAD51 foci in control and kd mice, suggesting RAD18-independent accumulation of RAD51 at SPO11-induced DSBs in meiosis (Fig. 6A).

### **RAD18 localizes to a small subfraction of meiotic DSB sites**

In mitotic HeLa cells, RAD18 accumulates as foci and colocalizes with both RAD51 and  $\gamma$ H2AX at DSBs [40]. In wild type meiotic cells, RAD18 accumulates as RAD51-like foci on the SC only in late zygotene, but not in either leptotene or early zygotene (Fig. 6B), suggesting that RAD18 does not immediately recognize the SPO11-induced DSBs, but may be recruited at a later stage, when some persistent meiotic DSBs are still present. The RAD18 foci at autosomes gradually disappeared during pachytene. Concomitantly, RAD18 started to accumulate on the chromatin surrounding the XY body (Fig. 6B). It is of interest to note that on the XY body of control early pachytene nuclei, RAD18 appears to localize first to the X chromosomal chromatin, which contains the persistent RAD51 foci, followed by a spread over the rest of the XY body (Fig. 6B). RAD51 foci on the unpaired X chromosome disappear in late pachytene/early diplotene, whereas RAD18 and  $\gamma$ H2AX remain on the XY body until late-diplotene (Fig. 6B, and Supplementary Fig. S1).

In order to study whether the RAD18 localization pattern depends on the presence of SPO11-induced DSBs, localization of RAD18 in *Spo11* mutant mice was examined. These mice carry a null-mutation at the catalytic site (D100Y), and the meiotic phenotype is morphologically indistinguishable from the *Spo11* knockout, no meiotic DSBs are generated (Fig. 6C; A. Inagaki, unpublished) [15,17]. In *Spo11* mutant mice, we could not detect RAD18 foci, whereas we still observed a very low level of accumulation of RAD18 in a mostly single large chromatin region that colocalized with the  $\gamma$ H2AX positive area (Fig. 6C). This region has been called the pseudo XY body [48]. The intensity of RAD18 that accumulated at the pseudo XY body was 90% reduced compared to the level on the XY body in wild type controls (Fig. 6D), and only a subfraction of the nuclei contained RAD18-positive pseudo XY bodies (42%),

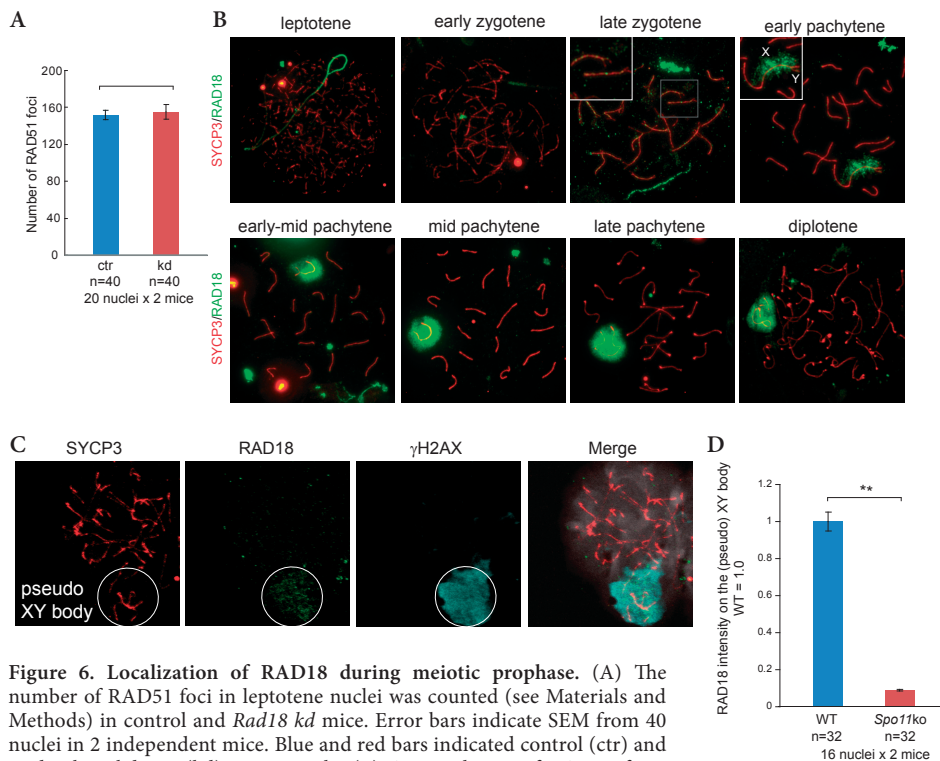


**Figure 6. Localization of RAD18 during meiotic prophase.** (A) The number of RAD51 foci in leptotene nuclei was counted (see Materials and Methods) in control and *Rad18 kd* mice. Error bars indicate SEM from 40 nuclei in 2 independent mice. Blue and red bars indicated control (ctr) and *Rad18* knockdown (kd), respectively. (B) Accumulation of RAD18 from leptotene to diplotene in wild type spermatocytes. In early pachytene, the XY body is shown in an enlarged picture, and X and Y chromosomes are indicated as X and Y. (C) Triple immunostaining of *Spo11* mutant spermatocyte nuclei with anti-SYCP3 (red), anti-RAD18 (green), and  $\gamma$ H2AX (light blue). The pseudo XY body is shown in the circle. (D) Graph showing the intensity of RAD18 on the XY body in wild type spermatocyte nuclei and on the pseudo XY body in *Spo11* mutant spermatocyte nuclei. The intensity of RAD18 on the XY body in wild type was set as 1.0. Error bars indicate SEM from 32 nuclei in 2 independent mice. Double asterisks indicate  $p < 0.01$  (Mann–Whitney *U* test).

whereas the vast majority of the nuclei (80%) contained a pseudo XY body identified by  $\gamma$ H2AX staining. This result shows that RAD18 accumulation at the pseudo XY body (in the absence of functional SPO11) is reduced compared to the accumulation of RAD18 on the XY body in wild type spermatocyte nuclei. The RAD18 foci on synapsed chromosomes in late zygotene and early pachytene, are SPO11-dependent, and thus most likely represent sites of (persistent, see also below) meiotic DSBs.

### Recruitment of RAD18 to IR-induced DSBs in spermatocytes

The lack of RAD18 recruitment to SPO11-induced DSBs in leptotene nuclei may be caused by specific factors that inhibit RAD18 recruitment to these sites. Alternatively, it may result from low expression of RAD18 at these stages. To examine this possibility, wild type mice were exposed to ionizing radiation with 5 Gy, and RAD18 foci formation was analysed after 3 hours. RAD18 was found to accumulate at radiation-induced DSBs from leptotene until late diplotene (Fig. 7), indicating that the amount

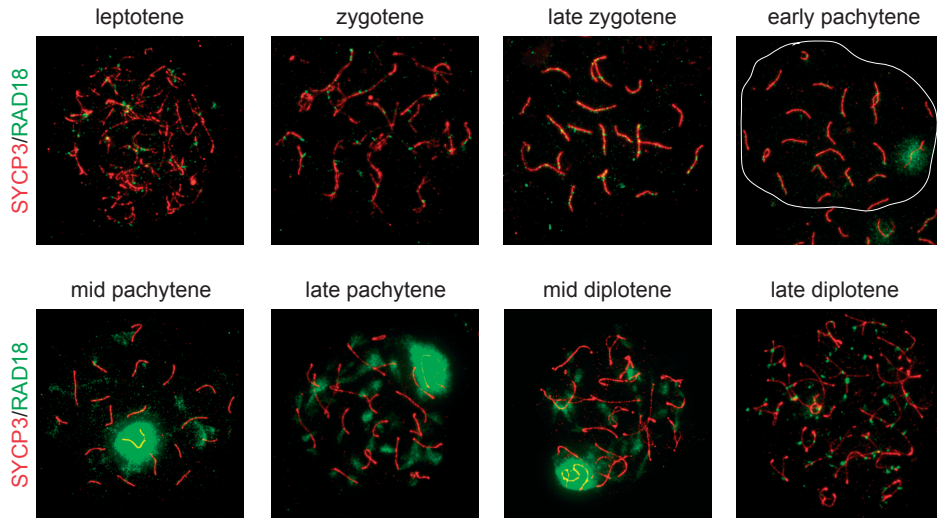


**Figure 7. Accumulation of RAD18 at IR-induced DSBs.** Localization of RAD18 in spermatocyte nuclei of wild type mice irradiated with IR at 5Gy. Three hours later, spread spermatocyte nuclei were prepared, and doublestained with anti-SYCP3 (red) and anti-RAD18 (green). The white line in the early pachytene image indicates the boundary of the nucleus.

of RAD18 that is present in leptotene nuclei is sufficient for recruitment to DSB sites. Intriguingly, we observed two different patterns of RAD18 accumulation. In leptotene, zygotene, and early pachytene nuclei, RAD18 accumulated as distinct foci, whereas a more diffuse accumulation pattern, similar to what is observed for  $\gamma$ H2AX, was observed in pachytene and early- to mid-diplotene (Fig. 7). These data suggest that depending on the substage of meiotic prophase, RAD18 accumulation in response to the formation of DSBs varies. Interestingly, the time point at which RAD18 localization changed from a focus-like pattern to a diffuse chromatin-associated pattern coincided with the accumulation of RAD18 at the XY body (Fig. 7). When RAD18 was lost from the XY body in late diplotene, RAD18 accumulated again as RAD51-like foci.

#### **RAD18 accumulates as foci at persistent DSBs in *Sycp1* knockout mice**

Our finding that RAD18 localizes to only a small subfraction of SPO11-induced DSBs, at a relatively late time point following the formation of these breaks, and the subsequent recruitment to the chromatin surrounding the persistent DSBs on the X, indicated that the recruitment of RAD18 to meiotic DSBs may only occur if these breaks persist. To study this further, we investigated RAD18 localization in spread spermatocyte nuclei from *Sycp1* knockout mice. SYCP1 is a transverse filament protein that connects the lateral elements to form a SC. In *Sycp1* knockout mice, chromosomes align, but synapsis is not achieved. In addition, repair of meiotic DSBs is stalled, as visualized by persistent  $\gamma$ H2AX and RAD51 staining, and no XY body is formed [38] (Fig. 8A and B). Intriguingly, in *Sycp1* knockout spermatocytes, RAD18 showed RAD51-like foci formation on all SCs in late zygotene (Fig. 8C). We also found foci-like accumulation

of RAD18 along the X chromosome, while RAD18 did not accumulate on the DSB-surrounding chromatin (Fig. 8C).

### RAD18 at persistent meiotic DSBs in *Rad54* knockout mice

RAD54 is a homologous recombination repair protein that may also function in meiosis. In yeast meiosis, meiosis-specific proteins appear to attenuate Rad54 functions, to facilitate interhomolog repair [49]. In mammals, two yeast Rad54 orthologs, RAD54 and RAD54B, have been identified [50]. Both *Rad54* single [39], and *Rad54/Rad54b* double knockout mice [51] are viable, fertile and show normal development. However, persistent RAD51 foci and their aggregation have been reported in diplotene spermatocyte of both *Rad54* and *Rad54/Rad54b*-double knockout mice [51]. Since this phenotype of persistent breaks in diplotene spermatocytes is somewhat reminiscent of what we observed in *Rad18* kd spermatocytes, we also examined accumulation of RAD18 in *Rad54* knockout mice. In early diplotene spermatocytes, more frequent accumulation of RAD18 at several areas of autosomal chromatin was found in *Rad54* knockout mice, compared to control wild type (Fig. 9A arrows, and B). Here, RAD18 does not accumulate as foci, but displays a more diffuse pattern on the chromatin, similar to the pattern that is observed at radiation induced breaks at this stage (late pachytene/early diplotene) (Fig. 7) [52]. At these RAD18 positive sites in *Rad54* knockout diplotene spermatocytes,  $\gamma$ H2AX accumulation was also observed (data not shown). Taken together, RAD18 is recruited to the sites where the DNA damage persists due to the lack of repair associated proteins, RAD54.

### Persistent $\gamma$ H2AX on autosomal chromatin in late diplotene spermatocytes of *Rad18* kd and *Hr6b*<sup>-/-</sup> mice

Similar to DSB-repair sites in mitotic cells, the surrounding chromatin of SPO11-induced DSBs is marked by  $\gamma$ H2AX in leptotene and zygotene nuclei [19] (Supplementary Fig.

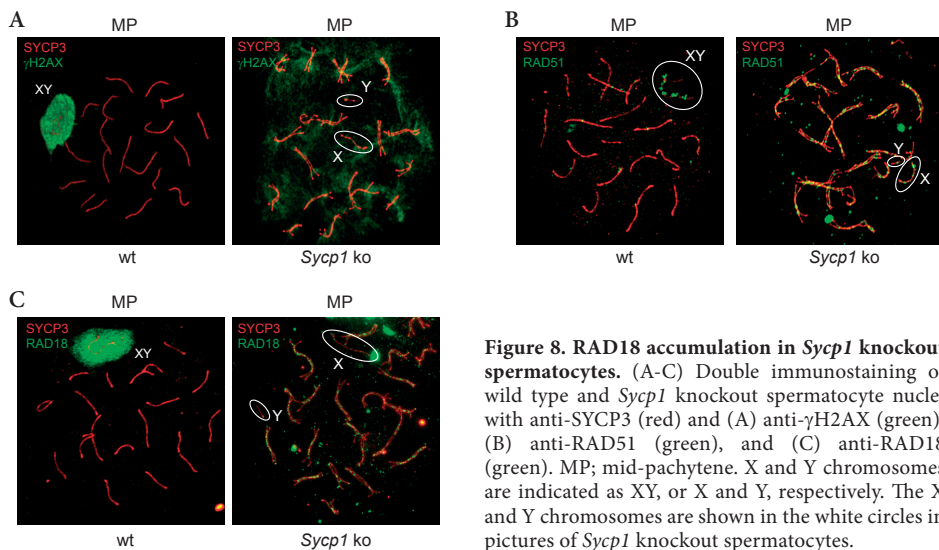


**Figure 8. RAD18 accumulation in *Sycp1* knockout spermatocytes.** (A-C) Double immunostaining of wild type and *Sycp1* knockout spermatocyte nuclei with anti-SYCP3 (red) and (A) anti- $\gamma$ H2AX (green), (B) anti-RAD51 (green), and (C) anti-RAD18 (green). MP; mid-pachytene. X and Y chromosomes are indicated as XY, or X and Y, respectively. The X and Y chromosomes are shown in the white circles in pictures of *Sycp1* knockout spermatocytes.

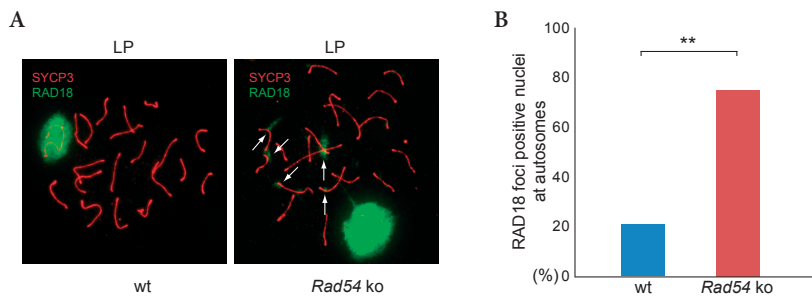


**Figure 9. RAD18 accumulation in *Rad54* knockout spermatocytes.** (A) Double immunostaining of wild type and *Rad54* knockout late-pachytene nuclei with anti-SYCP3 (red) and anti-RAD18 (green). Arrows indicated persistent RAD18 staining at autosomes. (B) The percentage of nuclei containing persistent RAD18 foci in late-pachytene is shown. 100 nuclei were examined in a control and a *Rad54* knockout mouse. Double asterisks indicate  $p < 0.01$  (Chi-squared test).

S1B). In addition,  $\gamma$ H2AX is known as the earliest marker of the XY body (Supplementary Fig. S1B, arrowhead) [19]. As pachytene progresses, the intensity of  $\gamma$ H2AX decreases at autosomes but not on the XY body, and  $\gamma$ H2AX has disappeared from autosomes in diplotene [19] (Supplementary Fig. S1B). We observed that  $\gamma$ H2AX was still present on the XY body just before entering metaphase (Supplementary Fig. S1B). In young as well as adult *Rad18* kd mice, the  $\gamma$ H2AX staining pattern was similar to that of control mice from leptotene to pachytene. However,  $\gamma$ H2AX positive sites still marked autosomes in 60% of late diplotene nuclei in *Rad18* deficient mice (Fig. 10A and B). This was much less frequently observed in control mice. To examine whether this function depends on the presence of a functional RAD18-HR6A/B complex, we examined  $\gamma$ H2AX staining in *Hr6b* knockout mice. Similar to *Rad18* kd mice, approximately 40% of late diplotene nuclei showed accumulation of  $\gamma$ H2AX at autosomal chromatin, compared to approximately 20% of the nuclei in wild-type testis (Fig. 10C).

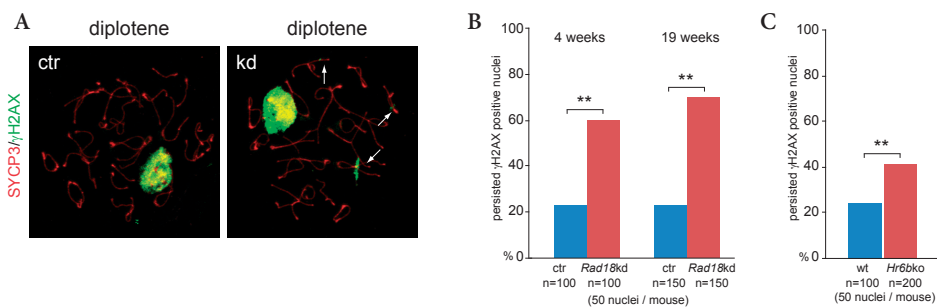


**Figure 10. Increased number of unrepaired meiotic DSBs in *Rad18* knockdown spermatocytes.** (A) Double immunostaining of control (ctr) and *Rad18* knockdown (kd) spermatocyte nuclei with anti-SYCP3 (red) and anti- $\gamma$ H2AX (green). Arrows point to  $\gamma$ H2AX, indicating persistent DSBs at autosomal regions. (B, C) Graphs showing the percentage of persistent  $\gamma$ H2AX foci in late-diplotene of 4-week-old (B, C) and 19-week-old (B) mice. Blue bars indicate control, and red bars indicate *Rad18* knockdown (B) or *Hr6b* knockout (C), respectively. The number of analyzed mice is indicated in the graph. Double asterisks indicate  $p < 0.01$  (Chi-squared test).

## DISCUSSION

### RAD18 and HR6A/B

RAD18 is most well known for its role in replicative damage bypass (RDB) that allows progression of DNA replication in the presence of DNA damage in mitotic cells (reviewed in [7]). In addition, RAD18 is also required for DSB repair [1,5]. Herein, we analyzed *Rad18* knockdown mice to study the role of RAD18 in meiotic DSB repair. RAD18 and HR6A/B function as a complex. It is thought that RAD18 may bind to DNA directly via its SAP domain, or indirectly via its Zinc finger, which may interact with ubiquitylated chromatin components such as ubiquitylated histones [53]. HR6A/B does not have any known direct DNA or chromatin binding properties. As expected, based on these properties of the proteins, we found that the localization of HR6A/B to chromatin, including the XY body, is at least partially dependent on RAD18. The intimate functional and physical relation between the two proteins would suggest that loss of the proteins may lead to similar phenotypes, and identification of overlapping phenotypic characteristics could help to distinguish between RAD18-dependent, and RAD18-independent functions of HR6A and HR6B. Previously, we have shown that HR6B at the XY body functions to decrease the H3K4me2 level, in association with a role in the maintenance of MSC1 [33,34]. Herein, we show that the regulation of the H3K4me2 level at the XY body appears to be RAD18 dependent. None of the other previously identified meiotic phenotypic characteristics of the *Hr6b* knockout mice were observed in the *Rad18 kd* mice. Apart from RAD18, HR6A/B also functions with other E3 ligases, such as RNF20 and RNF40 to ubiquitylate histone H2B at lysine 120 (H2BK120ubi) [54]. In addition, HR6A/B functions together with members of the UBR family of E3 ligases [55-57]. Thus, most likely the other functions of HR6B in meiosis depend on these, or yet unknown E3 ligases.

HR6B apparently also functions during postmeiotic spermatid differentiation, since condensing spermatids of *Hr6b* knockout mice showed severe morphological disturbances [58]. In addition, the expression of many genes (approximately 25% of the annotated genes) becomes disturbed in *Hr6b* round spermatids [34]. In *Rad18 kd* mice, we noted a milder disturbance of postmeiotic spermatid development. It is not excluded that a low level of remaining RAD18 expression in spermatids of *Rad18 kd* mice, generates a partial phenotype. However, the postmeiotic expression of X- and Y-linked genes may be affected in a similar way as in *Hr6b* knockout mice. Using immunocytology we do not detect RAD18 protein in postmeiotic spermatids, but on immunoblots the amount of RAD18 appears to be approximately equal in spermatocytes and spermatids [30]. Together, this indicates that part of the postmeiotic HR6B functions depend on RAD18.

Surprisingly, we observed an increased frequency of XY asynapsis in *Rad18* knockdown mice. This phenotype is not present in *Hr6b* knockout mice. It cannot be excluded that RAD18 carries out some HR6B-independent functions that may not require protein ubiquitylation. Still, we presume that it is more likely that this phenotype is related to systemic dysregulation in *Rad18 kd* mice that is evidenced by the overall decrease in body weight. Interestingly, in *Atm* knockout mice, a similar

effect on XY synapsis was described [59]. *Atm* deficient mice also display reduced body weight compared to their littermate controls [60]. In these mice, overall meiotic recombination was increased [59], indicating that the XY asynapsis could not be caused by decreased meiotic recombination. It is highly likely that the observed asynapsis results from premature desynapsis instead of a complete lack of synapsis. This conclusion is based on the fact that we did not observe any aberration in the frequency of MLH1 foci formation on the XY pair, and on the normal frequencies of X and Y bearing spermatids.

Sun et al. (2009) [61] described the testicular phenotype of *Rad18* knockout mice. They reported normal spermatogenesis in young mice, and progressive loss of stem cells in old (>12 months) *Rad18* knockout mice. Since they did not study meiotic prophase in detail in their mouse model, and the meiotic defects that we observed in the *Rad18* kd mice are rather subtle, it is not excluded that similar defects will be present in these males. Conversely, we do not exclude that upon aging, *Rad18* knockdown mice will show a similar loss of stem cells as was described for the *Rad18* knockout mice. The average litter size of the control mice in the study of Sun et al. (2009) is much lower compared to what we observed, indicating that the genetic background may also be different. Finally, the *Rad18* knockout allele was generated through insertional mutagenesis, and it cannot be excluded that (truncated) RAD18 is expressed in some tissues in the knockout mouse model, leading to a hypomorphic phenotype.

### **Recruitment of RAD18 to persistent meiotic DSBs and chromatin of the XY body**

In the present study, we found that RAD18 accumulates only at a small subset of meiotic DSBs in late zygotene to early pachytene, but not in leptotene, in a SPO11-dependent manner. This subset of meiotic DSBs may represent persistent DSBs, since in *Sycp1* knockout mice, in which many DSBs remain unrepaired due to the failure of complete chromosome pairing, many more RAD18 foci appear along the chromosomal axes. Our finding that RAD18 is able to associate with IR-induced DSBs in leptotene when the mice were irradiated with 5 Gy, indicates that the amount of RAD18 is not limiting at this stage. Thus, it appears that factors involved in recruiting RAD18 to damage-induced DSBs are absent or masked at SPO11-induced DSBs in leptotene. In mitotic cells, ubiquitylation of histone H2A at lysine 119 (uH2A) by the ubiquitin E3 ligase RNF8 functions as a key modification to transmit the signal further to downstream components of the DSB recognition pathway [62-64]. RNF8 deficient cells show no accumulation of RAD18 at IR-induced DSBs [1]. In leptotene and zygotene spermatocytes, we have not found uH2A accumulation at IR-induced DSBs (unpublished data), and it is also not present at SPO11-induced breaks at these stages [32]. Thus, most likely, some other component of the DSB-recognition pathway is capable of recruiting RAD18 to IR-induced DSBs in leptotene spermatocytes. In late zygotene, this unknown component may also have accumulated, or has become “unmasked” at SPO11-induced DSBs that have not yet been repaired. We suggest that the two known RAD18 interaction partners RPA [65] and RAD51C [1] are somehow involved in the recruitment of RAD18 only to the persistent meiotic DSBs.

Chromosomes or chromosomal regions without a pairing partner can only repair their meiotic DSBs in the unpaired regions through recombination with the sister chromatid or via NHEJ. Since both these pathways appear to be repressed during early meiotic prophase, meiotic DSBs in such regions may remain unrepaired. Indeed, persistent RAD51 foci are observed along the unsynapsed arm of the X chromosome in pachytene [47]. Surprisingly, these are only rarely observed along the unsynapsed part of the Y, suggesting that SPO11 generates only a few breaks in this region of the Y, or that these breaks are repaired via an alternative, rapid pathway. Corresponding to these persistent meiotic DSBs on the X chromosome in pachytene, RAD18 accumulates first on the chromatin regions of the X chromosome, and subsequently spreads to the synapsed chromatin and the region of the Y chromosome. This suggests that the persistent DSBs on the X may stimulate recruitment of RAD18 to the X chromosome, followed by spreading to the Y chromosome. Notably, uH2A shows a similar pattern of accumulation on the XY body, suggesting that uH2A may function to facilitate RAD18 recruitment to the chromatin surrounding the meiotic DSBs on the XY body.

#### **Possible role of RAD18 in intersister-mediated repair of persistent meiotic DSBs**

The repair mechanism for DSBs on the X and Y chromosomes remains unclear. Recent analyses of radiation-induced DSB repair in spermatocytes revealed that the NHEJ pathway is reactivated in late pachytene spermatocytes, and most damage-induced DSBs appear to be repaired via this pathway, although the HR pathway takes over when NHEJ is compromised [34]. For the persistent breaks at the XY body, it is not known whether NHEJ or HR (using the sister chromatid as a template for repair) is the favoured pathway. Since we did not observe a change in the dynamics of RAD51 foci on the XY body in *Rad18* kd mice, it is unlikely that RAD18 is required for the repair of these breaks. Moreover, the fact that RAD51 foci disappear from the XY body before  $\gamma$ H2AX, suggests that the NHEJ pathway may mediate repair of persistent DSBs on the unsynapsed XY axes. This would fit with the idea that intersister-mediated DSB repair should be inhibited as long as synapsis is not achieved, which maintains the interhomolog bias to stimulate chromosome pairing. In yeast, a protein named Hop1 triggers dimerization and activation of a kinase Mek1 [66,67]. Mek1 subsequently mediates phosphorylation of Rad54, which inhibits its activity, and is involved in mediating the interhomolog bias [49]. In mammals, two possible *Hop1* homologs, *Hormad1* and *Hormad2* have been identified [68]. HORMAD1 and 2 preferentially accumulate on unsynapsed chromosome axes in spermatocytes, and are removed upon synapsis. This is consistent with the idea that the interhomolog bias could be relieved upon synapsis. Thus, at synapsed autosomal sites, on paired chromosomes that repaired most of the breaks and formed at least a single crossover, the inhibition to repair via the sister may be relieved. At such DSB sites, RAD18 and RAD54 may function together to mediate inter-sister repair.

Taken together, our data indicate that RAD18, together with HR6B, may ubiquitylate an unknown substrate to facilitate repair of persisting meiotic DSBs at synapsed regions using the sister chromatid as a template for repair in late zygotene and early pachytene. In the absence of RAD18, these DSB sites persist until the NHEJ pathway

is reactivated in diplotene. At the XY body, the function of the RAD18-HR6B complex may be different. At the DSB sites along the unsynapsed X, it may try to stimulate HR, but fails to succeed due to the inhibition of inter-sister mediated repair. On the surrounding chromatin RAD18 may be involved in regulating chromatin structure and thereby help to maintain MSCI.

## ACKNOWLEDGEMENTS

We thank Dr. Hein te Riele and Dr. Sandra de Vries (The Netherlands Cancer Institute, Amsterdam, The Netherlands) for *Spo11* mutant mice, Dr. Albert Pastink (Leiden University Medical Center, Leiden, The Netherlands) for *Sycp1* knockout mice, and Dr. Roland Kanaar (Erasmus MC, Rotterdam, The Netherlands) for *Rad54* knockout mice.

This work was supported by the Netherlands Organization for Scientific Research (NWO) through ALW (VIDI 864.05.003).

## REFERENCES

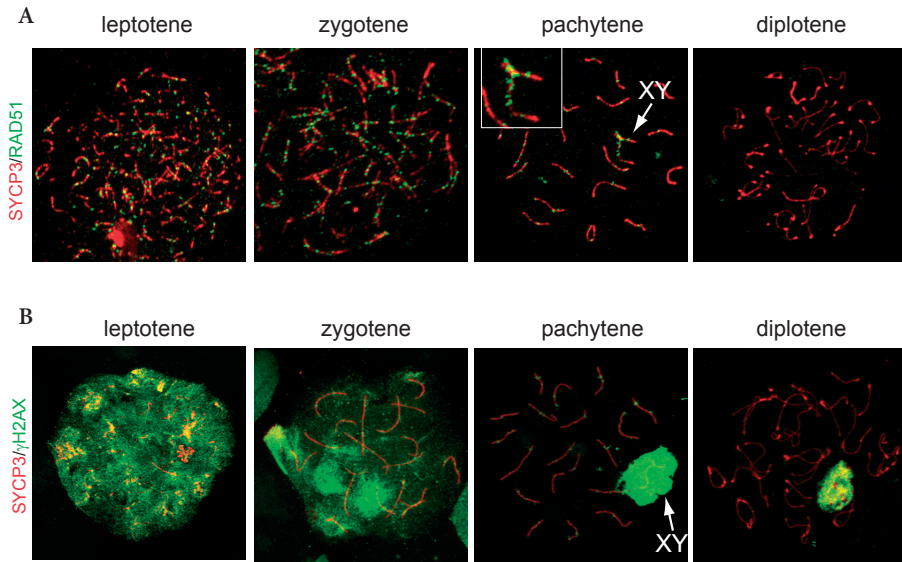
1. J. Huang, M.S. Huen, H. Kim, C.C. Leung, J.N. Glover, X. Yu, J. Chen, RAD18 transmits DNA damage signalling to elicit homologous recombination repair, *Nat Cell Biol* 11 (2009) 592-603.
2. S. Miyase, S. Tateishi, K. Watanabe, K. Tomita, K. Suzuki, H. Inoue, M. Yamaizumi, Differential regulation of Rad18 through Rad6-dependent mono- and polyubiquitination, *J Biol Chem* 280 (2005) 515-524.
3. S. Tateishi, H. Niwa, J. Miyazaki, S. Fujimoto, H. Inoue, M. Yamaizumi, Enhanced genomic instability and defective postreplication repair in RAD18 knockout mouse embryonic stem cells, *Mol Cell Biol* 23 (2003) 474-481.
4. N. Shiomi, M. Mori, H. Tsuji, T. Imai, H. Inoue, S. Tateishi, M. Yamaizumi, T. Shiomi, Human RAD18 is involved in S phase-specific single-strand break repair without PCNA monoubiquitination, *Nucleic Acids Res* 35 (2007) e9.
5. K. Watanabe, K. Iwabuchi, J. Sun, Y. Tsuji, T. Tani, K. Tokunaga, T. Date, M. Hashimoto, M. Yamaizumi, S. Tateishi, RAD18 promotes DNA double-strand break repair during G1 phase through chromatin retention of 53BP1, *Nucleic Acids Res* (2009).
6. M.H. Koken, P. Reynolds, I. Jaspers-Dekker, L. Prakash, S. Prakash, D. Bootsma, J.H. Hoeijmakers, Structural and functional conservation of two human homologs of the yeast DNA repair gene RAD6, *Proc. Natl. Acad. Sci. USA* 88 (1991) 8865-8869.
7. H.D. Ulrich, The RAD6 pathway: control of DNA damage bypass and mutagenesis by ubiquitin and SUMO, *Chembiochem* 6 (2005) 1735-1743.
8. R. van der Laan, H. Roest, J. Hoogerbrugge, E. Smit, R. Slater, W. Baarends, J. Hoeijmakers, J. Grootegoed, Characterization of mRAD18Sc, a mouse homolog of the yeast post-replication repair gene RAD18, *Genomics* 69 (2000) 86-94.
9. J.S. Jones, L. Prakash, Transcript levels of the *Saccharomyces cerevisiae* DNA repair gene RAD18 increase in UV irradiated cells and during meiosis but not during the mitotic cell cycle, *Nucleic Acids Res* 19 (1991) 893-898.
10. E.L. Dowling, D.H. Maloney, S. Fogel, Meiotic recombination and sporulation in repair-deficient strains of yeast, *Genetics* 109 (1985) 283-302.
11. F. Fabre, N. Magana-Schwencke, R. Chanet, Isolation of the RAD18 gene of *Saccharomyces cerevisiae* and construction of rad18 deletion mutants, *Mol Gen Genet* 215 (1989) 425-430.
12. J.C. Game, R.K. Mortimer, A genetic study of x-ray sensitive mutants in yeast, *Mutat Res* 24 (1974) 281-292.
13. S. Keeney, F. Baudat, M. Angeles, Z.H. Zhou, N.G. Copeland, N.A. Jenkins, K. Manova, M. Jasin, A mouse homolog of the *Saccharomyces cerevisiae* meiotic

- recombination DNA transesterase Spo11p, *Genomics* 61 (1999) 170-182.
14. S. Keeney, C.N. Giroux, N. Kleckner, Meiosis-specific DNA double-strand breaks are catalyzed by Spo11, a member of a widely conserved protein family, *Cell* 88 (1997) 375-384.
  15. F. Baudat, K. Manova, J.P. Yuen, M. Jasin, S. Keeney, Chromosome synapsis defects and sexually dimorphic meiotic progression in mice lacking Spo11, *Mol Cell* 6 (2000) 989-998.
  16. L. Cao, E. Alani, N. Kleckner, A pathway for generation and processing of double-strand breaks during meiotic recombination in *S. cerevisiae*, *Cell* 61 (1990) 1089-1101.
  17. P.J. Romanienko, R.D. Camerini-Otero, The mouse Spo11 gene is required for meiotic chromosome synapsis, *Mol Cell* 6 (2000) 975-987.
  18. S. Burma, B.P. Chen, M. Murphy, A. Kurimasa, D.J. Chen, ATM phosphorylates histone H2AX in response to DNA double-strand breaks, *J Biol Chem* 276 (2001) 42462-42467.
  19. S.K. Mahadevaiah, J.M. Turner, F. Baudat, E.P. Rogakou, P. de Boer, J. Blanco-Rodriguez, M. Jasin, S. Keeney, W.M. Bonner, P.S. Burgoyne, Recombinational DNA double-strand breaks in mice precede synapsis, *Nat Genet* 27 (2001) 271-276.
  20. T. Ashley, A.W. Plug, J. Xu, A.J. Solari, G. Reddy, E.I. Golub, D.C. Ward, Dynamic changes in Rad51 distribution on chromatin during meiosis in male and female vertebrates, *Chromosoma* 104 (1995) 19-28.
  21. A.L. Barlow, F.E. Benson, S.C. West, M.A. Hulten, Distribution of the Rad51 recombinase in human and mouse spermatocytes, *EMBO J.* 16 (1997) 5207-5215.
  22. W. Goedecke, M. Eijpe, H.H. Offenber, M. van Aalderen, C. Heyting, Mre11 and Ku70 interact in somatic cells, but are differentially expressed in early meiosis, *Nat Genet* 23 (1999) 194-198.
  23. A. Schwacha, N. Kleckner, Identification of joint molecules that form frequently between homologs but rarely between sister chromatids during yeast meiosis, *Cell* 76 (1994) 51-63.
  24. A. Schwacha, N. Kleckner, Interhomolog bias during meiotic recombination: meiotic functions promote a highly differentiated interhomolog-only pathway, *Cell* 90 (1997) 1123-1135.
  25. A. Inagaki, S. Schoenmakers, W.M. Baarends, DNA double strand break repair, chromosome synapsis and transcriptional silencing in meiosis, *Epigenetics* 5 (2010).
  26. C. Heyting, P.B. Moens, W. van Raamsdonk, A.J. Dietrich, A.C. Vink, E.J. Redeker, Identification of two major components of the lateral elements of synaptonemal complexes of the rat, *Eur J Cell Biol* 43 (1987) 148-154.
  27. M.J. Moses, Synaptonemal complex karyotyping in spermatocytes of the Chinese hamster (*Cricetulus griseus*). II. Morphology of the XY pair in spread preparations, *Chromosoma* 60 (1977) 127-137.
  28. V. Monesi, Differential rate of ribonucleic acid synthesis in the autosomes and sex chromosomes during male meiosis in the mouse, *Chromosoma* 17 (1965) 11-21.
  29. W.M. Baarends, J.W. Hoogerbrugge, H.P. Roest, M. Ooms, J. Vreeburg, J.H. Hoeijmakers, J.A. Grootegoed, Histone ubiquitination and chromatin remodeling in mouse spermatogenesis, *Dev Biol* 207 (1999) 322-333.
  30. R. van der Laan, E.J. Uringa, E. Wassenaar, J.W. Hoogerbrugge, E. Sleddens, H. Odijk, H.P. Roest, P. de Boer, J.H. Hoeijmakers, J.A. Grootegoed, W.M. Baarends, Ubiquitin ligase Rad18Sc localizes to the XY body and to other chromosomal regions that are unpaired and transcriptionally silenced during male meiotic prophase, *J Cell Sci* 117 (2004) 5023-5033.
  31. H.P. Roest, W.M. Baarends, J. de Wit, J.W. van Klaveren, E. Wassenaar, J.W. Hoogerbrugge, W.A. van Cappellen, J.H. Hoeijmakers, J.A. Grootegoed, The ubiquitin-conjugating DNA repair enzyme HR6A is a maternal factor essential for early embryonic development in mice, *Mol Cell Biol* 24 (2004) 5485-5495.
  32. W.M. Baarends, E. Wassenaar, J.W. Hoogerbrugge, G. van Cappellen, H.P. Roest, J. Vreeburg, M. Ooms, J.H. Hoeijmakers, J.A. Grootegoed, Loss of HR6B ubiquitin-conjugating activity results in damaged synaptonemal complex structure and increased crossing-over frequency during the male meiotic prophase, *Mol Cell Biol* 23 (2003) 1151-1162.

33. W.M. Baarends, E. Wassenaar, J.W. Hoogerbrugge, S. Schoenmakers, Z.W. Sun, J.A. Grootegoed, Increased phosphorylation and dimethylation of XY body histones in the Hr6b-knockout mouse is associated with derepression of the X chromosome, *J Cell Sci* 120 (2007) 1841-1851.
34. E. Mulugeta Achame, E. Wassenaar, J.W. Hoogerbrugge, E. Sleddens-Linkels, M. Ooms, Z.W. Sun, I.W.F. van, J.A. Grootegoed, W.M. Baarends, The ubiquitin-conjugating enzyme HR6B is required for maintenance of X chromosome silencing in mouse spermatocytes and spermatids, *BMC genomics* 11 367.
35. J. Seibler, B. Kuter-Luks, H. Kern, S. Streu, L. Plum, J. Mauer, R. Kuhn, J.C. Bruning, F. Schwenk, Single copy shRNA configuration for ubiquitous gene knockdown in mice, *Nucleic Acids Res* 33 (2005) e67.
36. B.L. Hogan, M. Blessing, G.E. Winnier, N. Suzuki, C.M. Jones, Growth factors in development: the role of TGF-beta related polypeptide signalling molecules in embryogenesis, *Dev Suppl* (1994) 53-60.
37. M.A. Bellani, P.J. Romanienko, D.A. Cairatti, R.D. Camerini-Otero, SPO11 is required for sex-body formation, and Spo11 heterozygosity rescues the prophase arrest of *Atm*<sup>-/-</sup> spermatocytes, *J Cell Sci* 118 (2005) 3233-3245.
38. F.A. de Vries, E. de Boer, M. van den Bosch, W.M. Baarends, M. Ooms, L. Yuan, J.G. Liu, A.A. van Zeeland, C. Heyting, A. Pastink, Mouse *Sycp1* functions in synaptonemal complex assembly, meiotic recombination, and XY body formation, *Genes Dev* 19 (2005) 1376-1389.
39. J. Essers, R.W. Hendriks, S.M. Swagemakers, C. Troelstra, J. de Wit, D. Bootsma, J.H. Hoeijmakers, R. Kanaar, Disruption of mouse RAD54 reduces ionizing radiation resistance and homologous recombination, *Cell* 89 (1997) 195-204.
40. A. Inagaki, W.A. van Cappellen, R. van der Laan, A.B. Houtsmuller, J.H. Hoeijmakers, J.A. Grootegoed, W.M. Baarends, Dynamic localization of human RAD18 during the cell cycle and a functional connection with DNA double-strand break repair, *DNA Repair (Amst)* 8 (2009) 190-201.
41. J. Essers, R.W. Hendriks, J. Wesoly, C.E. Beerens, B. Smit, J.H. Hoeijmakers, C. Wyman, M.L. Dronkert, R. Kanaar, Analysis of mouse Rad54 expression and its implications for homologous recombination, *DNA Repair (Amst)* 1 (2002) 779-793.
42. A.H. Peters, A.W. Plug, M.J. van Vugt, P. de Boer, A drying-down technique for the spreading of mammalian meiocytes from the male and female germline, *Chromosome Res* 5 (1997) 66-68.
43. M.E. van Royen, S.M. Cunha, M.C. Brink, K.A. Mattern, A.L. Nigg, H.J. Dubbink, P.J. Verschure, J. Trapman, A.B. Houtsmuller, Compartmentalization of androgen receptor protein-protein interactions in living cells, *J Cell Biol* 177 (2007) 63-72.
44. C. Hoege, B. Pfander, G.L. Moldovan, G. Pyrowolakis, S. Jentsch, RAD6-dependent DNA repair is linked to modification of PCNA by ubiquitin and SUMO, *Nature* 419 (2002) 135-141.
45. P.L. Kannouche, J. Wing, A.R. Lehmann, Interaction of human DNA polymerase  $\eta$  with monoubiquitinated PCNA: a possible mechanism for the polymerase switch in response to DNA damage, *Mol Cell* 14 (2004) 491-500.
46. S.H. Namekawa, P.J. Park, L.F. Zhang, J.E. Shima, J.R. McCarrey, M.D. Griswold, J.T. Lee, Postmeiotic sex chromatin in the male germline of mice, *Curr Biol* 16 (2006) 660-667.
47. P.B. Moens, D.J. Chen, Z. Shen, N. Kolas, M. Tarsounas, H.H. Heng, B. Spyropoulos, Rad51 immunocytology in rat and mouse spermatocytes and oocytes, *Chromosoma* 106 (1997) 207-215.
48. A. Chicheportiche, J. Bernardino-Sgherri, B. de Massy, B. Dutrillaux, Characterization of Spo11-dependent and independent phospho-H2AX foci during meiotic prophase I in the male mouse, *J Cell Sci* 120 (2007) 1733-1742.
49. H. Niu, L. Wan, V. Busygina, Y. Kwon, J.A. Allen, X. Li, R.C. Kunz, K. Kubota, B. Wang, P. Sung, K.M. Shokat, S.P. Gygi, N.M. Hollingsworth, Regulation of meiotic recombination via Mek1-mediated Rad54 phosphorylation, *Mol Cell* 36 (2009) 393-404.
50. T. Hiramoto, T. Nakanishi, T. Sumiyoshi, T. Fukuda, S. Matsuura, H. Tauchi, K. Komatsu, Y. Shibasaki, H. Inui, M. Watatani, M. Yasutomi, K. Sumii, G. Kajiyama, N. Kamada, K. Miyagawa, K. Kamiya, Mutations of a novel human RAD54 homologue, RAD54B, in primary cancer, *Oncogene* 18 (1999) 3422-3426.
51. J. Wesoly, S. Agarwal, S. Sigurdsson, W. Bussen, S. Van Komen, J. Qin, H. van

- Steege, J. van Benthem, E. Wassenaar, W.M. Baarends, M. Ghazvini, A.A. Tafel, H. Heath, N. Galjart, J. Essers, J.A. Grootegoed, N. Arnheim, O. Bezzubova, J.M. Buerstedde, P. Sung, R. Kanaar, Differential contributions of mammalian Rad54 paralogs to recombination, DNA damage repair, and meiosis, *Mol Cell Biol* 26 (2006) 976-989.
52. S. Schoenmakers, E. Wassenaar, W.A. van Cappellen, A.A. Derijck, P. de Boer, J.S. Laven, J.A. Grootegoed, W.M. Baarends, Increased frequency of asynapsis and associated meiotic silencing of heterologous chromatin in the presence of irradiation-induced extra DNA double strand breaks, *Dev Biol* 317 (2008) 270-281.
  53. V. Notenboom, R.G. Hibbert, S.E. van Rossum-Fikkert, J.V. Olsen, M. Mann, T.K. Sixma, Functional characterization of Rad18 domains for Rad6, ubiquitin, DNA binding and PCNA modification, *Nucleic Acids Res* 35 (2007) 5819-5830.
  54. J. Kim, M. Guermah, R.K. McGinty, J.S. Lee, Z. Tang, T.A. Milne, A. Shilatifard, T.W. Muir, R.G. Roeder, RAD6-Mediated transcription-coupled H2B ubiquitylation directly stimulates H3K4 methylation in human cells, *Cell* 137 (2009) 459-471.
  55. Y.T. Kwon, Z. Xia, J.Y. An, T. Tasaki, I.V. Davydov, J.W. Seo, J. Sheng, Y. Xie, A. Varshavsky, Female lethality and apoptosis of spermatocytes in mice lacking the UBR2 ubiquitin ligase of the N-end rule pathway, *Mol Cell Biol* 23 (2003) 8255-8271.
  56. Y.T. Kwon, Z. Xia, I.V. Davydov, S.H. Lecker, A. Varshavsky, Construction and analysis of mouse strains lacking the ubiquitin ligase UBR1 (E3 $\alpha$ ) of the N-end rule pathway, *Mol Cell Biol* 21 (2001) 8007-8021.
  57. T. Tasaki, Y.T. Kwon, The mammalian N-end rule pathway: new insights into its components and physiological roles, *Trends Biochem Sci* 32 (2007) 520-528.
  58. H.P. Roest, J. Klaveren van, J. Wit de, C.G. Gulp van, M.H.M. Koken, M. Vermey, J.H. Roijen van, J.T.M. Vreeburg, W.M. Baarends, D. Bootsma, J.A. Grootegoed, J.H.J. Hoeijmakers, Inactivation of the HR6B ubiquitin-conjugating DNA repair enzyme in mice causes a defect in spermatogenesis associated with chromatin modification, *Cell* 86 (1996) 799-810.
  59. M. Barchi, I. Roig, M. Di Giacomo, D.G. de Rooij, S. Keeney, M. Jasin, ATM promotes the obligate XY crossover and both crossover control and chromosome axis integrity on autosomes, *PLoS Genet* 4 (2008) e1000076.
  60. Y. Xu, T. Ashley, E.E. Brainerd, R.T. Bronson, M.S. Meyn, D. Baltimore, Targeted disruption of ATM leads to growth retardation, chromosomal fragmentation during meiosis, immune defects, and thymic lymphoma, *Gene Dev* 10 (1996) 2411-2422.
  61. J. Sun, K. Yomogida, S. Sakao, H. Yamamoto, K. Yoshida, K. Watanabe, T. Morita, K. Araki, K. Yamamura, S. Tateishi, Rad18 is required for long-term maintenance of spermatogenesis in mouse testes, *Mech Dev* 126 (2009) 173-183.
  62. N.K. Kolas, J.R. Chapman, S. Nakada, J. Ylanko, R. Chahwan, F.D. Sweeney, S. Panier, M. Mendez, J. Wildenhain, T.M. Thomson, L. Pelletier, S.P. Jackson, D. Durocher, Orchestration of the DNA-damage response by the RNF8 ubiquitin ligase, *Science* 318 (2007) 1637-1640.
  63. M.S. Huen, R. Grant, I. Manke, K. Minn, X. Yu, M.B. Yaffe, J. Chen, RNF8 transduces the DNA-damage signal via histone ubiquitylation and checkpoint protein assembly, *Cell* 131 (2007) 901-914.
  64. N. Mailand, S. Bekker-Jensen, H. Faustrup, F. Melander, J. Bartek, C. Lukas, J. Lukas, RNF8 ubiquitylates histones at DNA double-strand breaks and promotes assembly of repair proteins, *Cell* 131 (2007) 887-900.
  65. A.A. Davies, D. Huttner, Y. Daigaku, S. Chen, H.D. Ulrich, Activation of ubiquitin-dependent DNA damage bypass is mediated by replication protein a, *Mol Cell* 29 (2008) 625-636.
  66. J.A. Carballo, A.L. Johnson, S.G. Sedgwick, R.S. Cha, Phosphorylation of the axial element protein Hop1 by Mec1/Tel1 ensures meiotic interhomolog recombination, *Cell* 132 (2008) 758-770.
  67. H. Niu, L. Wan, B. Baumgartner, D. Schaefer, J. Loidl, N.M. Hollingsworth, Partner choice during meiosis is regulated by Hop1-promoted dimerization of Mek1, *Mol Biol Cell* 16 (2005) 5804-5818.
  68. L. Wojtasz, K. Daniel, I. Roig, E. Bolcun-Filas, H. Xu, V. Boonsanay, C.R. Eckmann, H.J. Cooke, M. Jasin, S. Keeney, M.J. McKay, A. Toth, Mouse *HORMAD1* and *HORMAD2*, two conserved meiotic chromosomal proteins, are depleted from synapsed chromosome axes with the help of TRIP13 AAA-ATPase, *PLoS Genet* 5 (2009) e1000702.

## SUPPLEMENTARY MATERIALS



**Supplemental Figure S1.** (A, B) Double staining of SYCP3 (red) and RAD51 (green) (A), or double staining of SYCP3 (red) and gH2AX (green) (B) from leptotene to diplotene in wild type spermatocytes. In pachytene, the XY body is shown as an enlarged picture (A), and indicated with arrows (A, B).

**Table S1.** Primer sets used for qPCR

gene name	fw/rev	sequence	annealing temperature
Sly	forward	GTCAGAACCAGACCCTGGAA	59
	reverse	GTTCTTGGTCCCCAAGTTCA	
Ssty	forward	ATACCACAGCAAGGCTACAG	59
	reverse	TCAGGGTGTGGAAGAAGAC	
Gm614	forward	AGACTCTGCCAGCAAATTCC	53
	reverse	TTCAGCATGGGCACAATAGC	
F14Rik	forward	ACCTGGAGCTTGTGGATGG	61
	reverse	CGAGGTACTCTAGGTTTGG	
Eif1ay	forward	CACTTCTCGGCGTTGCCCGT	60
	reverse	GCCTCTACGCCGTTTTTGCCT	
Pgk1	forward	GCACGCTTCAAAGCGCACG	60
	reverse	CACCCTCATCACGACCCGCT	
Atp7a	forward	GTGTCCGGACCATTGAACAG	61
	reverse	GGGGGTTAGCATTGTGGAGA	
Hprt	forward	GTTAAGCAGTACAGCCCCAAA	61
	reverse	AGGGCATATCCAACAACAAACTT	
Gla	forward	TCCCCAACGCTTTCCTAGTG	63
	reverse	CCCCAGTCAGCAAATGTCTG	
Sycp3	forward	TGGGATAATTGAAGATGTTGGA	59
	reverse	GGCTTTGAAAGAAGCTTTGG	
Hils1	forward	GCCAGGACAGACAGAAGAGC	60
	reverse	CACCCCTACGGACTCCTTTGA	
Cd24a	forward	TTCTGGCACTGCTCCTACCC	63
	reverse	CTGGTGGTAGCGTTACTTGG	
Spo11	forward	GCTCCTGGACGACAACCTTCT	60
	reverse	ATCTGCATCGACCAGTGTGA	
Creb3l4	forward	CCTCCGATTGCGATAGACAT	60
	reverse	GCCAGCAGTTGCTTTTCTTC	
Lzp-s	forward	GCCTGTGGGATCAATTGC	59
	reverse	CATGCTCGAATGCCTTGG	
Rad18	forward	TCTGTATGCATGGGACAGGA	59
	reverse	TCAGGTTCCAATTCCTCTGG	
actin	forward	CCGTGAAAAGATGACCCAG	50 - 65
	reverse	TAGCCACGCTCGGTCAGG	



5

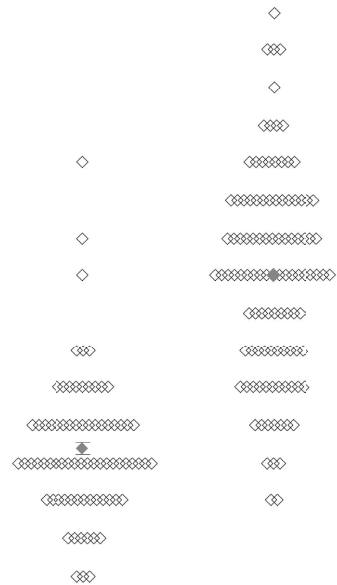
# MEIOTIC RECOMBINATION IS CONTROLLED BY PCNA K164 MODIFICATION

Manuscript in preparation

Akiko Inagaki<sup>1,4</sup>, Peter H. L. Krijger<sup>2,4</sup>, Esther Sleddens-Linkels<sup>1</sup>, Paul. C. M. van den Berg<sup>2</sup>, Evelyne Wassenaar<sup>1</sup>, Marja Ooms<sup>1</sup>, Sam Schoenmakers<sup>1</sup>, Jan H. J. Hoeijmakers<sup>3</sup>, J. Anton Grootegoed<sup>1</sup>, Heinz Jacobs<sup>2,4\*</sup> and Willy M. Baarends<sup>1,4\*</sup>

<sup>4</sup>These authors contributed equally to this work

\* Corresponding authors



<sup>1</sup> Department of Reproduction and Development, Erasmus MC - University Medical Centre, Rotterdam, The Netherlands,

<sup>2</sup> Division of Immunology, The Netherlands Cancer Institute, 1066 CX Amsterdam, Netherlands

<sup>3</sup> Department of Genetics and Cellbiology, Erasmus MC - University Medical Centre, Rotterdam, The Netherlands

## ABSTRACT

Proliferating cell nuclear antigen (PCNA) is known to be modified by either ubiquitin(s) or small ubiquitin-like modifier(s) (SUMO) at the conserved lysine 164 residue (K164) in *S. cerevisiae*, while no SUMOylated PCNA has been detected in mammalian cells to date. Previous studies have shown that homozygous *Pcna*<sup>K164R/K164R</sup> knockin mice display severe defects in germ cell development. Here we have analysed the function of PCNA modification in spermatogenesis in more detail. We show that the essential role of PCNA modification for primordial germ cell survival and/or proliferation is independent of a functional HR6B/RAD18 complex, that functions upstream of PCNA ubiquitylation. In addition, mutation of *Polymerase*  $\eta$  or double knockout of *Htfl/Shprh*, that are enzymes known to function downstream of the PCNA ubiquitylation, do not affect primordial germ cell development. However, we cannot exclude partial redundancy between different enzymes involved in translesion synthesis.

In heterozygote *Pcna*<sup>WT/K164R</sup> knockin mice, we observed an increase of 20% in meiotic recombination frequency in comparison to wild type controls. We show that although HR6B also modifies meiotic recombination, PCNA modification and HR6B most likely act independently in this mechanism. HR6B regulates the number of meiotic DSBs, whereas PCNA modification regulates the choice between crossover and noncrossover formation. We propose that PCNA SUMOylation rather than ubiquitylation is required to recruit an anti-recombinogenic downstream helicase in meiotic prophase nuclei. Increased meiotic recombination is the only phenotypic defect that has been observed to date in heterozygote *Pcna*<sup>WT/K164R</sup> knockin mice. This points to a possible requirement for SUMOylation of all three subunits of the homotrimeric PCNA ring, whereas ubiquitylation of a single PCNA subunit may be sufficient for functionality.

**Key words:** PCNA K164, meiosis, recombination, ubiquitylation, SUMOylation

## INTRODUCTION

Proliferating cell nuclear antigen (PCNA) is a processive clamp for DNA polymerases and an essential binding platform for numerous proteins involved in DNA replication, repair, and cell cycle regulation. PCNA forms a homotrimer that encircles double-stranded DNA, and operates as a sliding clamp to keep the DNA polymerase machinery firmly on the DNA during DNA replication (reviewed in [1]).

During DNA replication, the presence of unrepaired DNA lesions threatens to block progression of the replication machinery, which might result in the formation of DNA double-strand breaks (DSBs) and gross chromosomal rearrangements, or even to a permanent cell-cycle arrest and cell death. Replication damage bypass (RDB) is a special pathway that allows progression of DNA replication without actually removing the lesion (reviewed in [2]).

In *Saccharomyces cerevisiae*, the E2 ubiquitin-conjugating enzyme Rad6 is essential for this pathway. Depending on interactions with downstream components, error-free or error-prone sub-pathways can be activated. The first step in both pathways involves mono-ubiquitylation of PCNA at conserved lysine residue 164 (K164) by the Rad6-Rad18 complex, in which Rad18 acts as an ubiquitin ligase (E3 enzyme) [3]. Mono-ubiquitylation of PCNA by the Rad6-Rad18 complex recruits specific translesion synthesis (TLS) polymerases that can incorporate nucleotides in the strand opposite the site of the DNA lesions, and this process may usually be error-prone (reviewed in [4,5]). Alternatively, mono-ubiquitylation by the Rad6-Rad18 complex may be followed by Rad5-Mms2-Ubc13-mediated poly-ubiquitylation [3]. This polyubiquitylation involves the formation of K63-linked polyubiquitin chains. Ubc13 is the only known enzyme that can stimulate the formation of K63-linked polyubiquitin chains. K48-linked polyubiquitylation usually targets substrates for degradation by the proteasome, whereas K63-linkage does not. The E3 ubiquitin ligase Rad5 interacts with both the Rad6-Rad18 and the Mms2-Ubc13 complexes to stimulate poly-ubiquitylation of PCNA. Subsequently, polyubiquitylated PCNA enables template switching to the intact sister chromatid and as a consequence an error-free damage bypass pathway can be activated [6]. In *S. cerevisiae*, K164 residue of PCNA is known to be modified not only by ubiquitin but also by small ubiquitin like modifier (SUMO) [3]. This modification is mediated by the SUMO ligase Siz1 and causes the recruitment of a helicase Srs2 to replication forks during S phase in order to prevent unwanted crossover events through its ability to disrupt Rad51 nucleoprotein filaments [7-11]. Srs2 was originally identified as a suppressor of *rad6* and *rad18* mutants, and has been previously proposed to be a regulator of the Rad6-dependent pathways [12].

Functional orthologs of proteins involved in the RDB pathway have been identified in mammals, implying that this pathway is generally well conserved [13]. In mammalian cells, RAD18 complexes with the mammalian orthologs of yeast Rad6, HR6A (UBE2A) and HR6B (UBE2B) [14], and mediates PCNA mono-ubiquitylation at K164 when the replication machinery is stalled by UV-induced DNA damage to recruit one of the TLS polymerase families, Pol $\eta$  [15]. Mammalian orthologs of yeast Rad5, HLF and SHPRH, mediate PCNA polyubiquitylation with mammalian MMS2-UBC13, and

maintain genomic stability probably via the conserved error-free pathway of RDB [16-19]. PCNA is highly conserved as is K164, suggesting that PCNA might be regulated by SUMOylation as well as ubiquitylation in mammals, in a manner similar to that in *S. cerevisiae*. However, no SUMOylated forms have so far been detected in mammalian PCNA.

Recently, mice carrying a lysine (K) to arginine (R) mutation at lysine residue 164 of PCNA (K164R) were generated, using two different approaches [20,21]. In the first approach, knockin mice carrying the K164R mutation in *Pcna* were generated [20], whereas in the second approach a transgene carrying the K164R mutation was expressed on a *Pcna* knockout background [21]. Both K164R mouse models showed reduced somatic hypermutation and male infertility, but the K164R knockin mice showed a much severer phenotype, in particular in the testis [20] than the K164R transgenic mice. The latter displayed meiotic arrest in early pachytene with elongated chromosome axes [21], whereas no germ cells were detected in testes from K164R *Pcna* knockin mice [20]. The difference in phenotypes might be caused by differences in expression level of mutant PCNA; if the transgene is overexpressed, this may somehow help to overcome the lack of PCNA modification, resulting in a less severe phenotype. The role of PCNA modification in gametogenesis is at present unknown. The mammalian Rad6 orthologs HR6A and HR6B have essential functions in female and male gametogenesis, respectively [22,23], but it is not known whether any of the reproductive functions of HR6A and HR6B depends on the ability of HR6A and HR6B to ubiquitylate PCNA. Elongated chromosomal axes in spermatocyte nuclei as described for the transgenic K164R mice [21] have also been observed in *Hr6b* knockout mice [24]. In *Hr6b* knockout mice, these elongated axes are associated with increased meiotic recombination frequency ([24], see also below). This fits with the general correlation between chromosomal axis length and meiotic recombination frequency that has been described [25]. Meiotic recombination is initiated with the induction of meiotic DSBs by the topoisomerase II-like enzyme SPO11. In mitotic cells, DSBs may be repaired either through the non-homologous end-joining pathway (NHEJ) or via homologous recombination (HR). In meiotic cells, the error-prone NHEJ process is repressed [26], leaving HR as the only available pathway for repair. HR, using one of the chromatids of the homologous chromosome as a template for repair, may lead to the formation of crossovers. In mouse and man only a small minority of the DSBs lead to the formation of crossovers, but each chromosome pair has at least one (obligate) crossover. Repair of most meiotic DSBs leads to so-called gene conversions or noncrossovers (reviewed in [27]). Repair of meiotic DSBs is accompanied by, and essential for, chromosome pairing and synapsis of homologous chromosomes. Synapsis is achieved through the formation of the synaptonemal complex (SC) along the chromosomal axes of the paired chromosomes. The SC consists of two lateral elements that follow the chromosomal axes of each chromosome, connected by a central element. Before synapsis, the lateral elements are called axial elements, and these start to form in the leptotene stage of meiotic prophase, when the DSBs have just formed. In zygotene, the axial elements are complete and synapsis is initiated. In pachytene, synapsis is complete. At this stage, the crossover sites can be visualized through immunocytochemical analysis of the

mismatch repair enzyme MLH1. This protein forms a single focus at each crossover site on the SC. Subsequently, the SC is disassembled in diplotene, and in metaphase I, the actual crossovers are visible as chiasmata. The number of crossovers is tightly regulated. A mechanism termed crossover interference reduces the likelihood of two crossovers occurring in close proximity of one another. Furthermore, it is ensured that each chromosome pair contains at least a single crossover site. The most outspoken change in crossover frequency is observed in mice that are deficient for the ubiquitin conjugating enzyme HR6B [24]. *Hr6b* knockout male mice are infertile, associated with dysregulation of chromatin structure in meiotic and post-meiotic cells [23,24,28]. In late pachytene nuclei of these cells, the SCs are longer, and the number of MLH1 foci is 20% increased in comparison to controls [24], but crossover interference is not affected [29].

Herein, we analyzed the mice carrying a point mutation at lysine K164 (K164R) in *Pcna* to study the role of K164 modification of PCNA during spermatogenesis. In addition, we analysed the meiotic phenotype of several knockout mouse models that carry mutations in genes that function downstream or upstream of PCNA ubiquitylation in the RDB pathway.

## MATERIALS AND METHODS

### Mice

Generation of PCNA K164R knockin mice [20] and *Polh* knockout mice [30] has been described. *HLTF/SHPRH* double knockout mice were kindly provided by Kyungjae Myung (National Institute of Health, USA).

### Antibodies

For primary antibodies, we used the mouse monoclonal antibodies anti-MLH1 (Becton and Dickinson), the rabbit polyclonal antibodies anti- RAD51 [31], and anti-SYCP3 (gift from C. Heyting). For secondary antibodies, we used a goat anti-rabbit IgG alexa 488/564 or goat anti-mouse alexa IgG 488/564 (Molecular Probes).

### Meiotic spread nuclei preparations and immunocytochemistry.

Testis tissues were processed to obtain spread nuclei for immunocytochemistry as described by Peters et al [32]. Spread nuclei of spermatocytes were stained with antibodies mentioned above. Before incubation with antibodies, slides were washed in PBS (3x10 min), and non-specific sites were blocked with 0.5% w/v BSA and 0.5% w/v milk powder in PBS. Primary antibodies were diluted in 10% w/v BSA in PBS, and incubations were overnight at room temperature in a humid chamber. Subsequently, slides were washed (3x10 min) in PBS, blocked in 10% v/v normal goat serum (Sigma) in blocking buffer (supernatant of 5% w/v milk powder in PBS centrifuged at 14,000 rpm for 10 min), and incubated with secondary antibodies in 10% normal goat serum in blocking buffer at room temperature for 2 hours. Finally, slides were washed (3x10 min) in PBS (in the dark) and embedded in Prolong Gold with DAPI (invitrogen).

### Histological analysis and TUNEL assay

Testes were isolated from control, *Hltf/Shprh* double knockout, *Polη* knockout, heterozygous PCNA<sup>WT/K164R</sup>, and homozygous PCNA<sup>K164R/K164R</sup> mice that were 2 and 4 weeks old. Testes were fixed in 4% paraformaldehyde (TUNEL) or Bouin's fixative for morphological analysis, and embedded in paraffin according to standard procedures. For histological analysis, mounted sections were deparaffinized, rehydrated, and stained with hematoxylin and eosin. For TUNEL assay, sections were mounted on aminoalkylsilane-coated glass slides, dewaxed, and pretreated with protease K (Sigma) and peroxidase as described elsewhere [33]. Slides were subsequently washed in terminal deoxynucleotidyl transferase (TdT) buffer for 5 min [34] and then incubated for at least 30 min in TdT buffer containing 0.01 mM Biotin-16-dUTP (Roche) and 0.4 U of TdT enzyme (Promega). The enzymatic reaction was stopped by incubation in TB buffer, and the sections were washed [33]. Slides were then incubated with StreptABCComplex-horseradish peroxidase conjugate (Dako) for 30 min and washed in PBS. dUTP-biotin labelled cells were visualized with 3,3-diaminobenzidine tetrahydrochloride-metal concentrate (Pierce, Rockford). Tissue sections were counterstained with nuclear fast red-5% (wt/vol) (Al<sub>2</sub>(SO<sub>4</sub>)<sub>3</sub>). For each animal, the number of TUNEL (terminal deoxynucleotidyltransferase-mediated dUTP-biotin nick end labeling)-positive cells was counted in at least 200 tubule sections, and the average number of positive cells per 100 cross sections was calculated. Data were analyzed by using the Mann-Whitney U test.

### Confocal microscopy

Images of cells were obtained using a Zeiss LSM510NLO microscope (Carl Zeiss) with a 63 × /1.40 NA oil immersion lens. Proteins stained with alexa 488 were detected by exciting the probes with a 488 nm Argon gas laser and monitoring the emission through a 500-550 band-pass filter. Proteins stained with alexa 564 were detected by exciting the probes with a 543 nm helium neon laser and monitoring the emission through a long-pass 560 filter. To minimize the effect of photo-bleaching, images were taken with 10 μW for a 488 nm laser, and with 20 μW for a 543 nm laser. For quantification of immunofluorescent signal, slides were analyzed on the same day. Fluorescent images were taken under identical conditions for all slides, and images were analysed using the ImageJ software (Rasband, W.S., ImageJ, U.S. National Institutes of Health, Bethesda, Maryland, USA [<http://rsb.info.nih.gov/ij/>]). Nuclei were selected and the mean signal ( $\mu$ ) and standard deviation ( $\sigma$ ) was calculated by Image J software, and threshold was determined [35]. To count the number of RAD51 foci, threshold was set at;  $\mu + 2.5\sigma$ , and the number of foci was calculated using Image J. To prevent counting of non-specific background as RAD51 foci, areas less than 2 pixels were excluded from counting.

## RESULTS

### Lack of primordial germ cells in homozygous *PCNA<sup>K164R/K164R</sup>* mice, and increased apoptotic cells in heterozygous *PCNA<sup>WT/K164R</sup>* mice

We previously found that mutation of lysine 164 of PCNA (K164R) leads to infertility in both female and male mice, in association with complete absence of germ cells [20]. All wild-type, heterozygous, and homozygous mice showed similar body weight, while the testis of *PCNA<sup>K164R/K164R</sup>* mice weighed only 20% of testis of wild type and *PCNA<sup>WT/K164R</sup>* mice (Figure 1A). Next, we analyzed young mice to study whether some germ cells, including cells in meiotic prophase, might still be present in immature testes.

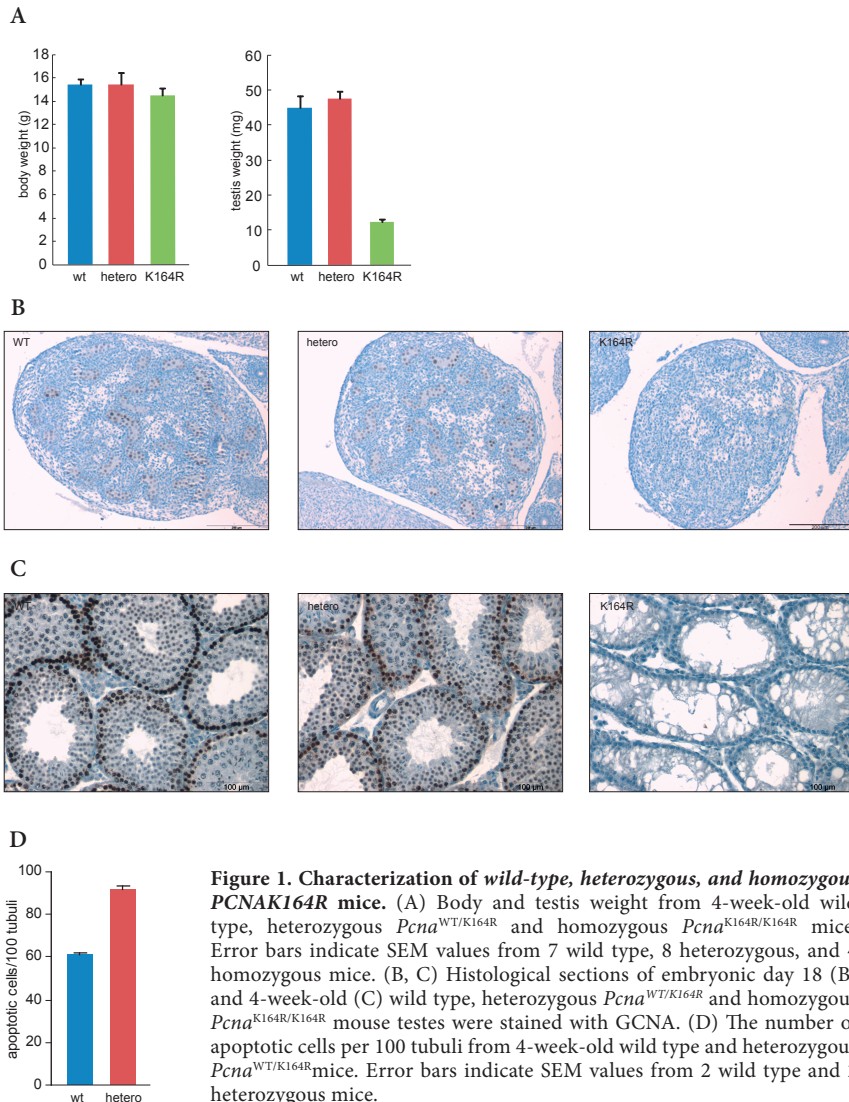


**Figure 1. Characterization of wild-type, heterozygous, and homozygous *PCNA<sup>K164R</sup>* mice.** (A) Body and testis weight from 4-week-old wild type, heterozygous *Pcna<sup>WT/K164R</sup>* and homozygous *Pcna<sup>K164R/K164R</sup>* mice. Error bars indicate SEM values from 7 wild type, 8 heterozygous, and 4 homozygous mice. (B, C) Histological sections of embryonic day 18 (B) and 4-week-old (C) wild type, heterozygous *Pcna<sup>WT/K164R</sup>* and homozygous *Pcna<sup>K164R/K164R</sup>* mouse testes were stained with GCNA. (D) The number of apoptotic cells per 100 tubuli from 4-week-old wild type and heterozygous *Pcna<sup>WT/K164R</sup>* mice. Error bars indicate SEM values from 2 wild type and 2 heterozygous mice.

However, similar to our previous observations [20], already in 4-week-old mice, the seminiferous tubules were devoid of germ cells. To investigate this further, we decided to analyse testes before birth. Primordial germ cells arise outside the gonads and migrate into the gonads around day 11 of mouse embryonic development (E11). During this period, the primordial germ cells increase in number through mitotic proliferation. Around E13, the germ cells enter a mitotic arrest, which is maintained until the process of spermatogenesis is initiated shortly after birth. In E18, neither seminiferous tubules formation nor primordial germ cells were found in PCNA<sup>K164R/K164R</sup> mice, suggesting a developmental retardation of gonads as well as primordial germ cells (Figure 1B). The lack of germ cells in homozygous PCNA<sup>K164R/K164R</sup> mice indicates that modification of PCNA is essential for the proliferation or survival of primordial germ cells. Heterozygous PCNA<sup>WT/K164R</sup> mice did not show any phenotype with respect to the number of germ cells compared with wild-type (Figure 1B and C). However, we observed an approximately 1.5-fold increase in the number of apoptotic spermatocytes in heterozygous PCNA<sup>WT/K164R</sup> mice by TUNEL at age of 4 weeks (Figure 1D). Downstream of PCNA monoubiquitylation by HR6A/B-RAD18, Pol  $\eta$  can be recruited to mediate error-prone RDB. Alternatively, RAD5 orthologs may mediate PCNA polyubiquitylation together with UBC13, to allow error free RDB. To analyse whether impairment of any of these downstream events may cause the loss of germ cells in the homozygous PCNA knockin mice, and the increased apoptosis of the heterozygote, we analysed testes from mice that carried mutations in both mouse RAD5 orthologs, *Hltf/Shprh* double knockout mice (Figure 2A) and from *Pol $\eta$*  knockout mice (Figure 2B). The total number of germ cells as well as the number of apoptotic spermatocytes was not different from controls in testis sections from these mice (Figure 2C and D).

### Normal SYCP3 length in pachytene spermatocytes of PCNA<sup>WT/K164R</sup> mice

Although we could not identify meiotic prophase cells in *Pcna*<sup>K164R/K164R</sup> testes, the increased apoptosis of spermatocytes in the heterozygotes suggested a meiotic phenotype in these mice. Since elongated chromosomal axes have been reported for spermatocytes from transgenic *Pcna*<sup>-/-tgK164R</sup> mice [21], we analysed this parameter in our heterozygous PCNA<sup>WT/K164R</sup> mice. The length of SYCP3 was measured in MLH1-positive mid-pachytene nuclei. In contrast to transgenic PCNA K164R mice, we did not find elongation of SYCP3 length in PCNA<sup>WT/K164R</sup> mice (Figure 3A).

### PCNA modification regulates meiotic recombination frequency

In *S. cerevisiae*, PCNA SUMOylation is mediated by the SUMO ligase Siz1 and this modification causes the recruitment of the helicase Srs2 to replication forks during S phase. At these sites, Srs2 prevents unscheduled crossover events through its ability to disrupt Rad51 nucleoprotein filaments [7-11,36]. To investigate whether PCNA modification may control meiotic crossover frequency in mice, we examined the nuclear localization of RAD51 and MLH1 in meiotic spread preparations of wild type and PCNA<sup>WT/K164R</sup> spermatocytes. RAD51 functions as a single-stranded DNA-binding protein that has DNA-dependent ATPase activity and stimulates strand exchange.

This protein accumulates in foci in leptotene and zygotene spermatocytes. These foci depend on the presence of the DSB-inducing enzyme SPO11, and are therefore thought to represent meiotic DSB repair sites. We observed no abnormalities in the overall pattern of RAD51 localization in PCNA<sup>WT/K164R</sup> spermatocytes (data not shown). In addition, the number of RAD51 foci in leptotene nuclei was not different between wild type and PCNA<sup>WT/K164R</sup> spermatocytes (Figure 3B). Subsequently, MLH1 foci were counted in mid-to-late pachytene spermatocytes to determine the crossover number. Intriguingly, we detected an increased number of MLH1 foci in PCNA<sup>WT/K164R</sup> pachytene spermatocytes (27.0 +/- 0.1) compared to wild type pachytene spermatocytes (22.3 +/- 0.2) (Figure 3C and D). The same analyses were performed for testes from *Hltf/Shprh* (Figure 4A), and *Polη* (Figure 4B) deficient mice, but no differences in the number of MLH1 foci between the knockouts and control mice were observed. Previously, we have shown that spermatocytes from *Hr6b* knockout mice also show a significantly increased number of MLH1 foci [24]. To analyse whether these effects on meiotic recombination could occur through the same pathway, we also analysed the number of RAD51 foci in *Hr6b* knockout mice. In contrast to the normal number of RAD51 foci in leptotene PCNA<sup>WT/K164R</sup> spermatocytes, an increased number of RAD51 foci was found in leptotene and zygotene *Hr6b* knockout spermatocytes compared with wild type spermatocyte (Figure 3E). This indicates that in *Hr6b* knockout mice, an increased number of meiotic DSBs can explain the increased number of MLH1 foci. In addition, we found that the increased number of RAD51 foci in *Hr6b* knockout mouse spermatocytes was not damage-induced but SPO11 dependent (Figure 3E). Taken together, these results suggest that the increased number of crossover sites observed in PCNA<sup>WT/K164R</sup> and *Hr6b* knockout mice are regulated by distinct mechanisms.

## DISCUSSION

In yeast, K164 of PCNA is known to be modified by ubiquitin, and also by SUMO, depending on the context [3]. PCNA SUMOylation is a key regulator to suppress unwanted homologous recombination and to facilitate error-free RDB during replication in yeast somatic cells [8,9]. Here we have analysed the role of PCNA K164 modification during spermatogenesis in mice.

### PCNA modification is crucial for proliferation of primordial germ cells

Our results show that disruption of the modification of PCNA at K164 residue results in the complete absence of primordial germ cells. The number of primordial germ cells was not reduced in the heterozygote, in *Polη*-deficient testes nor in testis of a double mutant for the mouse *Rad5* homologs. This raises the question whether this defect is caused by defective SUMOylation or ubiquitylation. PCNA ubiquitylation is thought to depend on the HR6A/B-RAD18 complex. Mice deficient for HR6A or HR6B have normal numbers of primordial germ cells (our own unpublished observations), and double-mutant mice are not viable. *Rad18* knockout mice show no overt defects in spermatogenesis in young adults, indicating that the number of spermatogonial stem cells is normal [37]. We have analyzed *Rad18* knockdown mice, and also observed that

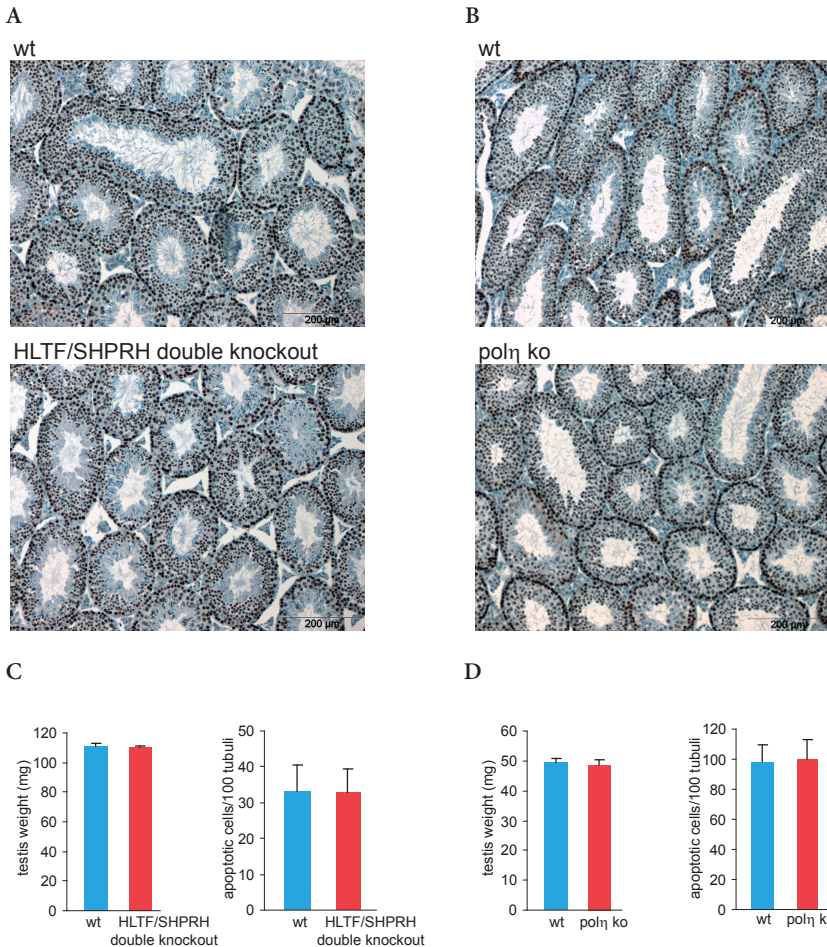


**Figure 2. Characterization of *Hltf/Shprh* double knockout and *Polh* knockout mice.** (A, B) Histological sections of 4-week-old wild type and knockout testes of *Hltf/Shprh* double knockout (A) and *Polh* knockout (B) mice were stained with GCNA. (C, D) Body and testis weight from 4-week-old wild type and knockout testes of *Hltf/Shprh* double knockout (C) and *Polh* knockout (D) mice. Error bars indicate SEM values from 3 wild type and 3 knockout mice.

the number of spermatogonial stem cells was normal (Inagaki et al., manuscript in preparation). These data indicate that primordial germ cell proliferation/survival might be independent of PCNA ubiquitylation. Alternatively, another E2/E3 complex may mediate basal PCNA ubiquitylation required for primordial germ cell proliferation/survival. In this context it is of interest to note that a severe reduction of stem cells has also been observed in *Rev1*-deficient mice (our own unpublished observations). These mice display transient growth retardation, and defects in C/G transversions in hypermutating immunoglobulin genes [38]. Similar to POL $\eta$ , REV1 is a Y polymerase that can be recruited to a damaged replication template by mono-ubiquitylated PCNA

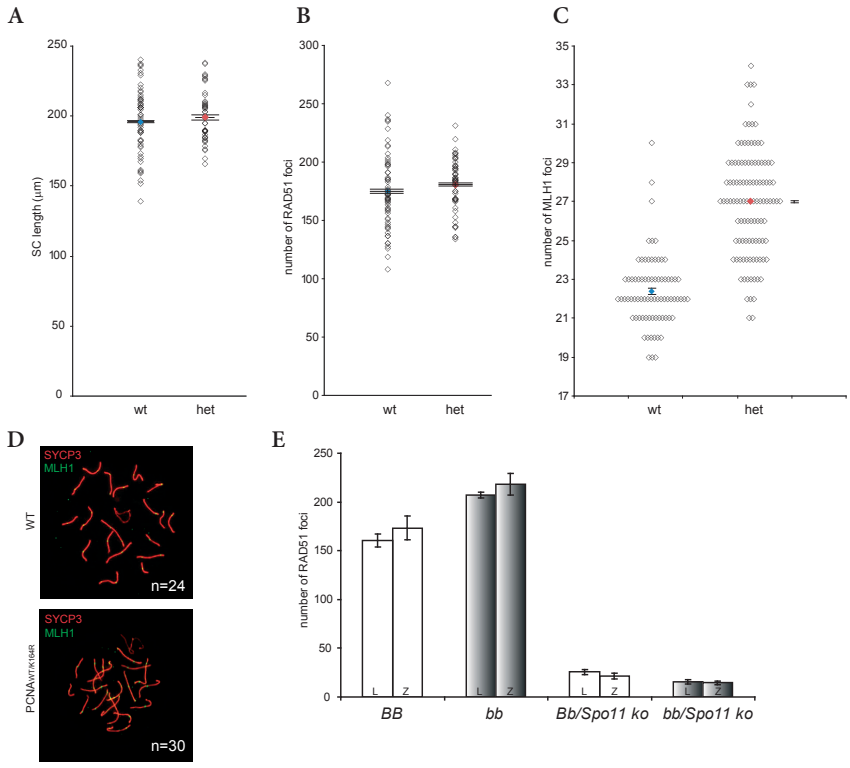


**Figure 3. Increased number of MLH1 foci in *PCNA*<sup>WT/K164R</sup> mice.** (A) The SC length was measured in pachytene nuclei (see materials and methods) of 4-week-old wild type (wt) and heterozygous *PCNA*<sup>WT/K164R</sup> (het) mice. Error bars indicate SEM values from 20 nuclei of 4 independent mice. (B) The number of RAD51 foci in leptotene nuclei was counted (see materials and methods) in 2-week-old wild type (wt) and heterozygous *PCNA*<sup>WT/K164R</sup> (het) mice. Error bars indicate SEM values from 30 nuclei of 2 independent mice. (C) The number of MLH1 foci in pachytene nuclei was counted in 4-week-old wild type (wt) and heterozygous *Pcna*<sup>WT/K164R</sup> (het) mice. Error bars indicate SEM values from 20 nuclei of 4 independent mice. (D) Double immunostaining of 4-week-old wild type and heterozygous *Pcna*<sup>WT/K164R</sup> spermatocyte nuclei with anti-SYCP3 (red) and anti-MLH1 (green). (E) The number of RAD51 foci in leptotene (L) and zygotene (Z) nuclei was counted (see materials and methods) in 4-week-old wild type (BB), *Hr6b* knockout (bb), heterozygous *Hr6b* in *Spo11* knockout (Bb/Spo11ko), and *Hr6b/Spo11* double knockout (bb/Spo11ko) mice. Error bars indicate SEM from 16 nuclei in 2 independent mice.

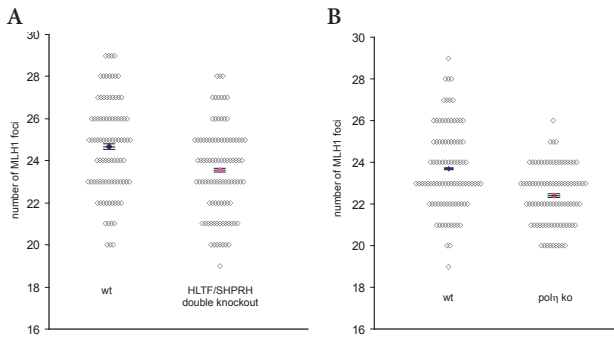


**Figure 4. Normal MLH1 foci numbers in *Hltf/Shprh* and *Polh* knockout mice.** (A, B) The number of MLH1 foci in pachytene nuclei was counted in 4-week-old wild type and *Hltf/Shprh* double knockout (A) and *Polh* knockout (B) mice. Error bars indicate SEM values from 20 nuclei of 3 independent mice.

[38-40]. Another DNA repair enzyme that is required for primordial germ cell survival and proliferation is FANCC [41]. This protein is part of an E3 ubiquitin ligase complex that ubiquitylates FANCD2/FANCI complex in the Fanconi anaemia (FA) pathway of DNA damage signalling. Apparently, primordial germ cells have special requirements for the RDB and FA pathways.

Roa et al. showed that in *Pcna*<sup>-/-</sup>*tg*<sup>K164R</sup> mice, germ cells are able to reach the early pachytene stage [21]. Although it is possible that the number of stem cells is also reduced in these mice, the phenotype is obviously milder. This difference may be explained by possible differences in genetic background (FVB versus C57BL/6J) of the two strains, or the two- to eight-fold overexpression of the mutant PCNA transgene in the *Pcna*<sup>-/-</sup>*tg*<sup>K164R</sup> mice may somehow rescue part of the defect [21].

### **HR6B modifies meiotic recombination frequency through regulation of the number of meiotic DSBs**

Crossovers are crucial for faithful meiotic chromosome segregation, and their formation requires the formation of programmed DSBs by SPO11 [42], followed by HR repair using one of the chromatids of the homologous chromosome as a template for repair. When DSB formation is reduced in *S. cerevisiae spo11* mutants, normal meiotic crossover frequencies are maintained. This phenomenon is referred to as crossover homeostasis [43]. Overexpression of Spo11 in *S. pombe* does not increase meiotic frequency above wild type levels [44], and in *C. elegans* there are indications that crossover homeostasis also quenches the effect of extra (radiation)-induced DSBs on crossover frequencies. In mice, the induction of approximately 100 extra DSBs through irradiation leads to only 1 extra crossover site on average, indicating that these breaks are preferentially repaired via noncrossover pathways. Previously, we had shown that *Hr6b*-deficient spermatocytes show an approximately 20% increase in meiotic recombination frequency. Here we show that this increase can be explained by a 15% increase in SPO11-induced DSB formation. Lynn et al. have shown that there appears to be a positive correlation between normal length of the SC and the number of meiotic recombination sites, indicating that the length of the SC reflects genetic rather than physical distance [25]. In *Hr6b* knockout mice, in accordance with the increased recombination rate, we also measured an increase in SC length in comparison to wild type, but this effect was only seen in late pachytene nuclei. This suggests that the increased SC length may be a manifestation of aberrant chromatin structure caused by *Hr6b* deficiency [24,28]. Still, aberrant chromatin structure, leading to a more open chromatin configuration, may allow the formation of more DSBs in leptotene, and subsequent extra crossover sites. In *C. elegans*, chromosome axis length is determined by condensin [45], which in turn controls the number of meiotic DSBs. Introducing extra DSBs with ionizing radiation or eliminating meiotic DSB formation altogether using a *Spo11* mutation had no effect on axis length in either the wild type or in the condensin I complex mutants [45], indicating that axis length is not influenced by DSBs, but axis structure regulates DSB frequency. If this mechanism is conserved from worm to mouse, it might be suggested that HR6B may functionally interact with

condensin, regulating chromosome structure and hence, the number of DSBs, SC length, and crossover frequency.

### PCNA modification at K164 regulates crossover frequency

In contrast to the positive correlation between the number of DSBs, SC axis length and crossover frequency in *Hr6b* knockout spermatocytes, we observed a 19% increase in the number of MLH1 foci in *Pcna*<sup>WT/K164R</sup> mice compared to controls, but no effect on the number of DSBs or SYCP3 length. Thus, although this indicates that both PCNA K164 modification and HR6B activity regulate meiotic crossover frequency to the same extent, they may operate via distinct and independent mechanisms. In support of this conclusion, we have not found an effect of RAD18 depletion in testes on meiotic recombination frequency (Inagaki et al., manuscript in preparation), indicating that HR6B regulates crossover frequency independent of the RDB pathway, possibly involving functional interaction with condensins, as described above. For PCNA, the regulation of crossover frequency through its modification at K164, most likely involves modification of the choice between crossover and noncrossover pathways, since the number of meiotic DSBs in leptotene was not different from controls. PCNA has been implicated in the suppression of recombination events during replication [8,9]. This function of PCNA requires its SUMOylation at K164. This modification recruits the helicase Srs2 [8,9]. Srs2 functions as an anti-recombinase through different mechanisms during separate stages of HR. At an early stage, Srs2 dismantles the RAD51 presynaptic filament. During the next stage of HR, when RAD51 coated ssDNA has invaded the homologous template, Srs2 disrupts the D-loop intermediate [7,46]. It has not yet been established whether this mechanism is also operative in mammals, but several possible functional homologs of Srs2 have been identified. Three different proteins, named RecQL5, FBH1 and BLM have been shown to be able to displace RAD51 from ssDNA and to suppress recombination [47-49]. BLM and an additional possible functional Srs2 homolog named RTEL1 have been shown to dissociate D-loop recombination intermediates [47,50]. In *C. elegans*, mutation of *Rtel1* leads to elevated numbers of crossover [51]. Taking these data into account it may be suggested that the effect of K164 mutation on recombination frequency that we observed is caused by a lack of PCNA SUMOylation, leading to decreased function of downstream anti-recombinogenic helicases at sites of meiotic DSB repair. An attractive candidate helicase that may function downstream of PCNA SUMOylation in meiosis is BLM. BLM localizes as foci in leptotene and zygotene nuclei. Using a conditional knockout approach, it was recently shown that deletion of *Blm* leads to a dramatic increase in meiotic recombination frequency in affected cells [52]. To obtain more insight in the possible anti-recombinogenic effect of the K164R mutation we analyzed RAD51 and RPA foci in zygotene and pachytene spermatocytes of wild type and *Pcna*<sup>WT/K164R</sup> mice, but no overt change in the patterns of RAD51 and RPA foci was observed (data not shown). However, it must be noted that the foci pattern were highly dynamic, making it impossible to detect subtle shifts in the appearance and disappearance of RAD51 and RPA foci. Further investigations are required to determine which, if any, helicase is recruited to regulate meiotic crossover frequency via SUMOylated PCNA. In addition,

it will be important to establish whether the distribution of crossovers is similar in spermatocytes of wild type and heterozygote mice.

### PCNA ubiquitylation and SUMOylation

Due to the virtually complete absence of germ cells from *Pcna*<sup>K164R/K164R</sup> mouse testes, we were unable to analyse the effect of complete absence of K164 modification on recombination frequency. Considering the homotrimeric structure of PCNA, wild type PCNA from control mice and mutated PCNA from homozygous *Pcna*<sup>K164R/K164R</sup> mice will form monomorph PCNA trimers that can be normally modified in the wild type, and for which all K164 modification is prevented in the homozygous mutant mice. In *Pcna*<sup>WT/K164R</sup> heterozygotes, four distinct compositions of the trimeric PCNA ring are possible from the combination of 3WT PCNA molecules, 2WT+1K164R PCNA molecule, 1WT+2K164R PCNA molecules, and 3K164R PCNA molecules at a ratio of 1:3:3:1. Langerak et al. described that the presence of only a single wild type *Pcna* allele might be enough for a normal damage tolerance function of ubiquitylated PCNA rings, since seven out of eight PCNA trimer complexes can be ubiquitylated at one site at least in heterozygous mice [20]. From this perspective, it is very surprising that we observed a relatively strong increase in meiotic recombination frequency in the heterozygote mice. The detrimental effect of the presence of 50% of K164R mutated and 50% wild type PCNA indicates that perhaps for this function of PCNA, all three subunits of the PCNA trimer need to be modified in order to function properly. Since this is expected to happen for only 1/8<sup>th</sup> of the trimeric PCNA rings, this may explain why the heterozygote displays such a dramatic effect on recombination frequency. Taken together with the above described data that point to a function of PCNA SUMOylation instead of PCNA ubiquitylation in the regulation of meiotic recombination, it might be suggested that SUMOylation is only effective when all three PCNA subunits are modified, whereas the ubiquitylation of a single PCNA in the ring is sufficient to stimulate the RDB pathway. SUMOylation of PCNA has not been reported for mammalian cells. So far, we have also been unable to establish that PCNA is modified by SUMO in wild type testes. This may be caused by active deSUMOylation during protein isolation, lack of proper antibody recognition, or actual lack of PCNA SUMOylation.

In summary, we have shown that PCNA modification at K164 is essential for the survival and/or proliferation of primordial germ cells. This most likely involves PCNA ubiquitylation, since the phenotype is similar to what we observed in *Rev1*-deficient mouse testes. However, since RAD18-deficient mouse testis appear to contain normal numbers of primordial germ cells, and the mutation in catalytic site of REV1 does not interfere the interaction with ubiquitylated PCNA, the observed lack of primordial germ cells in the *Pcna* mutant mice could be caused by defective SUMOylation instead of ubiquitylation. Moreover, it might be suggested although the phenotype of *Rev1* catalytic mutant mice and the PCNA K164 mutant are similar, they are not functionally related. Heterozygote *Pcna*<sup>WT/K164R</sup> mouse testes have normal numbers of spermatogonial stem cells, indicating that a single wild type allele is sufficient to rescue the primordial germ cells, similar to the wild type properties of *Pcna*<sup>WT/K164R</sup> mouse cells with respect to DNA repair. In contrast, meiotic recombination frequency is 20%

higher in heterozygote K164R mutant mouse spermatocytes compared to wild types. We speculate that this phenotype is caused by defective PCNA SUMOylation, resulting in reduced recruitment of a downstream anti-recombinogenic helicase, possibly BLM protein. We propose that this function requires SUMOylation of all three subunits of the homotrimeric PCNA ring.

## ACKNOWLEDGEMENTS

We thank Dr. Hein te Riele and Dr. Sandra de Vries (The Netherlands Cancer Institute, Amsterdam, The Netherlands) for *Spo11* mutant mice, Dr. Kyungjae Myung (National Institute of Health, USA) for *HLTF/SHPRH* double knockout mice, and Dr. Claude-Agnès Reynaud (Institut National de la Santé et de la Recherche Médicale, France) for *Polη* knockout mice.

This work was supported by the Netherlands Organization for Scientific Research (NWO) through ALW (VIDI 864.05.003).

## REFERENCES

- H.D. Ulrich, Regulating post-translational modifications of the eukaryotic replication clamp PCNA, *DNA Repair (Amst)* 8 (2009) 461-469.
- H.D. Ulrich, The RAD6 pathway: control of DNA damage bypass and mutagenesis by ubiquitin and SUMO, *Chembiochem* 6 (2005) 1735-1743.
- C. Hoegel, B. Pfander, G.L. Moldovan, G. Pyrowolakis, S. Jentsch, RAD6-dependent DNA repair is linked to modification of PCNA by ubiquitin and SUMO, *Nature* 419 (2002) 135-141.
- A.R. Lehmann, A. Niimi, T. Ogi, S. Brown, S. Sabbioneda, J.F. Wing, P.L. Kannouche, C.M. Green, Translesion synthesis: Y-family polymerases and the polymerase switch, *DNA Repair (Amst)* 6 (2007) 891-899.
- W. Yang, R. Woodgate, What a difference a decade makes: insights into translesion DNA synthesis, *Proc Natl Acad Sci U S A* 104 (2007) 15591-15598.
- W. Xiao, B.L. Chow, S. Broomfield, M. Hanna, The *Saccharomyces cerevisiae* RAD6 group is composed of an error-prone and two error-free postreplication repair pathways, *Genetics* 155 (2000) 1633-1641.
- L. Krejci, S. Van Komen, Y. Li, J. Villemain, M.S. Reddy, H. Klein, T. Ellenberger, P. Sung, DNA helicase Srs2 disrupts the Rad51 presynaptic filament, *Nature* 423 (2003) 305-309.
- E. Papouli, S. Chen, A.A. Davies, D. Huttner, L. Krejci, P. Sung, H.D. Ulrich, Crosstalk between SUMO and ubiquitin on PCNA is mediated by recruitment of the helicase Srs2p, *Mol Cell* 19 (2005) 123-133.
- B. Pfander, G.L. Moldovan, M. Sacher, C. Hoegel, S. Jentsch, SUMO-modified PCNA recruits Srs2 to prevent recombination during S phase, *Nature* 436 (2005) 428-433.
- T. Robert, D. Dervins, F. Fabre, S. Gangloff, Mrc1 and Srs2 are major actors in the regulation of spontaneous crossover, *Embo J* 25 (2006) 2837-2846.
- X. Veaute, J. Jeusset, C. Soustelle, S.C. Kowalczykowski, E. Le Cam, F. Fabre, The Srs2 helicase prevents recombination by disrupting Rad51 nucleoprotein filaments, *Nature* 423 (2003) 309-312.
- C. Lawrence, The RAD6 repair pathway in *Saccharomyces cerevisiae*: what does it do, and how does it do it?, *BioEssays* 16 (1994) 253-258.
- S. Prakash, R.E. Johnson, L. Prakash, Eukaryotic translesion synthesis DNA polymerases: specificity of structure and function, *Annu Rev Biochem* 74 (2005) 317-353.
- H. Xin, W. Lin, W. Sumanasekera, Y. Zhang, X. Wu, Z. Wang, The human RAD18 gene product interacts with HHR6A and HHR6B, *Nucleic Acids Res.* 28 (2000) 2847-2854.
- P.L. Kannouche, J. Wing, A.R. Lehmann, Interaction of human DNA polymerase

- eta with monoubiquitinated PCNA: a possible mechanism for the polymerase switch in response to DNA damage, *Mol Cell Biol* 14 (2004) 491-500.
16. A. Motegi, H.J. Liaw, K.Y. Lee, H.P. Roest, A. Maas, X. Wu, H. Moinova, S.D. Markowitz, H. Ding, J.H. Hoeijmakers, K. Myung, Polyubiquitination of proliferating cell nuclear antigen by HLTf and SHPRH prevents genomic instability from stalled replication forks, *Proc Natl Acad Sci U S A* 105 (2008) 12411-12416.
  17. A. Motegi, R. Sood, H. Moinova, S.D. Markowitz, P.P. Liu, K. Myung, Human SHPRH suppresses genomic instability through proliferating cell nuclear antigen polyubiquitination, *J Cell Biol* 175 (2006) 703-708.
  18. I. Unk, I. Hajdu, K. Fatyol, J. Hurwitz, J.H. Yoon, L. Prakash, S. Prakash, L. Haracska, Human HLTf functions as a ubiquitin ligase for proliferating cell nuclear antigen polyubiquitination, *Proc Natl Acad Sci U S A* 105 (2008) 3768-3773.
  19. I. Unk, I. Hajdu, K. Fatyol, B. Szakal, A. Blastyak, V. Bermudez, J. Hurwitz, L. Prakash, S. Prakash, L. Haracska, Human SHPRH is a ubiquitin ligase for Mms2-Ubc13-dependent polyubiquitylation of proliferating cell nuclear antigen, *Proc Natl Acad Sci U S A* 103 (2006) 18107-18112.
  20. P. Langerak, A.O. Nygren, P.H. Krijger, P.C. van den Berk, H. Jacobs, A/T mutagenesis in hypermutated immunoglobulin genes strongly depends on PCNAK164 modification, *J Exp Med* 204 (2007) 1989-1998.
  21. S. Roa, E. Avdievich, J.U. Peled, T. Maccarthy, U. Werling, F.L. Kuang, R. Kan, C. Zhao, A. Bergman, P.E. Cohen, W. Edelmann, M.D. Scharff, Ubiquitylated PCNA plays a role in somatic hypermutation and class-switch recombination and is required for meiotic progression, *Proc Natl Acad Sci U S A* 105 (2008) 16248-16253.
  22. H.P. Roest, W.M. Baarends, J. de Wit, J.W. van Klaveren, E. Wassenaar, J.W. Hoogerbrugge, W.A. van Cappellen, J.H. Hoeijmakers, J.A. Grootegoed, The ubiquitin-conjugating DNA repair enzyme HR6A is a maternal factor essential for early embryonic development in mice, *Mol Cell Biol* 24 (2004) 5485-5495.
  23. H.P. Roest, J. Klaveren van, J. Wit de, C.G. Gulp van, M.H.M. Koken, M. Vermey, J.H. Roijen van, J.T.M. Vreeburg, W.M. Baarends, D. Bootsma, J.A. Grootegoed, J.H.J. Hoeijmakers, Inactivation of the HR6B ubiquitin-conjugating DNA repair enzyme in mice causes a defect in spermatogenesis associated with chromatin modification, *Cell* 86 (1996) 799-810.
  24. W.M. Baarends, E. Wassenaar, J.W. Hoogerbrugge, G. van Cappellen, H.P. Roest, J. Vreeburg, M. Ooms, J.H. Hoeijmakers, J.A. Grootegoed, Loss of HR6B ubiquitin-conjugating activity results in damaged synaptonemal complex structure and increased crossing-over frequency during the male meiotic prophase, *Mol Cell Biol* 23 (2003) 1151-1162.
  25. A. Lynn, K.E. Koehler, L. Judis, E.R. Chan, J.P. Cherry, S. Schwartz, A. Seftel, P.A. Hunt, T.J. Hassold, Covariation of synaptonemal complex length and mammalian meiotic exchange rates, *Science* 296 (2002) 2222-2225.
  26. W. Goedecke, M. Eijpe, H.H. Offenber, M. van Aalderen, C. Heyting, Mre11 and Ku70 interact in somatic cells, but are differentially expressed in early meiosis, *Nat Genet* 23 (1999) 194-198.
  27. A. Inagaki, S. Schoenmakers, W.M. Baarends, DNA double strand break repair, chromosome synapsis and transcriptional silencing in meiosis, *Epigenetics* 5 (2010).
  28. W.M. Baarends, E. Wassenaar, J.W. Hoogerbrugge, S. Schoenmakers, Z.W. Sun, J.A. Grootegoed, Increased phosphorylation and dimethylation of XY body histones in the Hr6b-knockout mouse is associated with derepression of the X chromosome, *J Cell Sci* 120 (2007) 1841-1851.
  29. E. de Boer, A.J. Dietrich, C. Hoog, P. Stam, C. Heyting, Meiotic interference among MLH1 foci requires neither an intact axial element structure nor full synapsis, *J Cell Sci* 120 (2007) 731-736.
  30. F. Delbos, A. De Smet, A. Faili, S. Aoufouchi, J.C. Weill, C.A. Reynaud, Contribution of DNA polymerase eta to immunoglobulin gene hypermutation in the mouse, *J Exp Med* 201 (2005) 1191-1196.
  31. J. Essers, R.W. Hendriks, J. Wesoly, C.E. Beerens, B. Smit, J.H. Hoeijmakers, C. Wyman, M.L. Dronkert, R. Kanaar, Analysis of mouse Rad54 expression and its implications for homologous recombination, *DNA Repair (Amst)* 1 (2002) 779-793.
  32. A.H. Peters, A.W. Plug, M.J. van Vugt, P. de Boer, A drying-down technique for

- the spreading of mammalian meiocytes from the male and female germline, *Chromosome Res* 5 (1997) 66-68.
33. Y. Gavrieli, Y. Sherman, S.A. Ben-Sasson, Identification of programmed cell death in situ via specific labeling of nuclear DNA fragmentation, *J Cell Biol* 119 (1992) 493-501.
  34. W. Gorczyca, J. Gong, Z. Darzynkiewicz, Detection of DNA strand breaks in individual apoptotic cells by the in situ terminal deoxynucleotidyl transferase and nick translation assays, *Cancer Res* 53 (1993) 1945-1951.
  35. M.E. van Royen, S.M. Cunha, M.C. Brink, K.A. Mattern, A.L. Nigg, H.J. Dubbink, P.J. Verschure, J. Trapman, A.B. Houtsmuller, Compartmentalization of androgen receptor protein-protein interactions in living cells, *J Cell Biol* 177 (2007) 63-72.
  36. D. Branzei, F. Vanoli, M. Foiani, SUMOylation regulates Rad18-mediated template switch, *Nature* 456 (2008) 915-920.
  37. J. Sun, K. Yomogida, S. Sakao, H. Yamamoto, K. Yoshida, K. Watanabe, T. Morita, K. Araki, K. Yamamura, S. Tateishi, Rad18 is required for long-term maintenance of spermatogenesis in mouse testes, *Mech Dev* 126 (2009) 173-183.
  38. J.G. Jansen, A. Tsaalbi-Shtylik, P. Langerak, F. Calleja, C.M. Meijers, H. Jacobs, N. de Wind, The BRCT domain of mammalian Rev1 is involved in regulating DNA translesion synthesis, *Nucleic Acids Res* 33 (2005) 356-365.
  39. C.E. Edmunds, L.J. Simpson, J.E. Sale, PCNA ubiquitination and REV1 define temporally distinct mechanisms for controlling translesion synthesis in the avian cell line DT40, *Mol Cell* 30 (2008) 519-529.
  40. J.G. Jansen, A. Tsaalbi-Shtylik, G. Hendriks, H. Gali, A. Hendel, F. Johansson, K. Erixon, Z. Livneh, L.H. Mullenders, L. Haracska, N. de Wind, Separate domains of Rev1 mediate two modes of DNA damage bypass in mammalian cells, *Mol Cell Biol* 29 (2009) 3113-3123.
  41. J.J. Nadler, R.E. Braun, Fanconi anemia complementation group C is required for proliferation of murine primordial germ cells, *Genesis* 27 (2000) 117-123.
  42. S. Keeney, C.N. Giroux, N. Kleckner, Meiosis-specific DNA double-strand breaks are catalyzed by Spo11, a member of a widely conserved protein family, *Cell* 88 (1997) 375-384.
  43. E. Martini, R.L. Diaz, N. Hunter, S. Keeney, Crossover homeostasis in yeast meiosis, *Cell* 126 (2006) 285-295.
  44. W.D. Sharif, G.G. Glick, M.K. Davidson, W.P. Wahls, Distinct functions of *S. pombe* Rec12 (Spo11) protein and Rec12-dependent crossover recombination (chiasmata) in meiosis I; and a requirement for Rec12 in meiosis II, *Cell & chromosome* 1 (2002) 1.
  45. D.G. Mets, B.J. Meyer, Condensins regulate meiotic DNA break distribution, thus crossover frequency, by controlling chromosome structure, *Cell* 139 (2009) 73-86.
  46. S. Van Komen, G. Petukhova, S. Sigurdsson, P. Sung, Functional cross-talk among Rad51, Rad54, and replication protein A in heteroduplex DNA joint formation, *J Biol Chem* 277 (2002) 43578-43587.
  47. D.V. Bugreev, X. Yu, E.H. Egelman, A.V. Mazin, Novel pro- and anti-recombination activities of the Bloom's syndrome helicase, *Genes Dev* 21 (2007) 3085-3094.
  48. K. Fugger, M. Mistrik, J.R. Danielsen, C. Dinant, J. Falck, J. Bartek, J. Lukas, N. Mailand, Human Fbh1 helicase contributes to genome maintenance via pro- and anti-recombinase activities, *J Cell Biol* 186 (2009) 655-663.
  49. Y. Hu, S. Raynard, M.G. Sehorn, X. Lu, W. Bussen, L. Zheng, J.M. Stark, E.L. Barnes, P. Chi, P. Janscak, M. Jasin, H. Vogel, P. Sung, G. Luo, RECQL5/Recql5 helicase regulates homologous recombination and suppresses tumor formation via disruption of Rad51 presynaptic filaments, *Genes Dev* 21 (2007) 3073-3084.
  50. L.J. Barber, J.L. Youds, J.D. Ward, M.J. McIlwraith, N.J. O'Neil, M.I. Petalcorin, J.S. Martin, S.J. Collis, S.B. Cantor, M. Auclair, H. Tissenbaum, S.C. West, A.M. Rose, S.J. Boulton, RTEL1 maintains genomic stability by suppressing homologous recombination, *Cell* 135 (2008) 261-271.
  51. J.L. Youds, D.G. Mets, M.J. McIlwraith, J.S. Martin, J.D. Ward, O.N. NJ, A.M. Rose, S.C. West, B.J. Meyer, S.J. Boulton, RTEL-1 enforces meiotic crossover interference and homeostasis, *Science* 327 1254-1258.
  52. J.K. Holloway, M.A. Morelli, P.L. Borst, P.E. Cohen, Mammalian BLM helicase is critical for integrating multiple pathways of meiotic recombination, *J Cell Biol* 188 779-789.

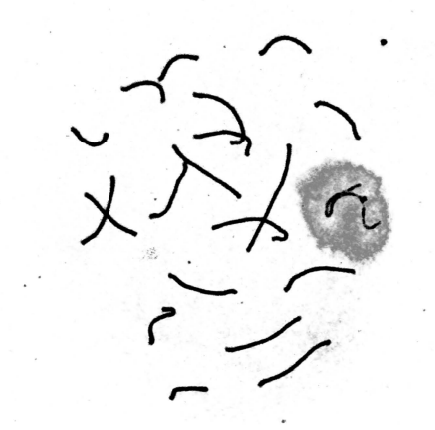
6

# RELATION BETWEEN RADIATION-INDUCED DNA DOUBLE-STRAND BREAKS, SYNAPSIS AND THE MSUC RESPONSE IN SPERMATOCYTES AND OOCYTES OF SPO11 MUTANT MICE

Manuscript in preparation

Akiko Inagaki, Sandra de Vries<sup>1</sup>, Sam Schoenmakers<sup>2</sup>, Christie Vermeulen<sup>3</sup>,  
Evelyne Wassenaar, Wiggert A. van Cappellen, Fabrizia Carofiglio,  
Esther Sleddens-Linkels, J. Anton Grootegoed, Hein P. J. te Riele<sup>1</sup>,  
Bernard de Massy<sup>4</sup>, and Willy M Baarends\*

\* Corresponding author



Department of Reproduction and Development, and <sup>2</sup>Department of Obstetrics  
and Gynaecology, Erasmus MC University Medical Center, Rotterdam, The Netherlands,  
<sup>1</sup>Division of Molecular Biology, Netherlands Cancer Institute, Amsterdam, The Netherlands,  
<sup>3</sup>Department of Medical Oncology, VU Medical Center, Amsterdam, The Netherlands.  
<sup>4</sup>Institut de Génétique Humaine, France

## ABSTRACT

The formation and repair of meiotic DNA double-strand breaks (DSBs) are required for homologous chromosome pairing and formation of the transcriptionally silenced XY body during male meiotic prophase in the mouse. These breaks are induced by the topoisomerase-like enzyme SPO11. Herein we show that haploinsufficiency for functional SPO11 reduces the number of meiotic DSBs in leptotene, but not in zygotene. In addition, the number of MLH1 foci, that localize to future crossover sites, was not different from wild type in spermatocytes of heterozygote mice. In SPO11 deficient spermatocytes as well as oocytes, a so-called pseudo XY body, highly enriched for the DSB-repair marker  $\gamma$ H2AX, forms on part of the asynapsed chromatin although meiotic DSBs are completely absent. A few foci of the homologous recombination repair protein RAD51 were detected in both spermatocyte and oocyte nuclei, indicating that some spontaneous DSBs were present. One or more of these spontaneous RAD51 foci frequently localized within the pseudo XY body, suggesting that spontaneous DSBs may trigger the formation of the pseudo XY body. In addition to RAD51 foci, many other DSB repair proteins accumulated on the chromatin of the pseudo XY body in spermatocytes. However, the complete histone replacement that accompanies normal XY body formation does not occur in the pseudo XY body in spermatocytes.

In the absence of functional SPO11, we find that heterologous synapsis is more extensive in spermatocytes compared to oocytes. Upon the induction of DSBs by irradiation in leptotene and zygotene nuclei, the pseudo XY body no longer forms. Instead, DSB repair proteins relocalize to the DSB repair sites. This process stimulates synapsis both in oocytes and spermatocytes.

We conclude that the amount of SPO11 in mouse spermatocytes is limiting, resulting in either delayed or reduced formation of meiotic DSBs in spermatocytes that are heterozygote for a null mutation in *Spo11*. In addition, radiation-induced DSBs can partially replace SPO11-induced DSBs for the achievement of chromosome synapsis. Our data are also consistent with the idea that persistent DSBs, damage- or SPO11-induced, facilitate recruitment of the machinery that initiates meiotic sex chromosome inactivation (MSCI) and meiotic silencing of unsynapsed chromatin (MSUC).

**Key words:** DNA double-strand break, SPO11, MSCI, MSUC, meiosis, XY body, pseudo-XY body

## INTRODUCTION

During meiotic prophase in yeast and mammals, the formation of DNA double-strand breaks (DSBs) by the topoisomerase-like enzyme SPO11 precedes the pairing and synapsis of homologous chromosomes [1]. Synapsis between chromosomes is achieved by the formation of a specific protein complex, consisting of lateral elements along the chromosomal axes that contain SYCP2, SYCP3 and cohesin, connected by a central element containing SYCP1 and several other meiosis-specific proteins (reviewed by [2]). In males, the X and Y chromosome form a very special pair; they synapse only in the short pseudoautosomal region in pachytene, and localize to the periphery of the nucleus. Furthermore, the chromatin is silenced by a process named meiotic sex chromosome inactivation (MSCI). This process requires the phosphorylation of H2AX [3], forming  $\gamma$ H2AX, by the checkpoint kinase ATR [4].  $\gamma$ H2AX is the earliest known marker of MSCI. This specific histone modification is also found in somatic cells, usually at sites of DNA DSB repair [5]. At the XY body, many DNA repair proteins accumulate, and histone modifications such as specific methylation, sumoylation and ubiquitylation marks also concentrate on the XY body (reviewed by [6]). The accumulation of DSB-repair proteins may be caused by delayed or stalled DSB repair in regions that fail to synapse. In early meiotic prophase cells, homologous recombination repair via the sister chromatid is thought to be repressed. In addition, essential components of the error-prone repair mechanism of nonhomologous end-joining (NHEJ) are suppressed in these cells [7]. Therefore, meiotic DSBs need to be repaired via homologous recombination, using one of the chromatids of the homologous chromosome as a template. Thus, in the absence of a homologous partner, meiotic DSBs will most likely persist. The specialization of the DSB-repair mechanism in meiotic prophase is necessary to stimulate the formation of crossovers between homologous chromosomes. These crossovers, in combination with the persistence of sister-chromatid cohesion along chromosome arms, provide the connection between homologous chromosomes at metaphase and are essential for correct chromosome segregation. Most meiotic DSBs are repaired as noncrossovers and a special mechanism, named crossover interference, reduces the chance of two crossovers occurring in close proximity. In addition, each chromosome must have at least one crossover event. It has been established that the length of the synaptonemal complex (SC) correlates to the number of crossover events [8]. For example, the average number of crossovers in FVB males and females is 22.5 and 32.1, respectively [9], and the average length of the SC is also increased in females compared to males [8]. However, it is not known if this correlation between SC length and crossover frequency is related to the number of induced meiotic DSBs. In fact, very little is known about the factors that regulate the number of DSBs. It has been suggested that the amount of SPO11 could be limiting, due to the fact that the meiotic block in spermatocytes that lack the checkpoint kinase ATM is partially suppressed on a *Spo11*<sup>+/-</sup> background [10].

In the complete absence of meiotic DSBs, synapsis is severely affected [11,12]. Some heterologous synapsis can occur, but the spermatocytes and oocytes do not proceed beyond the zygotene stage [11,12]. In *Spo11* knockout spermatocytes, a specific

chromatin structure that resembles the XY body, named pseudo XY body is formed [10]. This chromatin domain is marked by  $\gamma$ H2AX and ATR, and is transcriptionally silenced [13]. However, it does not localize to the XY pair, but to part of the unsynapsed chromatin. Based upon these characteristics, it has been proposed that the pseudo XY body is a manifestation of the process named meiotic silencing of unsynapsed chromatin (MSUC) [13], of which MSCI is thought to be a specialization. MSUC silences unsynapsed chromatin in male and female meiotic prophase cells. The exact cascade of events that leads to the transcriptional silencing is not known, but it has been established that there is a tight correlation between the presence of asynapsed chromosomal axes, the accumulation of ATR along these axes, the formation of  $\gamma$ H2AX, and the transcriptional silencing. Recently, two mammalian homologs of the yeast protein Hop1, named HORMAD1 and HORMAD2 have been identified [14-16]. The *S. cerevisiae* Hop1 is a component of the axial element protein cores in synaptonemal complexes [17]. Hop1 is involved in biasing meiotic DSB repair to occur between homologous chromosomes rather than between sister chromatids [18], and is important for effective chromosome segregation and for the meiotic recombination checkpoint [19]. The HORMA-domain is found in proteins that act as adapters on chromatin to recruit checkpoint or DNA repair proteins [20]. In meiosis of a wide range of species, HORMA-domain containing proteins regulate synapsis [21-24]. In mouse meiotic prophase, the HORMA-domain proteins localize to asynapsed axes of wild type as well as *Spo11*<sup>-/-</sup> spermatocytes [25]. Based upon these results, it has been suggested that the HORMAD proteins function upstream of ATR and  $\gamma$ H2AX in the regulation of MSCI and MSUC [25].

In *Spo11*<sup>-/-</sup> spermatocytes, the pseudo XY body forms only on part of the asynapsed chromatin. Somehow, the MSUC response is not complete. The restriction of MSUC to only part of the asynapsed chromatin is very surprising and raises the possibility that apart from asynapsis, also other mechanisms may contribute to the activation of MSCI and MSUC. Since all known players in these processes function also in DNA repair, it is tempting to speculate that persistent spontaneous DSBs on asynapsed axes may contribute to the activation of MSCI and MSUC. This notion is supported by the fact that irradiation-induced DSBs in leptotene cells enhance the efficiency of MSUC of a small translocation bivalent that carries a heterologous region of approximately 35-40 Mb [26]. In addition, recent data also provide a link between DSB-repair, the checkpoint kinase ATM, and transcriptional silencing of surrounding chromatin in somatic cells [27].

Herein we have investigated whether the amount of SPO11 limits the number of DSBs, and whether irradiation-induced DSBs can replace SPO11 with respect to its role in the stimulation chromosome synapsis. In addition we have studied the accumulation of DNA repair proteins on the pseudo XY body and asked how its formation is influenced by the presence of irradiation-induced DSBs.

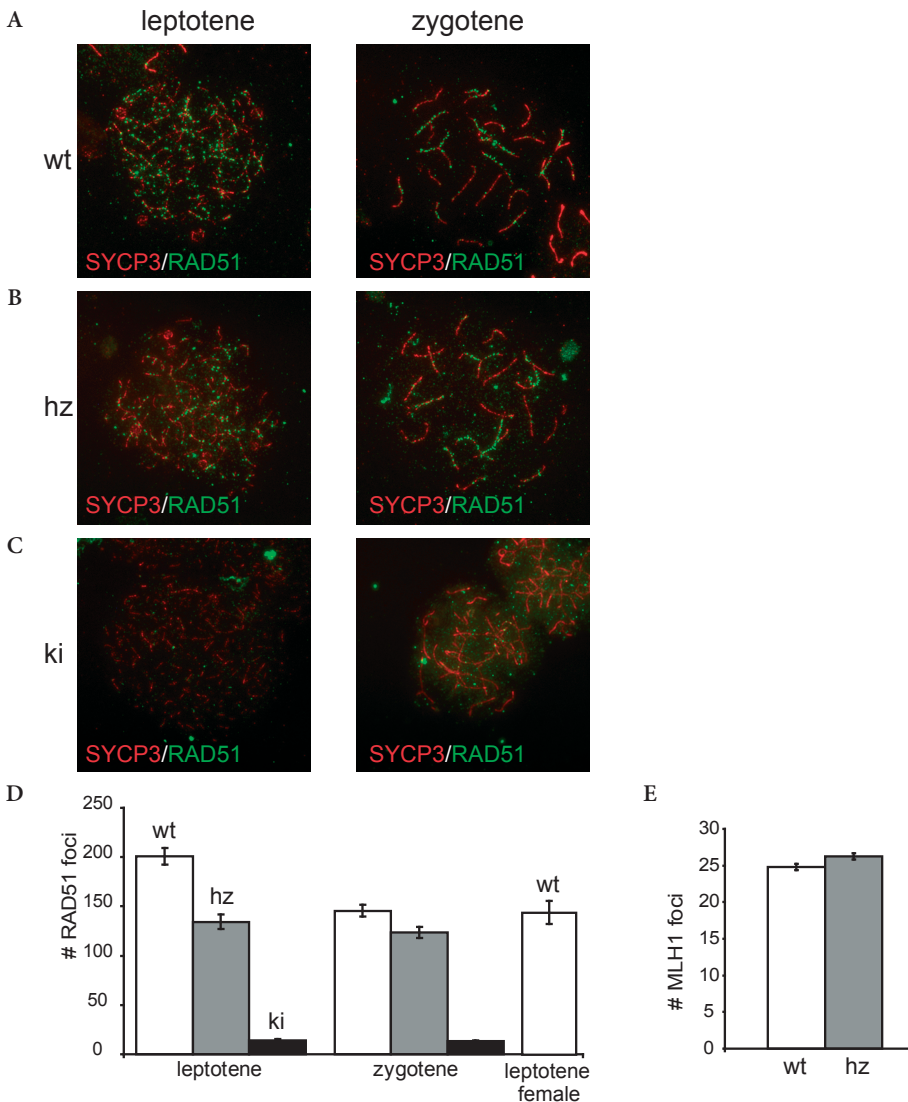


**Figure 1. Half the normal dose of functional SPO11 reduces the number of RAD51 foci in leptotene, but not in zygotene spermatocytes.** (A - C) Double immunostaining of wt (A), hz (B), and ki (C) of *Spo11* mutant spermatocyte nuclei with anti-SYCP3 (red), anti-RAD51 (green). (D) The number of RAD51 foci was counted in wt, hz, and ki leptotene and zygotene nuclei of *Spo11* mutant mice. White, gray, black bars indicate wt, hz, and ki *Spo11* mutant mice, respectively. Error bars indicate SEM for 20 nuclei from 2 independent mice. (E) The number of MLH1 foci in pachytene nuclei was counted in 4-week-old wt and hz *Spo11* mutant mice. Error bars indicate SEM for 30 nuclei from 2 independent mice.

## MATERIALS AND METHODS

### Mice

*Spo11* mutant mice were generated through a two-step recombination strategy. First, two heterospecific *lox* sites flanking the selectable marker hygromycin, replacing exons 4-8, were placed in the *Spo11* gene, in ES cells by homologous recombination. Next, a targeting vector containing the same heterospecific *lox* sites flanking exon 4-8 of *Spo11* with the point mutation generating Y100F at exon 4 was used to replace the selection marker by a site-specific double cross-over event (data not shown). The final modified *Spo11* locus carries a *loxP* site between exons 3 and 4, the point mutation generating Y100F at exon 4, and a *lox511* site between exons 8 and 9. ES cells carrying a single modified *Spo11* allele were used for blastocyst injection to generate chimeras, and heterozygotes were obtained upon germ line transmission of the mutated allele. Correct targeting was verified using Southern blotting with 5' and 3' probes outside the targeted region (data not shown).

Wild type, heterozygote and homozygote *Spo11* mutant mice were kept on a FVB background. To genotype the animals, the following primers were used: Forward, 5'CTGGTCGATGCAGATCCCTACGG3'; reversed, 5'TAGATGCACATTATCTCG-ATGCC3'

Adult *Spo11* mutant males were irradiated with 5 Gy with Elekta linear accelerator from a <sup>137</sup>Cs source (Crawley). Pregnant heterozygote females were irradiated with the same dosage of irradiation at E15.5. At 24h (females), 48h, and 120h (males) following irradiation, males and females were sacrificed. Testes were collected and spread as described below. Embryos were collected from the pregnant females and oocytes were spread from the ovaries. Tails from each embryo were used to genotype the embryos.

### Antibodies

For primary antibodies, we used mouse monoclonal antibodies anti-phosphorylated H2AX (Upstate), anti-ubiquitylated histone H2A (Millipore, #05-678), anti-BRCA1, anti-TOPBP1, anti-MDC1, anti-phospho H2A, anti-phospho H2AX (all from Upstate), anti-GMP1 (Zymed), and anti-MLH1 (Becton and Dickinson), rabbit polyclonal antibodies anti-H2AT119ph, anti-H2BT120ph, anti-H3.1 [28], anti-RAD18 [29], anti-RAD51 [30], anti-SYCP3 (gift from C. Heyting), and anti-H3K4me2 (Upstate), and rat polyclonal antibody anti-SYCP3 [28]. For secondary antibodies, we used a goat anti-rabbit/mouse IgG-peroxidase (Sigma), goat anti-rabbit IgG alexa 488/564, goat anti-mouse alexa IgG 488/564, or goat anti-mouse IgM alexa 564 (Molecular Probes).

### Meiotic spread nuclei preparations and immunocytochemistry

Testis tissues were processed to obtain spread nuclei for immunocytochemistry as described by Peters et al [31]. Spread nuclei of spermatocytes were stained with antibodies mentioned above. Before incubation with antibodies, slides were washed in PBS (3x10 min), and non-specific sites were blocked with 0.5% w/v BSA and 0.5% w/v milk powder in PBS. Primary antibodies were diluted in 10% w/v BSA in PBS, and incubations were overnight at room temperature in a humid chamber. Subsequently, slides were washed (3x10 min) in PBS, blocked in 10% v/v normal goat serum (Sigma)

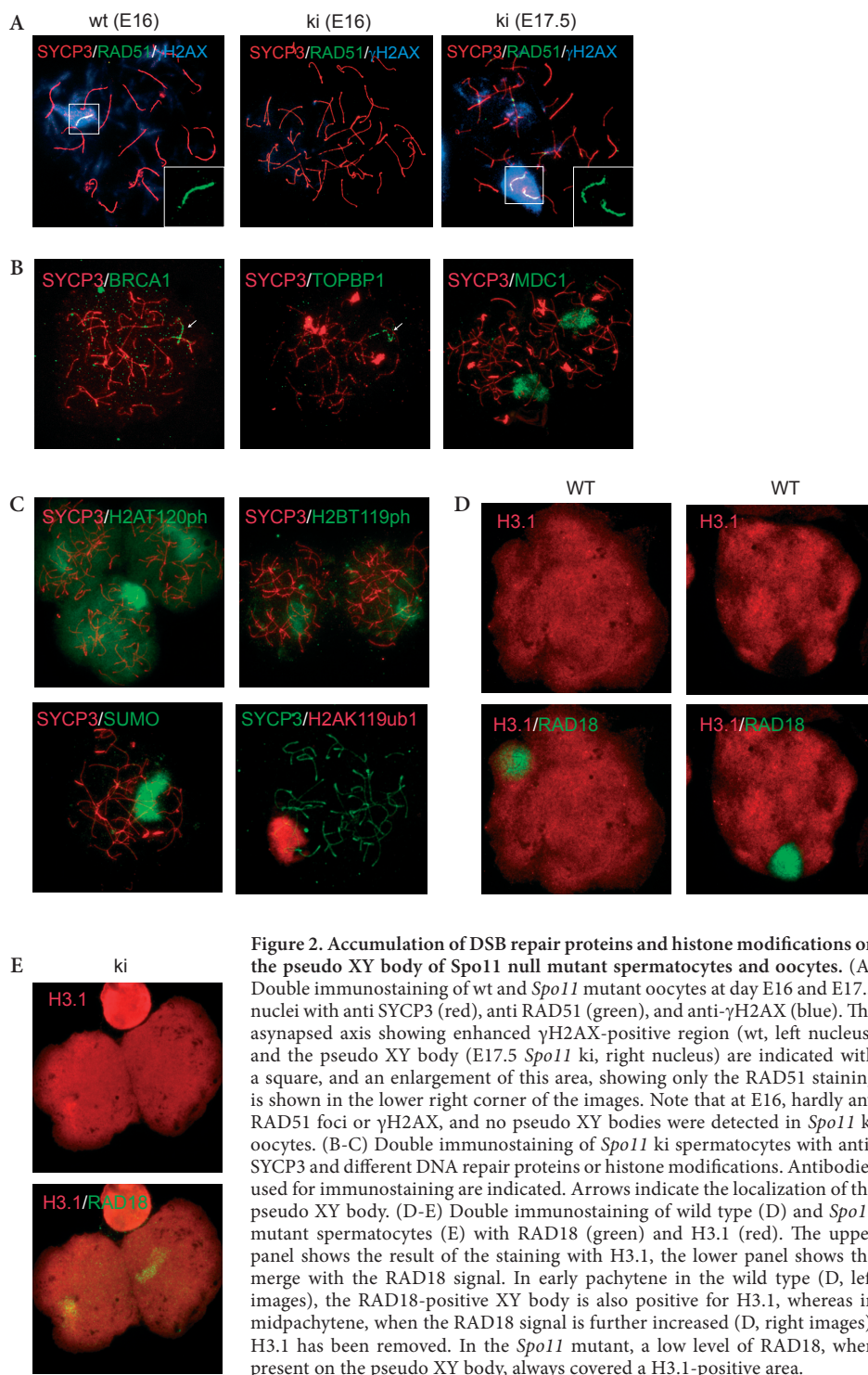
in blocking buffer (supernatant of 5% w/v milk powder in PBS centrifuged at 14,000 rpm for 10 min), and incubated with secondary antibodies in 10% normal goat serum in blocking buffer at room temperature for 2 hours. Finally, slides were washed (3x10 min) in PBS (in the dark) and embedded in Prolong Gold with DAPI (Invitrogen). Fluorescent images were observed by using a fluorescence microscope (Axioplan 2; Carl Zeiss) equipped with a digital camera (Coolsnap-Pro; Photometrics). Fluorescent images were taken under identical conditions for all slides, and images were analyzed using the ImageJ software (Rasband, W.S., ImageJ, U.S. National Institutes of Health, Bethesda, Maryland, USA [<http://rsb.info.nih.gov/ij/>]).

## RESULTS AND DISCUSSION

### **A two-fold reduction in the amount of functional SPO11 reduces the number of RAD51 foci at leptotene but not at zygotene**

We used a *Spo11* knockin mouse model in which the catalytically active Tyrosine (Tyr) 100 residue is replaced by a Phenylalanine (Phe). In yeast and plants, mutation of the analogous Tyr residue abolished meiotic DSB formation [32,33]. Identical to the *Spo11* knockout, male and female double-knockin mice (ki) are infertile, and meiotic prophase is blocked with spermatocytes and oocytes reaching a zygotene-like stage with variable degrees of heterologous synapsis (data not shown). First we analyzed the formation of meiotic DSBs in wild type (wt), heterozygote (hz) and ki mice through immunocytochemical analyses of the formation of RAD51 foci. RAD51 is a DNA-dependent ATPase that forms filaments on single-stranded resected DNA-ends at DSB-repair sites. It is essential for homologous recombination repair in mitotic cells [34,35]. In meiosis, RAD51 localizes to meiotic DSB sites, together with its meiosis-specific paralog DMC1 [36]. The number of RAD51 foci was analyzed in leptotene and zygotene nuclei (Figure 1). In leptotene, SPO11 is activated, and many DSBs are formed, concomitant with the assembly of short patches of axial element formation along the chromosomal axes (Figure 1A). In zygotene, repair of meiotic DSBs progresses, concomitant with homologous chromosome pairing and synapsis of the axial elements (now termed lateral elements), that occurs through the formation of the central element of the synaptonemal complex (SC) (Figure 1A). In wt spermatocyte nuclei, the number of RAD51 foci gradually decreases from leptotene to zygotene, and by mid-pachytene only the asynapsed axis of the X chromosome contains a few remaining RAD51 foci [36]. In hz *Spo11* mutant leptotene spermatocyte nuclei, the number of RAD51 foci was lower compared to wt (Figure 1B, D). However, in zygotene nuclei, no difference in the number of RAD51 foci between wt and hz nuclei was observed (Figure 1D). In the ki animals, only very few (approximately 13 on average) RAD51 foci were observed in leptotene and zygotene (Figure 1C, D).

These data indicate that in the hz mice, half of the normal amount of functional SPO11 is not capable of inducing the normal number of meiotic-DSBs in leptotene. However, the reduced SPO11 concentration may alter the kinetics of DSB formation, leading to a relative peak in DSB formation in zygotene in the heterozygote, and this may explain why the total number of RAD51 foci at this stage is near normal, and not reduced compared



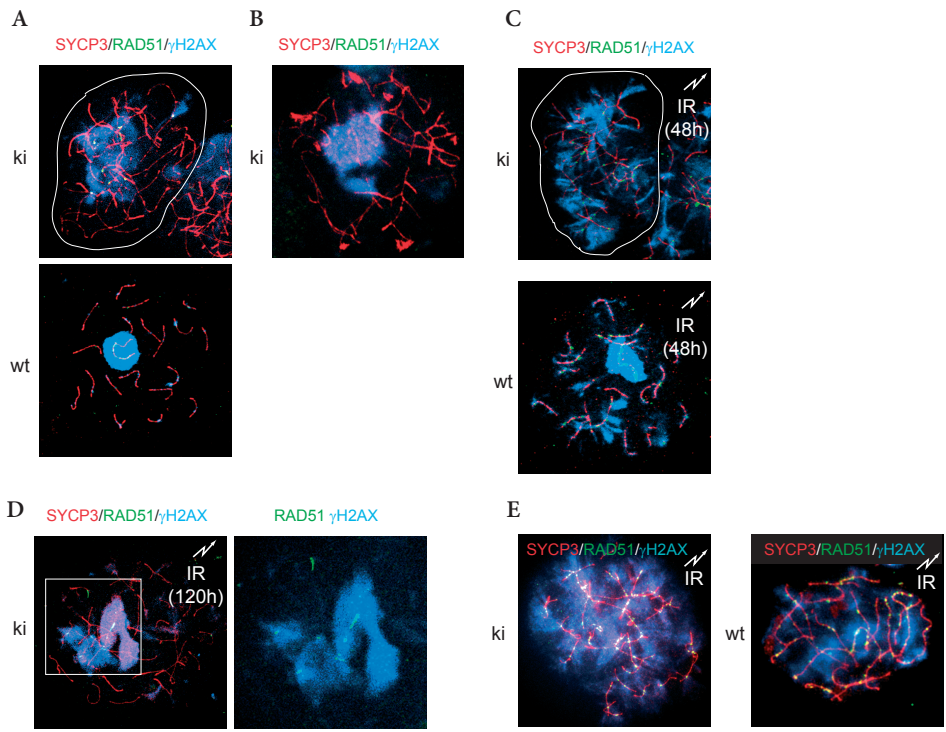


**Figure 3: RAD51 foci frequently localize to the pseudo XY body, and colocalize with  $\gamma$ H2AX and other DSB repair proteins in multiple chromatin domains following irradiation. (A-F) Immunostaining of wild type and *Spo11* mutant spermatocyte (A-D) and oocyte (E) nuclei. Spermatocytes and oocytes were immunostained with anti-SYCP3 (red), anti-RAD51 (green), and  $\gamma$ H2AX (blue). (A) Upper image, *Spo11* mutant late-zygotene-like spermatocyte with RAD51 foci in the pseudo XY body. Lower image, wild type pachytene spermatocyte, showing many persistent RAD51 foci on the X chromosome, and some on the autosomes, frequently colocalizing with  $\gamma$ H2AX. (B) Late-zygotene-like spermatocyte with a pseudo XY body that does not contain RAD51 foci. (C-E) Localization of  $\gamma$ H2AX and RAD51 in spermatocyte (C, D) and oocyte nuclei (E) of wild type and *Spo11* mutant mice irradiated with IR at 5Gy, and analyzed 48h (C), 120h (D), and 24h later (E). (D) Pseudo XY body is indicated with a square, and the enlarged image of the pseudo XY body is shown at the right. (E) Irradiated *Spo11* mutant (left) and wt (right) oocyte.**

to the leptotene stage. Analyses of the number of MLH1 foci revealed that indeed, the crossover frequency is not different between wt and hz pachytene spermatocytes (Figure 1E). In wt female leptotene oocytes, we found approximately 140 RAD51 foci (Figure 1D), which is somewhat lower compared to male wt leptotene nuclei. This is a surprising finding in light of the fact that oocytes have approximately 30% more MLH1 foci and corresponding crossovers compared to spermatocytes. It cannot be excluded that the dynamics of DSB repair differ between oocytes and spermatocytes. The time span between leptotene (induction of DSBs) and early pachytene (synapsis) is approximately 48 h in spermatocytes [37]. In oocytes, this time span is shorter (15-20h) [38], indicating that repair might occur somewhat faster, leading to an underestimation of the number of induced DSBs. Still, it is unlikely that the increased crossover number in wild type females compared to males is caused by an increase in the number of meiotic DSBs.

**Known markers of the XY body accumulate on the pseudo XY body in *Spo11* null spermatocytes, but this is not associated with histone eviction.**

The formation of the pseudo XY body has been described as an incomplete MSUC phenomenon, caused by the presence of asynapsed axes [13]. If this is the case, it would be expected that pseudo XY body formation also occurs during female meiotic prophase. Surprisingly, we did not observe a  $\gamma$ H2AX-positive chromatin domain in oocytes isolated from *Spo11* ki ovaries at embryonic day 16 (Figure 2A, ki, E16), despite the fact that pachytene oocytes are present in ovaries from wild type embryonic day 16 (Figure 2A, wt). Next, we analyzed *Spo11* ki ovaries at embryonic day 17.5 and did find a pseudo-XY body like,  $\gamma$ H2AX-positive region (Figure 2A, ki, E17.5). In addition, we detected spontaneous RAD51 foci which frequently colocalize with the pseudo XY body in *Spo11* ki oocytes.

We next asked whether known components of the DNA repair machinery accumulate on the asynapsed axes of the pseudo XY body (BRCA1, TOPBP1), or the surrounding chromatin (MDC1) in *Spo11* ki spermatocytes. Figure 2B shows that BRCA1, TOPBP1, and MDC1 all concentrate on the pseudo XY body of spermatocytes. However, for BRCA1 and TOPBP1, the signal is somewhat less pronounced compared to the intense marking of the axial elements of the X and Y in wild type nuclei (data not shown). In addition to these DNA repair proteins, several histone modifications are also known to accumulate on the XY body, and some of these also mark DSB repair sites; histone ubiquitylation and sumoylation (reviewed by [6]). The results shown in Figure 2C revealed that phosphorylation of histone H2A threonine 119 (H2AT119ph), phosphorylation of histone H2B theronine 120 (H2BT120ph), mono-ubiquitylation of histone H2A lysine 119 (H2AK119ub1) and chromatin SUMOylation all mark the pseudo XY body. However, the complete replacement of H3 that occurs on XY bodies and during MSUC [39], was never observed for the pseudo XY body (Figure 2D, E). We co-stained spermatocytes for H3.1, that normally disappears from the XY body in early-to-mid pachytene [39], and for RAD18, a ubiquitin ligase that starts to accumulate on the XY body in early pachytene and reaches its maximum during mid-to-late pachytene [40]. In wild type spermatocytes, a low level of RAD18 on the XY body was observed when H3.1 was still present (Figure 2D, left). Upon histone eviction, the RAD18 level has increased (Figure 2D, right). In the *Spo11* null spermatocytes, RAD18 levels on the pseudo XY body were very low, and we never observed depletion of H3.1 from the RAD18-positive region (Figure 2E). Together, these data indicate that DSB-repair proteins accumulate on the pseudo XY body in the absence of SPO11-induced meiotic DSBs. The slightly lower level of some proteins that is observed on the pseudo XY body compared to the level that is observed on the XY body, might be due to the fact that the cells never reach the stage that corresponds to mid-pachytene in wt spermatocytes, since histone eviction does not occur. Alternatively, the cells may reach this stage without performing the histone eviction, and this may be associated with less pronounced accumulation of BRCA1, TOPBP1, H2AK119ub1 and RAD18.

### **RAD51 foci frequently localize to the pseudo XY body**

The DNA repair-like response at the pseudo XY body may be a special adaptation of the DNA repair pathways in spermatocytes, triggered by the meiosis-specific processes associated with the formation of the SC. Asynapsed regions somehow recruit these proteins to elicit the MSUC response, independent of meiotic DSBs. Alternatively, or in addition, naturally occurring DSBs may play a role in nucleating the formation of the pseudo XY body in one or maximally two regions of the nucleus. To investigate this further, we performed co-immunostaining experiments for RAD51 to visualize DSB-repair sites,  $\gamma$ H2AX to visualize the pseudo XY body, and SYCP3 to assess the stages of the cells. We found that the pseudo XY body frequently contains several RAD51 foci in late-zygotene-like spermatocytes (Figure 3A, ki). At this stage, one or more RAD51 foci localized in the pseudo XY body in 89% (n=80) of the nuclei. The average number of RAD51 foci at this stage was 4.1, and 66% of these RAD51 foci was associated with the pseudo XY body. Note that some RAD51 foci were not located in the vicinity of the pseudo XY body, and were not marked by  $\gamma$ H2AX on the surrounding chromatin (Figure 3A, ki). Also in wild type nuclei,  $\gamma$ H2AX and RAD51 do not always colocalize in pachytene nuclei at autosomal regions (Figure 3A, wt). In later stages, RAD51 disappeared from the nuclei, while the pseudo XY body remained (Figure 3B), similar to what was observed in wt (data not shown). Together, this indicates that in accordance with what is observed on the normal XY body, naturally occurring RAD51 foci in *Spo11* null mice may persist in the pseudo XY body. This result suggests that naturally occurring DSBs may perform a functional role in nucleating the formation of the pseudo XY body in a certain sub-region of the nucleus. Alternatively, persistence of naturally occurring RAD51 foci may occur preferentially in the pseudo XY body. Real time analyses of the dynamics of RAD51 and  $\gamma$ H2AX would be required to define the actual sequence of events during pseudo XY body formation, but based on the SYCP3 patterns that we observed in *Spo11* ki spermatocytes with and without RAD51 foci, we favour the hypothesis that the formation of the pseudo XY body is triggered by a combination of the presence of naturally occurring DSBs and the presence of asynapsed chromatin. Furthermore, this hypothesis is supported by the fact that we did not detect any RAD51 foci nor any pseudo XY body in *Spo11* ki oocytes at embryonic day 16 (Figure 2A, ki, E16), while RAD51 foci and pseudo XY body appeared in *Spo11* ki oocytes at embryonic day 17.5, suggesting that spontaneous DSBs may trigger the formation of the pseudo XY body in the absence of SPO11-induced DSBs. Moreover, in these E17.5 *Spo11* ki oocytes, the colocalization between RAD51 foci and  $\gamma$ H2AX accumulation is striking in the pseudo XY body and also in other chromatin regions. In the pseudo XY body, RAD51 appears to coat the axial elements, instead of forming distinct foci. It is tempting to speculate that this may be related to the chromosome wide spreading of RAD51 that has been observed in chromatin immuno-precipitation experiments upon the induction of a single persistent DSB in yeast [41].

### **Induction of radiation-induced DSBs abolishes formation of the pseudo XY body**

Next, we introduced irradiation-induced DSBs in *Spo11* null mouse spermatocytes and oocytes to analyse the effect on the behaviour of DSB repair proteins, the pseudo

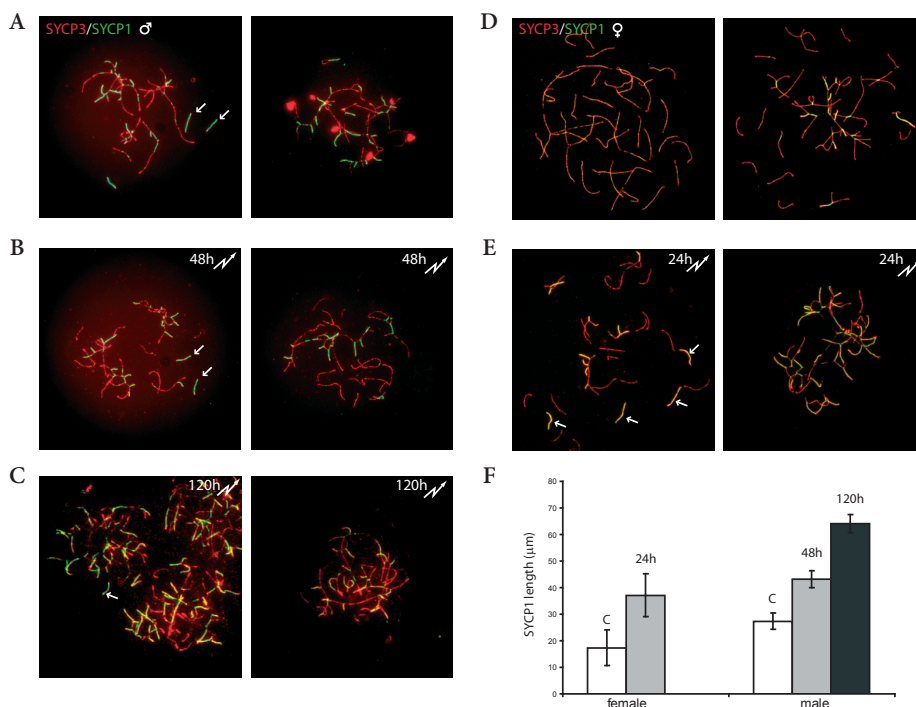


**Figure 4:** Irradiation-induced DSBs stimulate synapsis in SPO11-deficient oocytes but not in spermatocytes. (A-E) Spread spermatocyte (A-C) and oocyte (D, E) nuclei of *Spo11* mutant mice, non-irradiated (A, D), or exposed to 5Gy IR (B,C,E) and fixed at 48h (B) or 120h (C) after irradiation, or for the oocytes (E), at 24h following irradiation. Synapsis was analyzed via double-immunostaining for SYCP1 (green) and SYCP3 (red). (F) The total SC length (measured via SYCP1-signal analyses) in zygote-like nuclei of *Spo11* mutant mice described above was measured. Error bars indicate SEM for 30 nuclei from 2 independent mice.

XY body, and synapsis. Adult male *ki* mice were subjected to 5 Gy of irradiation and sacrificed 48h or 120 h following irradiation. Pregnant *h<sub>z</sub>* female mice that had mated with a *h<sub>z</sub>* male, were irradiated at E15.5 and sacrificed at E16.5 to prepare spread oocyte nuclei. Based upon previous experiments, 5 Gy is expected to generate approximately 60 DSBs in leptotene and zygotene spermatocytes and oocytes. Spread spermatocyte and oocyte nuclei were first analysed for RAD51 and  $\gamma$ H2AX staining. At 48h following irradiation, *Spo11* null zygotene-like spermatocytes lacked pseudo XY bodies. Instead,  $\gamma$ H2AX was present in multiple nuclear areas (Figure 3C, ki) that also contained many RAD51 foci (Figure 3C, ki). At 120h following irradiation, many nuclei displayed a single  $\gamma$ H2AX positive area, resembling the pseudo XY body (Figure 3D, ki). The number of RAD51 foci was higher at 48h compared to 120h, and RAD51 foci and linear aggregates localized to the pseudo XY body at 120h following irradiation in 70% (n=40) of nuclei. The IR-induced pseudo XY body may be the result of clustering of persistent-DSB-containing-chromosome domains (Figure 3D). A similar effect has been observed in mitotic G1 cells, in which DSBs formed at distant locations were able to subsequently be brought together to form a cluster [42]. Furthermore, during

meiosis, areas that are subject to MSC1 or MSUC also frequently colocalize to form a single chromatin domain that is  $\gamma$ H2AX-positive [43-47].

Previously, it has been shown that MSC1 is impaired when meiotic DSB repair is stalled, for example in *Dmcl* knockout mice [13] and in mice lacking the central element component of the synaptonemal complex SYCP1 [48]. Our data confirm and extend these observations, showing that there is a dynamic interplay between the pseudo XY body and DSB repair sites, irrespective of the fact that they are induced by SPO11 or irradiation. In *Spo11* null oocytes, at 24h following irradiation, a spread  $\gamma$ H2AX staining pattern and multiple RAD51 foci were induced upon irradiation (Figure 3E, ki), similar to what was observed in spermatocytes at 48h after irradiation. Further analysis needs to be performed to determine whether *Spo11* ki oocytes can form an IR-induced pseudo XY body at later time points following irradiation. In wild type pachytene oocytes, an MSUC response efficiently occurs when 1-3 chromosome pairs remain unsynapsed [49]. This occurs spontaneously in approximately 15% of the oocytes. However, if asynapsis is more extensive, such as in mouse mutants that display synaptic failure,  $\gamma$ H2AX accumulation is more diffuse and does not reach the high intensity that is normally observed at the XY body. In addition, in such nuclei, transcriptional silencing of the asynapsed regions does not occur [49]. We find pseudo XY bodies in E17.5 *Spo11* ki oocytes, in the presence of massive asynapsis (Fig 2A), indicating that in these nuclei, the MSUC-inducing proteins are not recruited to all the asynapsed axes, and are therefore still capable of inducing an MSUC response. The overall colocalization between RAD51 and  $\gamma$ H2AX accumulation in these nuclei, indicates that the presence of persistent naturally-occurring DSBs restrict the MSUC response to those regions that are both asynapsed and contain persistent DNA damage. For spermatocytes, we propose that the mechanism occurs in a similar fashion, although the MSUC response may be somewhat different from oocytes, as illustrated by the more prominent RAD51 accumulation on axes of the pseudo XY body in oocytes as compared to spermatocytes. A similar mechanism of induced transcriptional silencing of chromatin surrounding persistent DSBs was recently shown to be operative and has been termed DSB-Induced Silencing in Cis (DISC) [27].

### **Induction of radiation-induced DSBs stimulates synapsis in *Spo11* null oocytes and spermatocytes**

To analyse the effect of the induction of irradiation-induced DSBs on synapsis, we analysed SC formation using antibodies directed against the axial/lateral element component SYCP3 and the central element component SYCP1. In *Spo11* null spermatocytes and oocytes, the degree of synapsis is variable, with some nuclei showing no synapsis, whereas others show variable degrees of partial heterologous synapsis (Figure 4A, D). Occasionally, in spermatocytes, homologous synapsis between one or two chromosome pairs appears to occur, based upon the complete synapsis between lateral elements of equal length (Figure 4A, arrows). On average, the degree of heterologous synapsis is more extensive in *Spo11* null spermatocytes compared to oocytes (Figure 4F). Subsequently, we measured the total length of synapsed SC per nucleus in spermatocytes and oocytes upon irradiation. Both in *Spo11* null spermatocytes and

oocytes, the degree of synapsis was increased upon irradiation. In spermatocyte, the SYCP1 length was increased 1.5 fold and 2.3 fold compared to non-irradiated control, at 48h and 120h after irradiation, respectively (Figure. A-C, F). In oocytes, the SYCP1 length increased approximately two-fold compared to non-irradiated oocytes at 24h after irradiation (Figure 4 D-F). In addition, some homologous synapsis might occur, based upon the complete SCs that were occasionally observed (Figure 4B, C, E, arrows). These data show that irradiation-induced DSBs may replace SPO11-induced DSBs in stimulating synapsis in both oocytes and spermatocytes. Our data also indicate that in the absence of meiotic DSBs, spermatocytes achieve more extensive synapsis than oocytes. This may be due to the broader time period during which spermatocytes can attempt to complete synapsis compared to oocytes. However, the maximal levels of synapsis were higher at 24h after irradiation in oocytes, compared to 120h after irradiation in spermatocytes. Although complete synapsis was never observed, some oocytes reached a total SYCP1 length of 140  $\mu\text{m}$ , whereas a maximal length of 90  $\mu\text{m}$  was observed in the spermatocytes at 120h after irradiation (data not shown). This may be related to the fact that total synaptonemal complex length in oocytes is also higher in oocytes compared to spermatocytes.

The number of irradiation-induced breaks in our model (around 60) is approximately 25% of the normal amount of SPO11-induced DSBs. It is not known what the minimal number of SPO11-induced breaks is that is necessary to allow normal chromosome pairing. In contrast to the non-random distribution of SPO11-induced breaks, irradiation-induced DSBs are randomly distributed. Based on a random distribution, it is expected that each chromosome will obtain on average between 1 (chromosome 19) and 4 (chromosomes 1 and 2) DSBs, with one or more chromosomes lacking a DSB in approximately 70% of the nuclei. Based on the minimal effect of this number of extra DSBs on crossover frequencies in wild type mouse spermatocytes (only approximately 1 extra crossover upon induction of 60 DSBs) [26], it might be expected that irradiation-induced breaks may be not as efficient in stimulating homology recognition compared to SPO11-induced DSBs. Our data confirm and extend the observations made by Romanienko et al. (2000) that showed that cisplatin-induced DSBs could promote synapsis in *Spo11* knockout spermatocytes, providing a partial rescue of the synaptic failure in the absence of SPO11 [11]. Moreover, in yeast, irradiation-induced DSBs can also partially rescue the *spo11* mutant phenotype, although in this case, some cells appear to be able to perform correct meiotic segregation, based on the production of some viable spores [50]. The smaller size of the yeast genome compared to the mouse genome may explain the differential effects of irradiation on synapsis on a SPO11-deficient background in the two-species.

## CONCLUSIONS

A point mutation in the *Spo11* gene that leads to the replacement of a single Tyr by a Phe in the catalytic site of the enzyme leads to a complete lack of DSB formation in mouse oocytes and spermatocytes. Half the amount of functional SPO11 is sufficient to generate a normal number of crossovers, although the number of DSBs that are

generated in leptotene is reduced. In the absence of meiotic DSBs as in *Spo11* ki, DSB repair proteins accumulate on the so-called pseudo XY body in male and female nuclei. These proteins can be recruited from the pseudo XY body to actual DSB-repair sites upon irradiation, and this then abrogates the formation of the pseudo XY body in spermatocytes, due to the limiting amounts of components that function in both DNA repair and MSUC.

It is known that meiotic prophase is differentially regulated in males and females. One aspect is the 30% difference in the number of crossovers. Our data show that this difference is most likely not caused by an increased number of meiotic DSBs in oocytes. In addition, we can conclude that, similar to what has been observed in yeast, irradiation-induced DSBs can stimulate synapsis in both male and female SPO11-deficient meiotic prophase nuclei.

## ACKNOWLEDGEMENTS

This work was supported by the Netherlands Organization for Scientific Research (NWO) through ALW (VIDI 864.05.003).

## REFERENCES

1. S.K. Mahadevaiah, J.M. Turner, F. Baudat, E.P. Rogakou, P. de Boer, J. Blanco-Rodriguez, M. Jasin, S. Keeney, W.M. Bonner, P.S. Burgoyne, Recombinational DNA double-strand breaks in mice precede synapsis, *Nat Genet* 27 (2001) 271-276.
2. F. Yang, P.J. Wang, The Mammalian synaptonemal complex: a scaffold and beyond, *Genome dynamics* 5 (2009) 69-80.
3. O. Fernandez-Capetillo, S.K. Mahadevaiah, A. Celeste, P.J. Romanienko, R.D. Camerini-Otero, W.M. Bonner, K. Manova, P. Burgoyne, A. Nussenzweig, H2AX is required for chromatin remodeling and inactivation of sex chromosomes in male mouse meiosis, *Dev Cell* 4 (2003) 497-508.
4. J.M. Turner, O. Aprelikova, X. Xu, R. Wang, S. Kim, G.V. Chandramouli, J.C. Barrett, P.S. Burgoyne, C.X. Deng, BRCA1, histone H2AX phosphorylation, and male meiotic sex chromosome inactivation, *Curr Biol* 14 (2004) 2135-2142.
5. E.P. Rogakou, D.R. Pilch, A.H. Orr, V.S. Ivanova, W.M. Bonner, DNA double-stranded breaks induce histone H2AX phosphorylation on serine 139, *J Biol Chem* 273 (1998) 5858-5868.
6. A. Inagaki, S. Schoenmakers, W.M. Baarends, DNA double strand break repair, chromosome synapsis and transcriptional silencing in meiosis, *Epigenetics* 5 (2010).
7. W. Goedecke, M. Eijpe, H.H. Offenberg, M. van Aalderen, C. Heyting, Mre11 and Ku70 interact in somatic cells, but are differentially expressed in early meiosis, *Nat Genet* 23 (1999) 194-198.
8. N. Kleckner, A. Storlazzi, D. Zickler, Coordinate variation in meiotic pachytene SC length and total crossover/chiasma frequency under conditions of constant DNA length, *Trends Genet* 19 (2003) 623-628.
9. W.M. Baarends, E. Wassenaar, J.W. Hoogerbrugge, G. van Cappellen, H.P. Roest, J. Vreeburg, M. Ooms, J.H. Hoeijmakers, J.A. Grootegoed, Loss of HR6B ubiquitin-conjugating activity results in damaged synaptonemal complex structure and increased crossing-over frequency during the male meiotic prophase, *Mol Cell Biol* 23 (2003) 1151-1162.
10. M.A. Bellani, P.J. Romanienko, D.A. Cairatti, R.D. Camerini-Otero, SPO11 is required for sex-body formation, and Spo11 heterozygosity rescues the prophase arrest of *Atm*<sup>-/-</sup> spermatocytes, *J Cell Sci* 118 (2005) 3233-3245.
11. P.J. Romanienko, R.D. Camerini-Otero, The mouse Spo11 gene is required for meiotic chromosome synapsis, *Mol Cell* 6 (2000) 975-987.

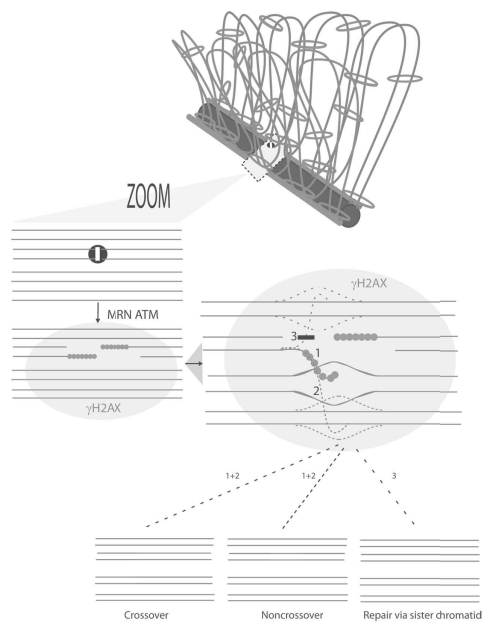
12. F. Baudat, K. Manova, J.P. Yuen, M. Jasin, S. Keeney, Chromosome synapsis defects and sexually dimorphic meiotic progression in mice lacking Spo11, *Mol Cell* 6 (2000) 989-998.
13. S.K. Mahadevaiah, D. Bourc'his, D.G. de Rooij, T.H. Bestor, J.M. Turner, P.S. Burgoyne, Extensive meiotic asynapsis in mice antagonises meiotic silencing of unsynapsed chromatin and consequently disrupts meiotic sex chromosome inactivation, *J Cell Biol* 182 (2008) 263-276.
14. Y.T. Chen, C.A. Venditti, G. Theiler, B.J. Stevenson, C. Iseli, A.O. Gure, C.V. Jongeneel, L.J. Old, A.J. Simpson, Identification of CT46/HORMAD1, an immunogenic cancer/testis antigen encoding a putative meiosis-related protein, *Cancer Immun* 5 (2005) 9.
15. S.A. Pangas, W. Yan, M.M. Matzuk, A. Rajkovic, Restricted germ cell expression of a gene encoding a novel mammalian HORMA domain-containing protein, *Gene Expr Patterns* 5 (2004) 257-263.
16. T. Fukuda, K. Daniel, L. Wojtasz, A. Toth, C. Hoog, A novel mammalian HORMA domain-containing protein, HORMAD1, preferentially associates with unsynapsed meiotic chromosomes, *Exp Cell Res* (2009).
17. T. de los Santos, J. Loidl, B. Larkin, N.M. Hollingsworth, A role for MMS4 in the processing of recombination intermediates during meiosis in *Saccharomyces cerevisiae*, *Genetics* 159 (2001) 1511-1525.
18. H. Niu, X. Li, E. Job, C. Park, D. Moazed, S.P. Gygi, N.M. Hollingsworth, Mek1 kinase is regulated to suppress double-strand break repair between sister chromatids during budding yeast meiosis, *Mol Cell Biol* 27 (2007) 5456-5467.
19. L. Wan, T. de los Santos, C. Zhang, K. Shokat, N.M. Hollingsworth, Mek1 kinase activity functions downstream of RED1 in the regulation of meiotic double strand break repair in budding yeast, *Mol Biol Cell* 15 (2004) 11-23.
20. L. Aravind, E.V. Koonin, The HORMA domain: a common structural denominator in mitotic checkpoints, chromosome synapsis and DNA repair, *Trends Biochem Sci* 23 (1998) 284-286.
21. N.M. Hollingsworth, L. Goetsch, B. Byers, The HOP1 gene encodes a meiosis-specific component of yeast chromosomes, *Cell* 61 (1990) 73-84.
22. A.P. Caryl, S.J. Armstrong, G.H. Jones, F.C. Franklin, A homologue of the yeast HOP1 gene is inactivated in the Arabidopsis meiotic mutant *asy1*, *Chromosoma* 109 (2000) 62-71.
23. K.I. Nonomura, M. Nakano, K. Murata, K. Miyoshi, M. Eiguchi, A. Miyao, H. Hirochika, N. Kurata, An insertional mutation in the rice PAIR2 gene, the ortholog of Arabidopsis ASY1, results in a defect in homologous chromosome pairing during meiosis, *Mol Genet Genomics* 271 (2004) 121-129.
24. S.A. Boden, N. Shadiac, E.J. Tucker, P. Langridge, J.A. Able, Expression and functional analysis of TaASY1 during meiosis of bread wheat (*Triticum aestivum*), *BMC Mol Biol* 8 (2007) 65.
25. L. Wojtasz, K. Daniel, I. Roig, E. Bolcun-Filas, H. Xu, V. Boonsanay, C.R. Eckmann, H.J. Cooke, M. Jasin, S. Keeney, M.J. McKay, A. Toth, Mouse HORMAD1 and HORMAD2, two conserved meiotic chromosomal proteins, are depleted from synapsed chromosome axes with the help of TRIP13 AAA-ATPase, *PLoS Genet* 5 (2009) e1000702.
26. S. Schoenmakers, E. Wassenaar, W.A. van Cappellen, A.A. Derijck, P. de Boer, J.S. Laven, J.A. Grootegeod, W.M. Baarends, Increased frequency of asynapsis and associated meiotic silencing of heterologous chromatin in the presence of irradiation-induced extra DNA double strand breaks, *Dev Biol* 317 (2008) 270-281.
27. N.M. Shanbhag, I.U. Rafalska-Metcalf, C. Balane-Bolivar, S.M. Janicki, R.A. Greenberg, ATM-dependent chromatin changes silence transcription in cis to DNA double-strand breaks, *Cell* 141 970-981.
28. W.M. Baarends, E. Wassenaar, J.W. Hooogerbrugge, S. Schoenmakers, Z.W. Sun, J.A. Grootegeod, Increased phosphorylation and dimethylation of XY body histones in the Hr6b-knockout mouse is associated with derepression of the X chromosome, *J Cell Sci* 120 (2007) 1841-1851.
29. A. Inagaki, W.A. van Cappellen, R. van der Laan, A.B. Houtsmuller, J.H. Hoeijmakers, J.A. Grootegeod, W.M. Baarends, Dynamic localization of human RAD18 during the cell cycle and a functional connection with DNA double-strand break repair, *DNA Repair (Amst)* 8 (2009) 190-201.
30. J. Essers, R.W. Hendriks, J. Wesoly, C.E. Beerens, B. Smit, J.H. Hoeijmakers, C. Wyman, M.L. Dronkert, R. Kanaar, Analysis of mouse Rad54 expression and its implications for homologous

- recombination, DNA Repair (Amst) 1 (2002) 779-793.
31. A.H. Peters, A.W. Plug, M.J. van Vugt, P. de Boer, A drying-down technique for the spreading of mammalian meiocytes from the male and female germline, *Chromosome Res* 5 (1997) 66-68.
  32. F. Hartung, R. Wurz-Wildersinn, J. Fuchs, I. Schubert, S. Suer, H. Puchta, The catalytically active tyrosine residues of both SPO11-1 and SPO11-2 are required for meiotic double-strand break induction in Arabidopsis, *The Plant cell* 19 (2007) 3090-3099.
  33. R.S. Cha, B.M. Weiner, S. Keeney, J. Dekker, N. Kleckner, Progression of meiotic DNA replication is modulated by interchromosomal interaction proteins, negatively by Spo11p and positively by Rec8p, *Genes Dev* 14 (2000) 493-503.
  34. D.S. Lim, P. Hasty, A mutation in mouse rad51 results in an early embryonic lethal that is suppressed by a mutation in p53, *Mol Cell Biol* 16 (1996) 7133-7143.
  35. T. Tsuzuki, Y. Fujii, K. Sakumi, Y. Tominaga, K. Nakao, M. Sekiguchi, A. Matsushiro, Y. Yoshimura, Morita T, Targeted disruption of the Rad51 gene leads to lethality in embryonic mice, *Proc Natl Acad Sci USA* 93 (1996) 6236-6240.
  36. M. Tarsounas, T. Morita, R.E. Pearlman, P.B. Moens, RAD51 and DMC1 form mixed complexes associated with mouse meiotic chromosome cores and synaptonemal complexes, *J. Cell. Biol.* 147 (1999) 207-220.
  37. E.F. Oakberg, Duration of spermatogenesis in the mouse and timing of stages of the cycle of the seminiferous epithelium, *The American journal of anatomy* 99 (1956) 507-516.
  38. H. Peters, Migration of gonocytes into the mammalian gonad and their differentiation, *Philos Trans R Soc Lond B Biol Sci* 259 (1970) 91-101.
  39. G.W. van der Heijden, A.A. Derijck, E. Posfai, M. Giele, P. Pelczar, L. Ramos, D.G. Wansink, J. van der Vlag, A.H. Peters, P. de Boer, Chromosome-wide nucleosome replacement and H3.3 incorporation during mammalian meiotic sex chromosome inactivation, *Nat Genet* 39 (2007) 251-258.
  40. R. van der Laan, H. Roest, J. Hoogerbrugge, E. Smit, R. Slater, W. Baarends, J. Hoeijmakers, J. Grootegoed, Characterization of mRAD18Sc, a mouse homolog of the yeast post-replication repair gen RAD18, *Genomics* 69 (2000) 86-94.
  41. M. Kalocsay, N.J. Hiller, S. Jentsch, Chromosome-wide Rad51 spreading and SUMO-H2A.Z-dependent chromosome fixation in response to a persistent DNA double-strand break, *Mol Cell* 33 (2009) 335-343.
  42. J.A. Aten, J. Stap, P.M. Krawczyk, C.H. van Oven, R.A. Hoebe, J. Essers, R. Kanaar, Dynamics of DNA double-strand breaks revealed by clustering of damaged chromosome domains, *Science* 303 (2004) 92-95.
  43. E.B. Baart, D.G. de Rooij, K.S. Keegan, P. de Boer, Distribution of Atr protein in primary spermatocytes of a mouse chromosomal mutant: a comparison of preparation techniques [In Process Citation], *Chromosoma* 109 (2000) 139-147.
  44. P. de Boer, A.G. Searle, F.A. van der Hoeven, D.G. de Rooij, C.V. Beechey, Male pachytene pairing in single and double translocation heterozygotes and spermatogenic impairment in the mouse, *Chromosoma* 93 (1986) 326-336.
  45. J. Forejt, Hybrid sterility in the mouse, *Trends Genet* 12 (1996) 412-417.
  46. W.M. Baarends, E. Wassenaar, R. van der Laan, J.W. Hoogerbrugge, E. Sleddens-Linkels, J.H. Hoeijmakers, P. de Boer, J.A. Grootegoed, Silencing of unpaired chromatin and histone H2A ubiquitination in mammalian meiosis, *Mol Cell Biol* 25 (2005) 1041-1053.
  47. R. van der Laan, E.J. Uringa, E. Wassenaar, J.W. Hoogerbrugge, E. Sleddens, H. Odijk, H.P. Roest, P. de Boer, J.H. Hoeijmakers, J.A. Grootegoed, W.M. Baarends, Ubiquitin ligase Rad18Sc localizes to the XY body and to other chromosomal regions that are unpaired and transcriptionally silenced during male meiotic prophase, *J Cell Sci* 117 (2004) 5023-5033.
  48. F.A. de Vries, E. de Boer, M. van den Bosch, W.M. Baarends, M. Ooms, L. Yuan, J.G. Liu, A.A. van Zeeland, C. Heyting, A. Pastink, Mouse Sycp1 functions in synaptonemal complex assembly, meiotic recombination, and XY body formation, *Genes Dev* 19 (2005) 1376-1389.
  49. A. Kouznetsova, H. Wang, M. Bellani, R.D. Camerini-Otero, R. Jessberger, C. Hoog, BRCA1-mediated chromatin silencing is limited to oocytes with a small number of asynapsed chromosomes, *J Cell Sci* 122 (2009) 2446-2452.
  50. L.W. Thorne, B. Byers, Stage-specific effects of X-irradiation on yeast meiosis, *Genetics* 134 (1993) 29-42.

7

# GENERAL DISCUSSION

Akiko Inagaki



## DISCUSSION

The aim of the work described in this thesis was to analyse RAD18 functions in mitotic and meiotic DNA repair pathways. RAD18 is most well known for its role in replication damage bypass (RDB). We have analysed the dynamic localization of RAD18 at sites where RDB is activated during S phase (Chapter 2), and also determined which RAD18 domains are required to ubiquitylate PCNA, which is the main substrate in the RDB pathway (Chapter 3). Although it has been known for some time that RAD18 also localizes to sites of DNA double-strand breaks (DSBs) (see also Chapter 2), and that *Rad18* deficient cells are sensitive to agents that induce DSBs [1-3], the functions of RAD18 at DSB repair sites remain elusive. To gain insight into these functions, it is important to understand what triggers recruitment of RAD18 to DSBs, and most essential, to identify interacting proteins that may be substrates for RAD18-mediated ubiquitylation. Here we will discuss the possible relevance of RAD18 recruitment to DSB-repair sites in mitotic and meiotic cells, and finally focus on the candidate substrates for RAD18 ubiquitylation that were identified in this context.

## 7

### RECRUITMENT OF RAD18 TO DSB REPAIR SITES IN MITOTIC CELLS

Two distinct modes of recruitment of RAD18 to sites of DNA damage can be discerned. First, RAD18 appears to have direct DNA binding properties mediated by the SAP domain. This binding requires the protein RPA, which binds to ssDNA and mediates recruitment of RAD18 to the DNA. RPA and the SAP domain of RAD18 are both required for PCNA ubiquitylation in the RDB pathway [4]. Second, recruitment of RAD18 to the chromatin surrounding DSB sites depends on the ubiquitin-binding Zinc finger domain of RAD18 (Chapter 3). Still, this mode of RAD18 recruitment also requires RPA (Chapter 3), although it is not clear whether in this situation RPA plays a direct role in RAD18 recruitment or acts further upstream. RAD18 localizes as a diffuse cloud to the region surrounding DSB sites within 2 minutes throughout the cell cycle (Chapter 2). Most likely, the Zinc finger domain mediates the binding of RAD18 to ubiquitylated chromatin components. The most well known ubiquitylated chromatin components that are enriched at sites of DSB-repair are ubiquitylated H2A and ubiquitylated H2AX [5-10]. The localization of ubiquitylated H2A and/or H2AX can be visualized using an antibody that targets conjugated ubiquitin (FK2; Biomol, PW 8810) or an antibody that recognizes ubiquitylated H2A (05-678, Upstate). The FK2 antibody recognizes all ubiquitylated proteins, mono- and poly- ubiquitylated. A related antibody, named FK1, recognizes only poly-ubiquitylated proteins, and another antibody (HWA4C4; eBioscience and Millipore, or Apu3.A8; Genetech and Millipore) recognizes only poly-ubiquitylated proteins that are linked via K63. Using such antibodies, it was shown that the majority of polyubiquitylated proteins at DSB sites are linked via K63 [11-13]. The antibody against ubiquitylated H2A is a mouse monoclonal IgM antibody that was fortuitously discovered in a screen for monoclonal antibodies that showed enhanced immunoreactivity in SV-40 transformed human fibroblasts

compared to the normal fibroblasts. Sequencing fragments of the immunoreactive band revealed that the recognized protein represented ubiquitylated H2A [14]. Still the specificity of this antibody for ubiquitylated H2A in immunocytochemistry has not been demonstrated unequivocally, and it is also not certain which ubiquitylated forms of H2A are recognized. The fact that the genome encodes many copies of the H2A gene complicates targeted mutagenesis studies, although a combined knockdown and transgenic approach might yield informative results. Huen et al.(2007) have shown that ubiquitylation of H2AX does not depend on K119/120, the major site for mono-ubiquitylation of H2A outside the context of DNA repair [6].

Our own immunoprecipitation experiments have shown that RAD18 interacts with mono-ubiquitylated H2A, and that the amount of co-precipitated mono-ubiquitylated H2A increases upon induction of DSBs (Chapter 3). This strongly suggests that RAD18 is recruited to DSB repair sites at least in part via interaction with mono-ubiquitylated H2A. This is also consistent with the fact that recruitment of RAD18 to DSB repair sites requires the function of RNF8, one of the main E3 ligases for H2A ubiquitylation [8]. In addition to the interaction of RAD18 with ubiquitylated H2A, our immunoprecipitation results also indicate that RAD18 interacts with many other ubiquitylated proteins, in a Zinc finger dependent way, making it highly likely that apart from H2A and H2AX, other ubiquitylated chromatin components will also be used by RAD18 to bind to chromatin near DSB repair sites. Our immunocytochemical analyses of FK2 in relation to the localization of RAD18 in HeLa cells indicate that RAD18 localization to chromatin is indeed dependent on the presence of ubiquitylated chromatin components (Chapter 3). To analyze whether RAD18 always localizes to regions that show enhanced H2A ubiquitylation, we analyzed human female primary fibroblast cultures. In these cells, dosage compensation has resulted in the inactivation of one of the two X chromosomes, and this chromosome is known to be enriched for ubiquitylated H2A. Immunocytochemical analyses of FK2 and RAD18 signals in these cells revealed that the Barr body was mostly not enriched for RAD18, even if FK2 staining was enhanced in this region. In a small percentage of the nuclei, RAD18 was detected at the Barr body (Chapter 3). Together with our immunoprecipitation experiments, that show a very different banding pattern of the input of ubiquitylated proteins compared to the output of ubiquitylated proteins whose precipitation by the RAD18 antibody depends on the presence of an intact Zinc finger domain, these data indicate that the interaction of RAD18 with ubiquitylated chromatin components is specific, and possibly regulated. Such regulation might occur via phosphorylation by ATM kinase, similar to what occurs for many other proteins involved in DNA damage response pathways (DDR). Using anti-Flag-tagged RAD18 co-immunoprecipitation followed by mass-spectrometry, we have found that RAD18 interacts with 14-3-3 proteins (data not shown), which recognize phosphorylated serine or threonine residue of substrates [15]. In addition, autoubiquitylation of RAD18 may render the protein inactive, since we did not observe an interaction between ubiquitylated H2A and ubiquitylated RAD18; only non-ubiquitylated RAD18 was co-immunoprecipitated upon precipitation of GFP-tagged H2A (Chapter 3).

## INTERACTING PROTEINS AND POSSIBLE DOWNSTREAM EFFECTS OF RAD18 RECRUITMENT TO DSB SITES IN MITOTIC CELLS

Recently, RAD51C was identified as a new interacting partner for RAD18 in mammalian cells [1]. RAD51C binds to the RING finger domain of RAD18, is a RAD51 paralog, and functions to stabilize RAD51 after DNA damage by protecting it from ubiquitin-mediated degradation [16]. It is not clear whether RAD51C is a substrate for RAD18. Huang et al. (2009) found that the number of irradiation-induced RAD51 foci is decreased in the absence of RAD18 [1], indicating that lack of interaction of RAD51C with RAD18 might somehow reduce the protective function of RAD51C and/or RAD51C is required for efficient loading of RAD51, like other RAD51 paralogs. Instead, we have found that RAD51 can still accumulate at sites of locally induced damage in the absence of RAD18, indicating that there is no absolute requirement for RAD18 in RAD51 foci formation (Chapter 2). Huang et al. (2009) found that the RING finger domain, but not its enzymatic activity, is required for the function of RAD18 in DSB repair, indicating that RAD18 may have a structural rather than an enzymatic function in DSB repair. However, we have found that the enzymatic activity of RAD18 is required for the recruitment of the checkpoint-related protein RAD9 to DSB repair sites (Chapter 3). Since we observed no direct interaction between RAD18 and RAD9, and also could not detect any ubiquitylated RAD9, the enzymatic role of RAD18 in this context may be indirect, involving a yet unknown substrate. Another known interaction partner for RAD18 is 53BP1 [3]. This protein plays an important role in the choice between HR and NHEJ; it stimulates NHEJ through interfering with DNA-end resection (Chapter 1). Watanabe et al. (2009) showed that RAD18 and 53BP1 are interdependent for foci formation after IR in G1 [3]. In this phase of the cell cycle, NHEJ is thought to be the preferred pathway for DSB repair, in the absence of a sister chromatid as the template for HR. We have found that RAD18 accumulates in one or two relatively large foci in G1 that may contain either Ku80 or RAD51 protein, suggesting that HR is initiated and probably persisted in approximately 47% of the spontaneous DSBs in G1 (Chapter 2). It is tempting to suggest that RAD18 may interact with 53BP1 to inhibit its NHEJ-stimulatory role, since Rad18 in yeast and chicken DT40 cells also inhibits NHEJ [17], and the interaction of RAD18 with RAD51C may facilitate HR. Intriguingly, 53BP1 interacts with RAD18 via the Zinc finger of RAD18 [3], suggesting that RAD18 may interact with ubiquitylated 53BP1.

Using two separate approaches we have also tried to identify novel RAD18 interacting proteins. As described above, we analysed RAD18-interacting proteins through a co-immunoprecipitation approach using FLAG-tagged wild type RAD18, and RAD18 mutated in the Zinc finger, expressed in HeLa cells. Co-immunoprecipitated proteins were identified through mass spectrometry. This approach yielded not only the 14-3-3 protein (see above), but also several other interesting candidate proteins such as the tumor suppressor protein JunB, and the breast cancer gene product BRCA2 [18]. BRCA2 protein interacts directly with the RAD51 recombinase [19,20] and regulates recombination mediated DSB repair by stabilizing the RAD51 filaments. In a second

approach, we performed a yeast two-hybrid screen, using full length mouse RAD18 as the bait and a cDNA library generated from mouse testis as the prey. This experiment yielded many clones encoding the protein MTBP for MDM2 (two)-binding protein. MTBP is highly expressed in testis and ovary, and was identified based on its MDM2-binding property [21]. *MDM2* is an oncogene that functions as an ubiquitin E3 ligase, it controls the activity of p53 as a transcription factor [22], and regulates the stability of p53 and MDM2 itself through ubiquitin-mediated proteasomal degradation [23,24]. MTBP may stabilize MDM2 by inhibiting autoubiquitylation of MDM2. This would enhance polyubiquitylation of p53 by MDM2 followed by the proteasome mediated degradation [25]. Knockout of MTBP leads to embryonic lethality [26], but haploinsufficiency increases tumor metastasis, indicating that MTBP may act as a tumor suppressor. To analyze a possible regulatory relationship between RAD18 and MTBP, we analyzed expression of MTBP and MDM2 in wild type and *Hr6b* knockout mouse spermatocytes and spermatids, and found that both proteins were upregulated in the knockout (data not shown). Together with the two-hybrid data, this suggests that HR6B, together with RAD18, may ubiquitylate MTBP, leading to its degradation, and concomitant destabilization of MDM2. This could then lead to stabilization of p53.

The two-hybrid system was also used to investigate possible interactions between RAD18 and components of the 9-1-1 complex. This complex is essential for the activation of cell cycle checkpoints at sites of DNA damage, and Rad18-mediated ubiquitylation of the Rad1 component of the 9-1-1 complex was reported to stimulate the activity of the 9-1-1 complex upon the induction of damage [27]. We did not detect any direct interaction between the components of the 9-1-1 complex and RAD18. Very recently, Davies et al. (2010) [28] reported that ubiquitylation of the 9-1-1 complex is independent of damage and the Rad6-Rad18 complex. Based on these observations, it appears that it is unlikely that RAD18 mediated ubiquitylation of some of the components of the 9-1-1 complex at sites of DNA repair. Most interestingly, although we have not found a direct interaction between RAD18 and the 9-1-1 complex, our results revealed a functional interaction; recruitment of RAD9 to G1 foci and to damage-induced DSBs requires RAD18. Based upon the fact that knockdown of RAD18 does not interfere with the activation of the checkpoint kinases that are downstream of 9-1-1 activation, CHK1 and CHK2, we propose that RAD9 performs a direct role in HR at these sites (Chapter 3).

## RAD18 RECRUITMENT TO MEIOTIC DSBs

In contrast to mitotic DSBs which may arise due to exogenous and endogenous DNA damage, meiotic DSBs are programmed and induced by the topoisomerase II-like enzyme SPO11. As discussed in Chapter 4, the processing of meiotic DSBs shows some resemblance to the processing of damage-induced DSBs, but specific aspects have been adapted to stimulate repair via homologous recombination, using the homologous chromosome as a template for repair, instead of the sister chromatid. RAD18 is not directly recruited to these DSBs, but only to a subset of approximately 30-40 breaks, based upon the number of foci that appears in zygotene. In these nuclei, RAD18 has a

focal appearance, and ubiquitylated H2A does not accumulate at these sites, indicating that RAD18 is recruited to these breaks independent of H2A ubiquitylation, and possibly also independent of its Zinc finger domain. This focal recruitment of RAD18 may depend on RPA that is loaded at many meiotic DSB-repair sites at this stage. Somehow, recruitment of RAD18 to SPO11-induced DSBs in leptotene is prevented, since radiation does induce focal RAD18 accumulation in these cells, indicating that RAD18 is present in sufficient amount. In pachytene, RAD18 accumulates as a diffuse cloud on the XY body, and colocalizes with ubiquitylated H2A. Interestingly, the presence of damage-induced DSBs in these cells also leads to a more diffuse accumulation of RAD18 to the region surrounding the DSBs, and this region is also enriched for ubiquitylated H2A. Taken together, this indicates that, similar to the situation in mitotic cells, two modes of RAD18 recruitment, a focal mode and a diffuse mode, are operative in meiotic cells. The diffuse mode of RAD18 accumulation most likely depends on the interaction between RAD18 and ubiquitylated H2A and/or possibly additional ubiquitylated chromatin components. Recently, the function of RNF8 in spermatogenesis has been examined and it was found that the ubiquitylation of H2A and H2B by this enzyme is essential for the histone-to-protamine transition that allows the tight packaging of the sperm genome [29]. Surprisingly, meiosis proceeds normally in *Rnf8* knockout mice, despite the fact that ubiquitylation of H2A on the XY body is disrupted [29]. It will be very intriguing to investigate whether RAD18 accumulates on the XY body in the *Rnf8* knockout mice.

## INTERACTION PARTNERS OF RAD18 IN MEIOTIC DSB REPAIR

RAD51C is one of the interaction partners of RAD18 in somatic cells [1]. In male spermatocytes, the pattern of RAD51C staining is strikingly similar to that of MLH1 [30]. In pachytene, one or two distinct RAD51C foci associated with each synapsed bivalent, and many of these RAD51C foci persist through diplotene, indicating that RAD51C targets crossover sites. *Rad51c* knockout mice are embryonic lethal [31]. To overcome the early embryonic lethality, a viable mouse model carrying a hypomorphic and null allele of *Rad51c* produced mice expressing 5-30% of the wild type level of RAD51C protein [32]. These *Rad51c* deficient mice are subfertile, and the number of RAD51 foci in leptotene and zygotene is significantly decreased, in association with abnormal synapsis between homologous chromosomes, and a decreased number of crossover sites and meiotic arrest [32]. This observation is surprising, in light of the fact that foci formation of RAD51C is not observed in leptotene and zygotene spermatocyte in wild type [30]. The decreased number of RAD51 foci is not due to a decrease in the number of SPO11-induced DSBs because the number of RPA foci is similar in both mutant and control mice [32]. Taken together, *Rad51c* deficient mice show clear defects in HR-mediated repair of meiotic DSBs. Spermatocytes of *Rad18* knockdown mice do not show such dramatic defects in HR repair, and RAD18 displays a different localization pattern, indicating that RAD51C and RAD18 may function independently in meiosis.

53BP1 is another obvious candidate interacting protein for RAD18 in spermatocytes. It colocalizes with RAD18 on the XY body in pachytene and diplotene spermatocytes.

However, *53BP1*<sup>-/-</sup> mice are fertile and the males have no noticeable defect in spermatogenesis [33,34]. In addition, the 53BP1 localization pattern is not different in *Rad18* knockdown spermatocytes compared to controls (unpublished data), indicating that RAD18 is not required for the localization of 53BP1 to the XY body.

As described above, MTBP may interact with RAD18 in spermatocytes, since both proteins are highly expressed in testis, and the level of MTBP protein was upregulated in *Hr6b* knockout spermatocytes and spermatids. To investigate this possibility further, it will be necessary to directly co-precipitate MTBP and RAD18 from testicular samples, and to study the effect of *Rad18* knockdown on MTBP protein expression in spermatocytes and spermatids.

### **POSSIBLE ROLE OF RAD18 IN INTERSISTER MEDIATED HOMOLOGOUS RECOMBINATION REPAIR OF PERSISTENT MEIOTIC DSBS**

In RAD18 deficient spermatocytes, and also in *Hr6b* knockout spermatocytes, we noted persistence of a few diffuse  $\gamma$ H2AX foci in diplotene (Chapter 4). This result indicates that the HR6B/RAD18 complex is required for repair of a small subset of meiotic DSBS. At the XY body, we do not observe any change in the dynamics of  $\gamma$ H2AX removal in *Rad18* knockdown spermatocytes compared to controls. It may be suggested that RAD18 stimulates HR at the XY body, but fails to succeed since repair via the sister chromatid and NHEJ are repressed. When NHEJ is reactivated in late pachytene spermatocytes [35], repair may occur via this pathway, independent of RAD18. This hypothesis is supported by the fact that both RAD51 and RAD18 disappear from the XY body before  $\gamma$ H2AX. At autosomal sites, where RAD18 shows a transient focal accumulation in late zygotene, RAD18 may be recruited to a small subset of meiotic breaks that has failed to initiate repair using the homologous chromosome as a template. On the autosomal chromosomes, synapsis may proceed in the presence of some persisting damage, once a certain threshold number of sites have progressed through the strand-invasion steps, and crossing-over sites have been designated. Synapsis may result in the removal of proteins that inhibit sister chromatid mediated HR, and thus persisting DSBS may then be repaired via the “normal” mitotic pathway. This process may be stimulated by RAD18, and on the *Rad18* knockdown background such breaks may persist until NHEJ is reactivated. Thus, RAD18 may stimulate intersister-mediated DSB repair at persisting DSBS on autosomes as well as on the X chromosome. At the X chromosome, this activity is inhibited since synapsis is not achieved (maintaining the interhomolog bias to stimulate chromosome pairing). However, at autosomal sites, where synapsis is achieved, this inhibition is relieved, and RAD18 helps to mediate the inter-sister repair. Based upon the number of RAD18 foci in late zygotene nuclei, it might be suggested that approximately 30-40 such sites of inter-sister repair occur per spermatocyte nucleus. RAD51C and BRCA2 are two putative interaction partners that could help to mediate this function of RAD18, although it remains to be established whether this also involves their ubiquitylation.

## PUTATIVE RAD18 FUNCTION IN TRANSCRIPTIONAL SILENCING COUPLED TO DNA REPAIR

In *Rad18* knockdown mice, the maintenance of meiotic sex chromosome inactivation (MSCI) appears to be impaired (Chapter 4), similar to what was observed for *Hr6b* knockout mice [36,37]. MSCI is thought to be triggered by the presence of asynapsed axial elements, but the process also resembles the DNA damage and requires ATR-induced  $\gamma$ H2AX formation. Recently, Shanbhag et al. (2010) elegantly showed that DSBs induce transcriptional silencing in cis, and that this requires ATM and ubiquitylation of H2A by RNF8 as well as additional K63-linked polyubiquitylation by RNF168. Since the X chromosome contains several persisting DSBs in pachytene, it is tempting to speculate that MSCI, and DSB-dependent silencing in cis, termed DISC, are evolutionary related ([38] and see also Chapter 4). Shanbhag et al. (2010) speculate that mono-ubiquitylation of H2A may be most directly involved in mediating DISC, whereas the formation of K63 polyubiquitin chains may function more in DNA damage recognition. Since we have observed a direct interaction between RAD18 and mono-ubiquitylated H2A, and observed an impairment of MSCI in RAD18 deficient spermatocytes, it might be suggested that RAD18 also functions in DISC in somatic cells. Perhaps its recruitment of RAD9 to DSB-repair sites is also functionally relevant in this context. The protein RAD1, a component of the 9-1-1 complex, has been shown to accumulate on the XY body [39]. For RAD9, this is not known. So far we have been unable to obtain specific antibodies that are useful for detecting components of the 9-1-1 complex at the XY body, and therefore, we cannot determine whether their recruitment is impaired in *Rad18* knockdown spermatocytes. To obtain more insight in the putative roles of RAD18 in DSB-repair, DISC and MSCI, it will be important to identify the (ubiquitylated) proteins that interact with RAD18 as observed in Chapter 3 by mass-spectrometry.

## REFERENCES

1. J. Huang, M.S. Huen, H. Kim, C.C. Leung, J.N. Glover, X. Yu, J. Chen, RAD18 transmits DNA damage signalling to elicit homologous recombination repair, *Nat Cell Biol* 11 (2009) 592-603.
2. N. Shiomi, M. Mori, H. Tsuji, T. Imai, H. Inoue, S. Tateishi, M. Yamaizumi, T. Shiomi, Human RAD18 is involved in S phase-specific single-strand break repair without PCNA monoubiquitination, *Nucleic Acids Res* 35 (2007) e9.
3. K. Watanabe, K. Iwabuchi, J. Sun, Y. Tsuji, T. Tani, K. Tokunaga, T. Date, M. Hashimoto, M. Yamaizumi, S. Tateishi, RAD18 promotes DNA double-strand break repair during G1 phase through chromatin retention of 53BP1, *Nucleic Acids Res* (2009).
4. A.A. Davies, D. Huttner, Y. Daigaku, S. Chen, H.D. Ulrich, Activation of ubiquitin-dependent DNA damage bypass is mediated by replication protein a, *Mol Cell* 29 (2008) 625-636.
5. A. Celeste, O. Fernandez-Capetillo, M.J. Kruhlak, D.R. Pilch, D.W. Staudt, A. Lee, R.F. Bonner, W.M. Bonner, A. Nussenzweig, Histone H2AX phosphorylation is dispensable for the initial recognition of DNA breaks, *Nat Cell Biol* 5 (2003) 675-679.
6. M.S. Huen, R. Grant, I. Manke, K. Minn, X. Yu, M.B. Yaffe, J. Chen, RNF8 transduces the DNA-damage signal via histone ubiquitylation and checkpoint protein assembly, *Cell* 131 (2007) 901-914.
7. N.K. Kolas, J.R. Chapman, S. Nakada, J. Ylanko, R. Chahwan, F.D. Sweeney, S.

- Panier, M. Mendez, J. Wildenhain, T.M. Thomson, L. Pelletier, S.P. Jackson, D. Durocher, Orchestration of the DNA-damage response by the RNF8 ubiquitin ligase, *Science* 318 (2007) 1637-1640.
8. N. Mailand, S. Bekker-Jensen, H. Faustrup, F. Melander, J. Bartek, C. Lukas, J. Lukas, RNF8 ubiquitylates histones at DNA double-strand breaks and promotes assembly of repair proteins, *Cell* 131 (2007) 887-900.
  9. G.S. Stewart, B. Wang, C.R. Bignell, A.M. Taylor, S.J. Elledge, MDC1 is a mediator of the mammalian DNA damage checkpoint, *Nature* 421 (2003) 961-966.
  10. A. Xie, A. Hartlerode, M. Stucki, S. Odate, N. Puget, A. Kwok, G. Nagaraju, C. Yan, F.W. Alt, J. Chen, S.P. Jackson, R. Scully, Distinct roles of chromatin-associated proteins MDC1 and 53BP1 in mammalian double-strand break repair, *Mol Cell* 28 (2007) 1045-1057.
  11. C. Doil, N. Mailand, S. Bekker-Jensen, P. Menard, D.H. Larsen, R. Pepperkok, J. Ellenberg, S. Panier, D. Durocher, J. Bartek, J. Lukas, C. Lukas, RNF168 binds and amplifies ubiquitin conjugates on damaged chromosomes to allow accumulation of repair proteins, *Cell* 136 (2009) 435-446.
  12. B. Sobhian, G. Shao, D.R. Lilli, A.C. Culhane, L.A. Moreau, B. Xia, D.M. Livingston, R.A. Greenberg, RAP80 targets BRCA1 to specific ubiquitin structures at DNA damage sites, *Science* 316 (2007) 1198-1202.
  13. G.S. Stewart, S. Panier, K. Townsend, A.K. Al-Hakim, N.K. Kolas, E.S. Miller, S. Nakada, J. Ylanko, S. Olivarius, M. Mendez, C. Oldreive, J. Wildenhain, A. Tagliaferro, L. Pelletier, N. Taubenheim, A. Durandy, P.J. Byrd, T. Stankovic, A.M. Taylor, D. Durocher, The RIDDLE syndrome protein mediates a ubiquitin-dependent signaling cascade at sites of DNA damage, *Cell* 136 (2009) 420-434.
  14. A.P. Vassilev, H.H. Rasmussen, E.I. Christensen, S. Nielsen, J.E. Celis, The levels of ubiquitinated histone H2A are highly upregulated in transformed human cells: partial colocalization of uH2A clusters and PCNA/cyclin foci in a fraction of cells in S-phase, *J. Cell Sci.* 108 (1995) 1205-1215.
  15. M.B. Yaffe, K. Rittinger, S. Volinia, P.R. Caron, A. Aitken, H. Leffers, S.J. Gamblin, S.J. Smerdon, L.C. Cantley, The structural basis for 14-3-3:phosphopeptide binding specificity, *Cell* 91 (1997) 961-971.
  16. B.T. Bennett, K.L. Knight, Cellular localization of human Rad51C and regulation of ubiquitin-mediated proteolysis of Rad51, *J Cell Biochem* 96 (2005) 1095-1109.
  17. A. Saberi, H. Hochegger, D. Szuts, L. Lan, A. Yasui, J.E. Sale, Y. Taniguchi, Y. Murakawa, W. Zeng, K. Yokomori, T. Helleday, H. Teraoka, H. Arakawa, J.M. Buerstedde, S. Takeda, RAD18 and poly(ADP-ribose) polymerase independently suppress the access of nonhomologous end joining to double-strand breaks and facilitate homologous recombination-mediated repair, *Mol Cell Biol* 27 (2007) 2562-2571.
  18. R. Wooster, G. Bignell, J. Lancaster, S. Swift, S. Seal, J. Mangion, N. Collins, S. Gregory, C. Gumbs, G. Micklem, Identification of the breast cancer susceptibility gene BRCA2, *Nature* 378 (1995) 789-792.
  19. P.L. Chen, C.F. Chen, Y. Chen, J. Xiao, Z.D. Sharp, W.H. Lee, The BRC repeats in BRCA2 are critical for RAD51 binding and resistance to methyl methanesulfonate treatment, *Proc Natl Acad Sci U S A* 95 (1998) 5287-5292.
  20. L.Y. Marmorstein, T. Ouchi, S.A. Aaronson, The BRCA2 gene product functionally interacts with p53 and RAD51, *Proc Natl Acad Sci U S A* 95 (1998) 13869-13874.
  21. M.T. Boyd, N. Vlatkovic, D.S. Haines, A novel cellular protein (MTBP) binds to MDM2 and induces a G1 arrest that is suppressed by MDM2, *J Biol Chem* 275 (2000) 31883-31890.
  22. J. Momand, G.P. Zambetti, D.C. Olson, D. George, A.J. Levine, The mdm-2 oncogene product forms a complex with the p53 protein and inhibits p53-mediated transactivation, *Cell* 69 (1992) 1237-1245.
  23. Y. Haupt, R. Maya, A. Kazaz, M. Oren, Mdm2 promotes the rapid degradation of p53, *Nature* 387 (1997) 296-299.
  24. M.H. Kubbutat, S.N. Jones, K.H. Vousden, Regulation of p53 stability by Mdm2, *Nature* 387 (1997) 299-303.
  25. M. Brady, N. Vlatkovic, M.T. Boyd, Regulation of p53 and MDM2 activity by MTBP, *Mol Cell Biol* 25 (2005) 545-553.
  26. T. Iwakuma, Y. Tochigi, C.S. Van Pelt, L.C. Caldwell, T. Terzian, J.M. Parant, G.P. Chau, J.G. Koch, C.M. Eischen, G. Lozano, Mtbp haploinsufficiency in mice increases tumor metastasis, *Oncogene* 27 (2008) 1813-1820.

27. Y. Fu, Y. Zhu, K. Zhang, M. Yeung, D. Durocher, W. Xiao, Rad6-Rad18 mediates a eukaryotic SOS response by ubiquitinating the 9-1-1 checkpoint clamp, *Cell* 133 (2008) 601-611.
28. A.A. Davies, A. Neiss, H.D. Ulrich, Ubiquitylation of the 9-1-1 checkpoint clamp is independent of rad6-rad18 and DNA damage, *Cell* 141 1080-1087.
29. L.Y. Lu, J. Wu, L. Ye, G.B. Gavrulina, T.L. Saunders, X. Yu, RNF8-dependent histone modifications regulate nucleosome removal during spermatogenesis, *Dev Cell* 18 371-384.
30. Y. Liu, M. Tarsounas, P. O'Regan, S.C. West, Role of RAD51C and XRCC3 in genetic recombination and DNA repair, *J Biol Chem* 282 (2007) 1973-1979.
31. S.G. Kuznetsov, D.C. Haines, B.K. Martin, S.K. Sharan, Loss of Rad51c leads to embryonic lethality and modulation of Trp53-dependent tumorigenesis in mice, *Cancer Res* 69 (2009) 863-872.
32. S. Kuznetsov, M. Pellegrini, K. Shuda, O. Fernandez-Capetillo, Y. Liu, B.K. Martin, S. Burkett, E. Southon, D. Pati, L. Tessarollo, S.C. West, P.J. Donovan, A. Nussenzweig, S.K. Sharan, RAD51C deficiency in mice results in early prophase I arrest in males and sister chromatid separation at metaphase II in females, *J Cell Biol* 176 (2007) 581-592.
33. J.C. Morales, Z. Xia, T. Lu, M.B. Aldrich, B. Wang, C. Rosales, R.E. Kellems, W.N. Hittelman, S.J. Elledge, P.B. Carpenter, Role for the BRCA1 C-terminal repeats (BRCT) protein 53BP1 in maintaining genomic stability, *J Biol Chem* 278 (2003) 14971-14977.
34. I.M. Ward, K. Minn, J. van Deursen, J. Chen, p53 Binding protein 53BP1 is required for DNA damage responses and tumor suppression in mice, *Mol Cell Biol* 23 (2003) 2556-2563.
35. E.A. Ahmed, M.E. Philippens, H.B. Kal, D.G. de Rooij, P. de Boer, Genetic probing of homologous recombination and non-homologous end joining during meiotic prophase in irradiated mouse spermatocytes, *Mutat Res*.
36. E.M. Achame, E. Wassenaar, J.W. Hoogerbrugge, E. Sleddens-Linkels, M. Ooms, Z.W. Sun, W.F. van Ijcken, J.A. Grootegoed, W.M. Baarends, The ubiquitin-conjugating enzyme HR6B is required for maintenance of X chromosome silencing in mouse spermatocytes and spermatids, *BMC genomics* 11 367.
37. W.M. Baarends, E. Wassenaar, J.W. Hoogerbrugge, S. Schoenmakers, Z.W. Sun, J.A. Grootegoed, Increased phosphorylation and dimethylation of XY body histones in the Hr6b-knockout mouse is associated with derepression of the X chromosome, *J Cell Sci* 120 (2007) 1841-1851.
38. N.M. Shanbhag, I.U. Rafalska-Metcalf, C. Balane-Bolivar, S.M. Janicki, R.A. Greenberg, ATM-dependent chromatin changes silence transcription in cis to DNA double-strand breaks, *Cell* 141 970-981.
39. R. Freire, J.R. Murguia, M. Tarsounas, N.F. Lowndes, P.B. Moens, S.P. Jackson, Human and mouse homologs of *Schizosaccharomyces pombe* rad1(+) and *Saccharomyces cerevisiae* RAD17: linkage to checkpoint control and mammalian meiosis, *Genes Dev* 12 (1998) 2560-2573.



&

## **ADDENDUM**

**Summary**  
**Samenvatting**  
**List of abbreviations**  
**Curriculum Vitae**  
**PhD portfolio**  
**List of publications**  
**Acknowledgements**

## SUMMARY

Cells are constantly exposed to internal and external factors that may cause DNA damage. To maintain genomic integrity, cells have developed elaborate DNA repair systems and various cell cycle checkpoints that ensure the repair of DNA lesions before cell cycle progression resumes. One of the most genotoxic lesions is a DNA double strand break (DSB). In mitotic cells, DSBs can arise when the replication fork collapses during S phase. In meiosis, DSBs are induced by the enzyme SPO11, as a first step in meiotic recombination. In addition, DSBs may arise, both in mitotic and meiotic cells, from exogenous factors such as ionizing radiation.

In this thesis, we focused on the role of RAD18 in DSB repair in mitotic and meiotic cells. RAD18 is an ubiquitin E3 ligase, which is most well known for its role in replication damage bypass (RDB), where it mono-ubiquitylates proliferating cell nuclear antigen (PCNA), in a cascade of events that allows DNA replication to proceed in the presence of damage. The function of RAD18 in DSB repair is much less clear. First, we analysed the dynamic localization pattern of YFP-tagged RAD18 during the cell cycle in living cells (**Chapter 2**). We show that the distribution pattern of YFP-RAD18 is mostly different from that of PCNA, but similar to that of the DSB repair-associated proteins RAD51 and  $\gamma$ H2AX. After induction of DSBs, using low power multi-photon laser irradiation, RAD18 accumulated at DSB sites, but PCNA did not. These findings suggest that RAD18 functions in DSB repair outside the context of RDB, and independent from PCNA mono-ubiquitylation. Next, we performed functional studies of RAD18 through analyses of the effects of mutations in the RAD18 RING finger, Zinc finger, SAP domain, and HR6A/B binding domain in **Chapter 3**. We show that RAD18 associates with DSBs via its Zinc finger domain through association with ubiquitylated H2A and other ubiquitylated chromatin components, which are enriched at chromatin surrounding DSBs. The association of RAD18 with DSBs allows recruitment of RAD9, one of the components of the 9-1-1 checkpoint complex. RAD9 may function directly in homologous recombination repair at DSBs, independent of downstream activation of the checkpoint kinases CHK1 and CHK2,

In meiotic cells, programmed DSBs are induced by an endogenous meiosis-specific topoisomerase-like protein called SPO11, at various locations in the genome at the beginning of the first meiotic prophase. The repair of SPO11-induced meiotic DSBs leads to the formation of crossovers and noncrossovers through homologous recombination. The role of mouse RAD18 in meiotic DSB repair is described in **Chapter 4**. We show that RAD18 is recruited to persistent meiotic DSBs in a SPO11 dependent manner. Analyses of the meiotic phenotype of *Rad18* knockdown mice revealed that RAD18 is required for the efficient repair of a small subset of meiotic DSBs. In addition, RAD18 is recruited to the chromatin of the XY chromosome pair that forms the transcriptionally silent XY body. The accumulation of RAD18 on the silenced chromosomal regions in meiosis occurs at least partially independent of SPO11-induced DSBs. At the XY body, RAD18 mediates the chromatin association of its interaction partners, the ubiquitin-conjugating enzymes HR6A and HR6B. HR6B is involved in regulation of histone modifications at the XY body, and required for



maintenance of sex chromosome silencing. We showed that this function is RAD18-dependent, since the level of dimethylation of histone H3 at lysine 4 in spermatocytes, and the maintenance of meiotic sex chromosome inactivation in spermatids were also affected in *Rad18* knockdown testes. Since PCNA is the most well known substrate for ubiquitylation by RAD18, it was also interesting to compare the phenotype of the *Rad18* knockdown mice with that of mice that carried a targeted mutation at the lysine (K164) that is normally ubiquitylated by RAD18 (**Chapter 5**). Surprisingly, homozygous *Pcna*<sup>K164R/K164R</sup> knockin mice display severe defects in germ cell development, indicating an essential role of PCNA modification during primordial germ cell survival and/or proliferation. Also, in heterozygous mice, carrying one mutated PCNA allele (*Pcna*<sup>K164R/+</sup>), we observed an increase in meiotic recombination frequency. This phenotype appeared to be independent of other components of the RDB pathway, indicating that perhaps not PCNA ubiquitylation, but PCNA sumoylation might be involved in the regulation of meiotic recombination frequency.

As described in **Chapter 6**, we have also analysed whether irradiation induced breaks can replace SPO11 to stimulate chromosome pairing during meiotic prophase. In addition, we have performed a detailed analysis of the relation between the accumulation of DNA repair proteins and the formation of the so-called pseudo-XY body in *Spo11* mutant spermatocytes. The pseudo-XY body is characterized by the formation of a transcriptionally silenced and  $\gamma$ H2AX-positive area, covering part of the asynapsed chromatin (not necessarily X and Y) in *Spo11*-deficient spermatocytes. We found that irradiation-induced breaks stimulate synapsis of synaptonemal complex formation in spermatocytes and oocytes. Shortly after irradiation, formation of the pseudo-XY body was not observed. Instead, multiple  $\gamma$ H2AX-positive areas, colocalizing with RAD51 foci, could be observed. In the absence of irradiation, spontaneous RAD51 foci also frequently colocalized with the pseudo-XY body. Taken together with our observation that a pseudo-XY body is formed in *Spo11* mutant oocytes, in association with RAD51 accumulation, we suggest that meiotic silencing may be triggered by the presence of persistent DSBs in oocytes and spermatocytes.

In **Chapter 7**, we discuss the possible relevance of RAD18 recruitment to DSB repair sites in mitotic and meiotic cells, and finally focus on the candidate substrates of RAD18 whose final identification will help to obtain more insight in the putative roles of RAD18 in DSB repair, DSB-dependent silencing in cis, and meiotic sex chromosome inactivation.



## SAMENVATTING

Cellen worden voortdurend blootgesteld aan interne en externe factoren die DNA schade kunnen veroorzaken. Om genomische integriteit te behouden hebben cellen daarom de beschikking over diverse DNA reparatie mechanismen. Daarnaast is er een controle-systeem dat ervoor zorgt dat schade aan het DNA gerepareerd wordt voordat de celdeling plaatsvindt. Eén van de meest genotoxische soorten DNA schade is de DNA dubbel-strengs breuk (DSB). In mitotische cellen kunnen DSB's ontstaan als de replicatie vork instort tijdens de S-fase. Verder kunnen DSB's ook ontstaan door externe factoren zoals ioniserende straling.

In dit proefschrift concentreren we ons op de rol van RAD18 in DSB reparatie in mitotische en meiotische cellen. RAD18 is een E3 ubiquitine ligase, en is vooral bekend vanwege zijn rol bij het passeren van DNA schade tijdens replicatie (replication damage bypass, RDB). Daar ubiquitineert het proliferating cell nuclear antigen (PCNA), in een reeks gebeurtenissen die ervoor zorgen dat DNA replicatie ondanks de schade kan doorgaan. Hoe RAD18 functioneert bij reparatie van DSB's is nog niet helemaal duidelijk.

Allereerst hebben we de dynamische lokalisatie van YFP-gekoppeld RAD18 gevolgd in levende cellen (**Hoofdstuk 2**). We laten zien dat het distributie patroon van YFP-RAD18 anders is dan dat van PCNA, het lijkt meer op het patroon van de DSB-reparatie eiwitten RAD51 en  $\gamma$ H2AX. Na inductie van DSB's met multi-foton laser bestraling accumuleert RAD18, maar niet PCNA, op DSB's. Dit suggereert dat RAD18 een rol heeft in DSB reparatie die onafhankelijk is van zijn rol in RDB en PCNA mono-ubiquitinatie.

Vervolgens hebben we functionele studies op RAD18 uitgevoerd door de effecten te bestuderen van mutaties in de RING-vinger, zink-vinger, SAP en HR6A/B domeinen (**Hoofdstuk 3**). We laten zien dat RAD18 via het zink-vinger domein aan DSB's bindt door associatie met geubiquitineerd H2A en met andere geubiquitineerde chromatine componenten die verrijkt zijn rondom DSB's. De associatie van RAD18 met DSB's zorgt ervoor dat RAD9, één van de componenten van het 9-1-1 checkpoint complex, wordt gerekruteerd. RAD9 zou een directe rol in homologe recombinatie kunnen spelen, die onafhankelijk is van activering van de checkpoint kinases CHK1 en CHK2.

In meiotische cellen worden geprogrammeerde DSB's gemaakt door het topoisomerase-achtige eiwit SPO11. Dit gebeurt op verschillende plekken in het genoom in de vroege meiotische profase. De reparatie van SPO11-geïnduceerde DSB's leidt via homologe recombinatie tot producten waarbij een hele chromosomale arm wisselt van chromosoom, of een product waarbij slechts een klein DNA fragment wordt uitgewisseld (respectievelijk genaamd crossovers en non-crossovers). De rol van RAD18 in meiotisch DSB herstel wordt beschreven in **Hoofdstuk 4**. Wij laten daar zien dat RAD18 wordt gerekruteerd naar persistente DSB's, en dat dit afhankelijk is van SPO11. Analyses van het meiotische fenotype van *Rad18* knockdown muizen laten zien dat RAD18 nodig is voor efficiënte reparatie van een kleine subset van meiotische DSB's. Bovendien wordt RAD18 gerekruteerd naar het chromatine van het XY chromosoompaar, dat de transcriptioneel inactieve XY body vormt. De



opeenhoping van RAD18 in transcriptioneel inactieve chromosomale regio's tijdens de meiose is tenminste deels onafhankelijk van SPO11-geïnduceerde DSB's. Op de XY body zorgt RAD18 voor de chromatine associatie van zijn interactie partners; de ubiquitine-conjugerende enzymen HR6A en HR6B. HR6B is betrokken bij de regulatie van histon modificaties op de XY body en bij het handhaven van transcriptionele inactivatie van de geslachtschromosomen. Wij hebben laten zien dat deze rol van HR6B afhankelijk is van RAD18, omdat het niveau van dimethylering op histon H3 op lysine 4 in spermatocyten, en het handhaven van geslachtschromosoom inactivatie in spermatiden ook aangedaan waren in testes waarin RAD18 uitgeschakeld was.

Omdat PCNA het bekendste ubiquitinatie substraat van RAD18 is, was het interessant om het fenotype van RAD18 knockdown muizen te vergelijken met dat van muizen met een mutatie in het lysine op PCNA (K164) dat normaal door RAD18 geubiquitineerd wordt (**Hoofdstuk 5**). Onverwachts lieten *Pcna*<sup>K164R/K164R</sup> knock-in muizen een ernstig defect zien in de ontwikkeling van de geslachtscellen, wat suggereert dat PCNA een essentiële rol heeft in de overleving en/of proliferatie van geslachtscellen. Bovendien zagen we dat heterozygote muizen met een enkel gemuteerd PCNA allel (*Pcna*<sup>K164/+</sup>) een verhoogde recombinatie frequentie in meiose hadden. Dit fenotype leek onafhankelijk van andere RDB-componenten, en doet suggereren dat niet PCNA ubiquitinatie, maar PCNA sumoylatie een rol zou kunnen spelen in het reguleren van de meiotische recombinatie frequentie.

In **Hoofdstuk 6** hebben we geanalyseerd of breuken die door straling worden geïnduceerd de functie van SPO11 kunnen vervangen en of deze breuken chromosoomparing kunnen induceren in meiose. Verder hebben we een gedetailleerde analyse uitgevoerd van de relatie tussen de accumulatie van DNA reparatie eiwitten en de vorming van het zogenoemde pseudo-XY body in *Spo11* mutant spermatocyten. Het pseudo-XY body wordt gekenmerkt door een transcriptioneel inactief gebied dat positief is voor  $\gamma$ H2AX en dat een deel van het niet-gesynapse chromatine in spermatocyten bedekt. Wij zagen dat stralings-geïnduceerde breuken synapsis en vorming van het synaptonemale complex in spermatocyten en oocyten stimuleren. Vorming van een pseudo-XY body kort na bestraling werd niet gezien, maar wel zagen we verschillende  $\gamma$ H2AX-positieve gebieden die samenvielen met RAD51 foci. Zonder bestraling vallen spontane RAD51 foci ook regelmatig samen met het pseudo-XY body. Onze waarnemingen dat het pseudo-XY body wordt gevormd in *Spo11* mutant oocyten en dat dit samenvalt met RAD51 accumulatie, geven samen aan dat meiotische inactivatie van transcriptie zou kunnen worden veroorzaakt door persisterende DSBs in oocyten en spermatocyten.

In **Hoofdstuk 7** bespreken we de mogelijke relevantie van RAD18 rekrutering naar DSB-reparatie gebieden in mitotische en meiotische cellen, en richten we ons op kandidaat-substraten van RAD18. De identificatie van deze substraten zou meer inzicht kunnen verschaffen in de mogelijke functies van RAD18 in de reparatie van DSB's, in DSB-afhankelijke transcriptionele inactivatie *in cis*, en in meiotische geslachtschromosoom inactivatie.

(Kindly translated by Daphne B. Pontier)



## LIST OF ABBREVIATIONS

BER	base excision repair
BIR	break-induced replication
bp	base pairs
cDNA	complement DNA
<i>C. elegans</i>	<i>Caenorhabditis elegans</i>
CPD	cyclobutane pyrimidine dimmers
CPT	camptothecin
Da	dalton
DNA	deoxyribonucleic acid
DISC	double-strand break-induced silencing in cis
DNA-PKcs	DNA-dependent protein kinase catalytic subunit
dsDNA	double-stranded DNA
DSB	double-strand break
E1	ubiquitin-activating enzyme
E2	ubiquitin-conjugating enzyme
E3	ubiquitin ligase
FHA	forkhead-associated
GCNA	Germ cell nuclear antigen
GFP	green fluorescent protein
$\gamma$ H2AX	phosphorylated histone H2AX
Gy	Gray
HJ	holliday junction
HR	homologous recombination
HR6BD	HR6A/B binding domain
HU	hydroxyurea
iFRAP	inverse fluorescence recovery after photo-bleaching
IR	ionizing radiation
MI	first meiotic division
MMS	methyl methanesulfonate
MPL	multi-photon laser
MSCI	meiotic sex chromosome inactivation
MSUC	meiotic silencing of unsynapsed chromatin
NER	nucleotide excision repair
NHEJ	nonhomologous DNA end-joining
PAR	pseudo autosomal region
PCNA	proliferating cell nuclear antigen
PIKK	phosphatidylinositol 3-kinase-like kinase
RDB	replication damage bypass
RNA	ribonucleic acid
SC	synaptonemal complex
<i>S. cerevisiae</i>	<i>Saccharomyces cerevisiae</i>
SCJ	sister chromatid junction



SDSA	synthesis-dependent strand annealing
shRNA	short hairpin RNA
siRNA	small interfering RNA
<i>S. pombe</i>	<i>Schizosaccharomyces pombe</i>
ssDNA	single-stranded DNA
SUMO	small ubiquitin-like modifier
TLS	translesion synthesis
TUNEL	Terminal deoxynucleotidyl transferase dUTP nick end labeling
uH2A	ubiquitylated histone H2A
UV	ultra violet
YFP	yellow fluorescent protein
Y2H	yeast two-hybrid
UBM	ubiquitin binding motif
UBZ	ubiquitin binding Zing-finger
UIM	ubiquitin interaction motif



## CURRICULUM VITAE

**Name** Akiko Inagaki

### Education

- 2006 - present *PhD student*  
Erasmus MC, The Netherlands
- 2004 - 2006 *Master's degree: Medical Science*  
University of Utrecht, The Netherlands
- 2000 - 2002 *Master's degree: Biochemical Science*  
Yokohama National University graduate school, Japan
- 1996 - 2000 *Bachelor's degree: Chemical Science*  
Yokohama National University, Japan
- 1993 - 1996 *Ibaraki high school, Osaka, Japan*

### Research experience

- 2006 – 2010 *Reproduction and Development; ErasmusMC, Rotterdam, The Netherlands.*  
Meiotic and mitotic functions of mammalian RAD18 in DNA double-strand break repair. Prof. J. A. Grootegoed, Prof. J. H. Hoeijmakers & Dr. W. M. Baarends.
- 2004 – 2006 *Department of Physiological Chemistry; University Medical Centre of Utrecht, The Netherlands.*  
Regulation of histone H3K4 tri-methylation and PAF complex recruitment by the Ccr4-Not complex. Modulation of Ubc4p/Ubc5p-mediated stress responses by the RING-finger-dependent ubiquitin-protein ligase Not4p in *Saccharomyces cerevisiae*. Prof. H.T. Timmers
- 2004 – 2004 *Department of Metabolic and Endocrine diseases, University Medical Centre of Utrecht, The Netherlands.*  
The Molecular genetics of Medullary Thyroid Carcinoma: Multistep Tumorigenesis. Prof. C. J. Lips
- 2000 – 2002 *Division of BioChemical Engineering, Yokohama National University, Japan.*  
Degradation of dibenzodioxins by *Streptomyces lividans*. Prof. J. Koizumi



# PHD PORTFOLIO - SUMMARY OF PHD TRAINING AND TEACHING

Name PhD student: Akiko Inagaki  
Erasmus MC Department: Reproduction and Development  
Research School: Medical Genetics Centre South-West Netherlands (MGC)  
PhD period: 2006-2010  
Promotors: Prof. dr. J. Anton Grootegoed / Prof. dr. Jan H. J. Hoeijmakers  
Supervisor: Willy M Baarends

## 1. PhD training

### *General courses*

Biomedical English Writing and Communication	2007
Safely working in the Laboratory	2009

### *Specific courses*

Course Molecular Medicine	2006
Biomedical Research Techniques V	2006
In Vivo Imaging "From Molecule to Organism"	2006
From Development to Disease	2006
Experimental approach to Molecular and Cell Biology	2006
Reading and discussing literature	2006
Antoni van Leeuwenhoek Advanced Microscopy Course	2008

### *Seminars and workshops*

Annual MGC graduate student workshop	2007-2009
--------------------------------------	-----------

### *Presentations*

Winterschool Kleinwalsertal	2007-2009
Annual MGC graduate student workshop	2007-2009

### *(Inter)national conferences*

Oct. 2006	Conference on 'Chromatin Mediated Biological Decisions', Marburg, Germany (poster contribution)
Nov. 2007	Annual meeting of Dutch microscopy association 'Molecular microscopy and Atoms at the interface'; Lunteren, The Netherlands Oral presentation: <i>Dynamic localization of RAD18 in living cells</i>
Mar. 2007	Gordon Research Conference on 'DNA Damage, Mutation & Cancer'; Ventura, USA (poster contribution)
Nov. 2008	Annual meeting of Dutch microscopy association 'Molecular microscopy and cellular traffic'; Lunteren, The Netherlands



- Mar. 2009 Oral presentation: *Dynamic accumulation of RAD18 at multi-photon laser induced damage in living cells*  
Keystone Symposium on ‘Genome Instability and DNA Repair’; Taos, USA (poster contribution)
- Sep. 2009 The EMBO meeting on ‘Advancing the life science’; Amsterdam, The Netherlands (poster contribution)
- Sep. 2009 The 19<sup>th</sup> MGC-Symposium, Rotterdam, The Netherlands  
Oral presentation: *The role of RAD18 in mitotic and meiotic cells.*
- Sep. 2009 EMBO meeting on ‘Meiosis’; L’Isle sur la Sorgue, France (poster contribution)
- Sep. 2010 EMBO meeting on ‘Interface between the Ubiquitin family and the DNA damage response’; Rovinj, Croatia (poster contribution)

## 2. Teaching

*Supervising practicals and excursions, Tutoring*

2007-2009 *Optical Image Centre, ErasmusMC, Rotterdam, The Netherlands*

Teaching assistant of OIC course “In Vivo Imaging; Cellular Imaging”

2006 – present Supervising master’s thesis research projects of Master students



## LIST OF PUBLICATIONS

**Inagaki A, de Vries S, Schoenmakers S, Vermeulen C, Wassenaar E, van Cappellen WA, Carofoglio F, Sleddens-Linkels E, Grootegoed JA, te Riele HP, de Massy B, Baarends WM.** Relation between radiation-induced DNA double-strand breaks, synapsis and the MSUC response in spermatocytes and oocytes of Spo11 mutant mice. (Manuscript in preparation)

**Inagaki A\***, Krijger PHL\*, Sleddens-Linkels E, van den Berg PCM, Wassenaar E, Ooms M, Schoenmakers S, Hoeijmakers JHJ, Grootegoed JA, Jacobs H\*, Baarends WM\*. Meiotic recombination is controlled by PCNA K164 modification. (Manuscript in preparation)

\*These authors contributed equally to this work

**Inagaki A, Sleddens-Linkels E, van Cappellen WA, Hibbert RG, Sixma TK, Hoeijmakers JHJ, Grootegoed JA, Baarends WM.** Human RAD18 interacts with ubiquitylated H2A and facilitates RAD9 recruitment to DNA double-strand breaks. Submitted

**Inagaki A, Sleddens-Linkels E, Wassenaar E, Ooms M, van Cappellen WA, Hoeijmakers JHJ, Seibler J, Vogt TF, Shin MK, Grootegoed JA, Baarends WM.** Meiotic functions of RAD18. Submitted

**Inagaki A, Schoenmakers S, Baarends WM.** DNA double strand break repair, chromosome synapsis and transcriptional silencing in meiosis. *Epigenetics*. 2010 May 5:4, 1-12.

**Dzyubachyk O, Essers J, van Cappellen WA, Baldeyron C, Inagaki A, Niessen WJ, Meijering E.** Automated Analysis of Time-Lapse Fluorescence Microscopy Images: From Live Cell Images to Intracellular Foci. *Bioinformatics*. 2010 Aug 11.

**Inagaki A, van Cappellen WA, van der Laan R, Houtsmuller AB, Hoeijmakers JH, Grootegoed JA, Baarends WM.** Dynamic localization of human RAD18 during the cell cycle and a functional connection with DNA double-strand break repair. *DNA Repair (Amst)*. 2009 Feb 1;8(2):190-201.

**Mulder KW, Inagaki A, Cameroni E, Mousson F, Winkler GS, De Virgilio C, Collart MA, Timmers HT.** Modulation of Ubc4p/Ubc5p-mediated stress responses by the RING-finger-dependent ubiquitin-protein ligase Not4p in *Saccharomyces cerevisiae*. *Genetics*. 2007 May;176(1):181-92.

**Mulder KW, Brenkman AB, Inagaki A, van den Broek NJ, Timmers HT.** Regulation of histone H3K4 tri-methylation and PAF complex recruitment by the Ccr4-Not complex. *Nucleic Acids Res*. 2007 March;35(7):2428-39.



## ACKNOWLEDGEMENTS

Life as a PhD student in Rotterdam was a very unique experience. Despite having a principle such as ‘You can always retake a test. But you can never retake a party’, I managed to reach this final point to finish my PhD thesis.

First of all, I would like to thank my supervisor, Willy M Baarends for the valuable guidance and advice. Thank you, Willy, for giving me an opportunity to work in your lab! I will never forget your first words to me, “Oh, I thought you were a man.” In truth, I thought you were a man, too! Thank you for all of your input about meiosis, meiotic repair mechanisms and the XY body. You inspired me greatly to work on all sorts of projects. Willy, you are one of the most honest and direct people I have ever met. At first, it took me a while to get used to your very straight remarks! Besides science, I had lots of fun with you in the lab, at daily lunch times, and especially during the conferences. At the Meiosis meeting in Isle sur la Sorgue, we all were very hardcore scientists!! These four years as a graduate student were a great experience thanks to you!

My PhD projects would not have been possible without my promoters, J Anton Grootegoed and Jan HJ Hoeijmakers. Anton, thank you for all the universal knowledge of spermatogenesis and meiosis that you provided in my projects. In addition to your serious and strict aspects toward science, it was very nice to discover your amusing and funny side! Jan, your enthusiasm for science always impresses me. Your very careful as well as very critical way to interpret all data is incredible. Thank you for all your interest in my DNA-repair projects.

My sincere gratitude also goes to my thesis committee members, Dik C van Gent, Heinz Jacobs and Titia K Sixma. All your helpful feedback stimulated me to improve and complete this thesis.

My dear two paranimfen, Iris Jonkers and Eskeatnaf Mulugeta Achame. Iris, it is so cool that you can come back for my thesis defense from Ithaca! It was great fun with you having many drinks in Rotterdam, Amsterdam, Zeeland, Kleinwalsertal, and Ithaca! You always created a very cheerful atmosphere in our lab. We all miss you and your powerful laughter, HAA HAA HAA HAA HAAAAAA. Eskeww, your high spirit and strong patience always amazed me. Thank you for joining my multi-cultural defense!!

Now many thanks go to my colleagues in the lab of Reproduction and Development. Esther, I cannot thank you enough for all your technical support and your generosity!! Our yeast two-hybrid screening would not have been successful without your enormous contribution. Dear Sam, you are a very funny person in a special way! It was extremely spectacular to see your transfer from the top of the mountain by helicopter. Good luck with your career as a Gynecologist. Please never sing in public! Peng, I wish you good luck with your new project! Evelyne, it was fun to expose Bouin fixation in the train!! Be ready for a live delivery during my thesis defense! Marja, thanks for slicing all my materials! Jos, you still have several months to bake an apple pie! To Joost, I have to say, “Wow!” When I first arrived in the department, you had a small group. Look at you now. Congratulations on your successful years. Eveline, you work like a playing musical! You are very unique! Cristina, your arrival to our lab supplied us with many new methods to approach research questions. Good luck with your new interesting protein, RT1!! Nilhan, kapsalon? Daphne, thank you for the translation of my Dutch ‘samenvatting’.



To other current and previous lab members, Catherine, Fabrizia, Federica, Stefan, Imke, Zeli, Kim, Annegien, Ruben, Maarten, Bas and Marieke, I thank you all!

For the last 4.5 years, I had great fun with many colleagues in cluster 15 at the lab-days, X'mas parties, AIO workshops, borrels, bowling competitions, and in Kleinwalsertal. Thank you all for your kindness! Marialuisa, Francesca, and Bianca, thank you all for our amusing trip to a big city, Chiavenna. My party mate, Aude, it was an amazing experience to be in New Zealand with you. We still need to go to South America! To some people, I would like to clear my identity. Vincenzo, I am NOT from Sapporo, and Job, I am NOT from Jamaica.

I would like to express my appreciation to OIC members, Gert, Adriaan and Alex. I have learned so many techniques and theories about microscopes. Thank you for giving me the opportunities to teach introduction courses. Sorry for having tried to sell all confocal microscopes at Marktplaats...

During my work at Erasmus MC, Benno, Jasperina and Jeanette smoothly managed all complicated arrangements. It is a pleasure to thank you all.

Many of my research projects would not have been done without my fruitful collaborations with the groups of Titia Sixma and Heinz Jacobs in NKI. I thank Rick, Peter, Nik, Paul, Heinz, and Titia for your massive input to the projects.

My life in the Netherlands would have been very boring without my waterpolo mates. I am heartily thankful to all of you! My special thanks goes first to all my teammates in Fysius het Ravijn. It is impossible to thank everyone individually, but I still am pleased to thank some girls from Dames 1 whom I always played with. Martina, Karin, Marlies, Rianne, Mayke, Yasmine, Marieke, Saskia, Mieke and Jane, we went to so many tournaments all over Europe, and I spent an amazing and unforgettable time with you all! Gerrit-Jan, Jan-Jacob, and Laurens-Jan, it was a very comical trip to Japan. My other thanks goes to all my teammates in ZPB H&L Productions. I had great party times with you all! A special thanks to Shari, Kirsten, Wendy, Jacqueline, Daphne, Lisette, Kimberly, Marina, Angela, Debbie, Esther, Danielle, Ingeborg, Brenda, Barbara, Marije, 3xKarin, Berbel, Danney, Jeroen and Martin. It was so much fun playing with you all!

Ben and Marion, I would not have survived in the Netherlands without you. I cannot ever thank you enough.

最後に、これまで心配と迷惑ばかりかけてきた両親に感謝の言葉で、この博士論文を締めくくりたいと思います。

「勉強と水球と、両立というよりはどっち付かずで、それでも何とかここまで辿り着くことが出来ました。なんやかんやで色々揉めることが多かったのですが、終わりよければ全てよし、という感じですかね。今までどうもありがとう。これからもよろしく。」

明子

Akiko Inagaki

IT'S PARTY TIME !!

